LA-8717-PR

Progress Report

C.3

Chemistry-Nuclear Chemistry Division

October 1979—September 1980

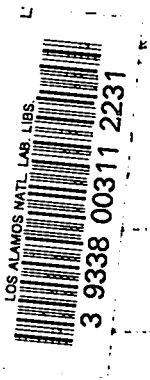

LOS ALAMOS SCIENTIFIC LABORATORY
Post Office Box 1663 Los Alamos, New Mexico 87545

This is the first report in this series.

Photocomposition by

IS-6 Composing Section

UNITED STATES
DEPARTMENT OF ENERGY
CONTRACT W-7405-ENG. 36

LA-8717-PR
Progress Report

UC-4
Issued: May 1981

Chemistry-Nuclear Chemistry Division

October 1979—September 1980

Compiled by

R. R. Ryan

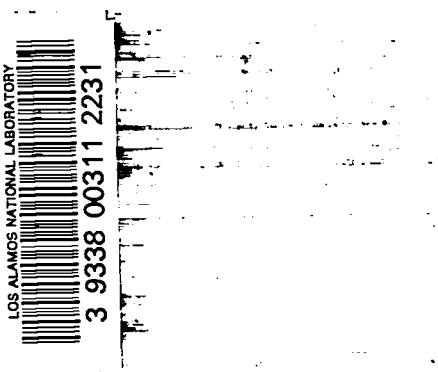

FOREWORD

DIVISIONAL OVERVIEW

Darleane C. Hoffman

It seems appropriate to reflect on the current state of the Division in our first annual report, prepared 10 years after formation of the Chemistry-Nuclear Chemistry Division in January 1971. On October 1, 1980 two new groups (CNC-3, Medical Radioisotopes Research, and CNC-7, Isotope Geochemistry) were formed in addition to our existing groups (CNC-2, Physical Chemistry-Chemical Physics, CNC-4, Inorganic and Structural Chemistry, and CNC-11, Nuclear and Radiochemistry. See Organization Chart below.) At the end of FY-1980, we had 155 people in the Division, including 95 professional scientists, 75 with the degree of Ph.D. During the year, we had 11 postdoctoral appointees, a postgraduate resident in nuclear medicine, and one of the recipients of the prestigious J. Robert Oppenheimer Fellowship awarded by the Laboratory each year to one or two outstanding young scientists. During the past year

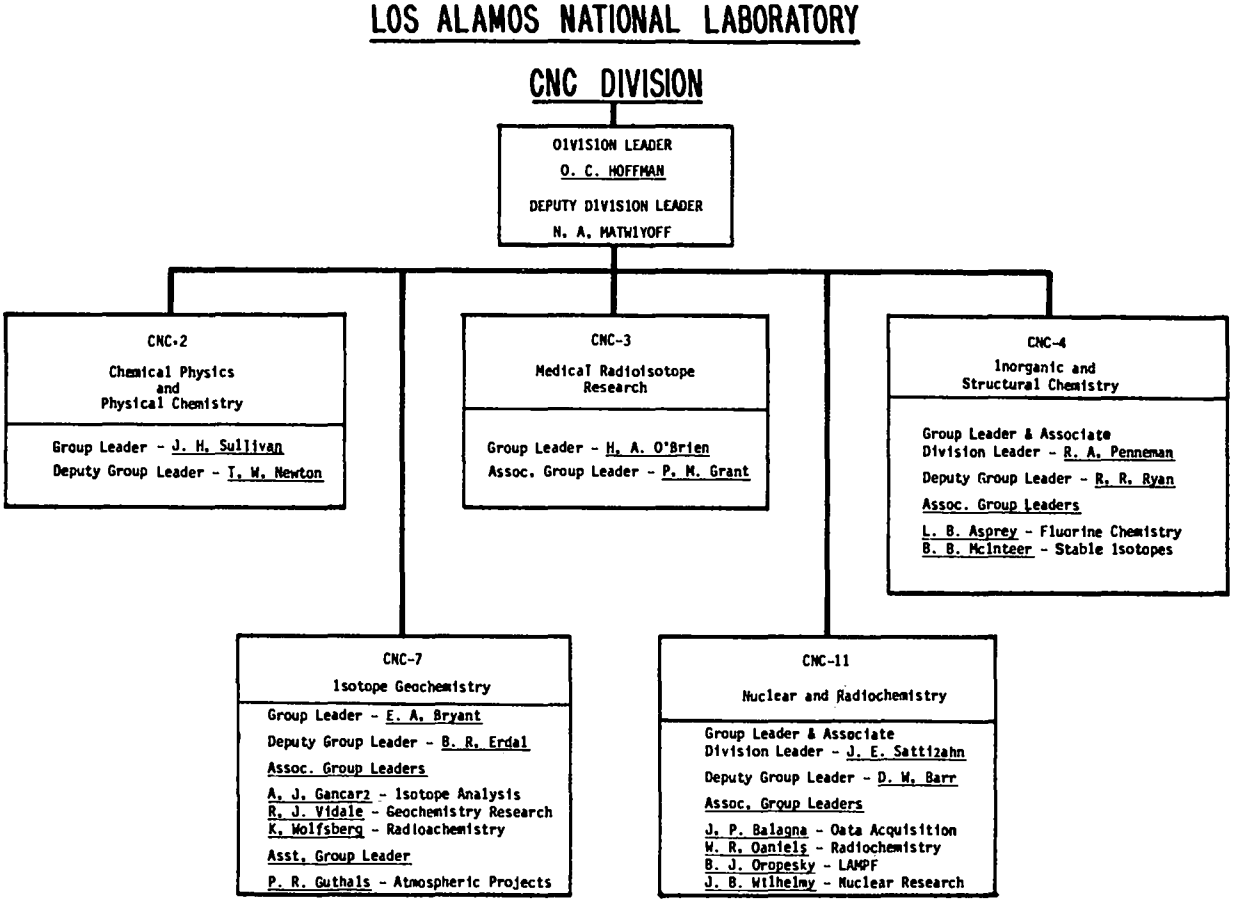

we have continued our close interactions with scientists from numerous universities and research institutes, both in this country and abroad. Some 50 visiting staff members and consultants contributed to a variety of projects within the Division, and an additional 30 research visitors used our nuclear chemistry facilities at the Los Alamos Meson Physics Facility (LAMPF). Advisory committees of eminent scientists reviewed our Medical Radioisotopes Research and Stable Isotopes Resource Programs. We hosted an Intermediate Energy Nuclear Chemistry workshop in June 1980 with 97 nuclear scientists (14 from abroad) in attendance. The Second Annual Divisional Information meeting was held in September 1980.

This report covers contributions during FY-1980 (October 1, 1979—September 30, 1980) to unclassified projects and to unclassified work related to the nuclear weapons program. Publications for all of calendar years 1978 and 1979 as well as FY-1980 are listed and total 198 (see Appendix A). Appendix B lists facilities provided by the Division.

The following are among our most notable accomplishments for FY-1980:

- Isotope separation of large amounts (kg/yr) of >99 at.% ^{13}C, ^{18}O, ^{15}N (plus 50% ^{17}O) has continued. Catalytic exchange of ^{12}CO with ^{13}CO (important in our CO distillation process for achieving 99% ^{13}C) has been found to proceed on γ-Al_2O_3 without the presence of ruthenium.
- A unique mass spectrometer system for rapid analysis of nitrogen isotope ratios has been developed. It can analyze several hundred samples per day in a fully automated fashion, from chemical processing to data print-out.
- Carbon-13 nuclear magnetic resonance studies of the interaction of the cancer chemotherapeutic agent, *cis*-diamine platinum (II), with the vitamin B_{12} derivatives, adenosylcobalamin and methylcobalamin, have shown that the platinum complex can inactivate the vitamin. This inactivation and resultant B_{12} deficiency may cause toxicity sometimes observed in the neural systems of patients with gynecological tumors treated with *cis*-diamine platinum (II).
- The validity of the use of heavy methanes ($^{12}CD_4$ and $^{13}CD_4$) as tracers of air movement over distances of 600 km and transit times of ~18 h has been demonstrated.
- Radiopharmaceutical cold kits, in common usage in nuclear medicine, permit radioactive labeling to be performed under sterile conditions in the clinic or hospital by trained nuclear medicine technologists. The recent development of two radioiodination cold kits in our laboratory will facilitate the use of ^{123}I in diagnostic medicine.
- The $^{68}Ge/^{68}Ga$ biomedical positron generator system is expected to play an important role in emission computed tomography studies in man. The development of spallation production of ^{68}Ge at LAMPF is an important step in creating an alternative, economical source for this nuclide.
- The achievement of high specific activity (600-1200 Ci/mmole) labeling of estrogen derivatives is a significant and essential development in the quest to obtain a useful *in vivo* estrogen-receptive tumor localizing agent. This search for a suitable agent is being conducted as a collaborative project involving Los Alamos, Washington University, the University of Illinois, George Washington University, and the University of Kansas.
- After more than 1.1-billion gallons of water were pumped from a well 90m from the Cambric underground nuclear test, only tritium and ^{85}Kr were positively detected.

- Sorption ratios for plutonium on tuff, granite, and argillite have been found to be independent of plutonium concentration in the 10^{-8} to 10^{-12} M range.
- Radiogenic lead mobilized from the mineralized strata at the Oklo mine has been found in the underlying conglomerate at concentrations as high as 3.4%.
- Muonic x-ray studies have provided the first experimental evidence for the orientation of the molecular electric dipole in NO as $^{-}NO^{+}$. (Meson capture should be related to electron density and was found to be appropriately larger for nitrogen in NO than in equimolar mixtures of $N_2 + O_2$ gas.)
- Our measurements of the theoretically important pion single-charge exchange reaction $^{13}C(\pi^{+},\pi^{o})\ ^{13}N$ as a function of pion energy show that the cross sections are substantially lower than previously reported values and are closer to theoretical predictions.
- A new coupled-channel theory for pion single-charge-exchange reactions was developed that goes beyond the first-order pion-nucleus interaction and includes the second-order interactions caused by true pion absorption and pion scattering from correlated nucleon pairs.
- Measurements of the excitation functions for the pion single-charge exchange reactions $^{27}Al(\pi^{-},\pi^{0})^{27}Mg$, $^{45}Sc(\pi^{+},\pi^{0})^{45}Ti$, and $^{65}Cu(\pi^{-},\pi^{0})^{65}Ni$ show no structure near the (3,3) pion-nucleon resonance as predicted by the impulse approximation and Fermi gas model, but exhibit a monotonic decrease in cross section approximately proportional to 1/E.
- Our measured ratios of the yields of radioactive products resulting from np and nn emission following the capture of a negative pion in selected target nuclei are consistent with an increasing probability for np pairs versus pp pairs in the nuclear surface with increasing target Z.
- Measurements of the intensities of several long-lived radionuclides in lunar rocks were used to show that the average flux of energetic protons emitted from the sun has varied during the last million years.
- Cross-section measurements have been made on several unique radioactive targets, for example, (n, 2n) and (n, np) reactions on 83-day ^{88}Zr and the (p,t) reaction and level structure studies on 75-yr ^{148}Gd.
- We have shown that a state-of-the-art, two-stage mass spectrometer can be used to measure "radiochemical detector" isotope ratios for nuclear weapons test diagnostics.
- Raman scattering studies of organic high explosives under extreme temperature (20-600K) and pressures up to 100 kbar show remarkable changes in the vibrational energies, line widths, and relative intensities; the implication is that selective coupling between phonon and molecular vibrations may control the energy transfer from the shock wave to the bonds that are broken in detonation.
- We have demonstrated a new experimental method for obtaining simple, interpretable Raman spectra for molecules whose spectra are usually unresolved or too complex for interpretation. The spectra were simplified by cooling the molecules in a free jet expansion and were obtained using ultrahigh-resolution coherent Raman techniques.
- Theoretical techniques were developed that, for the first time, enabled us to calculate rate constants for adsorption and desorption of atoms and molecules from solid surfaces. These techniques are unique in that they can be applied to sufficently large systems (10^2-10^3 atoms) to allow examination of the effects of adsorbate concentration and surface geometry on the rate constants.

- We have shown that Monte Carlo methods can be used to calculate electronic structures of molecules. This development is significant because it is applicable to larger molecules and because it allows calculation of properties where a molecular system is interacting with an extended system, as with chemisorbed H_2 on a crystal lattice.
- An atlas of uranium emission lines has been prepared, and it was demonstrated that the easily measured optogalvanic effect in a uranium hollow cathode discharge tube can be used to calibrate laser wavelengths simply and accurately.
- The structure of actinide molybdates, which can form during nuclear fuel reprocessing, is poorly known. We have completed the structure of $U(MoO_4)_2$.
- Carbamylmethylenephosphonates are valuable as acid extractants of actinides, and the first crystal structure containing this ligand has been determined.
- Unusual bonding and reactivity of SO_2 (with catalytic possibilities) are found on its coordination to molybdenum and tungsten carbonyls. We have found that SO_2 can be reduced to sulfur at medium temperature by H_2 over a catalytic surface of ruthenium on Al_2O_3.
- Rich new dynamics have been discovered in high-resolution studies of impurity-doped solids, including site-to-site exchange on the vibrational time scale. These results greatly expand our understanding of guest-host interactions and energy relaxation in condensed phase materials.

CNC
DIVISIONAL PERSONNEL AND FINANCIAL SUMMARY
FY-1980

	Funding[a] ($ K)	FTE[b] Average Level
DOE PROGRAMS		
Defense	$ 3 010	39
Supporting Research	2 347	28
Energy Research (ER)	1 154	11
Geothermal Energy (RA)	273	3
Atmospheric Projects (EV)	530	5
Medical Radioisotopes (EV)	890	11
Stable Isotopes Development (EV)	410	4
Stable Isotopes Inventory	586	7
TOTAL DOE PROGRAMS	$ 9 200	108
OTHER PROGRAMS		
NASA	83	1
NIH (Stable Isotopes Resource)	184	2
NV: Defense Radionuclide Migrations	150	2
Nevada Nuclear Waste Storage Investigations	768	8
Office of Waste Isolation	650	8
Miscellaneous	395	5
TOTAL OTHER PROGRAMS	$ 2 230	26
OVERALL TOTAL	$11 430	134

[a]Excluding capital equipment.
[b]FTE = full time equivalent rounded to nearest whole number. Not included are 12 postdoctoral appointees and 1 J. Robert Oppenheimer Fellow.

CONTENTS

CHEMISTRY-NUCLEAR CHEMISTRY DIVISION
OCTOBER 1979—SEPTEMBER 1980

Compiled by

R. R. Ryan

ABSTRACT

This report presents the research and development programs pursued by the Chemistry-Nuclear Chemistry Division of the Los Alamos National Laboratory. Topics covered include advanced analytical methods, atmospheric chemistry and transport, biochemistry, biomedical research, element migration and fixation, inorganic chemistry, isotope separation and analysis, atomic and molecular collisions, molecular spectroscopy, muonic x rays, nuclear cosmochemistry, nuclear structure and reactions, radiochemical separations, theoretical chemistry, and unclassified weapons research.

I. ADVANCED ANALYTICAL METHODS

A. Thermally Induced Laser Pulsing: A New Technique: to Measure Weak Absorptions of Solutions[1] (D. A. Cremers and R. A. Keller)

Pulsed operation of a normally continuously operating dye laser is achieved by inserting into the laser cavity a cell containing a solution having a small absorptivity ($\alpha \lesssim 10^{-4}\text{cm}^{-1}$). When the output coupler mirror is tilted off-axis, the laser goes into pulsed operation (Fig. 1). The width of each pulse is strongly dependent on the absorptivity of the solution. The frequency of the pulsing depends only upon the degree of misalignment of the cavity and the thermal conductivity of the solvent, not upon the absorptivity of the solution. Such data can serve as a calibration curve to determine the concentration of a dye in an unknown solution (Fig. 2).

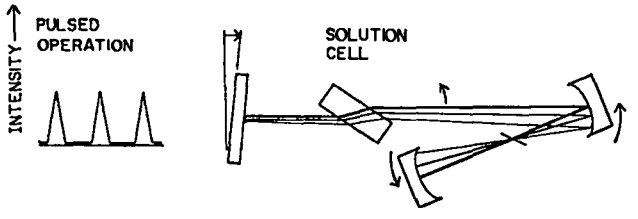

Fig. 1.
Thermally induced laser pulsing: A new technique to measure weak absorptions of solutions.

Experimentally and theoretically it is found that the energy absorbed during a pulse is a constant, independent of the solution absorptivity; that is,

$$(\alpha_o + \alpha_s)P\Delta t = \text{constant} \quad ,$$

where

α_o = solvent absorptivity ,
α_s = solute absorptivity ,
P = power of laser beam in cavity ,

and

Δt = pulse width.

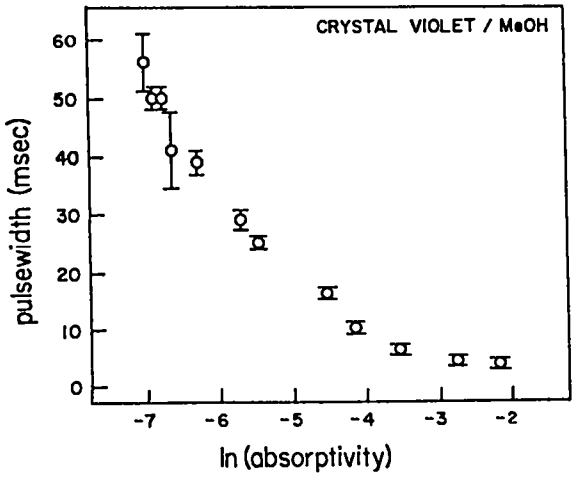

Fig. 2.
Dependence of pulse width on absorptivity of solutions. Experimentally $(\alpha_o + \alpha_s)\, P\, \Delta t = \text{constant}$.

Absorption of this amount of energy turns the laser off and causes the observed reciprocal relation between pulse width and absorptivity (Fig. 2).

Thermally induced laser pulsing can also be used to measure the absorptivity of a pure solvent as demonstrated in Fig. 3 for CCl_4. At low values of solute absorptivity, the pulse width remains constant, indicating $\alpha_o \gg \alpha_s$. The absorptivity of CCl_4 is found by fitting the equation, $(\alpha_o + \alpha_s)P\Delta t = \text{constant}$, to the data. The value we obtain is $\alpha_o = 9.2\times10^{-6}$ cm^{-1}, which agrees with a

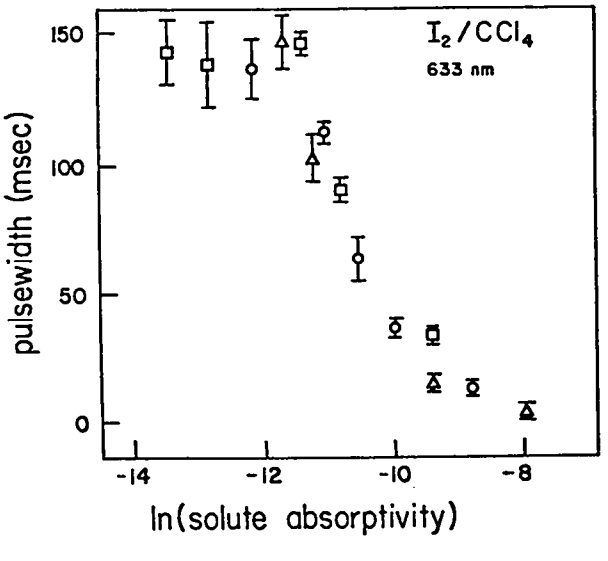

Fig. 3.
Determination of the absorptivity of a pure solvent: $\alpha_o(CCl_4) = 9.2 \times 10^{-6}$ cm^{-1}.

previously reported value of $\alpha_o < 10^{-5}$ cm^{-1}. This represents one of the smallest absorptivities yet measured for a solution.

B. Noise Considerations, Signal Magnitude, and Detection Limits in a Hollow Cathode Discharge by Optogalvanic Spectroscopy[2] (R. A. Keller and E. F. Zalewski*)

The optogalvanic effect is very sensitive for the detection of weak absorptions in a hollow cathode discharge, which leads to applications in spectroscopy and analytical determinations. It is therefore important to understand the limiting noise sources and the relationship between the magnitude of the impedance change and the number of photons absorbed.

Extensive measurements were made of the noise across a 25-kΩ ballast resistor in series with a hollow cathode discharge tube. Total noise was measured with a limited band-pass oscilloscope, and the frequency response of the noise was measured with a spectrum analyzer. Both measurements demonstrated that the noise was statistical in nature ($\sqrt{n}/n$ where n is the number of electrons moving in the circuit).

The magnitude of the laser-induced voltage change across the ballast resistor and the number of photons absorbed by the atomic species were simultaneously measured for uranium, sodium, europium, and zirconium in hollow cathode discharges. The results are summarized in Table I. The last column shows that the magnitude of the laser-induced impedance change per photon absorbed is essentially a constant. This ratio does not depend upon the ionization potential of the element, the mobility of the positive ion produced, the fill gas (neon or argon), or the current in the discharge tube. The numbers in the last column can be translated into an efficiency E $\sim10^{-3}$ (number of extra electrons produced per photon absorbed).

Knowledge of the impedance change per photon absorbed by the atomic system and the statistical nature of the circuit noise make it possible to calculate detection limits. For example, the calculated detection limit for uranium is 10^6 atoms/cm^3.

A mechanism that fits the data and appears to be quite plausible involves the use of the atomic system merely as a method of transferring laser energy into the electrons. In a hollow cathode discharge there is an equilibrium

*National Bureau of Standards, Washington, D. C.

TABLE I

RATIO OF THE LASER-INDUCED VOLTAGE CHANGE TO THE LASER POWER ABSORBED: U, Na, Eu, and Zr[a]

Element	I.P. (eV)	i (mA)	λ (Å)	I (mW)[b]	I_{abs} (mW)[c]	ΔV (mV)[d]	$\Delta V/I$ (mV/mW)[d,e]
U	6.1	24.9	5915.4	21.5	2.0	16	8.2 ± 2
U[f]	6.1	25.5	5915.4	26.5	2.7	33	12
Na	5.1	13.0	5895.9	0.277	0.09	0.956	11 ± 2
Na	5.1	13.0	5889.9	0.265	0.09	0.973	11 ± 2
Eu	5.7	15.6	6018.2	28.2	2.6	17.3	7 ± 1
Zr	6.8	30.6	6134.6	12	0.5	2.1	4 ± 1
Zr[g]	6.8	25.8	6134.6	10	0.5	3.2	6 ± 1

[a]With the exception of one Zr tube, the fill gas was neon (~5 torr); the ballast resistor was 26.9 kΩ.

[b]The laser was not single frequency, but its output consisted of three modes with an intermode separation ~1.5 GHz. Only the center mode, which contained about one-half of the intensity, overlapped the absorption band.

[c]Single pass absorption.

[d]The sign of ΔV depends upon whether ΔV is measured across the tube or the ballast resistor. The sign given here is for measurement across the ballast resistor.

[e]When error bars are given, two or three measurements were made. These values were reproducible from day to day.

[f]Different discharge tube.

[g]Ar fill gas (~5 torr).

established between the electron energy distribution and the atomic excitation distribution such that the electron temperature (T_e) and the electronic excitation temperature in the atom (T_a) are equal to the first approximation. This equilibrium occurs because of many elastic and superelastic collisions between the atomic system and the electrons. Laser irradiation is a small perturbation in this process. However, the numerous electron collisions prevent a significant change of the energy level population, and the energy supplied to the atomic system by the laser is filtered off to the electrons. This energy transfer distorts the electron energy distribution and creates an excess of electrons at an energy corresponding to that of the laser photons. The increased energy in the electrons results in a decrease in the impedance of the discharge. If the transit time of the electrons to the anode is long with respect to the electron-electron collision frequency, the excess energy is distributed among all the electrons, and the effective T_e increases. However, if an electron experiences few collisions on the way to the anode, the energy is not distributed among all the electrons, and the effective electron temperature does not change.

The efficiency measured here ($E \sim 10^{-3}$) compares quite well with fluorescence detection when one considers the quantum yield of fluorescence, the limited efficiency of collection of photons emitted over 4 π sr, and the conversion of collected photons into electrons. However, a big advantage of fluorescence is that the noise in the detection circuit is small in the absence of signal.

Previous workers have suggested that isotopically selective irradiation of a species in a gaseous discharge followed by cataphoresis is a possible method for isotope enrichment. If our mechanism is correct, irradiation of a particular species would not be a viable isotope enrichment scheme because it does not lead to preferential ionization of that species.

C. An Atlas of Uranium Emission Intensities in a Hollow Cathode Discharge[3] (B. A. Palmer, R. A. Keller, and R. Engleman, Jr.)

This atlas, a series of graphs depicting the spectrum of uranium and accompanied by tables of wave numbers, relative intensities, and assignments (see Fig. 4), provides an excellent source of information on the spectrum of uranium. Its wave-number accuracy makes this atlas useful for calibration of spectrographs, monochromators, and tunable lasers. The relative intensities of the spectral lines measured are accurate to ±8%, a result of the spectrometer used, and are useful in mapping the spectrum and determining relative oscillator strengths (gf values).

The spectral lines from our lamp, a commercially available hollow cathode discharge tube, are sharp and reproducible. The sharpness of the lines and the excellent wave-number accuracy of the Fourier transform spectrometer at Kitt Peak National Observatory result in a set of wave-number standards superior to any other with a comparable number of lines. The uranium emission spectrum has numerous very sharp lines widely distributed throughout the ir, visible, and uv spectral regions, resulting in a selection of strong lines in any given region of the spectrum.

This report provides an excellent source of information on the uranium spectrum. The tables list not only the wave numbers of the strong lines, but also the stage of ionization, energy levels, and J values for most of these transitions. This detailed knowledge is useful in working with uranium in plasmas, furnaces, or isotope enrichment. We are currently processing the data for similar compilations in the ir and uv spectral regions.

To check further the accuracy of the wave numbers reported in the uranium atlas and to provide several benchmarks of higher accuracy, we measured the wave numbers of 10 uranium lines.[4] The optogalvanic effect

LAMBDA(A)	SIGMA(CM-1)	INT	ION	E(EVEN)	J(E)	E(ODD)	J(O)
5919.6668	16888.1631	5.85	1	7828	4	23988	3
5919.2523	16889.3457	1.72	1	28566	7	11677	7
5915.3853	16900.3866	572.	1	16988	7	0	6
5915.8479	16901.3586	1.54					
5914.6882	16902.6878	5.19	1	26971	7	10069	7
5913.1387	16906.8303	3.48					
5911.9351	16910.1864	1.58	1	26979	8	10059	7
5911.5583	16911.3502	10.6	1	20712	8	3800	7
5911.0596	16912.7512	1.68					
5910.3573	16914.7638	3.77	1	24568	7	7645	8
5907.7532	16922.2196	2.73	1	38498	8	13567	7
5906.2320	16926.5781	1.76	1	24118	3	7191	2
5905.9744	16927.3161	1.59	1	23932	5	7805	6
5905.3383	16929.1624	1.62	1	27184	4	10254	5
5905.1222	16929.7598	3.17	1	16929	5	0	6
5902.6355	16935.8912	2.53	1	25793	3	8856	2
5902.4894	16937.3195	29.2	1	20885	3	3868	3
5902.1247	16938.3571	1.85	1	22788	4	5762	5
5901.9816	16939.9975	2.51	1	17559	5	628	5
5901.4551	16940.2789	1.11	1	31442	9	14501	8
5900.2237	16943.8144	2.63	1	14858	7	31882	8
5899.6828	16945.5978	2.88					
5898.7748	16947.9786	19.8	1	23197	7	6249	6

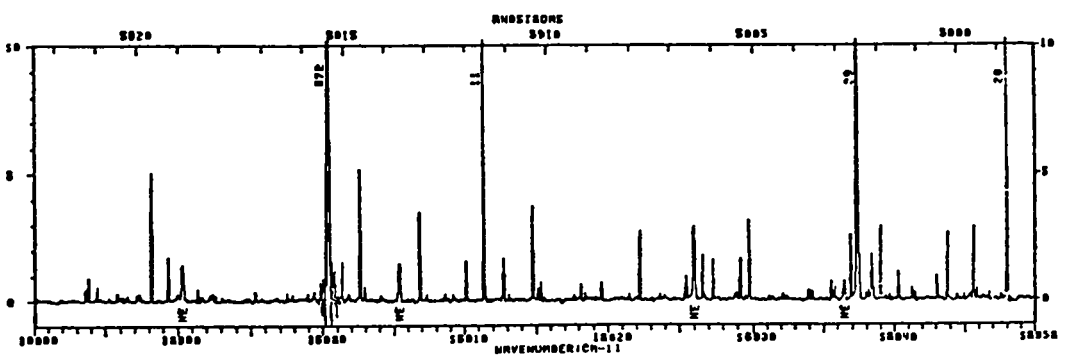

Fig. 4.
Sample page from uranium atlas.

was used to center a tunable dye laser in an optical transition, and the wave number of the dye laser was compared to the wave number of an iodine-stabilized He-Ne laser by using a lambda meter. The absolute wave numbers of these 10 lines were measured to an accuracy of ± 0.0006 cm^{-1}. The average difference between the atlas measurements and present work is $+0.0009$ cm^{-1}, which is well within the estimated accuracy of the atlas.

D. The Optogalvanic Effect as a Detector for Intracavity Atomic Absorption in a cw Dye Laser[5] (E. F. Zalewski,* R. A. Keller, and C. T. Apel)

The detection of trace optical absorptions can be enhanced several orders of magnitude by placing samples inside the cavity of a broadband laser. The absorption within the laser cavity inhibits lasing at wavelengths corresponding to the optical absorption. Sensitive detection of laser output reduction on the absorption line requires a spectrograph with resolution high enough to resolve the absorption line (5 m). Irradiation of gaseous discharges, at wavelengths corresponding to optical transitions of species present in the discharge, causes easily measurable changes in the impedance of the discharge (OGE). We have demonstrated the use of OGE as a simple, sensitive detector for intracavity absorption to replace the spectrograph.

An analytical flame is placed inside the cavity of a cw dye laser oscillating with a bandwidth ~4 Å centered on the sodium absorption (see Fig. 5a). The laser output is directed into a hollow cathode discharge containing sodium, producing an optogalvanic signal. As sodium is aspirated into the flame, the laser intensity at the sodium absorption wavelength and the OGE signal decrease. Note that the laser power remains constant. In Fig. 5b the normalized ΔOGE vs sodium is plotted. The S/N at 1 ppb is greater than 10, which is equivalent to the best reported sensitivity for sodium in flame atomic absorption spectroscopy. A comparison of the flame inside and outside the laser cavity is shown in Fig. 5c. The enhancement in sensitivity is ~4000. It is apparently possible to increase sensitivity at least 100 times by using a longer flame and operating the laser closer to threshold, where the enhancement factor should approach 10^5.

*National Bureau of Standards, Washington, D.C.

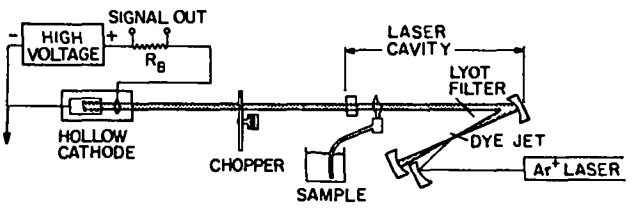

Fig. 5a.
OGE detector of intracavity absorption.

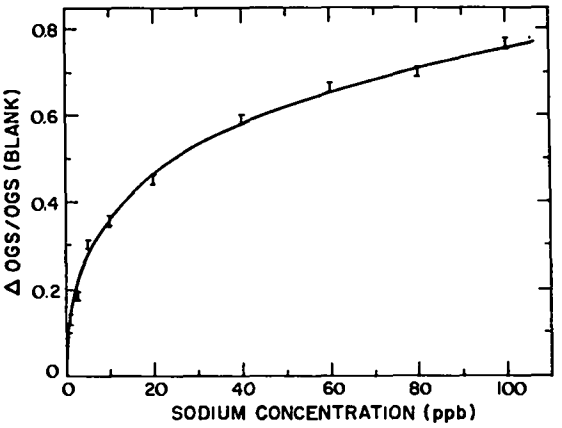

Fig. 5b.
Intracavity absorption of sodium atoms in a flame.

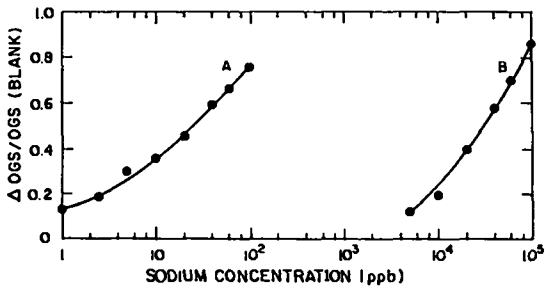

Fig. 5c.
Comparision of intracavity and extracavity absorption.

In essence this is the substitution of a one hundred dollar discharge tube for a several hundred thousand dollar spectrograph.

E. Ultrasensitive Analysis of Heavy Methane (M. M. Fowler, J. R. Tesmer, and J. B. Wilhelmy)

Heavy methanes ($^{12}CD_4$ and $^{13}CD_4$) are now being used as tracers for atmospheric dynamic studies. They

have several characteristics desirable for long-range atmospheric studies:

(1) In air there are essentially no contributions from species having mass 21. This suggests the possibility of using mass spectroscopic techniques for high-sensitivity studies.

(2) The heavy methanes are nonradioactive substances and thus free of the environmental objections associated with radioactive materials.

(3) The Los Alamos National Laboratory ICONs program provides reasonably large quantities of stable light isotopes, permitting inexpensive production of heavy methanes.

(4) Natural methane has an abundance of ~1.5 ppm in the atmosphere and thus should produce no unexpected chemical or physical effects to limit the usefulness of the tracers, as might occur from the introduction of nonstandard chemicals in a "carrier-free" state.

(5) Methane is believed to have a lifetime in the atmosphere of from 2-7 years. The heavy methanes will have even longer lifetimes because of isotopic effects, enhancing their usefulness for long-range global studies.

Current techniques for determining concentration of heavy methanes consist of chemically extracting methane from whole air samples and then looking for the mass-20 or -21 contribution by mass spectroscopy. Sensitivities as great as five parts in 10^{12} have been demonstrated for the methane fraction, resulting in a total sensitivity for mass-21 methane of $\sim 10^{-17}$ in the atmosphere. Although quite good, this is still an estimated two orders of magnitude greater than the anticipated natural background level. We are, therefore, attempting to develop a new technique to improve sensitivities for analytic detection.

The use of the vertical Van de Graaff facility at Los Alamos makes possible a double analysis technique consisting of reasonably high resolution mass analysis followed by molecular dissociation of the methane and unique detection of the electrostatic rigidities of the dissociated atoms (Fig. 6). A methane sample is introduced into a duoplasmatron ion source in the terminal of the accelerator, which is at a 6 to 8-MV positive potential. A magnet selects the positively charged mass-21 fraction and injects the ions into the accelerator. Following acceleration, the mass-21 fraction is again selected with an analyzing magnet having a resolution of $\sim 1/10^4$. This fraction then impinges on a 2 $\mu g/cm^2$ carbon foil, where the molecule is dissociated and the

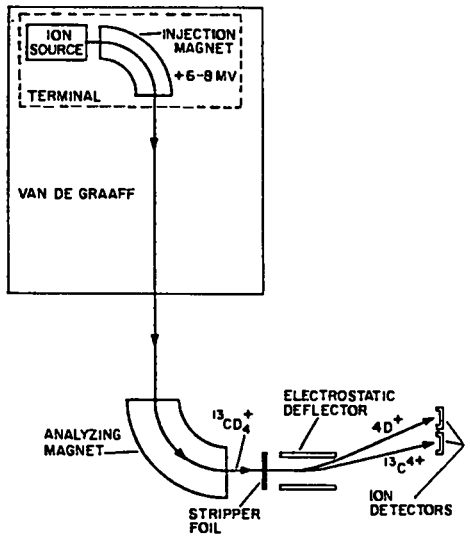

Fig. 6.
Schematic of proposed experimental configuration.

atomic constituents ionized. The ions enter an electrostatic deflector, which makes an energy/charge selection. The ions' paths are deflected and impinge upon solid-state detectors that record the energies. This double analysis should give a unique signal essentially free of background.

To date we have tested the most critical part of the proposal, that of ionizing the methane and extracting it with the injection magnet (Fig. 7). For the test, a small quantity of methane 20 ($^{12}CD_4$) was mixed with hydrogen carrier gas. The major extracted ions are

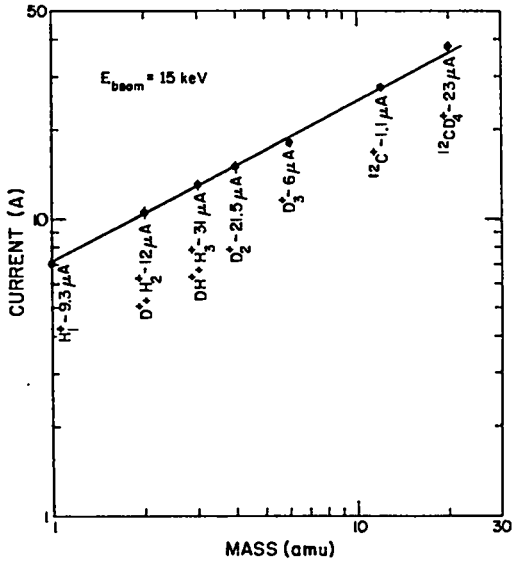

Fig. 7.
Mass of Ions observed from injection magnet as a function of electromagnet current for an extraction voltage of 15 KV.

shown along with their measured currents. The significant deuterium contamination is believed to be from recent deuterium runs in the source. Nevertheless the extracted methane was at a very high current and demonstrated the feasibility of the technique for use of a Van de Graaff facility for ultrasensitive molecular analysis.

Significant areas remaining for development include construction of the detection apparatus, adequate voltage regulation in the accelerator, determination of cross contamination between samples, and quantitative determination of the methane concentration.

II. ATMOSPHERIC CHEMISTRY AND TRANSPORT

A. The Heavy Methane Atmospheric Tracer Program (M. M. Fowler)

The large-scale development of energy sources such as coal or oil shale as alternatives to oil has heightened awareness of associated potential detrimental environmental effects. These effects will not be confined to the immediate areas containing the developing technology. There is a need for assessing the impact of related effluents not only nearby but also at a distance. Currently there are few numerical models that accurately estimate these impacts, and in complex environments there may be none.

An atmospheric tracer provides an alternative or complementary method for evaluating future or existing sites. This is not a novel tracer use, but current requirements are for applications at greater transport distances than previously encountered. Tracers can provide data to calibrate or fix the parametric variables of models, which can, in turn, provide more accurate predictions.

There are a number of additional areas where long-range atmospheric tracers are in demand, such as studies of chemical transformations in the atmosphere and verification of multidimensional transport and diffusion models relating to climatological studies. Although there is a recognized need for long-range atmospheric tracers, no current system is generally satisfactory. CNC Division of the Los Alamos National Laboratory is developing such a system.

An atmospheric tracer should be nontoxic and should not generate other environmental problems, which virtually eliminates radioactive tracers. It should also be sufficiently stable chemically in the atmosphere to allow completion of the anticipated applications, without being so long-lived that it contributes to the overall background. This problem plagues the traditional atmospheric tracer SF_6, which is now limited to transport distances of $\sim$100 km because of its anthropogenic background. Furthermore, there should be no extraneous sources of the tracer, so that tracer from other sources does not confuse the experiment in progress.

In addition to low tracer background, the tracer should be detectable at extremely low concentrations. Typically a tracer may be diluted with air a trillion fold, so that exceedingly small amounts of the tracer must be measurable. Of course as the distances increase, so do the difficulties with detection.

The tracer materials being studied by Group CNC-7 are methanes that are different in isotopic composition from normal methane. The two methanes of interest are $^{12}CD_4$ with a mass of 20 and $^{13}CD_4$ with a mass of 21, whereas normal methane, $^{12}CH_4$, has a mass of 16. The two fully deuterated methanes are unique in that they have no natural sources and no known large-scale industrial use, leading to the conclusion that there is virtually no background of these materials in the atmosphere. This assumption has been verified, and with our current analytical scheme we can say that the background for $^{13}CD_4$ is less than 1 part in 10^{18} parts of air by volume as an upper limit.

The employment of the heavy methanes is unique to Los Alamos because the CNC Division ICONs program provides highly enriched ^{13}C and depleted ^{12}C in reasonably large quantities and also provides for synthesis of $^{12}CD_4$ and $^{13}CD_4$.

Currently, the analytical scheme for these tracers involves the isolation of a methane fraction from a sample of atmospheric air followed by mass spectrometric analysis to determine the abundance of the tracer relative to normal methane. A tracer concentration of 1×10^{-18} in air by volume corresponds to a ratio of tracer to normal methane of $\sim 10^{-12}$, about the minimum measurable ratio for mass-21 methane in the mass spectrometer. The detection limit for mass-20 methane is $\sim$15 times poorer than for mass-21 methane, primarily because of background contributions from heavy water in the mass spectrometer. These measurements require $\sim$1 cm^3 of methane corresponding to 500-1000 ℓ of original air sample. In practice, it is not always possible to collect enough air to make the limiting measurement and, in these cases, the detection limit is higher. Typically, a 50-ℓ air sample will provide a

detection limit of ~10-20 times higher than the case for a sample of unlimited size.

During the past year a number of achievements related to this program have been realized.

(1) Methods for the preparation of absolute standards of CD_4 at low concentrations in CH_4 have been developed, and based on the standards prepared to date, the mass spectrometric measurements have a relative accuracy of a few percent for concentrations of $^{13}CD_4$ in CH_4 to less than 1 part in 10^9.

(2) The inlet system of the mass spectrometer has been redesigned to reduce the amount of methane required for analysis from 2 cm^3 to 1 cm^3. The analysis system has been improved so that the analysis of relatively large numbers of samples is now possible.

(3) Studies using the heavy methanes have been made of nocturnal drainage winds in a variety of locations with transport distances of up to 20 km.

(4) A new cryogenic sampler has been developed and tested in the field. A series of field experiments have tested new sampling methodology along with experiments to verify that the tracers are conserved to distances of up to 600 km (See Sec. II.B.)

(5) Finally, Los Alamos Groups CNC-11, CNC-7, and G-8 participated in the Atmospheric Studies in Complex Terrain (ASCOT), which took place in the geothermal power production area in northern California in September 1980. Much of next year will be spent in the analysis of samples and the interpretation of the resultant data.

B. A 600-km Atmospheric Tracer Field Test (M. M. Fowler)

A long-range application of the heavy methane tracer system has been carried out using both $^{12}CD_4$ and $^{13}CD_4$. This test had several objectives, including testing a newly developed cryogenic air sampler, testing a newly completed sample-handling apparatus, and demonstrating that the heavy methanes could be used to trace the path of air movement over distances up to 600 km and travel times of ~18 h.

This experiment was conceived and planned primarily by the Air Resources Laboratories (ARL) of the National Oceanic and Atmospheric Administration (NOAA) as a field demonostration of their new automated sampling system for their perfluorocarbon tracers. Los Alamos National Laboratory was invited to participate in this cooperative experiment. The use of the heavy methanes has been an important facet of this experiment, as there are no other long-range tracers against which to check the perfluorocarbon tracers.

The tracers were released over a period of 3 h at Norman, Oklahoma, during conditions (southerly wind) that were expected to give a transport trajectory in the desired direction but at a velocity somewhat greater than planned. The heavy methanes were premixed in an ~2:1 ratio ($^{12}CD_4$:$^{13}CD_4$) in a small cylinder. In this case the two methanes were to be compared with each other and with SF_6, which was also released at Norman, Oklahoma. The release consisted of 84 g of $^{13}CD_4$ and 153 g of $^{12}CD_4$, metered out at a constant rate over the 3-h period. In addition, 273 kg of SF_6 were released.

Sampling was carried out both on the surface and by aircraft at downwind distances of ~100 km and ~600 km (see Fig. 8). Sampling along the 100-km arc was at intervals of ~2.5° (~4.5 km) with a total of ~20 stations centered on the projected plume trajectory. Collections were made by using small pumps to inflate plastic bags over an 8-h period. The aircraft collections were made for periods of ~5 min over 21 km while the aircraft flew along the arc ~1 km above ground level. Heavy methane sampling at 600 km was made at six locations spaced at intervals of ~80 km, again centered on the predicted trajectory. Both cryogenically collected samples and bag samples were collected over 2-h periods at each site. A total of five sample pairs was collected at each site to give some sequential information. The aircraft sampling at 600 km was carried out at ~1.2 km above ground

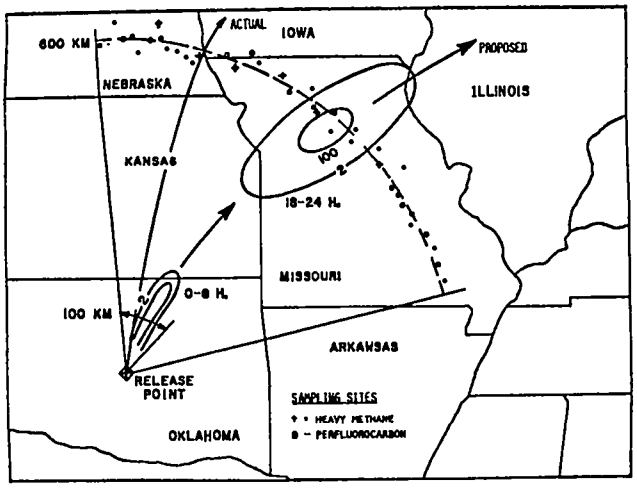

Fig. 8.
Experiment map (600 km). The arrows indicate a typcial plume trajectory, and the relative expected concentrations are indicated by contours.

level and each sample was collected over ~40 km of flight path. A total of 19 samples was collected in 2 passes along the 600-km arc.

At this time, about 3/4 of the samples have been analyzed and several observations can be made concerning the data.

(1) The cryogenic samplers developed by J. Frank and W. Shields worked well, and all of the samples desired were collected. These samples have been analyzed and have shown heavy methane tracer at two of the sites.
(2) The plume position and duration measured at 600 km agree qualitatively with similar measurements made using the perfluorocarbon tracers and agree with trajectory predictions.
(3) The amounts of SF_6 observed at both 100 and 600 km agree with those predicted from the heavy methane results. However, a factor of 2 uncertainty is associated with the SF_6 measurement at 600 km because of the small signal-to-noise ratio.
(4) The results from the aircraft samples collected at 100 km are in agreement with those collected on the ground.
(5) The new apparatus that transfers samples from bags to pressurized cylinders worked as desired and has been improved for use in the ASCOT experiments.
(6) Daily samples were also collected at four other sites: Argonne National Laboratory, National Bureau of Standards (Gaithersburg), AIRCO (New Jersey), and the Savannah River Plant. These samples have been analyzed and all sites except AIRCO provided samples with measurable amounts of $^{13}CD_4$. The arrival times of the tracer plume and the peak concentrations agree with model predictions. These results represent the detection and measurement of $^{13}CD_4$ at distances of nearly 2500 km from its release.

C. Project Airstream and Related Efforts in Atmospheric Chemical Measurements (E. J. Mroz)

1. Project Airstream. Project Airstream provides measurements of a number of stable and radioactive species (Table II) in the aerosol and gases that comprise the upper troposphere and lower stratosphere. A WB-57F aircraft especially equipped for high-altitude air sampling is flown for the Department of Energy (DOE) by the National Aeronautics and Space Administration (NASA) under the direction of the Johnson Space Center. Airstream missions are generally scheduled for April, July, and October. Figures 9 and 10 show the flight paths (altitude, latitude, longitude) flown on each mission. In addition, vertical profiles are flown at Anchorage, Alaska, Houston, Texas, and Panama City, Panama.

During fiscal year 1980, airstream missions 17, 18, and 19 were flown in October 1979, April 1980, and July 1980 as scheduled. Data obtained through Project Airstream are published in *Environmental Quarterly*, which is prepared by the DOE Environmental Measurements Laboratory.

TABLE II

CHEMICAL AND PHYSICAL MEASUREMENTS MADE ON THE WB-57F HIGH-ALTITUDE AIR-SAMPLING AIRCRAFT

Gases	Particles	Project
SF_6, N_2O, $^{14}CO_2$, CCl_4, CCl_3F, CCl_2F_2	$SO_4^=$, NO_3^-, NH_4^+, ^{7}Be, ^{90}Sr, ^{137}Cs, ^{144}Ce, ^{95}Zr, ^{239}Pu, ^{210}Pb	Airstream
H_2O, CO, O_3	Condensation Nuclei	CHAMP
Total Cl, Br, I	--	Total Halogen Exp
HT, HTO	--	Tritium Exp
--	Mass and size distribution, particle morphology, chemistry	QCM Exp

Fig. 9.
Airstream latitude coverage.

Concentration isopleths for ^{90}Sr during July 1978 are shown in Fig. 11. In its general features, the distribution of ^{90}Sr is typical of all species measured by Project Airstream. The contours generally follow the shape of the tropopause, and at any given altitude the concentration generally increases in the poleward direction. The region of maximum concentration is usually found in the higher latitudes. Figure 12 presents the stratosphere inventory for ^{90}Sr from 1963 to 1978. This figure is generally representative of all the fission products measured as part of Project Airstream. From these data the computed half-residence time for stratospheric air is about 10 months. Measurements of halocarbons, SF_6, and N_2O are being used to validate atmospheric circulation and photochemical models. Sulfate measurements have shown that volcanic events are important contributors to the stratospheric sulfate inventory.

2. Coordinated High-Altitude Measurement Project. The Coordinated High-Altitude Measurement Project (CHAMP) is a NASA-supported effort to augment the measurements made as part of Project Airstream (Table I) and to interpret jointly the data obtained from all of the on-board experiments discussed here. This project began in April 1980 when instrumentation arrived and plans for its installation on the WB-57F were formulated. Although the installation of the CHAMP instrumentation was not completed in time for the beginning of Airstream Mission 19 in July 1980, it was advanced enough to allow extensive flight testing of the

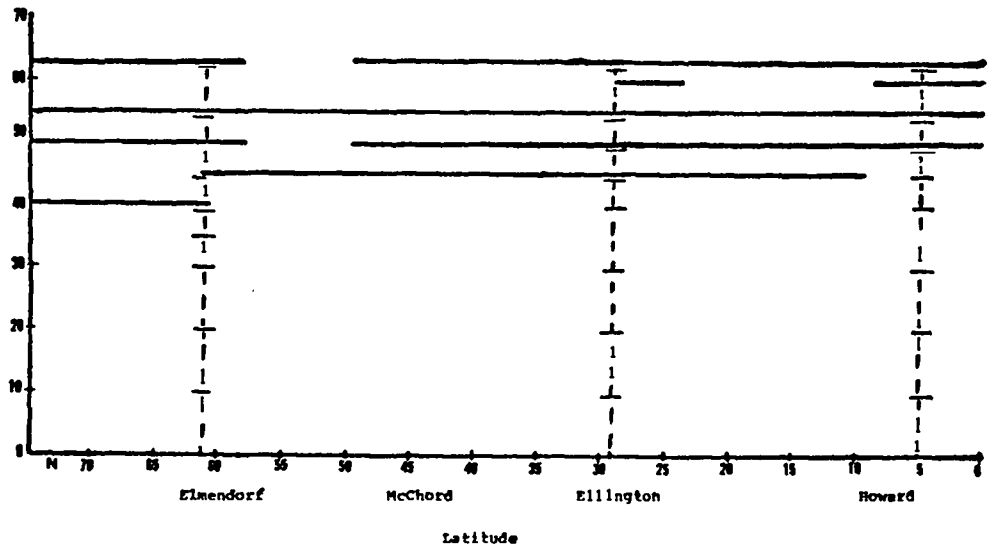

Fig. 10.
Airstream altitude coverage.

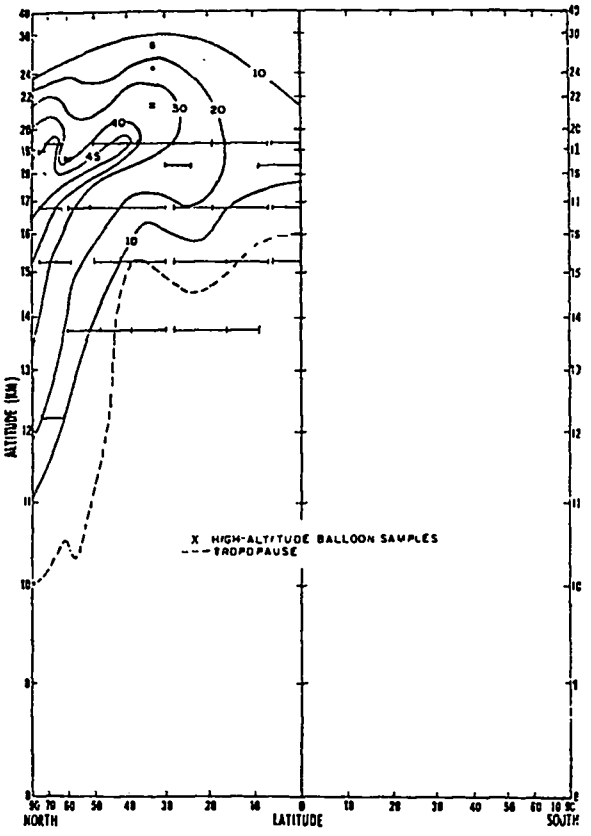

Fig. 11.
Concentration of ^{90}Sr in stratospheric air (pC1/100 SCM) July 1978.

CHAMP system. After Airstream Mission 19 was accomplished, the remainder of the installation work was completed. Design and construction were begun for a test stand to allow a more convenient means of maintaining, testing, and calibrating the CHAMP instruments. Development of data-processing procedures was also initiated.

3. Total Halogen Experiment. Under a cooperative agreement with the National Center for Atmospheric Research (NCAR), we are making measurements of the total chlorine, bromine, and iodine burdens in the upper troposphere and lower stratosphere. These measurements are crucial to understanding the role that compounds of these elements play in the destruction of ozone in the stratosphere.[6]

Initial results show a total chlorine concentration of ~3.0 ± 1.0 ppbv. This is in good agreement with estimates derived from summing the concentrations of the various halocarbon compounds known to be present in the stratosphere. A limited number of total bromine measurements exhibit a range of values between 7 and 40 pptv. Bromine has been shown to be a much more efficient catalyst for the destruction of ozone. However, the details of bromine chemistry in the stratosphere are still largely unknown. Total iodine values have been below our detection limit of ~3 pptv.

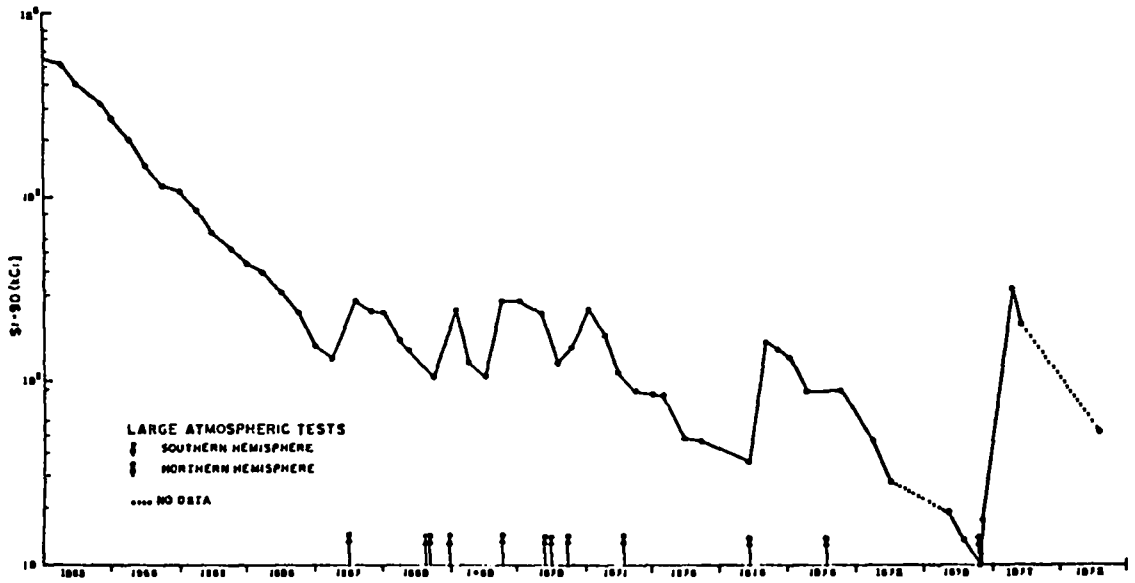

Fig. 12.
Stratospheric inventory of ^{90}Sr, northern hemisphere (kCl) 1963-1978.

4. Tritium Experiment. Under another cooperative agreement with the University of Miami Tritium Laboratory, we are assisting in measurements of HT and HTO. A comparison of tritium and ^{95}Zr data[7] has demonstrated that both are removed from the stratoshere at about the same rate. This implies that gravitational settling is an unimportant mechanism for the removal of small ($\sim$<1-μm-diam) particles from the lower stratosphere.

5. Quartz Crystal Microbalance Experiment. A quartz crystal microbalance (QCM) cascade impactor that was jointly developed by Group CNC-7 and a private consultant was installed on the WB-57F in July 1980. This instrument aerodynamically sizes particles and collects them on oscillating quartz crystals. The change in the frequency of the crystal is proportional to the mass of particles collected in each size fraction. The particles on each stage are then examined with an electron microscope aided by energy-dispersive x-ray analysis. The QCM provided data that aided in the identification of the plumes from Mt. St. Helens and Gareloi volcanoes.

6. Special Projects. The eruption of Mt. St. Helens on 18 May 1980 presented the community of atmospheric scientists with a unique opportunity to study the physics, chemistry, and climatological implications of a volcanic eruption plume. DOE elected to borrow two flights from Airstream Mission 19 in July 1980 to obtain measurements in the upper tropospheric and lower stratospheric plume of Mt. St. Helens. These two flights were flown on 20 and 21 May 1980. The plume passed over Kansas, Colorado, Wyoming, and northern New Mexico.

The results of these two flights together with the sulfate measurements made as part of Airstream Mission 19 in July and August 1980 were recently presented at a symposium in Washington, D.C.[8] The highlights of measurements made by the WB-57F are the following.

a. Sulfuric acid aerosol appeared in the stratospheric portions of the volcano plume very early—perhaps on the same day as the eruption and certainly within a few days.

b. Most, if not all, of the mass of volcanic ash injected into the stratosphere appears to have fallen out by August 1980. The remaining quantity of sulfuric acid aerosol in the stratosphere was about three times the pre-eruption levels. This represents ~0.2 to 0.5 × 10^9 kg of H_2SO_4 added to the stratosphere as a result of the Mt. St. Helens eruption.

c. Good agreement was found between satellite and WB-57F measurements of the total aeorsol burden in the stratosphere.

d. As a result of Airstream Mission 19 flights in the lower stratosphere over the Alaskan panhandle, we identified debris from the 8 August 1980 eruption of Gareloi volcano, located in the Aleutian Islands.

III. BIOCHEMISTRY

A. Carbon-13 Nuclear Magnetic Resonance Analysis of Metabolic Pathways for Glutamate Biosynthesis by *Microbacterium ammoniaphilum* (T. Walker, C. H. Han, V. Kollman, R. E. London, and N. A. Matwiyoff)

We have begun a major new research program directed toward the *in vivo* study of major metabolic pathways in microorganisms, the eventual goal being the efficient large-scale biosynthesis of isotopically labeled natural products. The initial focus is on the production of those labeled L-amino acids for which there is a need in human metabolic and nutritional studies and on the investigation of the structure and dynamics of enzymes enriched with labeled amino acids. Our general approach involves an attempt to produce ^{13}C and ^{15}N labels at specific sites in amino acids using strains of bacteria developed by the Japanese that "overproduce" specific amino acids.[9]

We have been highly successful with the organism *Microbacterium ammoniaphilum*, which produces L-glutamate in a 35-40% yield from glucose. So far, we have labeled glutamate starting with five different substrates: [^{15}N]ammonium sulphate, sodium [^{13}C]bicarbonate, [1-^{13}C]glucose, [1-^{13}C] and [2-^{13}C]acetic acid. These substrates yield [^{15}N]glutamate, [1-^{13}C] glutamate, [1,2,3,4-^{13}C]glutamate, [1,5-^{13}C] glutamate, and [2,3,4-^{13}C]glutamate, respectively. We have followed the incorporation of [1-^{13}C]glucose into glutamate, using ^{13}C nuclear magnetic resonance (NMR) to monitor the intermediates and to quantify the biosynthetic pathways involved. Preliminary ^{13}C NMR experiments have also been performed, using singly labeled acetate. The ^{13}C NMR experiments have not been done *in vivo* as described by other workers[10,11] because of the difficulty involved in maintaining the high level of aeration required by these cells. Instead, we have examined the growth media as a function of time, observing both a series of intermediates and the labeling pattern in the glutamate product.

The most interesting biosynthetic intermediate we have observed so far is trehalose, a nonreducing disaccharide produced from glucose. This sugar has previously been observed by ^{13}C NMR in yeast cells[10,12] and amoeba[13] although it is not known to occur in bacteria in the free state.[14] Trehalose is commonly found in yeasts, fungi, and insects, where it has been implicated as a structural component, as a reserve energy supply, and as an intermediate in glucose resorption or mobility.[14] Its presence in *Microbacterium ammoniaphilum* is a surprise, and the significance of its occurrence is under investigation.

The labeling patterns observed in the product glutamate can be used to predict which metabolic pathways are operative for the synthesis. The product derived from [1-^{13}C]glucose is approximately 40% enriched at C-2 and C-4, 10% at C-3, and 6% at C-1. This labeling pattern is extremely useful for ^{13}C NMR experiments because few ^{13}C-^{13}C multiplets are observed. The metabolic pathway to glutamate involves the conversion of [1-^{13}C]glucose to [3-^{13}C]phosphoenolpyruvate and [3-^{13}C]pyruvate by the Embden Myerhoff pathway followed by carboxylation to give [3-^{13}C]oxalacetate. The oxalacetate then reacts with [2-^{13}C]acetyl CoA to form citrate, which is then converted to α-ketoglutarate by the first third of the Krebs cycle and subsequently to glutamate. Carbon-2 of glutamate is labeled from the [3-^{13}C]oxalacetate, and C-4 is labeled from the [2-^{13}C]acetyl CoA. Carbon-3 is labeled by turns around the Krebs cycle or the glyoxalate cycle, whereas C-1 is labeled either from the HCO_3^- pool, which is labeled from C-1 of glucose by way of the pentose phosphate shunt or from turns around the Krebs cycle. Studies are currently in progress to quantify the various pathways involved.

Microbacterium ammoniaphilum will also grow on acetic acid, and specifically labeled [^{13}C]glutamate can be obtained from [1-^{13}C] and [2-^{13}C]acetic acid. Using [1-^{13}C]acetic acid, we obtain [1,5-^{13}C]glutamate, whereas from [2-^{13}C]acetic acid we obtain [2,3,4-^{13}C]glutamate. When grown on acetic acid, the glyoxalate pathway must be relatively more important, leading predominately to the triply labeled product rather than the doubly labeled product found when the cells were grown on glucose. Although we must still find optimum growth conditions for the cells on acetate, this may turn out to be the most economical way to label glutamate. In addition, we should be able to follow and quantify the pathways as was done for glucose.

B. Nuclear Magnetic Resonance Studies of an Isotopically Labeled Enzyme: Dihydrofolate Reductase

(R. E. London, R. L. Blakley,* J. P. Groff,* and L. Cocco*)

Nuclear magnetic resonance (NMR) is the only spectroscopic technique capable of probing individual nuclei of complex molecules or mixtures of molecules in solution. Biochemical applications of this method have generally been limited by the enormous complexity of these molecules, as well as by the inherent sensitivity limitations of the NMR technique. For the past several years, we have undertaken studies of specifically labeled enzymes that are biosynthesized on a medium containing isotopically labeled amino acids. This approach avoids both technique limitations because it is necessary to deal with only a particular subset of resonances corresponding to the labeled amino acid introduced into the enzyme and because the isotopic labeling greatly enhances the sensitivity of the experiment. For the past several years, our interest has focused on the bacterial enzyme dihydrofolate reductase. Interest in this enzyme derives in part from its clinical relevance—it is a target enzyme of drugs such as methotrexate, which is used in cancer chemotherapy, as well as drugs such as trimethoprim, which is used for treating a variety of infectious diseases. Labeling experiments have utilized [methyl-^{13}C]methionine, [guanido-^{13}C]arginine, and [γ-^{13}C]tryptophan.

During the past year, our particular emphasis has been on the effects of salts both on enzyme activity and on the NMR spectral parameters. This interest was sparked initially by the observation in studying the [γ-^{13}C]tryptophan labeled enzyme that one of the tryptophan residues gives rise to two resonances corresponding to a slow conformation equilibrium of the enzyme.[15] The intensity ratio R of the two tryptophan resonances was subsequently found to depend on the presence of KCl in the buffer. Up to this time, virtually all NMR studies of this enzyme had been done in high salt buffers because of the stabilizing effect of the salt. We have now found that in the absence of KCl the R value is low, that is, the enzyme exists in a nearly pure conformational state. Addition of KCl results in an increase in R to a limiting value of 35%. Another more recent result is that the R value is also altered by the addition of ligands such as the enzyme inhibitor methotrexate. Saturation of the enzyme with methotrexate in the absence (or presence) of salt results in a limiting R value close to the 35% figure.

*University of Iowa School of Medicine.

We have recently carried out studies of the effects of KCl on the [methyl-^{13}C]methionine and [guanidine-^{13}C]arginine labeled enzymes as well. In these cases, the limited resolution of the resonances restricts conclusions about the interaction. It was observed, however, that some of the resonances shift slightly more than others in response to salt, probably reflecting a generalized effect on molecular conformation. In parallel with the NMR investigations, we have studied the effect of various salts on enzyme activity, and we found that most salts activate the enzyme at low concentrations (~0.3 M) and inhibit the enzyme at higher concentrations.

A series of NMR studies dealing with the effects of the inhibitor trimethoprim and various analogs was also undertaken. Trimethoprin has proved one of the most interesting ligands in studies of the [methyl-^{13}C]methionine labeled enzyme, because very large downfield chemical shifts are observed. Of interest also is the different behavior of the [γ-^{13}C]tryptophan labeled enzyme resulting from trimethoprim compared with the structurally related analog pyrimethamine. We hope to deduce a more complete description of the interaction of these inhibitors with the enzyme on the basis of these chemical shifts.

C. Development of a Data Base for Carbon-13 Enriched Molecules (R. E. London)

The design of sophisticated biological nuclear magnetic resonance (NMR) experiments involving isotopic labeling requires a data base, which includes such parameters as relaxation behavior, coupling constants, ^{13}C assignments, etc. We have collected and published this data for such systems as carbohydrates and amino acids. Several studies have been carried out during the past year.

The extraction of coupling constants from ^{13}C enriched molecules is complicated by the presence of a distribution of isotopic isomers (for biosynthesized molecules), as well as by the possibility of high-order effects.[16-18] Although the latter possibility has generally received little attention for ^{13}C because of the large range of chemical shifts, we have noted a surprising number of such effects in many proton decoupled ^{13}C spectra of ^{13}C enriched molecules, as well as in the proton coupled ^{13}C spectra of singly enriched or unenriched molecules. Additional complications arise because some of the isotopic isomers present in solution may exhibit high-order effects whereas others may not. Our recent studies[19] have focused on the behavior of those weakly coupled ^{13}C spins which appear to be strongly coupled. As in the case of virtual coupled spins which are weakly coupled while exhibiting high order spectra, they cannot necessarily be considered first order. Spectral simulation indicates that this deceptive appearance is a consequence of the presence of unresolved splittings which, in turn, arise from strong coupling interactions elsewhere in the spectrum. Thus, even a moderately strong interaction, $J/\Delta\nu \sim 1/4$, can significantly perturb the spectra of many of the weakly coupled spins. The conditions under which such effects may be anticipated have been evaluated, based on the formalism developed by Pople and Schaefer[20] for a system containing only a single strong coupling interaction. The observation of spectral asymmetry for a weakly coupled spin can be used to draw several general conclusions about the spin system.

A second effort has involved the assignment of the ^{13}C resonances of the amino acid L-tryptophan based on ^{13}C labeling.[21] Isotopic enrichment constitutes the most reliable basis for making NMR assignments. An optimal labeling strategy depends on the relative ease of synthesis of the isotopically labeled species and the information content of the experiment. Carbon-13 enrichment is particularly favorable on the second basis because the many long-range couplings provide a basis for assigning remote nuclei if reasonable expectations exist for the coupling patterns. In this study, the $^{n}J_{CC}$ scalar coupling constants and chemical shift data have been used to assign the tryptophan ^{13}C resonances. The data have been supplemented with a Finite Perturbation Theory Self-Consistent Field Molecular Orbital calculation for comparison of the observed and predicted carbon-carbon couplings.

Several of our previous studies of ^{13}C labeled amino acids suggested a correlation between the carboxyl carbon shifts and the titration of the carboxyl group. A recent systematic study of this effect[22] demonstrated that a rough correlation does indeed exist between the carboxyl pK value and the total shift resulting from deprotonation of the carboxyl group. Generally, a plot of the shift in ppm vs pK leads to a curve with a slope close to 1.0. We expect this behavior to be valid only for carboxyl carbons in an aqueous environment. The titration behavior of carboxymethyl cyanocobalamin[23] indicates a dramatic deviation from this predicted behavior, presumably reflecting involvement of the carboxyl group in an intramolecular hydrogen bond. The observed

correlation may prove useful in characterizing the environment of carboxyl side chains in proteins.

IV. BIOMEDICAL RESEARCH

A. Radioisotopes

1. Bromine-77 Labeled Steroids for Detection of Hormone Associated Tumors (D. S. Wilbur). Radiobrominated steroids have potential applications for both early diagnosis of hormone-associated tumors and *in vivo* determination of hormone receptor content in certain tumors, the latter being important in the choice of therapy to be used. However, there are some formidable problems that must be addressed before these potential applications can be realized.[24] For instance, it is very important that the radiolabeled steroids have high specific activities, because there are so few receptor sites (fmol/mg tissue) available that essentially all of the steroid introduced needs to be radiolabeled. It is equally important that the radiolabeled product should retain its radiobromine both *in vitro* and *in vivo*.

Initial studies of radiobrominated steroids have been conducted with phenolic A-ring steroids (estrogens) because the brominations are relatively easily accomplished and the bromine should be less labile on the aromatic nucleus than it would be at other positions in the steroid molecules. Prior to radiobromination, methods of brominating the phenolic ring of estradiol *I* with stable bromine were investigated.[25] Although there were some previously reported methods of A-ring brominations,[26-28] none of the investigations described the product ratios obtained for the expected ortho regioisomers *II* and *III* and the dibromo compound *IV*. Bromination of the phenolic A-ring of estradiol was accomplished using a variety of brominating reagents and solvents. Direct brominations were carried out with bromine, N-bromosuccinimide (NBS), N-bromoacetamide (NBA), pyridinium bromide per bromide (PBPB), iodine monobromide, and a mixture of N-chlorosuccinimide (NCS) and bromide. Organometallic-assisted brominations were attempted with iron dust, mercuric acetate, and thallium trifluoroacetate. The results of these reactions are shown in Table III. The product ratios were determined by high-performance liquid chromatography (HPLC) on a silica (μ-porasil) column, eluting with a 100:1 mixture of chloroform and acetonitrile and using uv absorbance for detection.

The electrophilic brominating mixture of NCS/Br^- was chosen for the actual radiobrominations because the ^{77}Br used in the radiobrominations was in the bromide form when received.[29] Both estradiol *I* and 17α-ethynylestradiol *V* were radiobrominated.[30] The radiobrominated components in these reactions were separated by HPLC using a reverse-phase column, eluting with a 1:1 mixture of acetonitrile and water. Radiobrominations of *I* and *V* yielded mixtures of ortho isomers in roughly a 1:2 ratio for *II:III* and *VI:VIII*, respectively. All of the ortho isomers were found to be quite stable *in vitro*. Unfortunately, the ortho radiobrominated isomers accounted for only 50% of the activity injected into the HPLC. The largest amount of activity was found to be associated with an unstable species whose exact nature is not presently known.

Radiobrominations using the high specific activity ^{77}Br yielded specific activity ranges of 600-1200 Ci/mmol for the 4-bromo isomers *III* and *VII*. Investigation of the *in vivo* stability and biodistribution of these compounds will be conducted in the future. Studies are also planned for testing these compounds in rats containing estrogen-positive and estrogen-negative tumors. These studies will be conducted at the University of New Mexico Cancer Research and Treatment Center in collaboration with Dr. Fred Mettler.

The studies of radiobrominated steroids will broaden into radiolabeling in other positions in the steroid nucleus in the future but will continue to emphasize synthesizing radiolabeled steroids with high specific activities.

2. Radiohalogenating Fatty Acids in the Omega Position (D. S. Wilbur). The rapid metabolic turnover of fatty acids in myocardial tissue[31] makes it possible to use radiolabeled long chain carboxylic acids to study the regional distribution of myocardial perfusion. Investigations of radiolabeled fatty acids have shown that the best results are obtained when the radiolabel is in the terminal* (ω) position[32] rather than within the carbon chain[33] or adjacent (α) to the carboxylic acid function.[34] Labeling with radiohalogens in the ω position has been accomplished by halogen exchange[32] and by modification of the fatty acid to contain a terminal phenyl substituent,[35] which was radiolabeled electrophilically. However, these methods are limited by availability of appropriate starting materials.

*Terminal carbon refers to the carbon that is farthest removed from the carboxylic acid functionality.

TABLE III

BROMINATED ESTRADIOL PRODUCT RATIOS

A-Ring Brominated Products

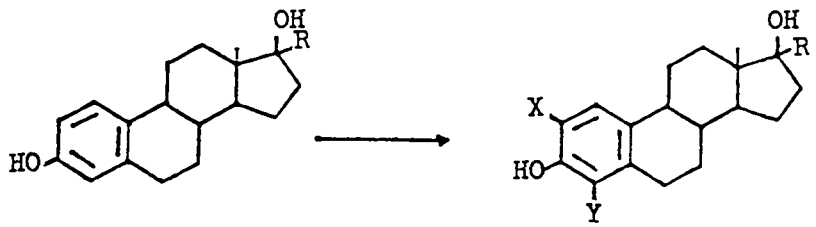

I:	R=H	V.	R=—C≡CH
II:	R=H; X=Br; Y=H	VI:	R=—C≡CH; X=Br,Y=H
III:	R=H, X=H; Y=Br	VII:	R=—C≡H, X=H; Y=Br
IV:	R=H; X=Br; Y=Br		

Reagents/Solvent	No. Equivalents	% II (2-Bromo E_2)	% III (4-Bromo E_2)	% IV (2.4-Dibromo E_2)	% Unidentified (one or more species)
Br_2/HOAc	0.5	41	59	trace	---
	1.0	40	51	9	---
	2.0	4	4	45	47
NBS/ETOH	0.5	24	67	9	---
	1.0	23	69	8	---
	2.2	---	trace	100	---
NBA/ETOH	0.5	29	64	trace	7
	1.0	25	69	6	---
	2.2	3	8	87	2
PBPB/HOAc	1.0	54	46	trace	---
PBPB/THF	1.0	42	51	7	---
PBPB/ETOH	1.0	28	69	3	---
IBr/ETOH	1.0	undefined	13	undefined	87
Fe(dust)/Br_2/HOAc	1.0/1.0	48	52	---	---
[a]$Hg(OAc)_2/Br_2$/HOAc	1.0/1.0	5	20	25	50
[a]$TI(TFA)_3/Br_2/CH_3CN$	1.0/1.0	23	47	12	8
NCS/Br/ETOH	1.0/1.0	25	61	13	---

[a]Values taken at ~50% reaction. Continuation of reaction yielded mostly unidentifiable components.

A synthetic reagent that may have application to labeling fatty acids in the ω position is Schwartz's reagent $(Cp)_2Zr(H)Cl$, which adds readily to double bonds in a process of hydrozirconation.[36] The initial hydrozirconation product is not observed; instead, the product obtained is the one that has the zirconium metal attached to the least hindered carbon atom (reaction 1). Thus, it may be possible to hydrozirconate unsaturated fatty acids and obtain the product that has the zirconium attached to the least hindered carbon in the carboxylic acid chain, the ω carbon. The loss of the unsaturation in fatty acids does not affect the myocardial uptake.[32] Once the zirconium-carbon bond is formed, it can be readily cleaved by electrophilic halogens (reaction 2). The

zirconium-carbon bond may also be cleaved by aluminum reagents,[37] permitting further synthetic transformations to be accessible via this route.

Because Schwartz's reagent is a strong reducing agent, it is not compatible with carboxylic functionalities. Therefore, the first attempted hydrozirconations were on the methyl ester of oleic acid (reaction 3). Although a reaction did occur, it was with the ester portion of the molecule and not with the double bond. Since the zirconium reagent is effectively blocked by steric hindrance, the very large trimethylsilyl and tert-butyldimethylsilyl esters of oleic acid were synthesized and reacted. These esters were also reduced. Two functionalities that are not affected by hydrozirconation are bulky ethers (e.g., tert-butyl ethers) and oxazolines.*

To utilize ether functions would ultimately require that these groups be converted to carboxylic acids, a transformation that requires strong oxidizing conditions. Such a synthetic path would offset the advantages gained by hydrozirconation.

Meyers[38] has shown that aromatic carboxylic acids may be converted to oxazolines readily and that the oxazolines can be easily removed to yield the starting acids. Unfortunately, all attempts to convert the carboxylic acid in oleic acid to an oxazoline yielded only the amide (reaction 4). Attempts to ring close the amide under dehydrating conditions (e.g., conc H_2SO_4, $SOCl_2$) were unsuccessful.

Research is continuing with further attempts to prepare the oxazoline of oleic acid as well as to explore other ester functions that may not be cleaved under the highly reducing conditions.

*This information was furnished by J. Schwartz, Princeton University.

3. Isotopic Exchange Procedures for Labeling Radiopharmaceuticals with Short-Lived Isotopes (P. M. Wanek). High yield labeling of pharmaceuticals with short-lived isotopes is difficult due to decay losses that result from transport, labeling chemistry, and quality assurance testing. One method to reduce such losses is the development of a biomedical radioisotope generator and rapid labeling chemistries. In the absence of a suitable generator system, the availability of labeling "cold kits" would greatly minimize decay losses. The term "cold kit" means that all the stable reagents required in the labeling chemistry are prepackaged as a sterile, pyrogen-free unit. When the radiopharmaceutical is needed, the sterilized radioisotope is purchased and the radiopharmaceutical manufactured in accordance with a well-established procedure. Radioiodination cold kits have been under development for some time in our laboratory in anticipation of the widespread availability of ^{123}I.

Among the numerous radioisotopes of iodine, ^{123}I is the most suitable for use in humans. The absence of beta particle emission together with the relatively short half-life (13.3 h) result in low radiation dose to the patient, and its major (86%) gamma photon of 159 keV is in the optimum energy range of the Anger camera.[39]

Previously reported methods for radioiodinating rose bengal, a hepatobiliary diagnostic agent, indicated that iodine exchange occurred via radioidine ($^*I_2$) at elevated temperatures.[40-42] We studied this reaction as a function of time, solution pH, solvent, reactant concentrations,

(1) $CH_3(CH_2)_nCH = CH(CH_2)_nCH_3 \xrightarrow{(Cp)_2Zr(H)Cl} CH_3(CH_2)_{2n+2}CH_2\text{-}Zr(Cp)_2Cl$

(2) $CH_3(CH_2)_yCH_2\text{-}Zr(Cp)_2Cl \xrightarrow{X_2 \text{ or } X^+} CH_3(CH_2)_yCH_2\text{-}X$

(3) $CH_3(CH_2)_7CH = CH(CH_2)_7CO_2CH_3 \xrightarrow{(Cp)_2Zr(H)Cl}$ Mixture of products - all still contain double bonds

(4) $CH_3(CH_2)_7CH = CH(CH_2)_7CO_2H \xrightarrow{HOCH_2C(CH_3)_2NH_2} CH_3(CH_2)_7CH = CH(CH_2)_7CONH\text{-}C(CH_3)_2CH_2OH$

(5) $CH_3(CH_2)_7CH = CH(CH_2)_7CONH\text{-}C(CH_3)_2CH_2OH \xrightarrow[\text{or } SOCl_2]{H_2SO_4} CH_3(CH_2)_7CH = CH(CH_2)_7C$ 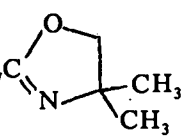

and temperature. The results demonstrated that 93 to 97% exchange of radioiodine could be achieved in 15 min at room temperature, and that the final product met the limit of ≤10% free $*I^-$ established by the U. S. Pharmacopeia.[43] An impurity found in the rose bengal starting material reduced the overall labeling yield of the rose bengal product. The optimum reaction conditions include purified rose bengal, a HCl-ethanol solvent maintained at a pH of <2 (1. O M HCl and ethanol, 1:11 v/v), KIO_3 (0.08 mg/mg of rose bengal) to oxidize $*I^-$ to $*I_2$, and reductant-free radioactive iodide solution (Fig. 13). The radiochemical purity of the labeled rose bengal was established using ascending paper radiochromatography, molecular sieve separation, uv spectroscopy, and chemical precipitation. Biologic confirmation of the movement of the labeled product through the hepatobiliary system was obtained in a rhesus monkey.

Another agent studied in our laboratory was radioiodinated o-iodohippuric acid (OIH), which is a well-established agent for diagnosing kidney dysfunction. Published reports[44-46] detail methods for exchange labeling of OIH using $*I^-$, *ICl, or $*I_2$ in several solvents and under varying reaction conditions. Major disadvantages

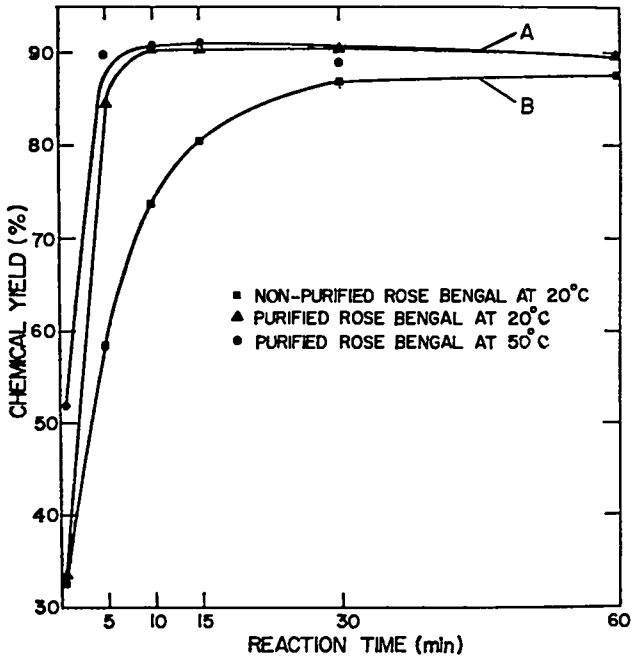

Fig. 13.
Chemical yield of ^{125}I rose bengal as a function of time. Curve A is the average yield of 3 determinations of 20°C and 3 determinations at 50°C using purified rose bengal. Curve B shows the average yield of 3 determinations at 20°C using non-purified rose bengal.

with these procedures include chemical breakdown of the OIH, low labeling yields, and nonadaptability to cold kit preparation.

Depending on the chemical supplier and the age of the sample, varying amounts of o-iodobenzoic acid (OIB) were found as an impurity in the OIH starting material. This impurity was more efficiently exchange labeled than OIH, and its presence at the start of the reaction substantially reduced the yield of labeled OIH. Thus, purification of the initial OIH is required.

The labeling procedure developed in our laboratory consists of placing 5 mg of purified OIH in a stoppered and crimp-sealed 10-cc serum vial and adding 0.3 mℓ of reductant-free Na*I (200-600 μCi) via syringe through the rubber septum. The mixture is autoclaved for 15 min, cooled to room temperature, diluted with 5.0 mℓ of sterile isotonic phosphate buffer solution, and is then ready for injection. This procedure consistently yields a product in which 99% of the radioiodine is attached to the OIH, while the other 1% is on the OIB. Confirmation tests of these results included ir spectroscopy, high performance liquid chromatography/uv detection, ascending paper radiochromatography, and melting point determinations. *In vivo* tests in a rhesus monkey demonstrated the movement of the labeled OIH through the renal system as expected.

Both labeling systems described here clearly demonstrate that rapid radioiodination labeling procedures that are adaptable to cold-kit preparations can be developed. These results have been made available to interested radiopharmaceutical firms for commercial development.

4. Strontium-82 and Rubidium-82 Biomedical Shipments in FY-1980 (J. W. Barnes, G. E. Bentley, T. P. DeBusk, M. A. Ott, F. H. Seurer, P. M. Grant, and H. A. O'Brien, Jr.). The ^{82}Sr-^{82}Rb generator system is of potential utility in diagnostic nuclear medicine for cardiovascular studies in conjunction with a high-resolution positron scintigraph device.[47,48] Noninvasive perfusion studies of the myocardium, cerebrum, and kidneys now appear to be the applications with the greatest promise, and Los Alamos National Laboratory has been producing and supplying ^{82}Sr to qualified medical investigators since 1978.

The activity is synthesized by irradiating metallic molybdenum targets with high-intensity medium-energy protons in the Isotope Production Facility at Los Alamos Meson Physics Facility.[49] Spallogenic ^{82}Sr is recovered and decontaminated by a hot-cell radiochemical procedure,[50] and shipments of typically ≲200

mCi are made to extramural researchers for animal and human studies with ^{82}Rb.

Before FY-1980, 27 different shipments of a total of 1.3 Ci of ^{82}Sr were delivered to 6 medical institutions. The shipments made during FY-1980 are summarized in Table IV.

5. Bromine-77 Biomedical Shipments in FY-1980 (J. W. Barnes, G. E. Bentley, T. P. DeBusk, M. A. Ott, F. H. Seurer, P. M. Grant, and H. A. O'Brien, Jr.). Use of ^{77}Br in nuclear medicine for pharmaceutical and protein labeling has been increasing in recent years.[51-53] In addition to its direct applications in compound labeling, ^{77}Br is also potentially useful indirectly as the generator of its ultrashort-lived ^{77m}Se daughter.[54,55]

The activity is synthesized by irradiating metallic molybdenum targets with high-intensity, medium-energy protons in the Isotope Production Facility at Los Alamos Meson Physics Facility.[56] Spallogenic ^{77}Br is recovered and decontaminated by a hot-cell radiochemical procedure[57] and shipments of typically $\lesssim$200 mCi are made to extramural and in-house researchers for labeling and biodistribution studies of diverse diagnostic agents.

Before FY-1980, 29 different shipments of a total of 2.2 Ci of ^{77}Br were delivered to 4 medical institutions. The shipments made during FY-1980 are summarized in Table V.

B. The National Stable Isotopes Resource (N. Matwiyoff)

The national stable isotopes resource (SIR) is operated as part of the ICONs program, named for the isotopes of carbon (^{12}C, ^{13}C), oxygen (^{16}O, ^{17}O, ^{18}O), and nitrogen (^{14}N, ^{15}N). The program encompasses the production of large quantities of the separated isotopes by the low-temperature distillation of CO and NO; the development of efficient synthetic methods for the incorporation of the isotopes into complex molecules; the improvement of techniques, especially nuclear magnetic resonance (NMR) and mass spectroscopy, for the analysis of isotopically labeled compounds; and participation with extramural investigators in cooperative research and development programs to develop the utility of stable isotopes in the biosciences and in environmental studies. The focus of the SIR, a joint effort of Groups CNC-4 and LS-5, is on developing uses of stable isotopes in the biosciences by

- Producing and providing enough separated ^{13}C, ^{15}N, and oxygen to support the program;
- Synthesizing labeled compounds for accredited investigators when those compounds are not readily available from commercial or other sources at acceptable costs;
- Developing an active program of research collaboration with investigators in the biosciences

TABLE IV

^{82}Sr SHIPMENTS IN FY-1980

Institution	Number of Shipments	Total Activity (mCi)
E. R. Squibb & Sons	4	1700
Hammersmith Hospital, London, England	4	680
Donner Laboratory, Berkeley	3	580
National Institutes of Health, Bethesda	2	300
Massachusetts General Hospital, Boston	2	240
Mt. Sinai Medical Center, New York	1	99
Johns Hopkins Hospital, Baltimore	1	50
VA Hospital, Madison, Wisconsin	1	25
Oak Ridge National Laboratory	1	2.4
Total	19	3700

TABLE V

^{77}Br SHIPMENTS IN FY-1980

Institution	Number of Shipments	Total Activity (mCi)
George Washington University Medical Center, Washington, D.C.	9	830
Los Alamos National Laboratory	8	760
Washington University, St. Louis	7	730
Kansas University Medical Center, Kansas City	8	450
Johns Hopkins Hospital, Baltimore	1	100
University of Massachusetts, Amherst	5	62
University of California, Davis	1	5
Total	39	2900

community, providing, as necessary, isotope labeled compounds and analysis and data interpretation with NMR and mass spectrometry;

- Advising and assisting investigators using isotopes of carbon, oxygen, and nitrogen;
- Hosting visiting scientists for training in use of stable isotopes and encouraging exchanges of talks, short courses, and extended research opportunities;
- Collaborating with other resources in synthesis and mass spectrometric and NMR analyses to speed development of isotope methodology; and
- Performing core research designed to keep the resource at a state-of-the art level.

Highlights of several projects supported by the SIR during the past year are described below.

1. Diagnosis of Fat Malabsorption by Breath Analysis of $^{13}Co_2$ after Oral Administration of ^{13}C Triolein. The fecal test for fat malabsorption in small children frequently requires patient restraint for 3 days to accomplish accurate stool collection. Expensive hospitalization may be required even when the patient is able to cooperate and is a hardship to children and parents. Using ^{13}C labeled fats supplied by the national SIR at the Los Alamos National Laboratory, J. B. Watkins, M.D., Director, Division of Gastroenterology and Clinical Nutrition, Children's Hospital of Philadelphia, Philadelphia, Pennsylvania; A. F. Hofman, University of California, San Diego, California; and P. D. Klein, Children's Nutrition Research Center, Texas Children's Hospital, Houston, Texas, have developed a rapid, convenient, noninvasive test for fat malabsorption based on the oral administration of the labeled fat followed by measurements of its oxidation to $^{13}CO_2$, which rapidly appears in the breath. The fats used in the test are the triglycerides, trioctanoin and triolein, labeled with ^{13}C in the carboxyl carbons of the fatty acid portion of the glycerides. When these are digested, absorbed, and metabolized, the CO_2 in the breath of the subject is also labeled with ^{13}C. If the fat is poorly digested and absorbed, most of it passes into the stool, and the breath CO_2 of the patient with malabsorption is only slightly and slowly labeled with ^{13}C. Watkins, Hofman, and Klein have shown that this simple breath test compares favorably with the fecal fat test in children with malabsorption caused by pancreatic insufficiency, and it is undergoing further clinical study by Dr. Michael Gelfand at the Children's Hospital Medical Center of the University of Cincinnati.

2. Reaction of the Chemotherapeutic Agent Cis-Platinum with Vitamin B_{12}. Scientists at the national SIR of the Los Alamos National Laboratory are using NMR spectroscopy together with specific labeling with the heavy nonradioactive isotope ^{13}C to study the structures and reactions of biologically active molecules. A noteworthy study accomplished recently was the investigation of the interaction of *cis*-diamine platinum(II) complexes with the vitamin B_{12} derivatives, adenosylcobalamin and alkylcobalamins. The antitumor

properties of *cis*-diamine dichloroplatinum(II) have been well documented, and at present this platinum(II) complex alone or in combination with other drugs is used extensively in the treatment of gynecological tumors. However, in some cases, the treatment produces severe side effects, such as hematological and renal toxicity and sometimes neurotoxicity. The peripheral neuropathy sometimes observed caught our attention because similar neurological symptons are associated with vitamin B_{12} deficiency. Using ^{13}C NMR spectroscopy and ^{13}C labeled cobalamins, we were able to show that *cis*-diamine platinum(II) does indeed react with the cobalamins by detaching the 5,6-dimethylbenzimidazole moiety from the cobalt(III) of the corrin. This suggests that patients treated with platinum(II) complexes can develop a vitamin B_{12} deficiency because the reaction between the corrinoid and the chemotherapeutic agent causes inactivation of the corrinoid coenzymes.

3. An Automated Mass Spectrometer for Nitrogen Isotope Analysis (B. B. McInteer). The design and construction of a unique spectrometer system capable of the rapid analysis of the ^{15}N:^{14}N ratios in thousands of samples per year from labeled nitrogen experiments has been completed, and the system has been carefully evaluated during the past year. The equipment processes several hundred samples per day in a fully automated fashion. Small vials of 0.15 mℓ volume are charged with 25μg of contained nitrogen in labeled ammonium salt sample solution. The tray of up to 137 samples is dried and then run at a rate of 150 s per sample. The equipment converts the ammonium salt to nitrogen gas using hypobromite reagent, purifies the sample using a cryogenic trap, measures the isotope abundance, prints out the results, and stores the data for the entire tray on magnetic tape for future reference.

Separated ^{15}N and ^{14}N in various chemical compounds are used for a wide variety of studies of the nitrogen cycle for agricultural research, forestry, biology, range sciences, animal nutrition, environmental studies of NO_x, and other disciplines. Heretofore, a serious obstacle to the use of these powerful tools has been the total isotopic analysis of the large number of samples that are generated in field studies. With this development, which is available for commercial exploitation, this obstacle is largely removed. With the appropriate modifications, the instrument will also be useful in the analysis of ^{13}C:^{12}C ratios in breath CO_2 samples from clinical studies.

V. ELEMENT MIGRATION AND FIXATION: GEOCHEMICAL STUDIES. (E. Bryant)

This section treats the phenomena of geochemical migration and fixation of elements, especially minor and trace elements, in rocks and pore solutions. We are studying the source, migration, and fixation of elements of particular interest in relation to geologic disposal of nuclear reactor waste and the extraction of geothermal heat. Present basic knowledge about the conditions and mechanisms of migration of elements in the Earth's crust is extremely limited, yet the potential application of such basic knowledge is very broad. The general questions of the geochemistry of these elements and, specifically, the rock types in which they are most abundant; which mineral phases incorporate them; under what circumstances they are concentrated in the intergranular regions; what processes free them from the source rocks; how and in what chemical form they migrate; how they are fixed at a new location; what role thermodynamics has in the solution-solid equilibration; and what are the kinetic controls on release and fixation are being addressed in a series of experimental studies presented in this section. In addition, a new fundamental research project has been initiated this year to extend these element migration studies beyond their program-oriented goals and to treat the above questions in a more general context.

A. Element Migration at the Key Lake Uranium Ore Deposit (D. B. Curtis and A. J. Gancarz)

1. Introduction. Geologic burial is the favored method under consideration for the disposal of commercially generated radioactive wastes. Efforts to evaluate the effectiveness of geologic media in isolating such wastes from the biosphere are limited by the necessity of considering periods of time much greater than those recorded by human experiences. The Natural Repository Analogue program is a research effort to study the retention and migration of elements in the Earth's crust by examining the geologic record, which *does* extend over appropriate periods of time. Previous efforts in this regard have been concerned with studies of the natural fission reactors found at the Oklo mines in the Republic of Gabon, Africa.[58-64] The work has been extended to the rich Precambrian uranium deposit discovered at Key Lake in the northwest corner of the Canadian province

of Saskatchewan.[65] Drill cores, taken as part of the exploration program at Key Lake, have provided well-documented samples from several million cubic meters of sandstone, metamorphic rock, and the uranium ores enclosed in these host rocks. The samples provide the opportunity to study elemental retention and migration in a chemical, physical, and geologic setting quite different from that found at Oklo.

Uranium and thorium decay through a series of radionuclides to form stable isotopes of lead. The relative abundances of actinide parent and stable lead daughter and the proportions of the four lead isotopes in any natural material are a function of the time that the material has been closed to the loss or gain of parent and daughter and the relative concentrations of the appropriate nuclides when the system became closed (the initial concentration). In principle, chemical and isotopic analyses of rocks for these three elements provide the means to understand aspects of the natural history of the rocks, that is, when they were formed, the relative abundances of actinide and lead in previous geologic history, the gain or loss of parent or daughter after formation, the nature of the physical and chemical processes involved in the fractionation, transport, and redeposition of these elements, and the date of these processes. This information is being developed by the analyses of samples from Key Lake.

2. Geology of Key Lake. Key Lake is located on the southeastern edge of the Athabasca formation, a fluviatile quartz sandstone deposit. The age of this deposit has been determined to be 1350 ± 50 million years (Myr) by Rb/Sr dating[66] and 1330 ± 30 Myr from lead isotopic data.[67] The Athabasca sandstone unconformably overlays rocks of the Wollaston Domain, a major structural province of the Canadian shield. The highly deformed basement complex consists of synforms and antiforms with granitoid Archean cores rimmed by Proterozoic metasediments.[68] Radiometric dating of the granitoid basement shows it to be at least 2.5×10^9 yr old. Multiple periods of metamorphism are observed in the metasediments. The major metamorphic period occurred about 1.7×10^9 yr ago with episodes as recent as 1.57×10^9 yr ago.[69,70] The entire region is overlaid by Pleistocene glacial debris.

The basement is predominately a biotite-feldspar-quartz gneiss interlayered with strata of graphite schist and coarse-grained pegmatoid rocks. Rocks of the Athabasca formation are composed almost entirely of quartz with traces of clay minerals and resistate minerals such as apatite, tourmaline, and zircon. A minor quartz conglomerate is formed at the base of the sandstone. There is a highly altered transition zone at the unconformity between this basal conglomerate and the crystalline rocks of the basement.[71]

Pre- and post-Athabasca faults are important structural features at Key Lake. They trend northeast-southwest and dip at 50-70° to the northwest, roughly parallel to the stratigraphic dip of the basement metasediments. The two Key Lake ore bodies are localized in fault zones that appear to impose a structural control on the mineralization. Ore localized at the northeast portion of the zone, the Deilmann orebody, is the subject of this study. Ores at Deilmann occur at the unconformity for distances of about 100 m to the southeast of the faulted region. They extend 150 m into the basement along the dip of the fault zone. The Athabasca sandstone that immediately overlays the ores is 40-60 m thick. To the northeast, at distances between 30 and 100 m, the sandstone thins dramatically, occasionally having thicknesses of <5 m.

Uranium and nickel are the major metallic elements in the ores, with smaller abundances of lead, zinc, and copper. Concentrations of the two major elements often run into the tens of percent. Three uranium minerals have been identified,[71] an oxide called pitchblende I, a more oxidized variety of pitchblende called sooty pitchblende or pitchblende II, and the silicate mineral coffinite.

3. Experiments. Samples representative of the Athabasca sandstone, the transition zone at the unconformity, the crystalline basement, and the ores were selected from the cores. Selections were made to provide an extensive spatial distribution around the Deilmann ore body. Approximately 10 g of rock were removed from the interior of core sections and crushed to <0.25 mm; 1-g aliquots were taken for determination of uranium and thorium concentrations. These two elements were analyzed by neutron activation analysis techniques using the automated analysis system at the Los Alamos Omega West Reactor. Lead isotope abundances were measured by isotope dilution mass spectrometry on 200 to 500-mg aliquots of the powdered samples.

4. Summary and Interpretation of Results. With a single exception, lead isotopic ratios in non-ore rocks from the Athabasca sandstone, from the transition zone at the unconformity, and from the crystalline basement define an age of 1.3×10^9 yr, when the sediments were

deposited in the Athabasca basin.[61,66] Both geologic evidence and radiometric age dates demonstrate that this is much later than the last metamorphic and deformational event affecting the basement. The time probably signifies a massive redistribution of lead and uranium in the underlying basement rocks associated with the deposition of the Athabasca sediments. The remarkable isotopic homogenization throughout much of this volume of rock at a particular time provides a temporal benchmark that can be used to identify subsequent fractionation and redistribution of uranium, thorium, and lead.

The majority of samples of all rock types, including the ores, manifest the fractionation and redistribution of lead and the actinide elements in the last 1.3×10^9 yr. Only 20% of the samples from above the unconformity and 38% of those from the basement rocks appear to have been chemically stable during this time. The Athabasca sandstone and the transition zone at the unconformity are a repository for lead. All the samples from that region are enriched in lead relative to uranium. The isotopic systematics cannot distinguish between lead excesses and uranium or thorium deficiencies. However, a positive correlation between the absolute abundance of lead and the proportion of radiogenic lead suggests an excess of lead. To determine the distances and direction of transport it is necessary to identify the source of this excess lead. The two ore samples that have been analyzed are highly deficient in radiogenic lead, which suggests that ores are a likely source. The quantity missing from 1 g of these ores is sufficient to increase the lead concentration in 1 kg of sandstone by an order of magnitude. Further analysis will attempt to establish if the excess lead in the sandstone has an isotopic composition consistent with lead missing from the ores. If such consistency can be established, it will provide evidence of a source-repository relationship between the ore and the sandstone and establish the spatial characteristics of the transport processes. It may be possible to define the extent of such a redistribution in the sandstone by the absence of excess lead.

B. Migration from Nuclear Explosion Cavities (D. C. Hoffman and W. R. Daniels)

A field study[72,73] of the distribution of radionuclides around an underground nuclear explosion cavity was initiated in 1974, about 9 yr after detonation. The goals of this Radionuclide Migration (RNM) project were to determine the rates of migration underground in various media at the Nevada Test Site (NTS) and the potential for movement both on and off the NTS of radioactivity from underground nuclear explosions. There was particular interest in possible contamination of water supplies. It was also envisioned that the study might provide data applicable to the underground disposal of radioactive waste. This ongoing project is sponsored by the Nevada Operations Office of the Department of Energy with the participation of the Los Alamos National Laboratory, the Lawrence Livermore National Laboratory, the United States Geological Survey, the Desert Research Institute, and appropriate support organizations.

The site of the 0.75-kt nuclear test Cambric, which was fired 73 m beneath the water table in tuffaceous alluvium, was chosen for initial studies. It is anticipated that eventually tests in other geologic media will be examined.

The cavity region was re-entered (Hole RNM-1) using standard drilling techniques, and sidewall core sampling was performed from 34 m below ground surface to 50 m below the detonation point to measure the vertical distribution of radionuclides. The hole was cased and the casing perforated to permit pumping of water from different regions. In this way, variations in the radionuclide content of water from the various intervals were determined. Most of the radioactivity and the highest specific activities of all radionuclides were still found in the region of the original explosion cavity 10 yr after the test. No activity above background was found 50 m below the cavity. Water from the region of highest radioactivity at the bottom of the cavity contained only tritium and ^{90}Sr at levels higher than the recommended concentration guides for drinking water in uncontrolled areas. Most of the radionuclides appear to be retained in the fused debris in the cavity region.

A satellite well (RNM-2S) was drilled 91 m from the Cambric re-entry hole. Pumping of RNM-2S induced sufficient artificial gradient to draw water from the Cambric cavity for study of radionuclide migration under field conditions. The appearance of tritiated water (HTO) in water from this satellite well signaled the forced breakthrough of water from the Cambric cavity region. By early October 1980, 5 yr after pumping started, 4.77×10^6 m^3 of water had been removed from RNM-2S. The only radionuclide other than tritium positively identified in this water is ^{85}Kr, a gas that appears to be dissolved in the water, although there is some evidence for the possible migration of small amounts of ^{106}Ru. Essentially all other radionuclides present in water in the Cambric cavity appear to sorb on

the alluvium so that they have not been transported to the satellite well.

Nearly 17% of the tritium produced in Cambric has been removed in water from the satellite well. The concentration continues to rise in an essentially linear manner (Fig. 14) except for two discontinuities that correspond to periods when the pump was inoperative. The arrival of tritium at RNM-2S was compared with the calculations of Sauty[74] for an instantaneous tracer injection in a radial, converging flow field, similar to the RNM experiment. The shape of the elution curve depends on the Peclet number, which is inversely porportional to the dispersivity; an excellent fit to the experimental data was achieved with Peclet number 10. The maximum in the elution curve for Peclet number 10 corresponds to a volume of 5.66×10^6 m^3 of water pumped, indicating that the tritium concentration in RNM-2S water should peak approximately August 1, 1981 with an uncertainty of 45 d.

The concentration of ^{85}Kr in water from RNM-2S is increasing at approximately the same rate as the tritium. The atom ratio of ^{85}Kr to tritium remains at about one-third that calculated for Cambric, suggesting that krypton travels in the water with the HTO but either at a slower rate or with some loss during transit. The relative positions of the tritium and krypton peaks should be informative.

Starting in May 1978 a 55-gal sample of RNM-2S water was taken each month in a plastic-lined barrel, and

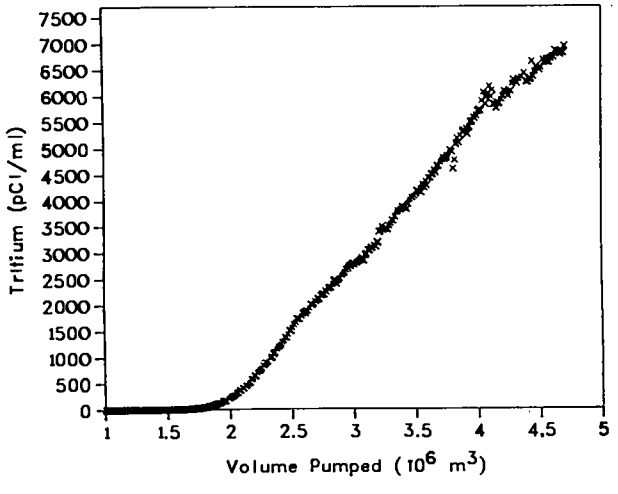

Fig. 14.
Tritium concentration (corrected to Cambric zero time) in water pumped from RNM-2S vs volume.

12 of these samples have been concentrated to solids and encapsulated in plastic for gamma-spectral analysis. The background sample used for the gamma-ray assay was obtained by evaporating 55 gal of water from Well 5B at the NTS. Essentially no radioactivity has been definitely observed above the Well 5B background sample with the exception of a 621.8-keV photopeak, presumably from the 9.75% branch in the ^{106}Rh daughter of 368.2-d ^{106}Ru. Assuming that the 621.8-keV photopeak is correctly identified as arising from ^{106}Ru, comparison of the ^{106}Ru-to-tritium ratios in RNM-2S water with those observed in RNM-1 cavity water and those produced in Cambric indicates that essentially all of the ^{106}Ru produced in Cambric remains in the fused debris but that which entered the cavity water has not been removed or delayed during transit to RNM-2S. The latter observation suggests that any ^{106}Ru present in the groundwater exists as an anionic species that does not sorb on the rock.

Nearly 17 000 gal (64.35 m^3) of water were pumped from RNM-1 on September 4, 1979 (Re-entry III), and water samples were taken at the surface hose bib in plastic bottles, gas-tight bottles, and in 55-gal, plastic-lined barrels. In Table VI, data from current and previous re-entries of RNM-1 are compared. Although the current ^{90}Sr and ^{137}Cs concentrations may be slightly lower, the higher ratios to tritium indicate that the tritium concentration is decreasing much more rapidly, presumably because of pumping at RNM-2S. The strontium and cesium results are consistent with the hypothesis that these elements are being replenished from the source term owing to their very high retention values.[73]

In conclusion, during 5 yr (over 1.1 billion gal of water) of pumping from the satellite well located 91 m from the Cambric cavity, only tritium, which is present as HTO and chemically the same as the water, and ^{85}Kr, which seems to be dissolved in the water, have been positively identified in water removed from this well, although there is some evidence for the possible migration of minute amounts of ^{106}Ru. These results are consistent with laboratory studies that indicate that, in general, sorption is sufficiently high to preclude the migration of most radionuclides from the original cavity to the satellite well in the near future. Pumping and radioassay of water from the satellite well will be continued to investigate the possible arrival of nonsorbing species.

TABLE VI
REPRESENTATIVE ACTIVITY LEVELS[a] IN RNM-1 WATER SAMPLES

Entry	Date	Total Volume from RNM-2S (10^6 m^3)	Concentration (dpm/mℓ) ^{90}Sr	Concentration (dpm/mℓ) ^{137}Cs	Atom Ratios ($\times 10^5$) ^{90}Sr/T	Atom Ratios ($\times 10^5$) ^{137}Cs/T
Original-Zone IV	8-8-75	0	~6	~1	1.8	0.31
Original-Zone V	8-14-75	0	~0.25	~0.2	0.23	0.18
Re-entry I[b]	10-4-77	1.17	1	~0.2	14	3.0
Re-entry II[b]	11-30-77	1.34	~0.6	~0.5	14	12
Re-entry III[b]	9-4-79	3.50	~0.2	~0.1	70	40

[a]All activity levels corrected to Cambric zero time.
[b]The water is believed to come primarily from Zone IV.

C. Radionuclide Transport and Retardation in Tuff (E. N. Vine, B. P. Bayhurst, W. R. Daniels, S. J. DeVilliers, B. R. Erdal, F. O. Lawrence, and K. Wolfsberg)

The suitability of tuff at the Nevada Test Site (NTS) for the isolation of radioactive waste is being investigated as part of the Nevada Nuclear Waste Storage Investigations. Tuff is a geological term applied to pyroclastic rocks composed of particles fragmented and ejected during volcanic eruptions. Such deposits are complex and may exhibit a wide range of properties, depending on their cooling and alteration history.[75] Related studies have been performed on other geologic media, especially granite and argillite.

The migration of radionuclides from a deep geologic nuclear waste repository would probably be the result of transport by groundwater. Retardation because of interactions with the surrounding geologic media should be a significant factor in minimizing such transport. Many lithologic types of tuff contain highly sorptive minerals. In addition, long hydrologic flow paths are typical of the NTS. These are both important reasons for the consideration of tuff as a geologic medium for isolation of radioactive waste.

An understanding of the mechanisms of transport and sorption-desorption is essential for prediction of the behavior of radionuclides during the time required for decay to safe levels and, thus, for demonstration of the effectiveness of tuff, or any potential medium, as a migration retardent. Sorptive properties of tuff are being studied with both batch measurements and flow experiments (crushed and solid rock columns). Studies were made on tuff core samples from two drill holes at the NTS at Jackass Flats and at Yucca Mountain. Water from Jackass Flats was pretreated at least 2 wk with crushed tuff from the core being studied before use in the experiments.[76-81]

The distribution coefficient K_d is commonly used to describe the partition of a radionuclide between solid and aqueous phases and is defined as the concentration of a species/gram of solid phase divided by its concentration/milliliter of liquid phase at equilibrium. We prefer to call it "sorption ratio" to avoid the implication of equilibrium. In column experiments the relative velocity of a radionuclide with respect to the groundwater velocity is measured. This retardation factor R_f is related to the sorption ratio K_d by the simple expression $R_f = (\rho/\varepsilon)K_d + 1$, where ρ is the density of the rock column and ε is the porosity.

The sorption ratios calculated from flow measurements can be compared with data obtained by batch techniques. Because the batch experiments are simple and fast, it is feasible to measure the influence on K_d of a large number of parameters.

1. Sorption Properties: Batch Measurements. Several parameters were studied with batch experiments. Particle size had the least effect on K_d values; little or no variation was obtained among fractions of <106 μm, 106-150 μm, 355-500 μm, and 106-500 μm. Measurements were also made at two temperatures, and sorption ratios at 70°C were generally greater than at 22° C. Strontium, cesium, and barium sorption ratios increased by factors of approximately 1.5 to 4, 1 to 2.8, and 2.5 to 5.6, respectively. Americium values changed very little.

Increases in K_d with sorption time were often observed, although the changes were generally small.

The effects of atmosphere on sorption behavior were investigated by comparing the results of studies performed in a pure nitrogen atmosphere having $\leqq$0.2 ppm oxygen and $\leqq$20 ppm CO_2 present with similar measurements made under natural atmospheric conditions on the same materials. The sorption ratios for technetium were most affected by atmosphere and were higher when measured under controlled atmosphere conditions, as was the sorption of plutonium. For nonzeolitized tuff from Yucca Mountain, the sorption ratios of uranium were not affected by atmosphere; however, they were somewhat higher in a nitrogen atmosphere for a zeolitized tuff. As expected, strontium, cesium, and barium were least affected by the presence or absence of oxygen and CO_2. Although sorption of cerium and europium on tuff was also unaffected, sorption of both those elements increased by a factor of 10 or more in a nitrogen atmosphere on granite and argillite. We have been able to observe apparently negative Eh values on some tuff-water systems but not on granite or argillite systems.

Groundwater composition may also influence the sorption ratio for many radionuclides. The two solutions used were selected to represent extremes for the media being studied. The sorption of cesium and barium was relatively insensitive to solution composition, whereas strontium sorption varied by a factor of 6 and cerium and europium by greater than a factor of 10. The results indicate the importance of the composition of the solutions.

Batch measurements are also providing relative sorption data on a wide variety of lithologic types of tuff. Although minor components in a rock sample can certainly play a major role in sorption, there is a fairly good correlation between sorption and major phases, as determined by x-ray diffraction, in the tuffs studied to date. A devitrified Yucca Mountain tuff exhibits some of the lowest sorption ratios of the samples studied. Sorption ratios for strontium, cesium, and barium on tuffs containing clinoptilolite or heulandite are at least one to two orders of magnitude larger than analcime-containing cores. Cerium and europium sorption, however, does not seem to be dependent on zeolite content. Ranges of sorption values obtained on samples containing quartz and feldspar (with and without analcime), samples containing glass (with and without clay), and samples containing clinoptilolite (heulandite) are summarized in Table VII. Intermediate values for strontium, cesium, and barium were obtained on glassy cores.

2. Sorption Properties: Column Measurements.

a. Crushed-Rock Columns. The migration of radionuclides through crushed-rock-core columns (35-106 μm) was measured. Groundwater pretreated with crushed tuff was used, and the columns were loaded with small volume spikes of the pretreated water containing the tracers. Flow rates generally ranged from 30 to 60 m/yr. The free column volumes (used to calculate the effective column porosity) were determined with both HTO and $^{131}I^-$, which gave identical results. Several kinds of elution behavior were observed: symmetric peaks where 50% of the activity was eluted at the peak, asymmetric peaks, and "no peaks," but instead a slow, usually uniform elution. With one exception the elution curves of ^{85}Sr were symmetric, and the column K_d values were one to three times lower than the corresponding batch K_d value. Strontium was eluted from the exceptional column at a rate of ~0.07%/day for ~72 days, then a small, sharp peak was observed, and then the slow, uniform "leaking" resumed. This column contained a highly vitric tuff, and the slow elution may be due to a gradual dissolution of the glass. This, however, would not explain the weak, sharp peak. Columns of Jackass Flats and Yucca Mountain tuff were also loaded with ^{137}Cs. The same slow leaking, without a sharp peak, was observed for ^{137}Cs on the tuff. The slow elution of ^{85}Sr and ^{137}Cs might be the result of exchange of the sorbed

TABLE VII

Major Phases	Sr	Cs	Ba	Ce	Eu
Quartz, feldspar (+/— analcime)	35-100	250-1200	210-980	140-1400	500-1400
Glass (+/— clay)	270-300	2000-7600	360-1000	24000	1700-20000
Clinoptilolite (heulandite)	1800-28000	8600-17000	1500-130000	550-36400	1200-49700

radioactive species with stable isotopes in the water, which contains $\sim 10^{-9}$ mol/ℓ cesium and $\sim 6 \times 10^{-7}$ mol/ℓ strontium.

Three columns were loaded with ^{85}Sr and tested at higher flow rates. The sorption ratio from one fast-flow column, run with ^{85}Sr added to the groundwater, was identical to that obtained from a slow-flow column loaded with a spike. However, an increase of 50% in K_d was obtained on another run at a fast flow rate. Granite columns run at 0.04 mℓ/h and 4.98 mℓ/h also exhibited a considerable increase in K_d at the faster flow rate. One would expect *a priori* that the K_d might be lower for faster flow if the sorption step is slow.

Three Yucca Mountain columns were run at two ^{137}Cs concentrations, 10^{-6}mol/ℓ and 10^{-9}mol/ℓ; the K_d value calculated for cesium was not affected by the cesium ion concentration. On a column with tuff from Jackass Flats there was a gradual elution of ^{137}Cs. In another fast flow Yucca Mountain column 50% of the total ^{137}Cs was eluted in only 7860 mℓ, in slowly increasing concentration; a sharp peak was never observed. A "column K_d" value of 21 900 mℓ/g, estimated from the volume required to elute 50% of the activity, is well above that obtained in batch measurements (8600 mℓ/g).

Columns loaded with ^{133}Ba showed peaks, followed in some cases by a gradual elution of activity. The K_d values are ~two to five times lower than the corresponding batch K_d values. A uranium elution peak was quite asymmetric, and the concentration slowly decreased.

b. Whole-Core Columns. Because studies using crushed rock involve newly exposed mineral surfaces, experiments were also undertaken with intact rock cores. An "elution" curve was obtained on one tuff core that was 15.9 mm high and 25.4 mm diameter. Approximately 40% of the ^{85}Sr loaded was eluted at a fairly constant, "peakless," rate in 1 year. The estimated sorption ratio of ~20 mℓ/g is less than the value obtained from batch measurements and similar to the value obtained on a crushed rock column of the same material.

c. Sorption Properties: Circulating System Measurements. Sorption ratios measured using a batch technique have frequently been observed to increase slowly with contact time. Experiments were initiated to determine whether this is the effect of "weathering" and self-grinding, which occur during the shaking operation used in the batch technique. A circulating system was used in which a 355- to 500-μm fraction of crushed tuff in a long polycarbonate tube was contacted with groundwater continuously circulated through the crushed tuff in a closed loop. Results for ^{85}Sr, ^{137}Cs, and ^{133}Ba from this circulating system are comparable to those from crushed-rock columns and lower than those from batch measurements.

3. Conclusions. Batch measurements provide an understanding of which experimental variables are important. For example, sorption ratios vary little with particle size and surface area. However, groundwater and rock composition are quite important. A general correlation has been identified between mineralogy (major phases) and the degree of sorption for strontium, cesium, and barium.

Data from crushed-tuff columns indicate that, except in simple cases where sorption coefficients are relatively low and ion-exchange equilibria not only exist but are the dominant mechanism for removal of radioisotopes from solution, the simple relation between the sorption ratio K_d and the relative velocity of radionuclides with respect to groundwater velocity may be insufficient to permit accurate modeling of the retardation of radionuclides. Additional work on whole-core columns and larger blocks of intact material is required to better understand radionuclide sorption and transport through rock.

D. The Leaching of Spent Fuel Elements in Water (A. E. Ogard, G. E. Bentley, E. A. Bryant, C. J. Duffy, G. F. Grisham, A. E. Norris, C. J. Orth, and K. W. Thomas)

This project developed from the Oklo natural fission reactor studies. It had been determined in the Oklo studies that many fission products and actinides remained in the reactor site during the periods of their radioactive decay following formation in the reactor zone 2 billion years ago. An explanation for this retention of fission products and actinides uses the extreme insolubility of uraninite (UO_2) in very reducing water environments. One can estimate from available thermodynamic data that the concentration of uranium in equilibrium with uraninite in pH 7 water that is free of dissolved oxygen is $\sim 10^{-11}$ mol/ℓ. This low value suggests that the reducing conditions that can occur in deep geologic burial would result in a very slow leaching of spent fuel elements in contact with water because spent fuel elements are largely sintered UO_2.

During our studies on the leaching of spent fuel elements, we found it difficult to duplicate readily the

reducing conditions of deep geologic burial. This result we inferred from the relatively high uranium concentrations that were found in the leachants rather than the low value listed above. However, it was observed that under our reducing condition as well as under an oxidizing atmosphere, some of the rare earth fission products and actinides behaved differently from the uranium, a behavior we attribute to a precipitation of the rare earths and actinides.

If the concentration of uranium and the activities of all radionuclides in the leachant are dependent only on the dissolution of the matrix UO_2, and all the fission products are homogeneously distributed through the UO_2, then the ratio of the fission products to uranium in the leachant should be comparable to the calculated radionuclide-to-uranium ratio in the original spent fuel element. Of these ratios the ones for europium, cerium, americium, and plutonium at 70°C under oxidizing conditions and plutonium at 25°C under reducing conditions are very much lower than the calculated ratios in the spent fuel element. These large differences in the ratios can occur if europium, cerium, americium, and plutonium are at their solubility limits and precipitate as some form of hydrous oxide as the UO_2 matrix continues to dissolve with time.

The data can be used for more quantitative comparisons. The uranium concentrations and activities of the radionuclides were used to calculate isotope concentrations. These isotope concentrations were then converted to elemental concentrations by using the calculated isotopic composition of the H. B. Robinson spent fuel element.[82] Based on these data the apparent solubility limits for some of the fission products are listed in Table VIII. These numbers assume kinetics did not prevent precipitation at either 25 or 70°C. Also, at 25°C the calculated numbers are largely lower limits because in most cases there was not evidence for precipitation from differences in the spent fuel-leachant ratios. For comparison, we can use the compilations of Baes and Mesmer[83] and the calculated solubilities of Newton et al.[84] Under oxidizing conditions and pH 4, uranium oxide would have a solubility of 10^{-1} to 10^{-2} mol/ℓ and under reducing conditions 10^{-7} to 10^{-11} mol/ℓ depending on which solid, the amorphous or the crystalline, is in equilibrium with the liquid. Similarly, the solubility of plutonium oxide would be 10^{-3} to 10^{-7} mol/ℓ for oxidizing and 10^{-7} to 10^{-14} mol/ℓ in reducing conditions. The solubility is dependent on the crystal form and the actual Eh of the system. These comparisons are probably as good as one could expect from such a heterogeneous and multicomponent system as a spent fuel element dissolving in water.

TABLE VIII

SOLUBILITIES AT pH 4, DEIONIZED WATER
(mol/ℓ)

Element	25°C	70°C	Condition
Eu	≧3 E-8	2 E-9	O & R
Ce	≧3 E-7	1 E-8	O & R
Am	≧5 E-8	2 E-9	O & R
Pu	3 E-7	1 E-8	O & R
U	>5 E-5	>E-4	O
		~2 E-6	R

The fission products ^{137}Cs, ^{90}Sr, and ^{125}Sb behave differently from the other products. Under reducing conditions and at both 25 and 70°C, ^{137}Cs, ^{90}Sr, and ^{125}Sb act similarly to uranium except that the concentrations of these isotopes in solution are far higher than expected from the isotope-to-uranium ratio in the spent fuel element. The ratios to uranium at 25 and 70°C for cesium and strontium are very high, especially the cesium-to-uranium ratios. Katayama et al.[85] in leaching experiments in air of H. B. Robinson spent fuel elements also found a higher fraction of some radionuclides, especially cesium, in the leachant than in the spent fuel element. They interpreted this higher concentration as indicating an absence of congruent dissolution. A higher concentration of radionuclides is not by itself sufficient reason to dismiss congruent dissolution. Postirradiation examinations of spent fuel elements have shown that the radionuclides can be inhomogeneously distributed through the fuel, especially the more volatile elements, such as cesium and iodine. If the cesium were concentrated at the grain boundaries of the fuel and at the colder exterior of the fuel pellet but were still largely incorporated into the UO_2 matrix, its concentration in the leachant could be controlled by the dissolution of the UO_2 matrix but at a higher cesium-to-uranium ratio. The behavior of cesium, strontium, and uranium appears to be very similar but at different concentration levels.

We conclude that the solubilities of some radionuclides, especially rare earths and actinides, may be important and controlling factors in leaching of waste

forms. These solubilities should be measured accurately as a function of pH and not as a part of a multicomponent system.

Although the amount of data is small, it is interesting to postulate that a negative temperature coefficient of solubility is being exhibited by the actinides and rare earths. Individual solubilities should be measured as a function of temperature to determine if a kinetic effect is being observed in the data. A negative temperature coefficient of solubility for actinides and rare earths in water would have important consequences for nuclear reactor safety and for the management of nuclear wastes.

E. Preliminary Considerations Concerning Actinide Solubilities (T. W. Newton, B. P. Bayhurst, W. R. Daniels, B. R. Erdal, and A. E. Ogard)

The principal practical reason for studying the near-neutral solution chemistry of the lighter actinides is to provide quantitative information for input to models being developed for prediction of the transport of these elements by groundwater. Information is needed on the oxidation states, actual species present, and maximum concentration, governed by solubility. Additional important uses for this information are the interpretation of the results of laboratory and field studies of the sorptive behavior of geologic media and the design of meaningful studies of the partitioning of actinides between rock and groundwater.

During the past year, work on fundamental solution chemistry pertinent to radioactive waste management has been initiated.[86-89] Thus far, work has been confined to preliminary considerations of the problems involved in understanding the precipitation and dissolution behavior of actinide compounds under environmental conditions. For the first step, the considerations have been restricted to equilibrium solubilities in the absence of complexing agents for actinide oxides and hydrated oxides, or hydroxides.

To get a preliminary idea of the solubility behavior, we attempted to calculate solubility as a function of Eh and pH using the appropriate thermodynamic data. If the solubility products, hydrolysis constants, and oxidation potentials are available, the solubilities can be calculated in a direct way. Unfortunately, almost none of the required data have been accurately determined, so recently published estimates[90] have been used. The results are presented in terms of "contour maps" showing lines of constant solubility as a function of Eh and pH. Calculations have been made for the +4 oxides and hydrous oxides of uranium, neptunium, and plutonium. The results for $PuO_2 \cdot nH_2O$ are shown in Fig. 15. The diagrams were constructed under the assumption that conversions of the hydrated oxides to the more stable crystalline oxides are slow compared with the establishment of the solubility equilibria. In spite of the uncertainty in the input data the results are very instructive; they show that the Eh and pH dependences are certainly quite complex. In addition, these results will be of value in planning solubility experiments and in interpreting the data.

The solubility diagram for $PuO_2 \cdot nH_2O$ (Fig. 15) is divided into two regions by a solid diagonal line; below this line the solid phase is the +4 hydrated oxide, while above the line the +6 hydroxide is stable. Abrupt changes in solubility occur when this line is crossed. The upper dotted line on the diagram represents the potential of the water/oxygen couple, $2H_2O = O_2 + 4H^+ + 4e^-$; systems with apparent Eh values below this line are thermodynamically unstable in the presence of one atmosphere of oxygen. Reactions involving this couple are usually very slow, so the potential for the more rapid H_2O_2/O_2 couple, $H_2O_2 = O_2 + 2H^+ + 2e^-$, is also shown. Systems with potentials below this line are expected to react reasonably rapidly with oxygen.

The diagram shows that the calculated minimum solubility occurs at the bottom of a basin with approximately triangular contours. Three distinct principal solubility equilibria are associated with the regions showing diagonal, horizontal, and vertical contour lines, respectively. In the lower left of the diagram the contour

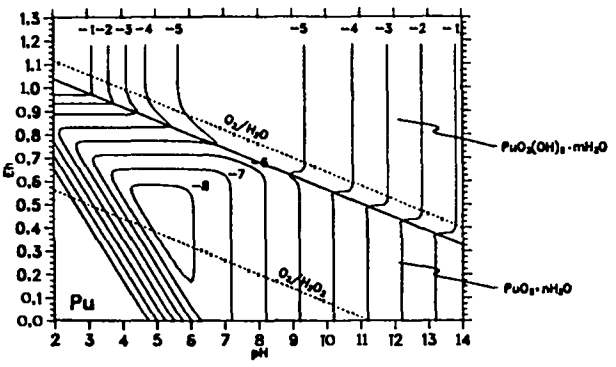

Fig. 15.
Lines for constant log (solubility) vs Eh and for plutonium hydrous oxides.

lines show a slope of about -4×0.059, and the plutonium half-reaction for the principal equilibrium is

$$PuO_2 \cdot nH_2O + 4H^+ + e^- = Pu^{3+} + (2 + n)H_2O. \quad (1)$$

Farther up on the diagram where the contours are horizontal, the half-reaction is

$$PuO_2 \cdot nH_2O = PuO_2^+ + nH_2O + e^-. \quad (2)$$

This result is consistent with the observations of Rai and coworkers at Battelle Pacific Northwest Laboratory, who showed that where Pu(V) is the principal solution species in contact with $PuO_2 \cdot nH_2O$, the solubility depends on the Eh but is essentially independent of pH. In the lower part of the diagram where the contours are vertical, the solubility is independent of Eh, and the principal equilibrium is

$$PuO_2 \cdot nH_2O + OH^- = Pu(OH)_5^- + (n - 2)H_2O. \quad (3)$$

This analysis shows that if the input for the calculations is reasonably correct, the only parameters that contribute significantly to the solubility of $PuO_2 \cdot nH_2O$ are (1) the solubility product, (2) the $Pu^{3+} - Pu^{4+}$ standard potential, (3) the $Pu^{4+} - PuO_2^+$ standard potential, and (4) the *fifth* hydrolysis constant for Pu^{4+}.

This discussion indicates that only a limited number of properly chosen experiments are required to predict the solubility of $PuO_2 \cdot nH_2O$ over the whole range of Eh and pH. Because there is a fairly reliable value for the $Pu^{+3} - Pu^{4+}$ standard potential,[91] the solubility product could be determined from a set of solubility measurements in the $3 \leqq pH \leqq 4$ and $0.5 \leqq Eh \leqq 0.6$ V range where Eq. (1) is the principal equilibrium. Careful measurements in the $3.5 \leqq pH \leqq 6$ range where Eq. (2) is the principal equilibrium could be used for an independent determination of the solubility product with the difficulty that the estimated uncertainty in the required potential for the $Pu^{4+} - PuO_2^+$ couple is quite large.[91] The equilibrium constant for Eq. (3) could be determined in any convenient region with $pH \geqq 7$ or 8 and $Eh \lesssim 0.5$ V.

The diagram shows that careful measurement and control of the Eh will be required for meaningful solubility determinations in regions where Eqs. (1) and (2) are the principal equilibria. A good method probably is to use Eh moderators or buffers together with a potentiostat. The requirements for such a moderator in actinide solubility studies are:

- Formal potentials in the range −0.5 to 0.9 V, approximately.
- Stable for many days with respect to decomposition in either the oxidized or reduced forms in the pH range from ~2 to ~9.
- Relatively rapid redox reactions with actinide species, but no other reactions such as precipitation or complexation.
- Reversible redox reactions at the working electrode of a potentiostat.

Bondietti and Lee at Oak Ridge National Laboratory have used redox indicators as Eh buffers in their work on technetium. They report that Nile Blue, Thionine, and 2,6-dichloroindophenol (DCIP) at concentrations of 10^{-6} M gave Eh values in agreement with the theoretical ones within 10-20 mV at a pH of ~8.25. The reported potentials[92] for Thionine and DCIP are such that they might be useful for $PuO_2 \cdot nH_2O$ solubility studies in the regions where Eqs. (1) and (2) are the principal equilibria, and for $NpO_2 \cdot nH_2O$ where equilibria analogous to Eqs. (2) and (3) are predominant. However, DCIP probably would not be suitable for the present purposes because it is insoluble in acid solutions, unstable in strongly alkaline solutions, and decomposes slowly even in neutral solutions.[92] In addition, it forms anions that might complex actinide species. Other dyes should be considered; for example, Bindschedler's Green forms cations, shows Eh versus pH similar to that for DCIP, is useful in the $2 \leqq pH \leqq 9.5$ range, and shows instability only at the extremes of pH. In addition, it shows evidence for semiquinone formation, which may facilitate the one-electron steps required in the redox reactions of the actinides.

Inorganic couples also should be considered for use as redox buffers or moderators. Professor Henry Taube at Stanford University, who has had considerable experience with a wide variety of inorganic complexes, suggests that although many ruthenium complex couples have desirable potentials they are probably not stable enough. Certain osmium complexes are much more stable, and Taube suggests that the II-III couples such as $Os(bipyridyl)_3$ and $Os(bipyridyl)_2(CN)_2$ should be tried.

A preliminary list of possible Eh moderators is given in Table IX, together with the formal potential at pH 7

TABLE IX

POSSIBLE Eh MODERATORS

	E_m^7 (V)	pH range
Os(II)-Os(III) couples		
tris (1,10-phenanthroline)	0.88	
2,2′-bipyridine	0.88	
dicyano-bis-(2,2′-bipyridine)	0.78	
4,7-dimethylphenanthroline	0.68-0.73	
3,4,7,8-tetramethylphenanthroline	0.68-0.73	
Co(II)-Co(III) sepulchrate	−0.3	
Organic couples[a]		
Bindschedler's Green	0.224	2-9.5
Induline Scarlet	−0.299	3.0-8.6
Rosinduline 2G	−0.281	4.8-11.4
Lissamine Blue BF	−0.253	1-11
N,N′-dimethyl Viologens	−0.446[b]	8.4-13
Indigo Carmine	−0.125	<9[c]
Pyocyanine	−0.034	1-12

[a]Data taken from Ottaway, 1972.

[b]Potentials of substituted viologens are independent of pH and follow the simple Nernst equation $Eh = E_o + (RT/F)_{\ell n(Co/Cr)}$.

[c]Semiquinone is formed above pH 9.

(E_m^7) and the pH range under which they can be investigated.

The preliminary conclusions discussed here indicate some important experimental work that should be done. Solubility and distribution studies require control of Eh, so for this purpose various redox couples should be tested for stability and for rapidity of reaction with actinide species of trace concentrations.

F. Rock-Water Interactions (R. W. Charles and R. J. Vidale)

1. Introduction. The experimental rock-water interactions are conducted to model some of the expected rock-fluid reactions that will be encountered in the Fenton Hill Hot Dry Rock System as the system matures, that is, as the system approaches a steady state chemically after perturbations caused by initial drilling and reservoir establishment have abated. This is a granitoid-water system. A small effort has been started with basalt-fluid systems. The latter are of interest if such rocks are to be used as rad-waste repositories.

The rock is reacted in a dynamic (circulation) system by flowing fluid over rock disks (or prisms). The rock is subjected to temperature (either fixed or in a controlled gradient) up to 310°C and pressures up to 1/3 kbar for experiments up to 9 months in duration. The rock is examined for etching and secondary mineralization by scanning electron microscopy, electron microprobe, and optical microscopy. Modeling of the system can be done after the method of Schreinemakers (1915-1925)[93] as modified by Korzhinskii (1959),[94] Zen (1966),[95] and Zen (1974).[96] Work done with this approach follows.

2. Multisystems. A magnetic tape of the program REACTION developed by L. W. Finger, Carnegie Institute of Washington, and D. M. Burt, Arizona State University, was obtained in FY-1980. The program is now running at Los Alamos National Laboratory's central computing facility (CCF). Although the program was correct as written, 10 fatal errors had to be

corrected along with several compilation inconsistencies because of differences in language between the computer for which the program was originally written and the CCF.

The program is of immediate use in determining all possible reactions between a series of phases, and it prints them in descending order of degeneracy. One must then take these univariant reactions and assemble them by hand in intensive variable space with possibly negative degrees of freedom (Korzhinskii, 1959). This net produces a useful framework of univariant equilibria which, if properly oriented, will define a series of phase assemblages stable under different μ_i - μ_j conditions.

The REACTION program has now been combined with a computer plotting routine to place all of the calculated invarient and univariant equilibria in μ_i - μ_j' space. Systems as large as two negative degrees of freedom can be handled at this time. Currently, the program is in HPL for the HP 9825 calculator with 9866B printer and 9872A plotter. We plan to enlarge this to handle systems of $F = -3$ and convert to FORTRAN.

This development relates observed mineral assemblages in intensive variable space, allows identification of other assemblages not observed directly, and defines the univariant equilibria separating the divariant assemblages. An example follows.

3. Biotite Granodiorite + Distilled Water Reacted in a Temperature Gradient. The complete experiment reacting biotite granodiorite with distilled water is described in Los Alamos National Laboratory report LA-8566-MS. To summarize: the reacting phases [(thomsonite (T), stilbite (S), beidellite (B), plagioclase (P), K-spar (K), anorthite (A), and sericite (M)] are described by the components Na_2O-K_2O-Al_2O_3-CaO with H_2O and SiO_2 mobile. A connected net for this $f = -1$ multisystem is shown in Fig. 16. The relevant intensive variables for the experiment are P, T, μ_{SiO_2}, and μ_{H_2O}. A number of X-Y plots relate the relevant divariant assemblages

low T: B+P+K+M (AST) (to 119°C) ,
intermediate T: S+P+K+M (ABT) (161°C) ,
high T: T+P+K+M (ABS) (209°C to 310°C) ,
and very high T: A+P+K+M (BST) (above 310°C) ,
by the method of displaced equilibria:

$$-\Delta S dT + \Delta V dp - \Delta n_{H_2O} d\mu_{H_2O} - \Delta n_{SiO_2} d\mu_{SiO_2} = 0.$$

Note that divariant assemblages, for example, (AST), are named by absent phases. Holding any two of these intensive variables constant, the slopes of the generated X-Y plot may be calculated. Six are possible for this system. Most relevant to the current experiment is the case of P and μ_{H_2O} constant yielding,

$$\frac{dT}{d\mu_{SiO_2}} = \frac{-\Delta n_{SiO_2}}{\Delta S}$$

Exact orientation is not possible because the entropies of some of the phases are unknown. However, we do know the sequence of divariant assemblages with temperature and μ_{SiO_2}. The diagram may be oriented as shown in Fig. 17 with the reaction path as shown.

The diagram predicts the disappearance of zeolite at higher temperature and does not require additional divariant assemblages to be found experimentally. In addition, a number of univariant curves separate these divariant assemblages, which may be relevant depending upon the bulk composition of the experimental system.

Some interesting conclusions were drawn from this. Although the experiment is in an open system, for long periods of time the solution burden is constant, which indicates steady-state equilibrium with secondary material on the rock surface. To state this another way, for small changes in bulk composition the system behaves as if it were a closed system. Another point observed is that although the system is initially silica supersaturated (biotite granodiorite) it becomes silica undersaturated (thomsonite bearing) after reaction.

4. Sentinel Gap Basalt Reacted in a Temperature Gradient. Reaction between water and a basalt reservoir in a temperature gradient must be defined if basalt is to be used for geothermal energy extraction or radioactive waste deposition. Six prisms (2.4 cm by 0.8 cm by 0.8 cm) of Sentinel Gap basalt were reacted along a temperature gradient of 72 to 310°C at 1/3 kbar for 2 months with initially distilled water under flow conditions of 2-3 cc/min.

The fresh basalt consists of two pyroxenes, plagioclase, and Ti-magnetite. The matrix is a micropegmatite with a rhyolite norm. Natural alteration of the basalt to nontronite is extensive. Under experimental conditions, recrystallization of the basalt is apparent throughout the *volume* of the sample even though no attempt is made to flow fluid through the rock. Weight

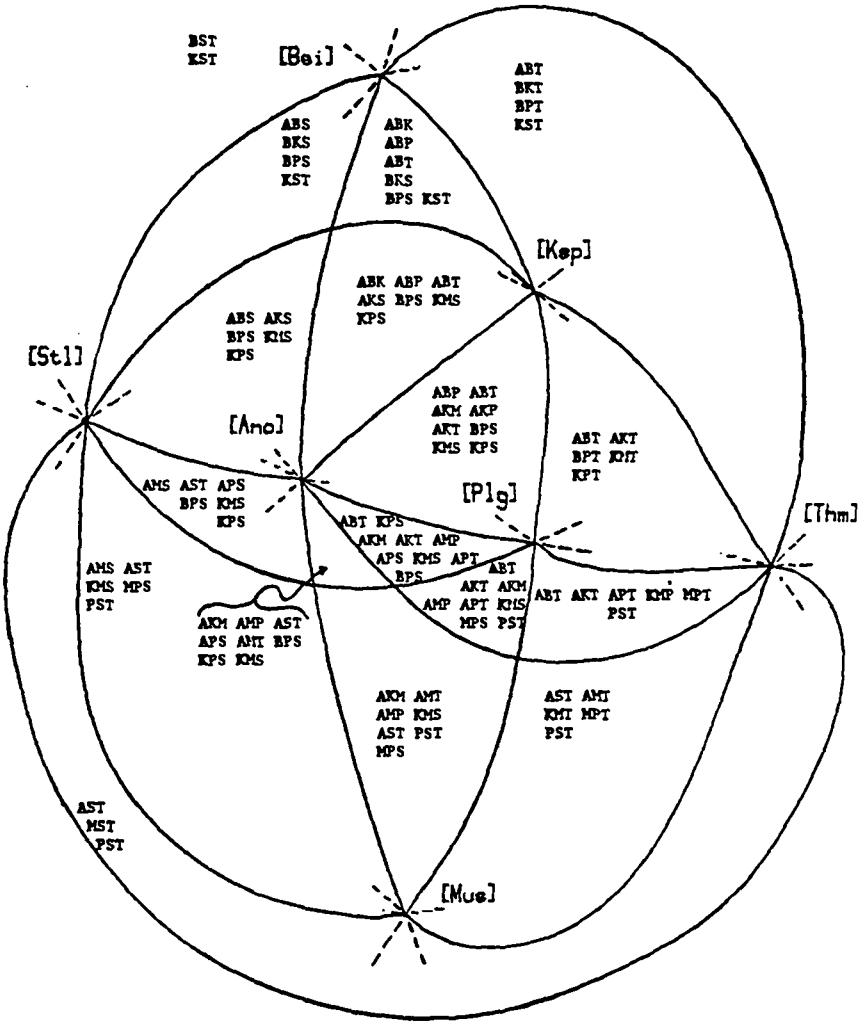

Fig. 16.
Connected net showing all possible divariant fields for the biotite granodiorite + water system.

loss varies from 5% at 72°C to 14% at 310°C. Surface and internal assemblages evolve to a smectite-like clay and an illite, respectively. While the pyroxenes, plagioclase, and Ti-magnetite are resistant to reaction, the nontronite and micropegmatite are extensively recrystallized at all temperatures. Most of the micropegmatite is dissolved at higher temperatures.

G. The Application of Fluid Chemistry Studies to a Hot Dry Rock System: Neutron Activation Studies (R. Vidale, I. Binder, and A. Gancarz)

Neutron activation analysis methods were developed for determination of element concentrations in geothermal system waters, bulk rock samples, separated mineral phases, and intergranular salts from a hot dry rock geothermal system. Selected trace and major element concentrations were determined by neutron activation for (1) 39 water samples taken during the course of a 75-day experimental run of the Fenton Hill hot dry rock system, including both the injected cool water and the heated water emerging from the system; (2) a bulk rock core section from 8904 ft (2714 m); (3) each of the seven major phases present in the rock; and (4) a sample of intergranular salts obtained by leaching the disaggregated rock at 25°C.

Sodium, cesium, bromine, and europium continued to increase in the fluid during the 75-day test run and were added to the circulating fluid almost exclusively by the deep reservoir. Sudden changes in their concentration may indicate significant events in the system just before

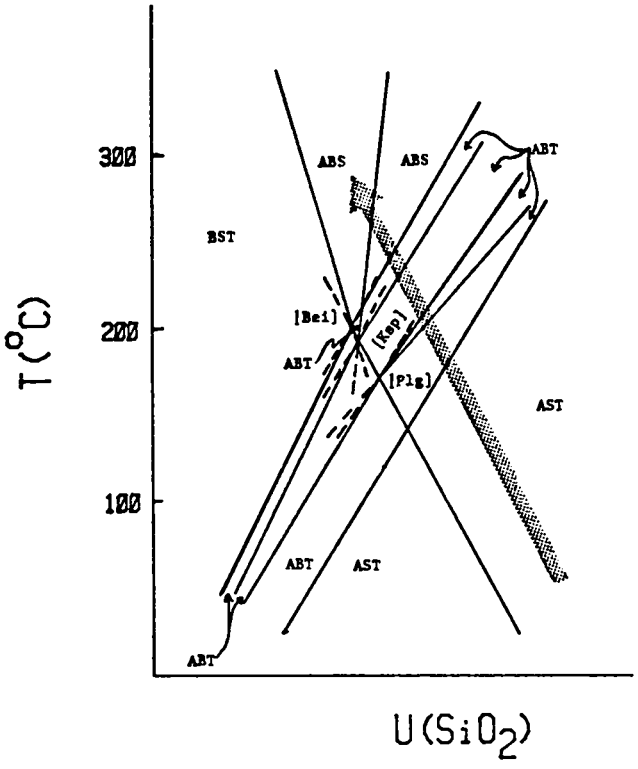

Fig. 17.
T vs μ_{SiO_2} for the observed divariant assemblages. Reaction proceeds according to the arrow. Only the relevant divariant assemblages are labeled.

days 23, 46, 55. Potassium, calcium, strontium, barium, iron, and cobalt also continued to increase and were added both by surface sources and the deep reservoir. Many of their concentrations also changed just before days 23, 46, and 55. Zinc, molybdenum, arsenic, antimony, and tungsten appeared to reach a steady state within 75 days.

Plagioclase is the major rock source for sodium and a major source for calcium. The disproportionately low increase of calcium relative to sodium in the working fluid suggests dissolution of plagioclase by pore fluid or circulating fluid and the formation of a calcium-bearing alteration mineral at depth. This is in agreement with laboratory circulating system data.

The major possible sources of elements added to the working fluid in the deep reservoir are mineral/water interaction during circulation, local saline pore solution and interstitial salts that have already interacted with the rock, and the moving deep hot brine of the Jemez system. Mineral/water interaction is known to be significnt from experimental work. Local interstitial salts, in the limited rock sample available, seem to occur in different element proportions from those in the working fluid. Limited addition of the Jemez deep hot brine will be considered carefully before further inferences are drawn about system behavior from solution chemistry.

H. Permeability Measurements (C. Duffy)

Matrix permeability (permeability of unfractured rock) provides a measure of the minimum permeability of a rock mass. The permeability measurements described below are for cylinders, 1 in. (25.4 mm) in diameter by approximately 1 in. (25.4 mm) long, cut from drill core samples from the Fenton Hill hot dry rock site. The primary importance of the measurements is in understanding the water loss mechanisms in the hot dry rock system. Water losses above those that can be explained by matrix permeation would indicate water loss owing to fracture permeation or perhaps the presence of high permeability rock that was not sampled by coring.

Permeability measurements are also important in understanding mass transfer between fluid and rock because permeability influences the amount of rock that

interacts with the fluid. This consideration is of secondary importance at Fenton Hill, but in areas such as nuclear waste isolation it may be of primary importance.

The permeabilities of six samples from the EE-2 drill hole at Fenton Hill have been measured as a function of effective confining pressure P_e (confining pressure minus pore pressure) at room temperature (23°C). P_e ranges from ~2 to 30 MPa. Permeabilities k in the 2- to 5-MPa range are generally in the 10^{-17} to 10^{-18} -m^2 range, whereas those near 30 MPa are in the 10^{-19}- to 10^{-20} -m^2 range.

The samples examined were 11743-3, 12854-6, 13461-2A, 13965-1, 14502-3, and 14964-1. The sample number to the left of the hyphen is the bore hole depth in feet. All of these samples except 12854-6 show some foliation. Three cores of 11743-3 cut in orthogonal directions were tested and despite the presence of foliation showed no dependence of permeability on direction. The data for these three cores are shown in Fig. 18. Permeability in all three directions is adequately described by the relation

$$k = \frac{2.12 \cdot 10^{-12}}{(1 + 447.1P_e)^{1.88}},$$

where k is in m^2 and P_e is in MPa. The permeability of this sample was measured only after P_e had been raised to ~30 MPa. This is also true of sample 13956-1; its permeability can be described by

$$k = \frac{3.78 \cdot 10^{-18}}{(1 + 0.327P_e)^{1.40}}.$$

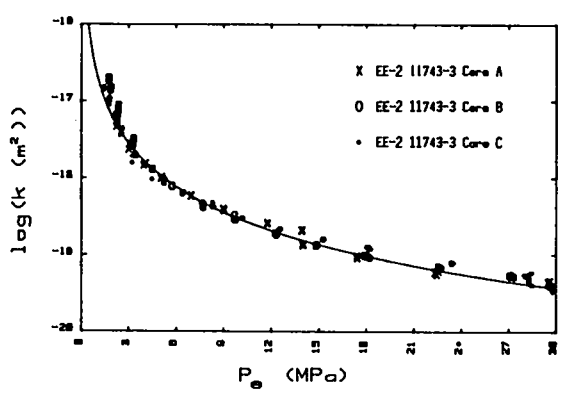

Fig. 18.
Permeability of EE-2 11743 as a function of effective confining pressure measured in three orthogonal cores.

It was noted that for this specimen the permeability did not increase below ~2 MPa.

In the remainder of the samples, permeability was initially measured with increasing P_e. These samples showed an irreversible change in permeability with increasing P_e. After pressurization to a P_e of 25-30 MPa, permeabilities measured at low P_e were as much as an order of magnitude lower than observed initially. This behavior is illustrated by the data for EE-2 13461-2A, which are shown in Fig. 19. It seems probable that the irreversible change in k is due to reduction of porosity, which was created by extraction of the sample from the bore hole and subsequent cooling. Apparently the laboratory permeabilities represent only upper bounds on *in situ* matrix permeabilities.

For these latter specimens k as a function of P_e has been fit only to those data obtained after maximum pressurization. These relations are:

for 12854-6,

$$k = \frac{8.31 \cdot 10^{-18}}{(1 + 0.222P_e)^{10.08}} + \frac{4.68 \cdot 10^{-20}}{(1 + 0.60P_e)^{1.80}},$$

for 13461-2A,

$$k = \frac{3.55 \cdot 10^{-16}}{(1 + 254.7P_e)^{0.94}},$$

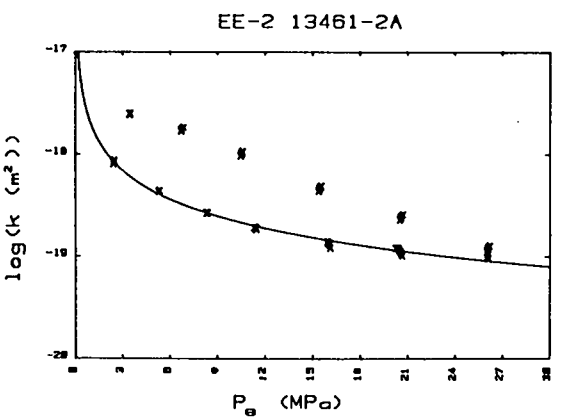

Fig. 19.
Permeability of EE-2 13461-2A as a function of effective confining pressure showing reduction of permeability with pressurization of the sample. Higher values of permeability were obtained upon initial pressurization of the sample, lower values upon depressurization.

and for 14502-3,

$$k = \frac{6.73 \cdot 10^{-17}}{(1 + 251.4P_e)^{0.90}} .$$

Only increasing P_e data were collected for 14961-1. It was similar to data for 13461-2A and 14502-3.

I. Element Transport in Solids: The Interaction of Water and Fenton Hill Granite (L. A. Blatz and C. E. Holley, Jr.)

In connection with the geothermal project at Fenton Hill we have studied the interaction of water with biotite-granodiorite rock (drill cuttings from the 9560- to 9570-ft level of EE-1 at Fenton Hill) at 198, 235, and 275°C. The rock had an approximate modal composition of 26% quartz, 36% plagioclase, 19% microcline, 12% biotite, and 7% other minerals.

The samples were shaken with varying degrees of vigor in Teflon, titanium, or various steel containers, all encased in steel bombs for 2, 4, 7, 16, 24, 48, and 96 h and more rarely for 8, 16, 32, and 65 days. In most cases the same rock samples were repeatedly extracted, usually five times, with fresh water for each extraction.

The quantities studied in the aqueous phase included the monomeric and total silica concentrations (by both silco-molybdate and atomic absorption analyses), the pH (at room temperature), and, less frequently, the (Na^+), (K^+), (Al^{+++}), (Ca^{++}), (Mg^{++}), (ΣFe), (F^-), and (Cl^-) concentrations.

Studies on the solid phase included weight changes after each extraction, some surface examination of the rock samples before and after extraction, and qualitative observation of the precipitates left on white micropore filters after filtration of the aqueous phases.

For 275°C, the concentrations of monomeric silica as a function of time and the number of extractions are shown in Fig. 20. A family of curves, one for each set of extractions, is obtained. Each curve has a different limiting slope at zero time. The rate law for the dissolution of silica was assumed to be

$$\frac{d(SiO_2)}{dt} = ak\,\{(SiO_2)_{sat} - (SiO_2)\} ,$$

where a is the ratio of the rock area to the fluid volume, k is the rate constant which equals f (T, rock composition, agitation rate, surface conditions, pH, etc.), $(SiO_2)_{sat}$ is the value of (SiO_2) obtained after a relatively long time

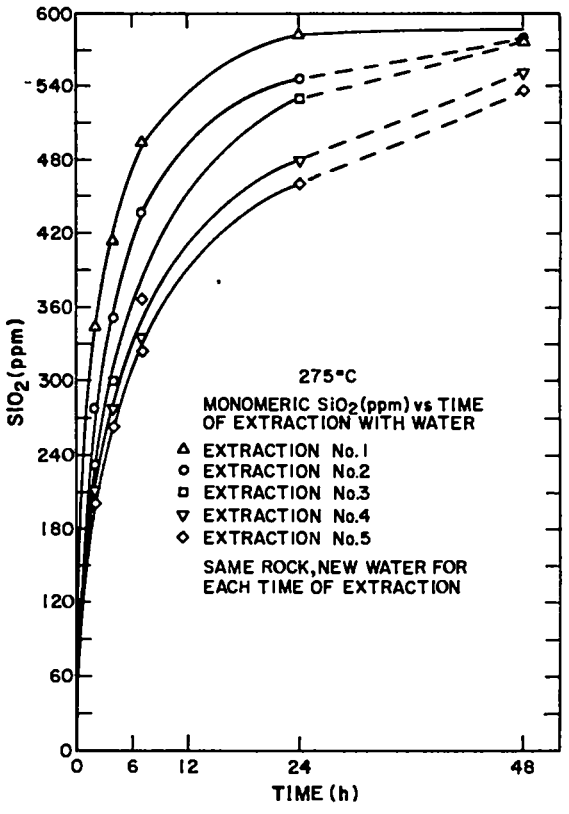

Fig. 20.
Monomeric silica vs time of extraction with water.

(590 ppm and 96 h for the data of Fig. 20), and (SiO_2) is the instantaneous silica concentration. The integrated form of this rate law is

$$\ln\left\{\frac{(SiO_2)_{sat} - (SiO_2)}{(SiO_2)_{sat}}\right\} = -\,akt .$$

Figure 21 shows the lines obtained for the first, third, and fifth extractions (to avoid unnecessary complexity in the figure) when the quantity on the left is plotted vs t for each set of extractions. It can be seen that the data for the shorter times, 2-7 h, follow reasonably well the straight line defined by the equation. However, the data for the longer times of 24 h and more depart markedly from the straight lines.

Several factors are involved in the observed behavior of this system. (1) Very fine particles (<1μm) are adsorbed on the rock particles, and these fine particles dissolve faster and more or less completely in the shorter times. (2) The rock surfaces contain sharp edges, corners, and other areas of greater reactivity that for the most part disappear in the shorter times. (3) The rate at

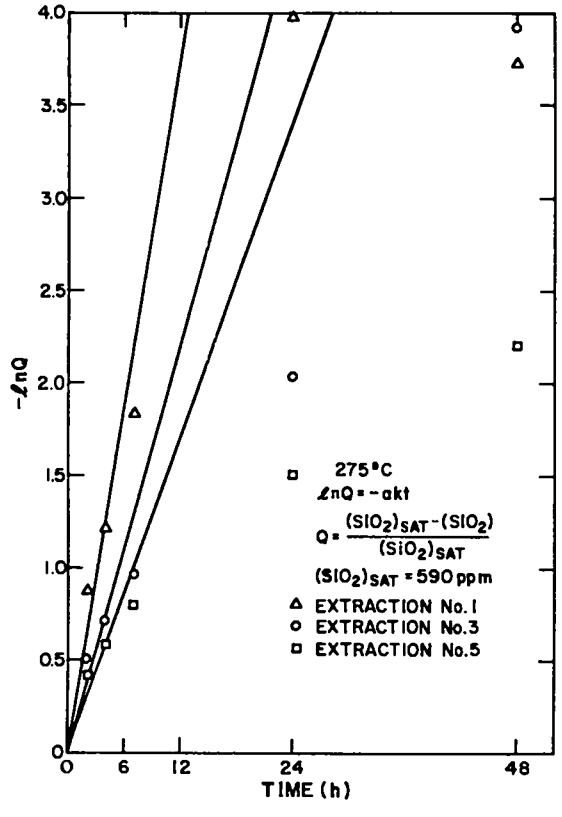

Fig. 21.
Data from Fig. 20 plotted according to the integrated rate equation given in the text.

which silica dissolves depends in part upon the OH^- concentration in the aqueous phase, and this quantity changes with time. (4) The rock surfaces may be at least partly coated with insoluble silicates or metal ions during the course of the reaction and/or coated with mineral alteration products so that the reactive surface area decreases with time. (5) The amount of rock present may decrease. After five 48-h extractions at 275°C, the amount of silica removed was 5.4% of the weight of the rock. If it all came from the quartz, between 15 and 20% of the quartz was removed. This decrease in the amount of quartz could itself explain much of the behavior at 48 h, although the effect on the surface area is not accurately known. However, at the shorter times the weight loss was much smaller, and the other factors must be involved.

The values of $(SiO_2)_{sat}$ obtained in the first extraction were within 5% of the values given by Morey, Fournier and Rowe[97,98] for the solubility of quartz and were within ~10% of the values given by Van Lier, Bruyn, and Oberbeek.[99] (Also see Iler.[100])

J. Amphiboles on the Join Pargasite-Ferropargasite (R. W. Charles)

The thermodynamic properties of a number of minerals as noted by Robie et al.[101] are at best incomplete. This observation is particularly true for complex, yet common, minerals, such as the amphiboles and micas. We are proposing to grow some of these minerals to obtain their enthalpies of formation. Our focus will be the fluoro-amphiboles and micas. Both are commonly found in solid solution with their OH end members. This paper is based on experimentally grown amphiboles in the series pargasite-ferropargasite and shows our capability to grow minerals and to determine some of their crystallographic properties.[102]

Amphiboles have been grown across the join $NaCa_2Mg_4AlSi_6-Al_2O_{22}(OH)_2-NaCa_2Fe_4AlSi_6$ $Al_2O_{22}(OH)_2$ on QFM and CCH_4 oxygen buffers to gain insight into the iron-magnesium substitution in an amphibole without the local charge imbalance caused by sodium in the M(4) site. Oxygen fugacity was found to have no effect upon the unit cell dimensions of amphibole. Unit cell parameters (C 2/m) for amphibole grown across the series are:

Composition	a(A)	b(A)	c(A)	β	v(A)³
Mg_4	9.892(1)[a]	17.941(2)	5.277(1)	105°33′(1)	902.2(3)
Mg_3Fe	9.904(1)	17.989(5)	5.291(2)	105°27′(1)	908.6(5)
Mg_2Fe_2	9.915(3)	18.031(7)	5.301(3)	105°24′(1)	913.6(1.0)
$MgFe_3$	9.930(5)	18.104(6)	5.320(2)	105°16′(1)	922.6(9)
Fe_4	9.953(5)	18.152(3)	5.330(2)	105°16′(2)	928.8(4)

[a]Parenthesized figures represent the estimated deviation (esd) in terms of least units cited for the value to their immediate left; thus 9.892(1) indicates an esd of 0.001.

No change in cell parameters is observed with temperature on a given buffer. The essentially linear trend indicates disorder of magnesium and iron in M(1), M(2), and M(3) sites. In all cases plagioclase and pyroxene were present in the charge. The amount ranged from a few percent to >30% without affecting the unit cell parameters of coexisting amphibole.

VI. INORGANIC CHEMISTRY

A. Small Molecule Chemistry

1. Alumina Catalyzed Isotope Exchange in CO (D. C. Moody, M. Goldblatt, B. B. McInteer, and T. R. Mills). Carbon-13 nuclear magnetic resonance spectroscopy has developed into an extremely powerful tool for the chemist. Thus, the demand for the isotope has increased rapidly. Fractional distillation of CO has proved to be a convenient method for ^{13}C enrichment up to approximately 94%. Interference by the various oxygen isotopes prevents direct enrichment beyond this. Isotope exchange or scrambling is thus an important step in the ultimate production of >99% ^{13}CO.[103] Although a variety of systems have been reported to promote this exchange, the great majority of the work has been performed with hot metal or metal-carbide filaments.[104] These systems are not readily adaptable to flow conditions where large volumes of gases are involved.

Previous studies at room temperature had found only slight activity for γ-alumina in the isotope exchange of CO. High catalytic activity had been observed in the more easily reduced systems such as the nickel, copper, and iron oxides.[105] At higher temperatures, however, we have found that γ-alumina is an excellent catalyst for this exchange and because it is not easily reduced, little or no CO_2 is formed.

Because ruthenium/alumina has been observed to an effective Fischer-Tropsch catalyst where the CO is activated toward reaction with hydrogen, we had expected that this would be a good catalyst for the isotope exchange in CO; and, indeed, we observed K's between 0.6 and 0.7 after 1 h at 500°C in a closed system. This K is defined as the following ratio of masses:

$$K = \frac{(28)(31)}{(29)(30)} \quad (28 = {}^{12}C^{16}O;\ 29 = {}^{12}C^{17}O,\ {}^{13}C^{16}O;$$

$$30 = {}^{13}C^{17}O,\ {}^{12}C^{18}O;\ 31 = {}^{13}C^{18}O)\,.$$

As complete exchange occurs, this should approach unity. However, because of varying amounts of ^{17}O in an enriched ^{13}CO, K's in excess of 0.9 are not observed. Much to our surprise, however, 99% γ-alumina was found to be an even better catalyst, yielding essentially complete exchange (K = 0.83) under the same conditions. Analytical data on this alumina did not indicate the presence of substantial amounts of impurities, such as iron and copper oxides that might be expected to catalyze the CO exchange. However, to minimize further the possibility that an impurity might be the active species in the exchange, an ultrapure grade of alumina (99.999%) was examined under the same conditions. Essentially identical results were obtained (K = 0.84).

For both ruthenium/alumina and alumina some preferential site exchange between oxygen in the catalyst and CO is observed. This phenomenon was observed earlier in the room temperature studies on alumina.[105] No indication of bulk oxygen exchange with the catalyst has been observed, however. Likewise, extremely small amounts of carbon appear to be deposited on the catalysts, and exchange with the carbon in the CO occurs. It is unlikely that these two mechanisms would account for all the isotope exchange that we are observing, and because no appreciable amount of CO_2 is formed, we feel that CO/CO_2 exchange is also not a major contribution.

The exact nature of the exchange process is thus unknown. But it is interesting that the exchange occurs readily on pure γ-alumina. Because this is the support of choice for many metal systems that are active in the conversion of CO/H_2 to hydrocarbons, one has to wonder what role the alumina might be playing in the overall reaction scheme, and whether some activation of the CO might not be coming from the support. Similarly, the use of zeolites as supports is becoming more commonplace, and although not as active as γ-alumina, molecular sieves have also been found to catalyze this exchange in CO.

The results of this study have been incorporated into the operation of the Los Alamos ICONs facility and a scrambler using γ-alumina has been operating continuously for months with no loss of activity.

2. Catalytic Reduction of SO_2. (D. C. Moody, R. R. Ryan, and K. V. Salazar) Many processes have been used with varying degrees of success for removal of SO_2 from flue gases. Quite a few more have been proposed. One type of process that seems quite attractive is the reduction of the SO_2 to sulfur. Numerous papers and

patents pertaining to this subject have appeared. Bauxite- and alumina-supported systems,[106] in particular, have received attention. A variety of reducing agents have been used, the most common of which are H_2, CH_4, and CO. Operating temperatures between 300 and 600°C are generally required, and substantial amounts of H_2S thus result from reactions of the sulfur produced with hydrogen. Thermodynamic and kinetic studies of this system suggest that temperatures much lower than 400°C should be used to minimize the H_2S formation.[107] In those cases where CO has been used as the reductant, COS formation often plagues the systems.

The present work examines the effect of using an extremely active hydrogenation catalyst to promote the reduction of SO_2 with H_2 at temperatures low enough to minimize H_2S formation. Ruthenium on γ-alumina was examined and found to be quite active at temperatures as low as 150°C. All experiments were performed under static conditions in an apparatus consisting of a 250-mℓ round bottom flask equipped with a greaseless stopcock connected to a manifold (~100 mℓ) with inlets for SO_2, H_2, and vacuum. Pressure drop was monitored as a measure of the reaction rate. These conditions are by no means optimum for this type of reaction, so the extreme activity observed for ruthenium/alumina is indeed remarkable. This reactivity can be calibrated somewhat by comparison to the reactivity of γ-alumina under the same conditions. The 0.5% Ru/Al_2O_3 shows good reactivity at 156°C (0.5 torr/min) whereas γ-alumina is essentially unreactive at this temperature (Table X). At temperatures where γ-alumina has appreciable activity (300°C, 0.2-0.3 torr/min), 0.5% Ru/Al_2O_3 is almost too reactive to get anything but an estimate of the rate (300°C, 0.2-0.3 torr/min), 5% Ru/Al_2O_3 was the most active of the catalysts tested and gave a reduction rate ~10 times faster than 0.5% Ru/Al_2O_3. Because the rate increased proportionally to the ruthenium percentage, 10% Ru/Al_2O_3 and ruthenium metal were tested. The surface-impregnated 10% Ru/Al_2O_3 catalyst showed only slight activity, whereas ruthenium metal had no activity as a catalyst for the reduction of SO_2 with H_2. Surface area differences for these catalysts limit the accuracy of the comparisons, especially for the ruthenium metal.

An important consideration in SO_2 reduction experiments where sulfur is generated is catalyst poisoning. A series of repeated runs using 0.5% Ru/Al_2O_3 showed a slow decrease in reaction rate. This decrease in rate, we feel, is a consequence of our static system, which allowed sulfur to drop back onto the catalyst and perhaps hinder gas contact. This hypothesis is not inconsistent with the return of 100% of the activity for this catalyst simply by heating under vacuum and subliming off sulfur. Under flow conditions we do not expect to experience any decrease in activity that would necessitate reactivation of the catalyst.

The data presented in Table XI indicate that the stoichiometry of the reactants (SO_2 and H_2) need not be controlled precisely. Clearly, some excess H_2 is desirable, but an acceptable rate is observed when stoichiometric

TABLE X

EFFECT OF Ru CONCENTRATIONS IN $Ru/\gamma\text{-}Al_2O_3$ CATALYSTS FOR SO_2 REDUCTION

SO_2 (torr)	H_2 (torr)	Temp (°C)	Catalyst	Pressure Drop (torr/min)
200	400	156	0.5% Ru/Al_2O_3	~0.5
200	400	200	0.5% Ru/Al_2O_3	~1.1
160	320	250	0.5% Ru/Al_2O_3	~3
160	320	300	0.5% Ru/Al_2O_3	~10-12
160	320	300	$\gamma\text{-}Al_2O_3$	~0.2-0.3
200	400	156	5% Ru/Al_2O_3	~4-5
200	400	156	10% Ru/Al_2O_3	<0.05
200	400	156	99.95% Ru metal	No reaction

TABLE XI

PERCENT SO_2 CONVERSION ON 0.5% Ru/Al_2O_3 AT 156°C AFTER 5-1/2 h

SO_2 (torr)	H_2 (torr)	SO_2 Converted to Sulfur (%)
50	550	>90%
100	500	~31%
200	400	~20%
400	200	~3%

amounts of SO_2 and H_2 are available. Because of the low temperature of operation (156°C), the reaction of sulfur with excess H_2 to yield H_2S does not occur at an appreciable extent even where a large excess of H_2 is available and >90% of the SO_2 has been consumed. Both characteristics would be particularly advantageous should such a system be applied directly to the removal of SO_2 from flue gases.

A number of other potentially reactive species are present in flue gases in additional to SO_2. Thus, a variety of experiments were performed to test the effects of such species as NO, CO, and CH_4 on the reaction under study. The reduction of NO with H_2 has been examined extensively, and Ru/Al_2O_3 not only catalyzes the reaction but promotes N_2 formation.[108] For comparison, this reduction was examined under our experimental conditions using 5% Ru/Al_2O_3, and then a mixture of NO, SO_2, and H_2 was examined. Reduction of both NO and SO_2 was observed to occur with a total pressure drop of 2-3 torr/min. The products obtained were N_2, S_8, H_2O, and a trace of N_2O, in addition to unreacted NO and SO_2.

The reaction of CO and SO_2 has also been studied quite extensively over a variety of catalysts.[109] Under our conditions even at 200°C, no appreciable reaction of CO with SO_2 was observed over 5% Ru/Al_2O_3. Because Ru/Al_2O_3 catalyzes the conversion of CO and H_2 to hydrocarbons (Fischer-Tropsch reactions) at moderate temperatures, the mixture of CO, SO_2, and H_2 was not examined. Methane, however, is a major product of this Fischer-Tropsch chemistry, so the reaction of CH_4 with SO_2 was studied. Again, numerous such studies over a variety of catalysts have been reported.[106,110] However, at 152°C under our experimental conditions, no reaction of CH_4 with SO_2 was observed over 5% Ru/Al_2O_3 catalyst. These data suggest that NO, CO, and CH_4 will not hinder the reduction of SO_2 with H_2 over Ru/Al_2O_3 under our experimental conditions. The Fischer-Tropsch reaction of CO and H_2, however, does present one complication that might arise should this catalyst be used directly in the reduction of SO_2 with H_2 in flue gas streams. The increased H_2 consumption would probably necessitate the removal of the CO from the NO and SO_2 before the reduction step with H_2.

In summary, Ru/Al_2O_3 is quite active as a catalyst for the reduction of SO_2 with H_2 to sulfur and water at temperatures low enough that H_2S formation is not a problem. The stoichiometry of reactants does not have to be precisely controlled. Poisioning of the catalyst has not proved to be a problem. Nitric oxide reduction occurs readily under the same conditions with no apparent complication arising from the simultaneous reduction of both NO and SO_2. These data suggest that this catalyst should be examined for possible direct application to desulfurization of flue gases.

3. Novel Reactivity and Structure of $Ru(CO)_2(\eta_2SO_2 \cdot SO_2)(PPh_3)_2$ (D. C. Moody, R. R. Ryan, and K. V. Salazar). Since our discovery of η^2-SO_2 bonding in transition metal complexes,[111] there has been considerable interest in this bonding mode and in the extent to which S-O bond activation actually occurs and whether it can be exploited in reaction chemistry studies.

In this regard, the complex $Ru(CO)_2(SO_2)(PPh_3)_2$ (Ref. 112) appeared quite interesting because a trigonal bipyramidal structure with an equatorial η^2-SO_2 was expected by analogy to the known structure of $RuCl(NO)(SO_2)(PPh_3)_2$ (Ref. 113). Reinvestigation of the infrared spectrum of $Ru(CO)_2(SO_2)(PPh_3)_2$ revealed υ(SO) peaks at 1105 cm^{-1} and 850 cm,$^{-1}$ which shifted to 1060 cm^{-1} and 815 cm^{-1} when the complex was prepared with $S^{18}O_2$. This pattern indicated η^2-SO_2 coordination,[111,114] and the extremely low frequency of the second υ(SO) peak suggested substantial S-O bond lengthening. These structural features have been verified through a single crystal x-ray diffraction study. The complex crystallizes in the monoclinic space group $P2_1/n$ with $a = 20.276(3)$, $b = 16.158(3)$, $c = 10.691(2)$, $\beta = 96.42(1)°$ and $D_c = 1.54$ g cm^{-3} for $Z = 4$ ($T = -60°C$). The structure was solved by Patterson and difference Fourier techniques and refined to $R = 0.035$ and $Rw = 0.035$ for 3976 reflections. As can be seen in Fig. 22, the

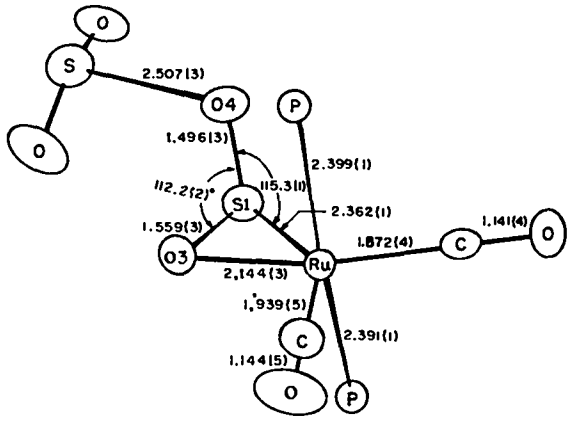

Fig. 22.
Structure of $Ru(CO)_2(\eta^2-SO_2\cdot SO_2)(PPh_3)_2$.

geometry around the metal is trigonal bipyramidal with an equatorial η^2-SO_2 similar to that reported for $RuClNO(\eta^2-SO_2)(PPh_3)_2$ (Ref. 113). The dihedral angle between the Si-O4 bond and the Si-Ru-O3 plane is 107.9° as compared to 110.3° in the latter complex. In addition, another SO_2 is coordinated to the terminal oxygen of the η^2-SO_2. The geometry about the ligand-bound SO_2 is similar to that observed in metal halide- (and pseudohalide-) bound SO_2, which characteristically exhibits rather long S-X distances and pyramidal geometry about the sulfur atom.[115] The 2.5-Å S-O distance is approximately midway between the sum of the van der Waals radii (3.25 Å) and the sum of the covalent radii (1.7 Å).[116] The interaction is thus best described with a bond order less than one, consistent with the extreme lability of this second SO_2 molecule. This lability necessitated the low-temperature structure determination and accounts for the failure to detect infrared peaks of the ligand-bound SO_2 in room temperature nujol mull spectra.

The bonding of η-SO_2 has been suggested to primarily involve π-donation from the metal to the LUMO of SO_2, which is antibonding with respect to the S-O bond and bonding with respect to the O-O vibration.[117,118] This type of interaction would be expected to lengthen S-O distances and increase the terminal oxygen basicity. It follows that such an increase in basicity should enhance coordination by Lewis acids like SO_2. The present complex exhibits the longest coordinated SO bond and the lowest υ(SO) value of any of the reported η^2-SO_2 complexes.[118]

During the synthesis and attempted crystallization of $Ru(CO)_2(SO_2)(PPh_3)_2$ an unusual reactivity was observed. The complex slowly reacts with excess SO_2 in the absence of oxygen to generate the bidentate sulfate complex $Ru(SO_4)(CO)_2(PPh_3)_2$ (Ref. 119), the same complex that is obtained on reaction with molecular oxygen,[112] plus PPh_3S and an unidentified ruthenium species, which appears to contain bridging carbonyls. The only products obtained in the presence of excess PPh_3 are $Ru(SO_4)(CO)_2(PPh_3)_2$ and PPh_3S. When liquid SO_2 is used as the solvent, the reaction rate is significantly enhanced. This is the expected result if coordination of a second SO_2 to the metal-bound SO_2 is important in the overall reaction scheme, and because the reaction ultimately involves oxygen transfer from one SO_2 to another, the importance of such an interaction would not be unreasonable.

We are currently varying the size and basicity of the phosphine ligands in an attempt to understand more completely this unique reaction. This is the first report of electrophilic attack on an η^2-SO_2 and indicates that further studies of η^2-SO_2 with Lewis acids may lead to interesting results.

4. Coodinatively Unsaturated Mo(0) and W(0) Complexes and Their Reactions with Small Molecules (G. J. Kubas and R. R. Ryan). The ability of transition metal complexes to achieve coordinative unsaturation nearly always plays a vital role in their function as homogeneous catalysts. Precious metal complexes are usually suitable in this regard but are, of course, inappropriate for applications where disposable catalysts are desired. We have focused our attention on more available Group 6 metals and have found the first example of a stable coordinatively unsaturated tungsten (0) complex, $W(CO)_3(PCy_3)_2$ (Cy = cyclohexyl), and only the second example of a 5-coordinate Mo(0) complex, $Mo(CO)_3(PCy_3)_2$ (Ref. 120). These complexes can be synthesized quite conveniently and can reversibly bind small molecules such as dinitrogen, ethylene, and hydrogen and irreversibly coordinate CO, SO_2, and nitrogen donor ligands (see Table XII).

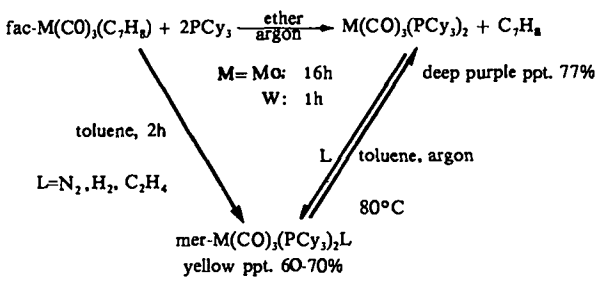

TABLE XII

RESULTS OF ADDITION OF SMALL MOLECULES TO $M(CO)_3(PCy_3)_2$ (M = Mo or W)[a]

Reversible Binding of:	Irreversible Binding of:	Anomalous Reactions with:[b]	No Reaction with:
N_2	CO	O_2	NEt_3
H_2	SO_2	NO	$NHEt_2$
C_2H_4	NH_3	CO_2	C_2F_4
H_2O	NH_2R	CS_2	cyclohexene
ROH	CH_3CN	CH_3NO_2	propylene
acetone	pyridine	CH_2Cl_2	butadiene
acetaldehyde	pyridine N-oxide	CH_3I	R_2O[c]
Et_2S	formaldehyde	HCl	furan
thiophene (M=W)	dimethyl-formamide	PhSH	tetrahydrofuran[c]
		PhC≡CPh	thiophene (M=Mo)

[a]In toluene solution at room temperature.

[b]Oxidative addition, disproportionation, or multiple product formation occurs.

[c]Weak interaction. Unstable complexes formed in ether or THF solutions.

Although these complexes have not yet proven to be active catalysts, a better understanding of zero-valent Group 6 complexes and their potential as catalysts is being achieved.

The bulky, mutually *trans* tricyclohexylphosphine ligands appear to be unique in stabilizing the 5-coordinate species and their adducts. (Many other phosphines of varying size and basicity have been tried without success.) Several other aspects of the complexes are also intriguing. Because of steric limitations imposed by the phosphines, $M(CO)_3(PCy_3)_2$ selectively coordinates only those ligands that "fit." Thus, NH_3 and NH_2Et readily add to the sixth position but $NHEt_2$ and NEt_3 do not. (See Table XII for further examples). One can consequently view $M(CO)_3(PCy_3)_2$ as a rather bulky Lewis acid. The complexes obtained with certain energy-related small molecules, such as hydrogen, alcohols, and water, are interesting because of their seemingly anomalous infrared absorptions. In the complexes containing the reversibly bound hydroxylic ligands, very low carbonyl stretching frequencies are observed, and the value of Δ (the difference between the second and third listed CO frequency) is much higher than that observed for non-hydroxylic ligands (Table XIII). Furthermore, the value of the lowest ν(CO) shifts upon deuteration (L = H_2O vs D_2O). Although the latter phenomenon may be explainable on the basis of mixing of δ(H_2O) with ν(CO), the possibility that there is a weak interaction between carbonyl and H_2O ligands on the same or neighboring molecules cannot be discounted. The water molecule

TABLE XIII

IR DATA FOR $W(CO)_3(PCy_3)_2L$

L	ν(CO)(cm^{-1})			Δ
SO_2	1994	1909	1873	36 cm^{-1}
H_2	1961	1843	1843	0
---	1946	1932	1811	21
NH_2Bu^n	1936	1811	1788	23
DMF	1925	1801	1775	26
py	1925	1791	1757	34
EtOH	1941	1806	1744	62
MeOH	1931	1821	1721	100
H_2O,$H_2{}^{18}O$	1928	1798	1705	93
HDO	1928	1798	1700	98
D_2O	1928	1798	1695	103

may also have split on coordination into hydrido and hydroxo ligands, for which there is precedence in certain Pt(0) complexes.[121] The υ(OH) region of the infrared spectrum of solid $Mo(CO)_3(PCy_3)_2(H_2O)$ contains four peaks in the 3300-3660 cm^{-1} range, further clouding the issue. If an unusual bonding situation is occurring, it would be relevant to the water gas shift reaction, $H_2O + CO \rightarrow H_2 + CO_2$.

The infrared spectrum of $W(CO)_3(PCy_3)_2(H_2)$ is unusual in that υ(W-H) (1568 cm^{-1}) is significantly lower than usually observed for metal hydrides, whereas δ(W-H) (951 cm^{-1}) is higher than normal. Coupled with the highly reversible nature of the H_2 binding, this raises the possibility that the H_2 is coordinated in an unprecedented molecular fashion, rather than as a dihydride. X-ray crystallography has revealed that the nonhydrogen ligands are arranged in an octahedral fashion, but the hydrogens could not be located in the sixth coordination site for either the molybdenum or tungsten complexes, even at -80°C. Neutron diffraction studies in collaboration with Phillip Vergamini of Los Alamos Group P-8 are in preliminary stages.

Finally, attempts were carried out to synthesize complexes similar to the above but containing *two* reversibly or weakly bound ligands, that is, $Mo(CO)_2(PCy_3)_2(H_2)_2$. If such species could be made, the possibility for catalytic behavior would be increased because of the presence of two potential open coordination sites. However, this is a very difficult synthetic problem, and so far coordinately unsaturated dicarbonyl complexes have not been obtained.

5. Molybdenum and Tungsten SO_2 Complexes (G. J. Kubas, G. Jarvinen, and R. R. Ryan). Our work on the coordination chemistry of SO_2 contributes significantly to knowledge of structure and bonding in transition metal complexes and has the potential to lead to much improved methods for controlling this major pollutant. The η^2(side-on) bonding mode of SO_2, first definitively characterized at Los Alamos National Laboratory,[122] has increasingly attracted our attention because this form of coordinated SO_2 has shown some intriguing examples of reactivity quite different from that presently known for the better studied η^1-planar, η^1-pyramidal, or bridging SO_2 coordination modes. Our study of molybdenum and tungsten complexes of SO_2 began in order to show that $Mo(CO)_3(phen)(SO_2)$ and $Mo(CO)_2(bipy)(SO_2)_2$ contain η^2-SO_2 ligands, whereas η^1-planar SO_2 was found in all previously structurally characterized SO_2 complexes of d^6 metals.[123] Subsequent work has shown that the bonding mode of the SO_2 in these octahedral d^6 systems is quite sensitive to the type and arrangement of the ancillary ligands. For example, the bonding mode of SO_2 varies with L in the complexes *cis, trans*-$Mo(CO)_2(PPh_3)_2(SO_2)L$: for L = pyridine or CH_3CN, an η^2-SO_2 is observed; for L = CO or p-tolylisocyanide, an η^1-SO_2 is found; and remarkably, for L = alkylisocyanide, η^1-planar *and* η^2-SO_2 are apparently formed. These observations were quite helpful in deriving bonding concepts for the η^1 vs η^2 geometries, which have been set forth in our recent review article on SO_2 complexes.[124]

Further studies have been carried out on these complexes. An x-ray crystal structure of $Mo(CO)_2(PPh_3)_2(CNCy)(SO_2)$ confirmed the coexistence of both η^1-planar and η^2-SO_2. This is the first example of room-temperature stable SO_2 linkage isomerism.[125] ^{31}P and ^{17}O solution NMR studies[126] were performed on these and related complexes to determine whether or not separate resonances for the bound and unbound oxygens of η^2-SO_2 could be distinguished. As can be seen from the data in Table XIV, only one major ^{31}P resonance was located for $Mo(CO)_2(PPh_3)_2(CNCy)(SO_2)$, even down to -50°C. Because infrared studies indicated that the η^1-*planar form predominates in solution*, the NMR peak at 44.8 ppm is most likely due either to the chemically equivalent *trans*- PPh_3 in this isomer or to an average signal for both isomers. For the CN(p-tolyl) analogue, which contains only η^1-SO_2, a resonance is observed at slightly lower chemical shift (the 24.3-ppm signal is apparently due to a decomposition product). The non-SO_2 containing complexes, $Mo(CO)_2(PPh_3)_2(CNR)_2$, gave resonances at ~10 ppm higher field. In regard to the ^{17}O NMR results, in all cases only one resonance was observed for complexes with isotopically enriched SO_2, even for $Mo(CO)_3(py)_2(\eta^2\text{-}SO_2)$, which may have been expected to give separate signals for the bound and unbound oxygens of the η^2-SO_2. Thus, exchange averaging of the oxygens is apparently occurring, even at −50°C. Interestingly, however, the chemical shift for the η^2 complex is much lower than for those with η^1-SO_2. To summarize, it appears that structural changes involving the coordinated SO_2 occur rapidly on an NMR time scale, and in certain cases little energy difference exists between the η^1 and η^2 forms of SO_2 binding.

TABLE XIV

^{31}P AND ^{17}O NMR DATA

Compound	$\delta(^{31}P)$ (ppm)[a]	$\delta(^{17}O)$ (ppm)[b]	^{17}O Signal Width at Half Height (Hz)
$Mo(CO)_2(PPh_3)_2(CNCy)(SO_2)$	+44.8	420	800
$Mo(CO)_2(PPh_3)_2[CN(p\text{-tolyl})](SO_2)$	+43.5, +24.3	416	800
$Mo(CO)_3(py)_2(\eta^2\text{—}SO_2)$		234	300
$Mo(CO)_2(PPh_3)_2(CNCy)_2$	+54.3		
$Mo(CO)_2(PPh_3)_2(CNBu^t)_2$	+54.2		
$Mo(CO)_2(PPh_3)_2[CN(p\text{-tolyl})]_2$	+53.3		

[a] CH_2Cl_2 solutions. Reference: Me_3PO_4.

[b] CH_2Cl_2 solutions of complexes with isotopically enriched SO_2 (33% ^{17}O). Reference: H_2O. For free SO_2, $\delta = 512$ ppm.

The first example of SO_2 coordinated to metals by way of all three of its atoms, $[Mo(CO)_2(PPh_3)(py)(SO_2)]_2$, has been synthesized. It contains bridging η^2-SO_2 (Fig. 23) and forms in CH_2Cl_2 solution from *cis, trans*-$Mo(CO)_2(PPh_3)_2(py)(\eta^2\text{-}SO_2)$, which apparently first undergoes rearrangements to a *cis*-PPh_3 isomer and then loses a phosphine and dimerizes. The basicity of the previously terminal oxygen atom (O4) is apparently substantial, since the dimer is not readily cleaved by pyridine. Phosphine substitution occurs instead to give $[Mo(CO)_2(py)_2(SO_2)]_2$. Experiments have been carried out to determine the reactivity of the terminal oxygen of η^2-SO_2 coordinated to Mo(0) and W(0). Use of reagents such as BF_3 and $MeSO_3F$ (methylating agent) has thus far led to extensive decomposition of the complexes, making it difficult to ascertain the nature of the reactions. Experiments involving less reactive Lewis acids are planned.

Our attempts to synthesize a phosphine analog of the complexes *fac*-$Mo(CO)_3(N\text{-}N)(\eta^2\text{-}SO_2)$ (N-N = phenanthroline and bipyridine) using the bidentate phosphine bis (1,2-diphenylphosphino)ethane (dppe) yielded the interesting chemistry outlined below.

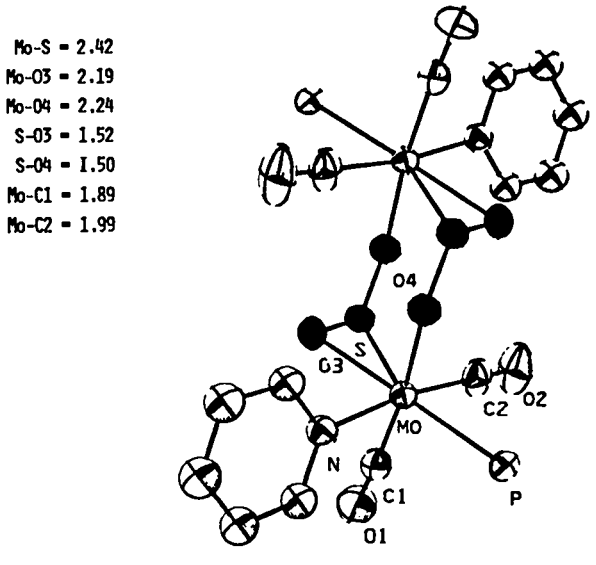

Fig. 23.
Molecular structure of $[Mo(CO)_2(PPh_3)(py)(SO_2)]_2$. (Phenyl groups have been omitted for clarity.)

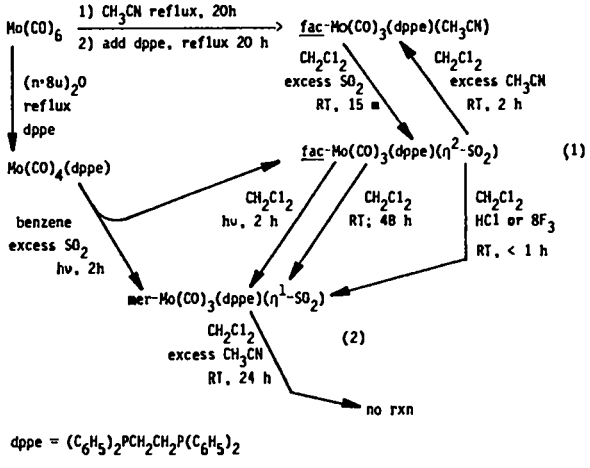

dppe = $(C_6H_5)_2PCH_2CH_2P(C_6H_5)_2$

The η^2-SO_2 complex *fac*-$Mo(CO)_3(dppe)(\eta^2$-$SO_2)$ (1) initially formed from the reaction of excess SO_2 with *fac*-$Mo(CO)_3(dppe)(CH_3CN)$ is gradually converted in solution to the meridional isomer (2), where the SO_2 adopts an η^1-planar bonding mode. This is another example of the interconversion of the η^1-planar and η^2-SO_2 geometries and the first where geometrical isomers of a complex show different modes of SO_2 bonding. The η^2-SO_2 ligand in (1) is readily displaced by other ligands, including CH_3CN as shown, to give *fac*-$Mo(CO)_3(dppe)L$ complexes. By contrast, the η^1-SO_2 ligand in (2) is much less labile. The complex (2) presumably represents a more thermodynamically stable arrangement of the ligands around the metal atom. The photochemical reaction of $Mo(CO)_4(dppe)$ and SO_2 yields primarily complex (2), but a small amount of (1) is also present. Because (1) has been shown to be photochemically converted to (2) at a moderate rate, the initial product of the photochemical reaction of $Mo(CO)_4(dppe)$ and SO_2 may also be (1).

Our previous work on η^2-SO_2 complexes has indicated that the terminal oxygen possesses considerable basicity. An attempt to protonate the terminal oxygen of (1) with a slight excess of HCl led to rapid isomerization to (2). A similar rapid isomerization occurred upon addition of BF_3, another Lewis acid, to (1). The reason for the acid catalysis is not clear. The rate-determining step in the isomerization would not appear to be dissociation of the η^2-SO_2 ligand because substitution of the η^2-SO_2 by excess CH_3CN, which presumably involves a rate-determining dissociation of SO_2, proceeds much faster than the isomerization. Therefore, the presence of the acids must increase the rate of some other process involved in the isomerization. A variety of mechanisms can be proposed for the isomerization of (1) to (2) involving dissociative or nondissociative processes, but there is no basis now for favoring one mechanism over another. It will also be of interest to determine if the Lewis acid catalysis is specific to the SO_2 complex (1) or occurs more generally for other ligands.

B. Actinide Chemistry

1. Uranium(V) Fluoride Chemistry (P. G. Eller, G. W. Halstead, and M. P. Eastman*). In connection with the investigation of organo U(V) compounds, we have also been developing the chemistry of U(V) fluorides. Our entry to this field was the investigation of the thermal reduction reaction:[127]

$$UF_6 + SO_2 \xrightarrow{\Delta} SO_2F_2 + \alpha\text{-}UF_5 + U_2F_9 + U_3F_{13} + \cdots .$$

At an appropriate temperature it was found that excellent single crystals of the long known compounds α-UF_5 and U_2F_9 could be obtained. Single-crystal x-ray diffraction studies were carried out to verify the structures deduced on the basis of x-ray powder diffraction studies. A linear chain of UF_6 octahedra with bridging fluorides forms the basic structure of α-UF_5, whereas U_2F_9 has a three-dimensional bridge structure with the basic uranium coordination of a tricapped trigonal prism. Microspectrophotometry measurements on U_2F_9 showed the presence of both U(IV) and U(V) and thus indicated that U_2F_9 should not be considered to have a delocalized, intervalence electronic structure.

We also developed a large-scale synthesis of β-UF_5 by the photolysis of UF_6 in the presence of SO_2 or CO (Refs. 128,129).

$$UF_6 + \tfrac{1}{2}\,CO \xrightarrow{h\nu} \beta\text{-}UF_5 + \tfrac{1}{2}\,COF_2 .$$

The ready availability of multigram quantities of β-UF_5 allowed us to carry out an extensive investigation of the behavior of β-UF_5 in more than 50 nonaqueous solvent systems.[130] It was thus possible to show that β-UF_5 possesses a fairly extensive chemistry in selected coordinating nonaqueous solvents. A predominant reaction in such systems is autoionization to give UF_6^- anions and solvated UF_4^+ cations; that is,

$$2UF_5 + xDMF \longrightarrow UF_6^- + UF_4(DMF)^+_x .$$

The presence of the product species was definitively shown by near ir-visible and ir spectrophotometry, EPR, conductivity, and elemental analyses. An example of the identification by near ir-vis spectrophotometry of UF_6^- in solutions of β-UF_5 in dimethylsulfoxide (DMSO) and dimethylformamide (DMF) is shown in Fig. 24.

The availability of milligram quantities of β-UF_5 also allowed an improved synthesis of uranium pentaethoxide[128,129] as well as other desired species, such as $(PPN)(UF_6)$.[130,131] The latter species is significant

*University of Texas at El Paso, Texas.

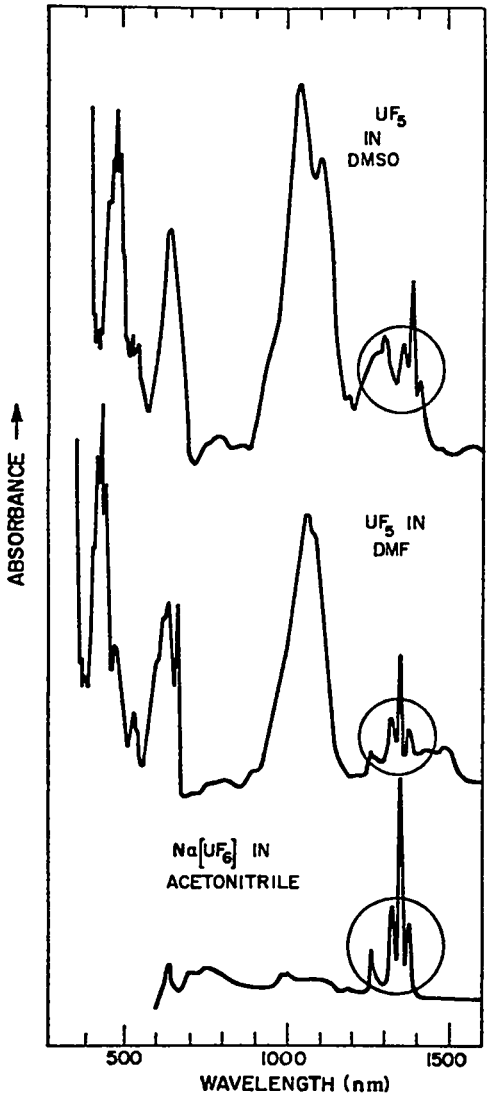

Fig. 24.
The near ir spectrum of β-UF_5 and $Na[UF_6]$ in various nonaqueous solvents.

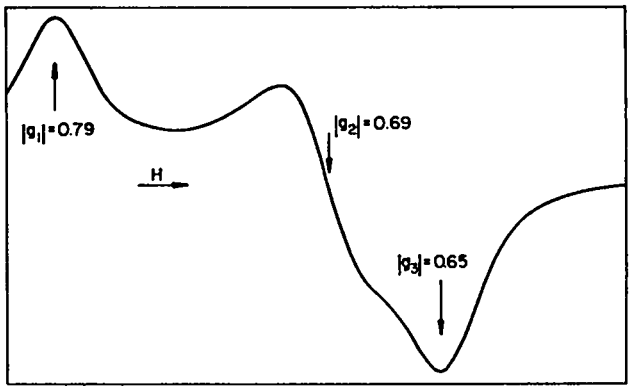

Fig. 25.
The EPR spectrum of polycrystalline $[PPN](UF_6)$ at 100°K (ν = 9.049 GHz).

because we feel that it may be isostructural with the unknown protactinium analog. Note that MUF_6 species have been shown to contain either six or eight coordinate uranium, depending upon the cation, whereas the few $MPaF_6$ compounds that have been studied all have a protactinium coordination of eight. Another unusual aspect of $(PPN)(UF_6)$ is that near ir-vis and ir spectra indicated the presence of an octahedral UF_6^- anion with little or no distortion, whereas the EPR spectrum exhibited an orthorhombic g-tensor (Fig. 25) almost unprecedented for an actinide compound.[131] A single crystal x-ray study verified the existence of a UF_6^- anion that is octahedral within experimental error and suggested that the observed EPR spectrum should be attributed to the low (triclinic) site symmetry and/or very small distortions of the UF_6^- octahedron.

2. Uranium(V) Alkoxides (P. G. Eller and P. J. Vergamini). An ongoing program is concerned with synthesis and characterization of interesting compounds containing pentavalent uranium, one of the less studied valence states of uranium. Uranium(V) alkoxides have been known since the Manhattan Project,[132] but recent studies have expanded greatly the knowledge of these interesting compounds.[133] $U(OC_2H)_5$ and $U(OC_2H_5)_6$ are the only known uranium compounds that are *liquid* at ambient conditions. Our investigations[134] commenced with the preparation of several new uranium(V) reactions with uranium pentaethoxide:

$$U(OC_2H_5)_5 + \text{xs } HOR_f \rightarrow$$

$$U(OR_f)_x(OC_2H_5)_{5-x}(HOC_2H_5)\ ,$$

$x = 4$, $R_f = C_4F_9$ or $CH(CF_3)_2$,

$x = 5$, $R_f = C_6F_5$.

The new compounds were characterized by chemical reactivity, analyses, variable temperature NMR (^{13}C, ^{19}F, ^1H), and, in the case of $U(OC_4F_9)_4(OC_2H_5)(HOC_2H_5)$, single-crystal x-ray diffraction. The new compounds possess moderate thermal stability but are not unusually volatile. The compounds' lack of volatility despite their highly fluorinated nature may be attributed to their large molecular weights.

A particularly useful result of our investigation was the demonstration that high-resolution ^{13}C, ^{19}F, and ^{1}H NMR can be useful tools for characterizing U(V) compounds. Despite the paramagnetism of these f^1 systems, reasonable resonance linewidths are observed and the spectra are amenable to interpretation. For example, consider the ^{13}C NMR spectrum of $U(OC_6H)_5$, shown in Fig. 26. As expected, at 15°C four resonances are observed with linewidths clearly reflecting the distances of the particular resonating nuclei from the paramagnetic uranium. As the temperature is lowered, the spectrum becomes more complex because of cluster formation and/or freezing out of geometrically inequivalent phenoxy groups.

By ^{1}H NMR and solution molecular weight measurements, nonfluorinated derivatives such as $U(OC_2H_5)_5$ and $U(OC_6H_5)_5$ are believed to be polynuclear.[132,133] However, our single-crystal x-ray study revealed a *monomeric cis*-octahedral structure for $U(OC_4F_9)_4(OC_2H_5)(HOC_2H_5)$. Although the "ethanol" proton was not located, it is assumed to be hydrogen-bonded between the *cis*-ethoxides. Unusual U-O-C angles are present, 173° for U-O-C(C_4F_9) and 158° for U-O-C(C_2H_5), consistent with the large steric congestion anticipated for this molecule and the lack of total ethoxide substitution by the much larger perfluoro-t-butoxy groups.

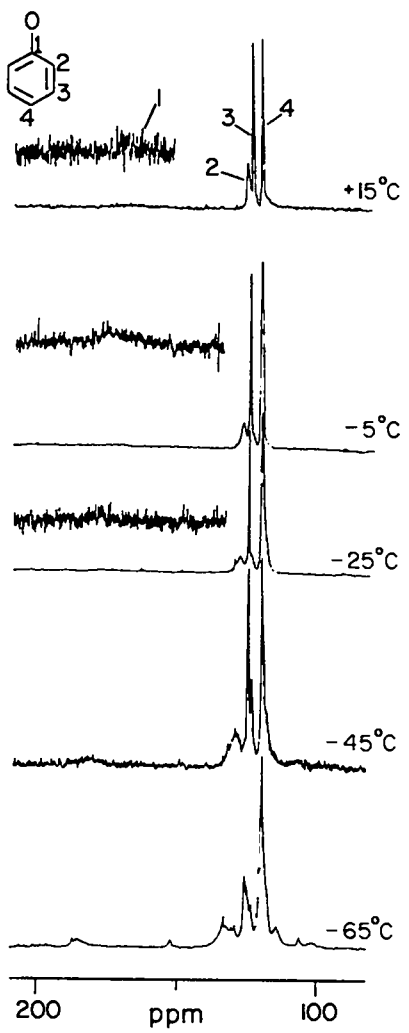

Fig. 26.
The C^{13} NMR spectrum of uranium pentaphenoxide.

Some reaction chemistry has also been explored for uranium(V) alkoxides, and an improved synthesis of uranium pentaethoxide has been developed.[135,136]

$$UF_5 + 5\ NaOC_2H_5 \rightarrow 5\ NaF + U(OC_2H_5)_5\ .$$

3. Interactions of 4f and 5f Cyclopentadienides with SO_2 (P. G. Eller). The objective is to search for novel metal-SO_2 interactions by using oxophilic 4f and 5f complexes as substrates. Such species might well favor oxygen and side-on binding of the SO_2 and perhaps reactions in which S-O bond activation occurs. Thus far we have studied the intereactions of several 4f and 5f cyclopentadienides with SO_2 (Ref. 137). An example is:

$$Cp_3UCl \xrightarrow{xs\ SO_2} Cp_3UCl\cdot 2\ SO_2\ ,$$

where Cp = cyclopentadienyl.

The substrate does, in fact, bind 2 moles of SO_2, but the product has properties unexpected for a simple adduct. The product is nearly air stable, contains irreversibly bound SO_2, is insoluble in common organic solvents and thus probably is polymeric, and has an infrared spectrum which suggests a radical change in the bonding of at least some of the Cp groups and the absence of free S-O groups. The compound is formulated as the O,O′-sulfinate $CpU(CpSO_2)_2Cl$ that results from insertion into M-Cp groups (Fig. 27). Similar results were obtained with Sm, La, and Th cyclopentadienides:

$$Cp_3Sm \xrightarrow{xs\ SO_2} Cp(CpSO_2)_2Sm\ ,$$

$$Cp_3La \xrightarrow{xs\ SO_2} Cp(CpSO_2)_2La\ ,$$

and

$$Cp_4Th \xrightarrow{xs\ SO_2} Cp(CpSO_2)_3Th\ .$$

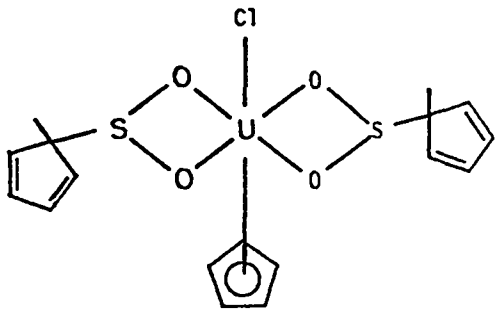

Fig. 27.
Proposed structure of "$Cp_3UCl \cdot 2SO_2$". Polymeric structures involving bridging sulfinate groups are also possible.

Thus, 4f and 5f cyclopentadienides in general appear to undergo Cp insertion reactions with SO_2. Possibly the ionic nature of the Cp bonding in the organometallic precursors and/or the oxygen-loving nature of the 4f and 5f metals determine the course of these reactions. Note that among the hundreds of known transition metal cyclopentadienides, Cp insertion has been reported only with certain Zr compounds (Table XV).[138]

4. Actinide Extractant Chemistry (S. M. Bowen* R. T. Paíne*, C. F. Campana*, P. G. Eller, and N. C. Schroeder**). The compound dihexyl-N,N-diethylcarbamylmethylenephosphonate (DHDECMP) has been useful in partitioning +3 valent actinides out of highly acidic high-level liquid waste (HLLW) from reprocessing commercial light water reactor (LWR) fuels.[139]

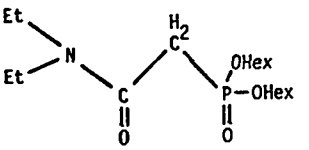

DHDECMP has been reported[139] to extract Am(III) as $AmL_2(L\text{-}H)(NO_3)_2$, where L-H is a deprotonated DHDECMP with a postulated "acac" type binding to Am (III), that is,

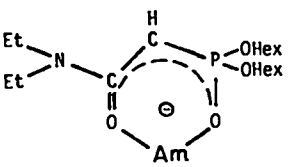

In conjunction with R. T. Paine and co-workers at the University of New Mexico and N. C. Schroeder at the Idaho Falls National Engineering Laboratory, we have attempted to crystallize complexes of DHDECMP (and similar derivatives), in the belief that structure determinations on such compounds will aid interpretation and design of improved extraction systems, for which the true extracted species are rarely (if ever) known.[140]

We have succeeded in crystallizing and determining the single-crystal structure of mercury(II) complexes of the deprotonated DHDECMP ligand Hg-(DHDECMP-H)(NO_3) and the diethyl analog Hg(DEDECMP-H)(NO_3). In contrast to the O,O bonded structure proposed for the extracted Am(III) species, in the Hg(II) compounds the primary metal-ligand interaction is through the methine carbon atom. A primary Hg-O(NO_3) is also present, and secondary interactions to phosphoryl and amide oxygens from a neighboring molecule lead to formation of dimeric units. A view of the structure of the diethyl complex, in which the central coordination geometry was found to be identical to that in the dihexyl compound, is shown in Fig. 28. Very recently, the x-ray crystal structure of a Th(IV) complex of DEDECMP was carried out, and O,O′ binding, as proposed for the extracted AM(III) species mentioned above, was formed.† Thus, these

*University of New Mexico.
**Idaho Falls National Engineering Laboratory.

TABLE XV

REACTIONS OF SO_2
WITH SOME M-Cp COMPLEXES

No Reaction with Cp	Cp Insertion
Cp_2Fe	Cp_3Sm
Cp_2TiCl_2	Cp_3La
Cp_2HfCl_2	Cp_4Th
$CpTiCl_3$	Cp_3UCl
$CpRh(C_2H_4)(SO_4)$	$Cp_2Zr(CH_3)Cl$
$CpMn(CO)_2(SO_2)$	$[Cp_2ZrCl]_2O$
$(C_6H_6)Cr(CO)_2(SO_2)$	$Cp_2Zr(CH_3)_2$
	Cp_4Zr

†This information was provided by R. T. Paine.

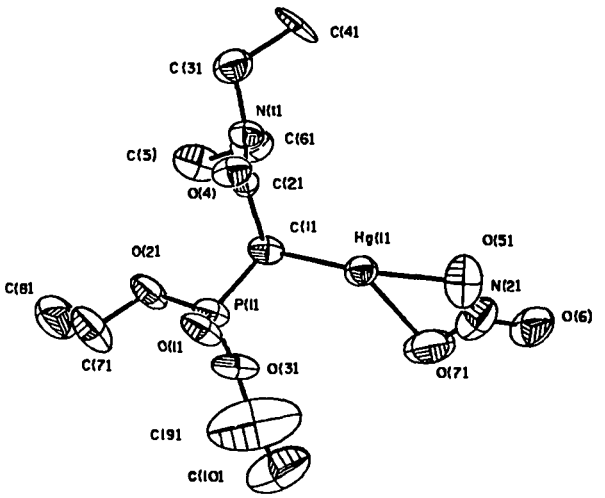

Fig. 28.
The structure of the UF_6^- anion in [PPN](UF_6).

phosphonate ligands indeed possess an unanticipated degree of binding complexity, and further structural work is mandated.

5. Valence, Size, and Coordination Demands of Actinides as Applicable to Storage in Synthetic Materials (R. A. Penneman). Actinides, and especially americium, are the major long-term contributors to nuclear waste hazards. From about 500 years to 50 000 years, ^{241}Am and ^{243}Am lead all other elements.[141] Actinide ions are Chatt-Ahrland Class A cations and strongly attract hard anions such as F^- and $O^=$. There is no doubt that the actinide 3+ and 4+ ions can be incorporated into cavities of the right (large) size, which can provide oxide coordination of eight or greater. It still must be determined whether radiation effects on the actinide valences and on the surrounding lattice will affect actinide retention in a nonleachable state.

There are many suggested matrices that can act as hosts for actinide storage: glass, cement, various synthetic minerals, etc. All of these share a common basis; that is, the actinide is *always* coordinated by oxygen. The nearest neighbors surrounding, for example, an Am^{4+} ion are oxygens, usually derived from a regular polygon. Extremes range from simple oxide ions, as those in ThO_2, to oxygens primarily bound to representative elements such as silicon (silicate) and phosphorous (phosphate) and include oxygens shared with small, highly charged transition elements such as titanium (titanates) or molybdenum (molybdates). In all but the simplest structures, tetrahedra, octahedra, or more complicated oxygen polyhedra are packed around cavities that can accommodate ions of various sizes and charges.

The ions of neptunium, plutonium, and americium have different valences and, hence, different sizes. It is extremely important in regard to these elements to consider the effects of valence, size, and concomittant oxygen coordination number requirements (cavity size and geometry). The reasons are several.

(1) Alpha radiation and recoils can cause metamictization of the host material,
(2) reduction of the actinide guest ion by radiation effects will cause lattice expansion,
(3) oxidation of the actinide guest ion by radiation effects will cause lattice contraction, and
(4) there can be changes in leachability of the actinide as consequences.

Because actinide ions are the largest for their charge types in the periodic system of elements, it is useful to start with this consideration.

In Fig. 29 are shown *differences* in radii (for example, Th^{4+} is 0.24 Å larger than Zr^{4+}).[142] Even though the radius of the higher actinides decreases by way of the 5f contraction, the Bk^{4+} ion (Bk is one past the series midpoint) is still 0.06 Å larger in radius than its lanthanide (rare earth) counterpart, terbium.

Indeed, when people focus solely on electronic configuration to select the lanthanide congener of an actinide (say europium for americium), they often fail to notice the size discrepancy. For the early part of the two series, it is appropriate to displace the lighter 4f series ~3 elements to the right to approximate ion-size equality. Figure 30 shows this point and compares La^{3+} with U^{3+} and Pr^{4+} with Pu^{4+}. Even so, the oxidation chemistries of the two elements will differ widely; for example, Pr^{4+} is a far more powerful oxidant than Pu^{4+} or Am^{4+} and is about equal to Cm^{4+}.

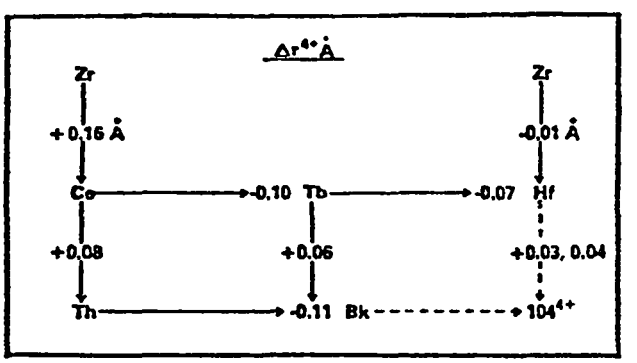

Fig. 29.
Trends in size differences of tetravalent elements.

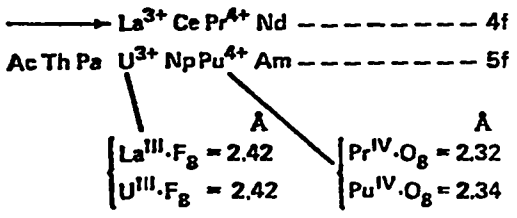

Fig. 30.
For approximate size equivalence, 4f/5f: Slide 4f series ~3 elements to right.

Most of the host structures proposed to accommodate guest actinides have not been studied with actinides actually present, and all are deficient in that no studies have been conducted with the actinide in different valence states, for example, +3, 4, 5, or 6.

In the absence of data we can calculate the effect of valence changes by using the equations of W. H. Zachariasen, which relate bond to bond strength and are based on well-established structural data.[143] Thus, while one intuitively feels that a valence change of +3 to +4 in the same oxygen coordination, say 8, would cause bond shortening, Zachariasen's formulas provide quantitative figures.

Zachariasen's equations are of the form

$$D(s) = D_1 - B \ln(s) \quad ,$$

where D_1 is the bond length normalized to unit bond strength and (s) is the bond strength at bond length D(s).[142] For a simple example, in ThO_2 there is cubic coordination and Th^{4+} is bound to eight equivalent oxygens. For $Th^{4+} - O_8$, $s = 4/8 = 0.5$; for Th, $D_1 = 2.181$. $B = 0.35$ Å for $s \leqq 1$. Thus,

$$D(s) = 2.181 - 0.35 \ln(0.5) = 2.42 \text{ Å}.$$

If we put La^{3+} in place of Th^{4+} and remove oxygens statistically to allow just six oxygens per La^{3+} vs the eight for Th^{4+}, the La^{3+}-O_6 distance is 2.43 Å, nearly identical to that of Th^{4+}-O_8 [obtained from $D(s) = 2.20 - 0.339 \ln(0.5)$].[143]

In the case of americium, the effect of valence and oxygen coordination number is demonstrated in Table XVI.

The major fact to be observed from the table is that, at the same coordination, there is a major *increase* of ~0.15 Å in the M-O bond distance on reduction of a tetravalent actinide to the trivalent state. Such a change could well be disruptive, encouraging ion migration and expulsion from the host.[144]

TABLE XVI

AMERICIUM-OXYGEN BOND DISTANCES

Coordination Number	Bond Distances (Å) Trivalent	Tetravalent
8	2.47	2.33
10	2.55	2.40
12	2.62	2.47

In the case of a simple structure such as ThO_2, oxygen loss can allow accommodation. However, when the oxygens are bound to other elements (as in silicate and phosphate), such oxygen migration and loss are not possible. Thus, reduction of M^{4+} to M^{3+} must be accompanied by a localized internal pressure in the lattice, trying to expand it to allow for attainment of the now-longer equilibrium M^{3+} —O bond distance demanded by the lowered bond strength.

When equilibrium bond distances can be attained, oxygen coordination increases the stability of the tetravalent state over the trivalent. Information on stabilization of the actinide tetravalent states over their trivalent states can be derived from the formation of heteropolytungstates and molybdates,[144] whose structures provide cavities in the oxide matrix that can accommodate M^{3+} and M^{4+} ions. Studies have shown that Pu(III) and Pu(IV) are both complexed in solution by heteropolytungstates[145] but that Pu(IV) is much more stable[146] (as would be expected from the known chemistry of plutonium). Another study[147] has shown that Cm(IV) in aqueous polytungstate solution is completely reduced in a zero-order reaction to Cm(III) in 1.5h when the alpha-emitter ^{244}Cm is used. The studies of polytungstates and polymolybdates were conducted in the presence of water and suggest an increased stabilization of M^{4+} over M^{3+} of ~1 V. Because the Pu^{3+}/Pu^{4+} couple is ~1 V, it is clear that Pu^{4+} will be greatly stabilized. The comparable americium couple is ~—2.4 V, so that stabilizing tetravalent americium by 1V will still leave it unstable towards reduction to Am^{3+}. It must

be determined whether Am^{3+} or Am^{4+} will be the stable form, especially where radiation is present to eject electrons into different lattices. We predict that Pu^{4+} will be very stable and Am^{4+} metastable, but that Cm^{4+} will be unstable. There is one catch: little is known about the relative stabilities of the various oxidation states of neptunium, plutonium, americium, and curium, when incorporated in *anhydrous* minerals in the presence of ionizing radiation. Their stabilities will be strongly influenced by specific site size and also the presence or absence of other reducible transition elements, for example, molybdenum, iron, etc.

6. Actinide Molybdates (P. G. Eller, T. Cremers, R. A. Penneman, and C. Herrick). The dissolution of zirconium-clad nuclear fuel rods in high-acid media can lead to varying amounts of plutonium-containing insoluble residues (up to several percent plutonium content).[148,149] The possibility has been considered that fission product molybdenum can allow formation of heteropolymolybdates that can incorporate plutonium into large heteropoly cages (see Fig. 31).[150] Some structural and synthetic information is available on actinide-molybdates, but for the most part the area is chaotic. Our objective is to prepare and structurally characterize selected actinide molybdate phases, with the hope of gaining better insight into the formation of the insoluble plutonium-containing phases mentioned above.

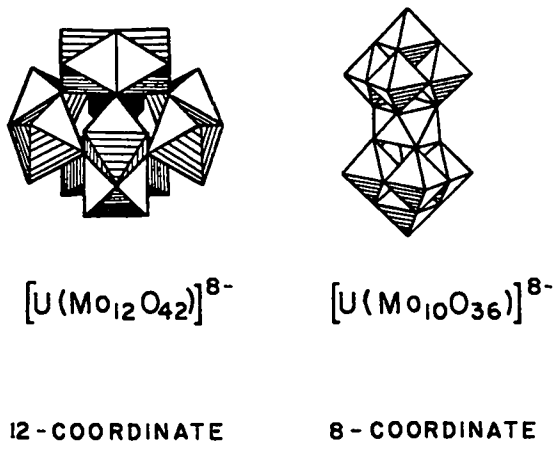

Fig. 31.
Sketches of the heteropoly uranium molybdates $[U(Mo_{12}O_{42})]^{8-}$, which contains 12 coordinate uranium,[a] and $[U(Mo_{10}O_{36})]^{8-}$, which contains 8 coordinate uranium.[b] The octahedral units represent octahedral (MoO_6) polyhedra.

Our recent successful attempt in this area[151] produced a "low-temperature" phase of uranium molybdate, $U(MoO_4)_2$, by the following reaction:

$$UO_2 + 2MoO_3 \xrightarrow{1200°C} U(MoO_4)_2 .$$

A single crystal selected from the solidified melt was examined by single-crystal x-ray diffraction and shown to possess a structure (Fig. 32) with sheets containing uranium, molybdenum, and oxygen connected by short, nearly linear U-O-U linkages (U-O = 2.059 Å). Uranium-oxygen bond lengths in the sheets are 2.39 (1)Å, 2.32 (2)Å, and 2.20 (2)Å. Molybdenum-oxygen bond lengths range from 1.869 to 2.002 Å within the plane and are 1.674 and 2.438 Å between the sheets. Space Group: Orthorhombic Pban, a = 20.069(4), b = 7.328(1), c = 4.1148(7)Å, and R = 0.058 for 954 reflections with $I \geq 2\sigma(I)$. This structure differs radically from the high-temperature α form of UMo_2O_8, in which MoO_4 tetrahedra (Mo-O = 1.62 - 1.96 Å) bridge between UO_6 octahedra (U-O = 2.12 - 2.64 Å).[152] The relatively large difference in volume/formula unit, 177.0 $Å^3$ for the

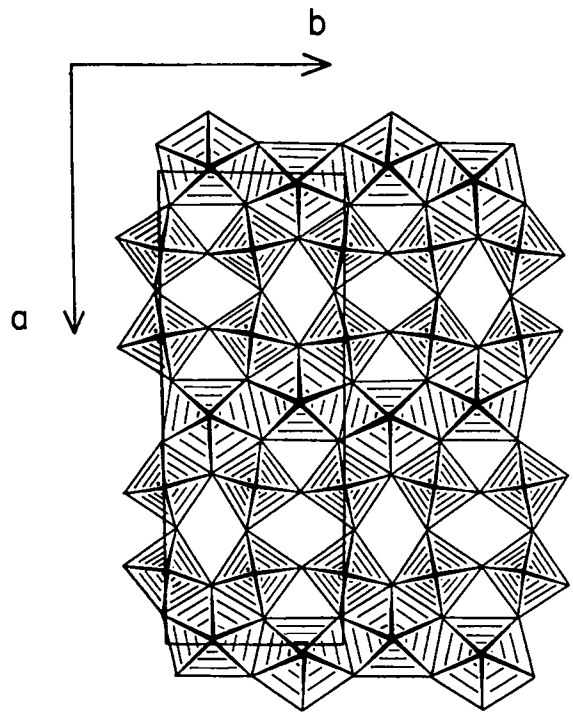

Fig. 32.
The structure of the low-temperature (orthorhombic) form of UMo_2O_8.

α form and 151.3 Å^3 for the β form, also is consistent with the lower coordination numbers for the α form.

A few other phases, both synthetic and naturally occurring, are listed in Table XVII. A number of other uranium-molybdenum oxide phases are also known.

An interesting aspect that the β-UMo_2O_8 structure shares with many seemingly dissimilar oxouranium structures is the occurrence of sheets separated by short, nearly linear U-O-U linkage with an interplanar distance of 4.1 Å. Some other structures in which this feature occurs are:

	U-O (Å)	d (Å) Ref.
α-U_3O_8	2.073	155
β-U_3O_8	2.080	156
UO_2Br	2.054	157
UVO_5	2.05	158

7. Bond Lengths and Bond Strengths in Actinide Fluorides (R. A. Penneman). In this section Zachariasen's formulas for actinide fluorides are tested and applied.[159,160] The decision between atom positions of fluorine and oxygen in PuOF, which resulted in a reversal of the positions formerly assigned, provided a striking demonstration of their utility. In the compounds of the class MOF (M = Pu, La, etc.), the x-ray data can be fit equally well, with either the Pu-O or the Pu-F distance being the shorter of the two. In Table XVIII each choice is assessed.

The bond strengths can be calculated from the known bond distances in the structure. The formula $D(s) = D_1 - B \ln(s)$ is solved for bond strength (s) and summed for the elements. In Set 1, the bond strength sums to ridiculous values, in contrast to Set 2 where the values sum nicely to the expected valences in Pu^{3+}, O^{2-}, F^{1-}.

Thus, the Pu-O distance is the smaller of the two, whereas the free ion O^{2-} is larger than F^- and this size order was used as the basis for the original assignment. The shortening is a direct consequence of the bond strength. That is, each oxygen and fluorine ion is shared by 4-plutonium ions so that the bond strength of the Pu-O bond is 2/4 = 0.5 (vs 0.4997 calc) and each Pu-F bond is 1/4 = 0.25 (vs 0.2363 calc from the formulas of W. H. Zachariasen[159,160]).

In a similar manner all known actinide fluoride compounds were tested, resulting in some atom position reassignments.[159] Some representative compounds are listed in Table XIX.

TABLE XVII

SOME PREVIOUSLY REPORTED PHASES
RELATED TO β-URANIUM MOLYBDATE

Formula	Crystal System	a	b	c	Ref.	Metal Coord. No.
$U(MoO_4)_2$ Sedovite	Monoclinic or orthorhombic	3.36(6)	11.08(3)	6.42(5)	153	Unknown
α-$U(MoO_4)_2$	Trigonal	17.30(1)		6.145(1)	154	Mo tetrahedra, U octahedra
α-$Th(MoO_4)_2$	Trigonal	17.61(2)		6.259(5)	154	Mo tetrahedra, Th octahedra
$Pu(MoO_4)_2$	Orthorhombic	3.34	10.97	6.32	148,149	Unknown

TABLE XVIII

PuOF

- Locating the light atoms in oxyfluorides, LaOF, PuOF.
- X-ray diffraction studies.
- Cannot distinguish between O and F.
  W. H. Zachariasen, Acta. Cryst. 4, 231 (1951).
- Ionic radii $\bar{\bar{O}} > F^-$; is M-O > M-F?

Use Bond Length — Bond Strengths

Set 1:	Pu-4O	Pu-4F
	2.569 Å	2.385 Å
	s = 0.2952	s = 0.3745

$\sum$ Pu = 2.68; $\sum$ O = 1.18; $\sum$ F = 1.50

Interchange O and F Positions

Set 2:	Pu-4O	Pu-4F
	2.385 Å	2.569 Å
	s = 0.4997	s = 0.2363

$\sum$ Pu = 2.94; $\sum$ O = 2.00; $\sum$ F = 0.95

TABLE XIX

Compound	Coordinate	Dobsd (Å)	Dcalc (Å)
γPuOF	Pu-4F	2.58	2.55
	Pu-4O	2.39	2.39
Li_3ThF_7	Th-9F	2.377	2.37
KTh_6F_{25}	Th-3F	2.32	2.33
	Th-4F	2.35	2.36
	Th-2F	2.51	2.49
K_5ThF_9	Th-8F	2.33	2.33
$CsUF_6$	U-6F	2.057	2.06
$(NH_4)_4UF_8$	U-8F	2.28	2.28
NH_4UF_5	U-9F	2.33	2.33
UO_2F_2	U-2O	1.74	1.76
	U-6F	2.429	2.42

8. Actinide Oxo Chemistry (P. G. Eller, R. A. Penneman, and T. L. Cremers). In parallel with our studies on oxide phases (actinide molybdates) pertinent to Purex process problems (Sec. VI.B.6), we are also investigating unusual complexes of "yl" or "oxo" cations such as UO_2^+ and PaO_2^+. In particular, we wish to crystallize complexes of such species and to determine whether the linear geometry (as in all uranyl and known MO_2^{2+} species) or the angular geometry (as in nearly all transition metal "yl" species such as MoO_2^{2+}) results. This point is particularly significant for pentavalent protactinium, which possesses certain chemical properties (such as hydrolysis/polymerization in acid media and propensity for binding "soft" donor ligands) more akin to d-block than to f-block metals. Additionally, studies of such species are significant because protactinium is by far the least studied of the early actinides and because oxo favoring conditions are encountered in virtually all nuclear waste cycles.

We have begun to investigate the reduction of uranyl ion with reductants such as Cr(II) and Ti(III) in nonaqueous solvents as a possible route to stable UO_2^+ species. Unlike the reported situation in water,[161] in a variety of nonaqueous systems such as DMF and DMSO the resulting UO_2^+ (identified spectroscopically) seems to be quite stable (weeks, in some cases), and we are optimistic that crystalline UO_2^+ complexes may be isolated and studied crystallographically. We have also repeated French work, which claimed that UO_2Cl can be prepared by the hot tube reaction of UCl_4 and U_3O_8 at 590°C (Ref. 162). This reaction, indeed, appears to work as described, and we have collected an x-ray data set on single crystals resulting from this reaction. A complete structure determination is in progress. Attempts thus far to dissolve this material in strongly coordinating solvents in order to prepare a complex containing a discrete, mononuclear UO_2^+ complex have been unsuccessful, but work continues. Similar chemical studies are being carried out for the reported UO_2Br compound.[162,163] Electrochemical reduction of nonaqueous uranyl solutions will also be used. Subsequently, we will proceed to prepare and characterize analogous PaO_2X systems by similar means. Structural parameters for the MO_2^+ moiety will be compared with those of other known MO_2^{n+} species and correlated with theoretical studies of such species.

Properties of actinide monoxo species are also being investigated. For example, we have discovered that

UOF_4 forms stable, soluble complexes with a variety of strongly coordinating organic molecules including nitriles, sulfoxides, amides, and alcohols. The preliminary results indicate that for UOF_4 an extensive chemistry may exist, similar to that observed with UF_5 (Ref. 164). These results suggest that other actinide fluorides and oxo species may also be solubilized and complexed, thus providing synthetic routes to new, unusual, and perhaps volatile actinide compounds. Crystal structure studies are planned for several key mixed-donor compounds.

We are also attempting to engage the aid of theoreticians in understanding the reasons for the geometric difference between f-block (linear) and d-block (angular) "yl" species. Despite many theoretical studies on the uranyl ion, the fundamental reasons for the strong stabilization of the linear geometry remain unclear. This point is borne out by controversy over a recent paper which ascribes uranyl linearity to a cooperative interaction between filled 6p and empty 7s orbitals, a type of interaction not possible with d-block metals.[165]

9. Fluorination Reactions of UF_6 with Organic Compounds (L. B. Asprey and P. G. Eller). Numerous inorganic fluorides have been used to introduce fluorine into an organic compound or to rupture the compound into various smaller organic fragments containing a fluorine atom. Several classification schemes have been proposed to describe the behavior of these fluorinating agents. Probably the best known is that of Meshri and White,[166] which divides these agents into hard, moderate, and soft. Under this scheme, strong oxidizing agents containing fluorine, such as ClF, ClF_3, OF_2, K_2NiF_6, and UF_6, are hard agents. Moderates include HgF_2, SbF_5, $SbF_3/SbCl_5$, and AsF_3 among others; these are for the most part nonoxidative or slightly so. The soft class includes alkali fluorides AgF, HF, SF_4, COF_2, and others, which are strictly metathetical in their fluorination behavior. The distinctions between the several classes are blurred, and several well-known fluorinators such as WF_6 are omitted.

Because we have worked extensively with UF_6 for some years, we decided to study reactions of this hard agent and compare it to the behavior of nonclassified WF_6 and to the soft SF_4. An extensive study of SF_4 as a fluorinating agent by Hasek et al.[167] and a study of UF_6 by Olah et al.[168] have been reported.

Our work has been on the reaction of UF_6 and WF_6 with a number of simple organic molecules. Alcohols, ethers, ketones, and acids, both aliphatic and aromatic, were included. The results of Hasek et al.[167] on the use of SF_4 as a fluorinating agent were used for comparison. Olah's studies[168] of UF_6 as a fluorinating agent were focused only on the organic part of the reaction, and his suggestions as to the fate of the UF_6 were incorrect; we therefore carried out our own examinations with UF_6. Because very little data concerning fluorinations by WF_6 exist, we investigated these reactions also.

Both inorganic and organic compounds formed in the fluorination reactions were identified when possible. Powder x-ray and analytical methods, as well as some ir spectroscopy, were used on solids. Spectroscopic methods used included ^{19}F and ^1H NMR, ir, mass spectrometry, and visible uv. Gases, liquids, and solids resulting from the reaction were examined.

a. Experiments. Unless otherwise noted, WF_6 and UF_6 were diluted with $CFCl_3$ (Freon 11) in order to moderate reactions, some of which are quite violent. Reactions where ^{19}F and ^1H NMR were used for characterization were carried out in polyfluoroethylene (PFE) plastic tubes resistant to both fluorination and oxidation. A Varian 390 NMR spectrometer was used. Large-scale reactions where ir was used for analysis were carried out in 30 mℓ Kel-F tubes. Metal ir cells with AgCl windows were used for the ir measurements on a Pekin-Elmer Model 180 spectrometer. Solids were examined by Debye-Scherrer powder methods. All solids were loaded into capillaries in an inert atmosphere box. A Cary Model 14 spectrometer was used for visible-uv spectra. For mass spectrometry, a Bendix Time-of-Flight machine was used.

All compounds employed were of reagent grade and dried thoroughly before use. WF_6 and UF_6 were purified by trap-to-trap distillation to remove HF.

A typical experiment consisted of loading the desired organic compound, usually 1-2 mmols, in a plastic NMR tube, distilling in 3-5 mmols of Freon 11 followed by the desired amount of WF_6 or UF_6. The tube was sealed off and placed in a standard glass 5-mm-o.d. NMR tube for examination. A similar procedure was followed for ir study except that the amounts were increased to 5-10 mmols of organic compound, the amounts of other reagents increased correspondingly, and the reactions were carried out in a 19-mm-o.d. Kel-F tube. The resulting gases were then expanded into an ir cell for measurement. After removal of the volatiles, the tube containing solids was transferred to an inert atmosphere box for loading of x-ray capillaries.

b. Results and Discussion. Alcohols: Methyl alcohol in Freon 11 solution reacts cleanly with SF_4 to give CH_3F, SOF_2, and HF. UF_6 also gives CH_3F, solid β-UF_5, and an unidentified material. However, using CH_3OH as the solvent leads to reduction of U(VI) with formation of a solution of UF_5 in CH_3OH and formation of HF. WF_6 behaves very differently, with methoxy groups replacing the fluorides in WF_6 one by one, which results in a whole series of $WF_x(CH_3O)_{6-x}$ compounds.

SF_4 plus ethyl alcohol in Freon 11 yields C_2H_5F and SOF_2 cleanly, whereas UF_6 gives C_2H_5F, CH_3F, and CO, which shows C-C bond breakage. As with methyl alcohol, WF_6 forms an entire series of ethoxy-fluoro-tungsten(VI) compounds.

Ketones: Acetone reacts smoothly with SF_4 to give the difluoroalkane $CH_3CF_2CH_3$ and SOF_2. In this case, WF_6 behaves similarly, with WOF_4 being the solid product. However, UF_6 oxidizes acetone to give a considerable amount of tar and some $CH_3CF_2CH_3$, UOF_4, CO, and HF; all of the latter could be identified.

Benzophenone reacts with SF_4 to give ϕ-CF_2-ϕ in the presence of a catalyst and heat.[167] WF_6 in Freon 11 does not appear to react. However, UF_6 in Freon 11 reacts smoothly to give ϕ-CF_2-ϕ and the orange solid, UOF_4.

Acids: Acetic acid does not appear to react with SF_4 or WF_6 under the mild conditions used. However, UF_6 does react with glacial acetic acid to yield UO_2F_2 and other unidentified products that contain UOF_4 and UO_2F_2, probably $UO_2F_2 \cdot UOF_4$, $UO_2F_2 \cdot 2UOF_4$, etc. Other organic products were not identified.

Trifluoroacetic acid reacts with UF_6 by two paths. One is light-catalyzed and yields UOF_4, CF_3COF, and HF. In the dark, however, the predominant products are UF_5, CF_4, and CO_2, which shows breakage of a C-C bond.

Ethers: Tetrahydrofuran's behavior with SF_4 was not studied and did not appear in the literature. WF_6 in Freon 11 reacts smoothly to open the ring and give CH_2F-CH_2-CH_2-CH_2F and solid WOF_4. UF_6 in Freon 11 added to tetrahydrofuran resulted in a very violent reaction, almost an explosion, and was not further investigated.

Aromatics: Benzene does not react with either SF_4 or WF_6 at room temperature. However, a violent reaction occurs with UF_6 with the production of tar. No further study was made.

Alkanes: SF_4 and WF_6 do not react with heptane at room temperature. Addition of UF_6 to a large excess of heptane results in the formation of tar.

c. Summary. From the above results, it can be seen that the fluorinating behavior of WF_6 is like that of SF_4 in most cases. It tends to react gently with functional oxygen groups to substitute fluorines for the oxygen, with WOF_4 the inorganic product. It is also unreactive in many cases where there are no organic functional groups, as with alkanes and with aromatics such as benzene.

The behavior of UF_6 is very different from both SF_4 and WF_6. UF_6 is a strong oxidizing agent and tends to break C-C bonds, forming fluorinated fragments from the original compound and being itself reduced to U(V) as UF_5. Occasionally, it remains as U(VI) and replaces an oxygen, forming UOF_4 in a manner analogous to WF_6.

VII. ISOTOPE SEPARATION AND ANALYSIS

A. Separation of Stable Isotopes (Carbon, Nitrogen, and Oxygen) and Production of Labeled Compounds (T. R. Mills, M. Goldblatt, and R. C. Vandervoort)

The stable isotope separation program has the objectives of providing separated stable isotopes of carbon, oxygen, and nitrogen (ICONs) for research purposes and also of developing new or improved techniques for incorporating the separated isotopes into commonly desired chemical forms. As part of the stable isotopes resource (SIR) at Los Alamos, the isotope separation program distributes isotopic materials to SIR- approved researchers. The remainder of isotopic materials are sold at cost to Los Alamos investigators or to the general research community through Mound Facility. The value of isotopic materials produced for sales during FY-1980 was $585K.

The isotopes are separated by cryogenic distillation of CO for carbon isotopes and of NO for both nitrogen and oxygen isotopes. During FY-1980, the quantities of isotopes separated were 5.6 kg ^{13}C at 90% enrichment, 4.3 kg ^{13}C (99%), 1.2 kg ^{15}N (60+%), 0.7 kg ^{15}N (98%), 58.2 kg ^{16}O (99.98%), 0.1 kg ^{17}O (20%), 0.1 kg ^{17}O (50%), and 0.7 kg ^{18}O(10%).

The distillation columns, which are up to 225m long, are of unique design.[169] Several significant improvements were made in the separation plant in FY-1980. As part of the ^{13}C enrichment system it is necessary to promote isotopic exchange of CO species. A new CO exchanger was built, using the new

alumina-catalyzed exchange method (see Section VI.A.1). The exchanger works at exchange rates up to 15 mole/day with complete exchange and without losses caused by disproportionation. Also, the process control CEC-621 mass spectrometer was automated for increased speed and improved reliability. In early FY-1981 the spectrometer will be fully automated to permit totally unattended analyses.

Most of the isotopically enriched CO or NO is converted to other labeled compounds for use by researchers. A variety of forms were prepared in FY-1980 in batches ranging from several grams to several kilograms of compound. Some products were made using precursors produced in previous years. Table XX summarizes these conversions.

B. Automatic Nitrogen Analysis (B. B. McInteer and J. G. Montoya)

Nitrogen isotopes are used globally as tracers for field and laboratory experiments directed toward clarification of the nitrogen cycle. Thousands of samples requiring isotope ratio determinations result from these studies. Heretofore these samples in the form of ammonium salts have been processed using a routine laboratory procedure capable of handling 20-50 samples per day. Because this capacity limits the use of nitrogen isotopes for tracer experiments, we have developed automatic equipment capable of handling several hundred samples per day, unattended.

The basic instrument is an isotope-ratio mass spectrometer* whose inlet system has been completely replaced by the new equipment. The circuitry has been slightly modified to permit automatic data monitoring and fine automatic adjustment to the analyzer magnet current for mass peaking. Samples containing 0.25 mg nitrogen are pipetted into small plastic vials with 0.15mℓ vol. After drying by flowing gas stream, they are mounted in a movable sample tray holding up to 137 vials. The samples are then processed one after another and results are printed out and also stored on magnetic tape for later listing of the complete tray.

The procedure used for sample proceessing is similar to that developed manually since the first use of sodium hypobromite by Rittenburg.[170] The reagent solution is only half as concentrated and is squirted through capillary tubing 0.05 mℓ per sample. The greatest novelty of the basic procedure is the use of a condensible purge gas, Freon-12, to displace the air above the sample instead of evacuating the sample. This permits most

*Model 3-60, manufactured by Nuclide, Inc., 62 E. College Ave., State College, Pennsylvania.

TABLE XX

Product	Reactions	Quantity (mol)
$^{13}CO_2$	$^{13}CO + CuO \rightarrow {}^{13}CO_2 + Cu$	346
$^{13}CH_3OH$	$^{13}CO_2 + 3H_2 \xrightarrow[cat]{Cu,Ni} CH_2OH + H_2O$	15
$^{12}C^{18}O$	$^{12}C + 1/2{}^{18}O_2 \rightarrow {}^{12}C^{18}O$	0.1
$^{13}CF_4$	$^{13}CO_2 + SF_4 \rightarrow {}^{13}CF_4 + 2SOF_2$	0.02
$^{12}C^{16}O^{18}O$	$Cu + 1/2{}^{18}O_2 \rightarrow Cu^{18}O$	
	$Cu^{18}O + {}^{12}C^{16}O \rightarrow {}^{12}C^{16}O^{18}O$	5.6
$^{12}C^{18}O^{18}O$	$^{12}C + 2{}^{15}N^{18}O \rightarrow {}^{12}C^{18}O^{18}O + {}^{15}N_2$	1.6
$^{14}N_2$	$2{}^{14}NH_3 + 3CuO \rightarrow 3Cu + {}^{14}N_2 + 3H_2O$	0.5
$^{15}NH_3$	$^{15}NO + H_2 \xrightarrow[cat]{Pt} {}^{15}NH_3 + H_2O$	59
$H^{15}NO_3$	$2{}^{15}NO + H_2O + 3/2O_2 \rightarrow 2H^{15}NO_3$	19
$K^{15}NO_3$	$H^{15}NO_3 + KOH \rightarrow K^{15}NO_3 + H_2O$	17
$(^{15}NH_4)_2SO_4$	$^{15}NH_3 + H_2SO_4 \rightarrow (^{15}NH_4)_2SO_4$	38
$^{15}N_2$	$2{}^{15}NH_3 + 3CuO \rightarrow 3Cu + {}^{15}N_2 + 3H_2O$	16
$H_2{}^{17}O$, $H_2{}^{18}O$	$N^*O + H_2 \xrightarrow[cat]{Pt} H_2{}^*O + NH_3$	50
$^{18}O_2$	$H_2{}^{18}O \xrightarrow{electrolysis} H_2 + 1/2{}^{18}O_2$	3.6

sample processing to be at ambient pressure. After the reagent has caused the sample to release N_2 gas, the resulting gas mixture flows to a small U-trap of stainless steel capillary tubing, which is chilled with liquid nitrogen. This freezes out the Freon-12 as well as trace impurities of the evolved gas, and the resulting purified N_2 flows to the mass spectrometer for isotope ratio measurement. Tiny pneumatic valves were specially designed for this machine. The total volume occupied by the sample gas is ~ 0.5 cm^3.

Many of the procedures necessary for accurate, reproducible results are like those of a manual procedure for good mass spectrometry. A reference gas is run regularly, and a record is maintained and checked in computer memory for stable results. Similarly, the background peaks at Mass-29 and -28 are monitored. In addition, sets of standard samples of NH_4SO_4 of various isotopic compositions have been prepared for routine checking of the machine. Incidentally, enough interest has been generated in other laboratories for these standards to be distributed internationally throughout the scientific community.

Certain sources of error are distinctive to this automatic machine. The Freon gas available commercially has an unacceptable level of nitrogen impurity, and we have designed and built a small distillation column, operating at ambient temperature, to purify the purge gas. The seal between the polyethylene vial and the holder has also proved unreliable, and a neoprene O-ring is now used for a more reliable seal. The pressurization of the reagent reservoir with gas causes some gas solubility and subsequent evolution in the sample vial, so we have used purified Freon there, too. Fresh reagent is prepared for each tray, and it is degassed under vacuum before use.

The result of this development has been a capability of running a tray of samples at 120-150 s per sample. Our laboratory has processed about 4000 samples in its first year of operation and has capacity for many more.

C. Modernization of Isotope Separators (J. P. Balagna)

The isotope separators that are presently in use are 16 and 10 years old, and the designs are even older. These separators have become a necessary tool in the weapons diagnostic program of the group. The ability to measure an isotope produced by an n,2n or n,3n reaction after separation from a high-abundance n,γ product has made it possible to improve weapons diagnostic techniques.

The necessary conditions for successful isotope separation are a high transmission of rare species and the lowest possible cross contamination of the low-abundance isotopes with the nearby high activity of an n,γ isotope. This phenomena, called tailing, is presently at the 5×10^{-4} level at the M-1 position, where M is the most abundant isotope. In many cases this is still one or two orders too high for good, rapid measurement of the n,2n species. State-of-the-art separators are two to three orders better than ours at present.

A modernization program has been in progress for the past year to retrofit these separators with new electronic, vacuum, and magnetic components to improve their performance. In addition, new ion sources develop a capability to measure isotopes of elements not previously available to this method. Gold, iodine (as a positive ion), the platinum group, and other rare earths in addition to europium, thulium, and lutetium are under active development. The goal of the ion sourcery effort is to have sources with sufficient versatility to produce a useful ion beam from any element of interest.

The ion optics of these separators are far from optimum. The aberrations caused by both electrostatic and magnetic imperfections are under study, using available computer codes. Some lens redesign has resulted in much less electrical breakdown in our lens system. The magnet optics are quite poor in view of today's technology. A study has begun to determine if quadrapole and sextupole coils in the magnet gap will improve magnet performance.

A large program is under way to provide ion beam diagnostic techniques that can guide the development and improvement of the separators. Present tools for this purpose are rudimentary.

The twin needs of high transmission of material loaded into the ion source and small tailing effects are the proximate goals. Their accomplishment will give the weapons diagnosticians many more elements to use.

VIII. ATOMIC AND MOLECULAR COLLISIONS

A. Molecular Dynamics of the NO and Ozone Chemical Reaction (J. J. Valentini, J. B. Cross, and G. H. Kwei)

The chemical reaction between NO and ozone to produce NO_2 and oxygen is important and familiar to chemists and atmospheric scientists. It is one step in the NO_x catalyzed destruction of "odd" oxygen (oxygen

atoms and ozone) in the stratosphere and is central to the photochemistry of the polluted troposphere. It is also one of the most extensively studied of all chemical reactions, there being more than 20 papers in the literature dealing with it. Despite its familiarity, the dynamics of the NO/ozone reaction have not been clearly elucidated, because the reaction is quite complicated. The five reactant and product electronic states that are accessible in the reaction give rise to several possible reaction potential energy surfaces.

We have completed a crossed molecular beam study of this reaction, the results of which show one striking new feature of the dynamics and clarify others. Figure 33 shows the angular distribution of the NO_2 product of the reaction at two collision energies. A slight but unambiguous bimodality is evident. This results from the existence of two reaction channels, one leading to $^2B_{1,2}$ electronically excited NO_2, the other to ground state $^2A_1$ NO_2. This bimodality is more clearly evident in the center-of-mass recoil angle and velocity distribution of Fig. 34, obtained by transforming the scattering data from the space-fixed laboratory coordinate system to a coordinate system in which the center-of-mass motion has been removed. Here we see a very narrow, strongly backward NO_2 peak and a broad sideways NO_2 peak. Conservation of energy considerations require that the backward peak be assigned to $^2A_1$, NO_2 and the sideways peak to $^2B_{1,2}$ NO_2.

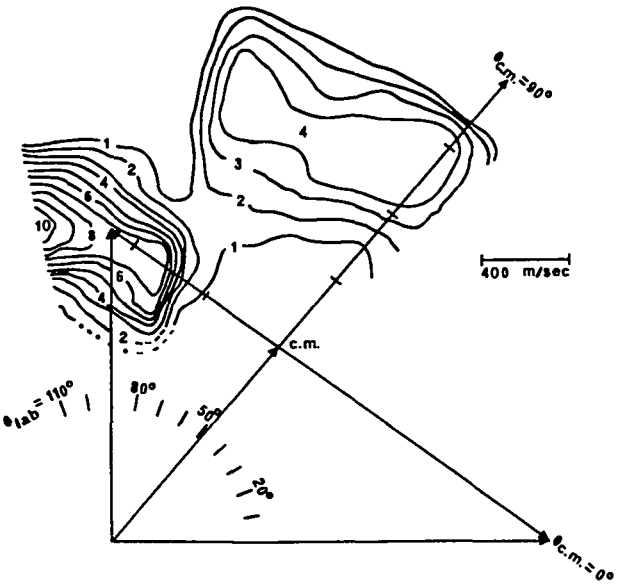

Fig. 34.
Center-of-mass recoil angle and velocity flux contour map of the NO_2 product from the NO + O_3 reaction at a relative translational energy of 14.2 kcal/mole. Contour map is superimposed on the "Newton diagram" showing the most probable NO ($\theta_{lab} = 0°$) and O_3($\theta_{lab} = 90°$) velocity vectors.

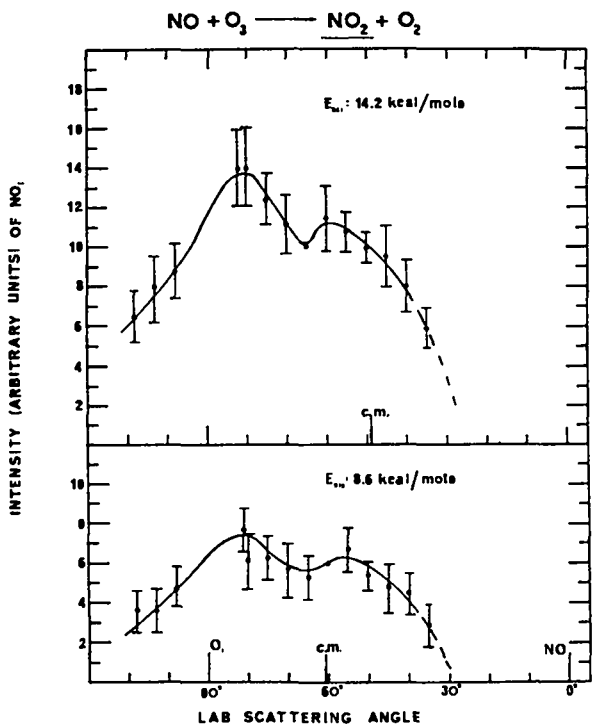

Fig. 33.
Angular distribution of the NO_2 product from the NO + O_3 reaction at relative translational energies of 8.6 and 14.2 kcal/mole. O_3 beam at 90°, NO beam at 0°.

Although it is admittedly difficult to draw conclusions about the character of the reaction potential energy surface from the angle-velocity distributions for such a complex system, we can find no other explanation for the strongly backward peaked ground state NO_2 than that it comes about because the NO abstracts the central oxygen atom of ozone, with consequent strong product repulsive interaction. Such a mechanism, while not without precedent, is a surprising feature of the dynamics.

Our results also seem to contradict previous observations of an anamolously strong dependence of the reaction yield on collision energy. Over the energy range of 5 kcal/mol to 14 kcal/mol, we find that the overall yield of both $^2B_{1,2}$ NO_2 and $^2A_1$ NO_2 approximately quadruples. Previous measurements based on measurement of the chemiluminescence from the $^2B_{1,2}$ products, as compared to our mass spectrometric measurements, indicated an increase of more than a factor of 50.[171] We believe that there are features of the chemiluminescence from this reaction, such as an energy-dependent spectral

"blue" shift or a slightly energy-dependent branching ratio between states of widely varying radiative lifetime, that seriously affect the chemiluminescence yields and lead to overestimating the energy dependence of the reaction.

B. High-Repetition-Rate Pulsed Gas Beam Source (J. B. Cross and J. J. Valentini)

Major advances in molecular collision dynamics and spectroscopy have been made possible through exploiting the unique properties of molecular beams produced by the supersonic expansion of gas through a small orifice. These properties, low temperatures (1-10 K) and high number densities (10^{13}-10^{16} molecules/cm^3), allow high signal-to-noise experiments to be performed with a very nearly state selected group of molecules; that is, the partition function of the system is nearly unity. Continuously operating supersonic nozzles have been most often used to produce these beams because of their simplicity and high reliability. However, these gas beam sources generally require high pumping speed vacuum systems, which are bulky and expensive. Because of this, pulsed nozzle sources have been developed, in which the gas flow through the nozzle orifice is rapidly switched on and off by some type of valve. Such pulsed sources require only modest vacuum systems, because the gas flow is reduced by the duty factor of the valve, that is, the product of "on" time and the repetition rate, and at low duty cycle the reduced flow can permit the use of peak nozzle throughputs 10 to 1000 times greater than is possible with cw nozzles.

These pulsed sources are well suited to spectroscopic or other experiments in which the intermittent nature of the beam is not a hindrance. The pulsed sources currently available, however, generally require complex and expensive electronic driving circuits, have low repetition rates and a limited range of pulse widths, and are often somewhat unreliable. We have developed an inexpensive, reliable, simple, high-repetition-rate pulsed gas beam source. The source was constructed by modifying a commercial piezoelectric leak valve and is driven by a small signal generator whose square wave output is amplified by a simple one-transistor amplifier.

The valve is highly reliable; we have obtained nearly 10^7 pulses without failure. It is also very flexible, producing pulse widths from 50 μs to several ms at repetition rates of more than 500 s.$^{-1}$ Significantly, the pulse width and repetition rate can be varied while the source is in operation; no physical adjustments are required.

Comparisons of the mechanical temporal profile of the valve, measured by optical techniques, and the gas beam temporal profile, measured by laser-induced fluorescence of I_2 expanded in helium carrier gas, show excellent agreement, with the gas pulse being 5-10% shorter than the mechanical pulse. The pulse-to-pulse stability is very high, fluctuations in gas pulse intensity being less than 5%.

This pulsed gas beam source produces a nearly ideal supersonic gas expansion. Extensive measurements of the temperature of the molecules in the beam, made by inverse Raman spectroscopy, show close agreement with continuum mechanics predictions for ideal isentropic flow. For a pure methane expansion with a 0.50-mm orifice and 50 psi backing pressure, we have observed a rotational temperature of 9 K at a distance 32 mm downstream, where the pressure is 0.040 torr. The predicted temperature here is 10 K.

The valve can be employed in a variety of molecular beam spectroscopy experiments and because of its high repetition rate should even prove useful in crossed molecular beam dynamics experiments.

C. Coupling of Chemical Reaction with Ambipolar Diffusion in a Flowing Afterglow Experiment: Application to Ion-Molecule Reactions of Uranium Hexafluoride (G. E. Streit and T. W. Newton)

The flowing afterglow technique yields rate constants for ion-molecule reactions that are generally in good agreement with the results of other methods, such as merged beams, high-pressure mass spectrometry, and ion cyclotron resonance spectrometry; it is thus well accepted for measuring the rates of such reactions.[172]

An accurate determination of rate constants from flowing afterglow experiments requires the solution of the transport equation

$$V(r)\frac{\partial[A^-]}{\partial z} = (D_{A^-})\left[\frac{1}{r}\frac{\partial[A^-]}{\partial r} + \frac{\partial^2[A^-]}{\partial r^2} + \frac{\partial^2[A^-]}{\partial z^2}\right] - k[A^-][B], \quad (1)$$

where V(r) is the radial velocity distribution, $[A^-]$ and [B] are the reactant ion and neutral molecule concentrations, D_{A^-} is the ambipolar diffusion coefficient, and k is

the second-order rate constant for the reaction between A^- and B. The negative charge on A was chosen only to be specific; it could as well be positive. Several groups have solved this equation by either analytical or numerical techniques[173-176] using various simplifying assumptions. One of these is that loss of A^- by diffusion is governed by a diffusion coefficient that is independent of the extent of reaction. For many reactions of interest this assumption is not valid, and in our work[177] we have made D_{A^-} a function of the ion composition and solved Eq. (1) numerically. We consider a three-ion system in which a reactant ion is converted to a product ion in the presence of a nonreacting ion of the opposite sign. The ion concentrations are such that the diffusion is ambipolar. Equations for the required ambipolar diffusion coefficients have been derived by Oskam[178] and for a positive ion and two negative ions are:

$$D^a_+ = \frac{2D_+D}{D_+ + D}\ ,$$

$$D^a_1 = \frac{2D_+D_1}{D_+ + D}\ , \qquad (2)$$

$$D^a_2 = \frac{2D_+D_2}{D_+ + D}\ ,$$

where $D = (\eta_1 D_1 + \eta_2 + D_2)/(\eta_1 + \eta_2)$, D_+, D_1, and D_2 are the ambipolar diffusion coefficients, D_+, D_1, and D_2 are the free diffusion coefficients, η_1 and η_2 are the number densities, the subscript + indicates the positive ion and the subscripts 1 and 2 indicate the two negative ions. If the free diffusion coefficients D_1 and D_2 differ significantly, all three ambipolar diffusion coefficients will depend on the relative concentrations of the two negative ions. This is illustrated in Fig. 35.

Our numerical solutions of Eq. (1) show that when the two free diffusion coefficients are equal, a plot of the logarithm of the reactant ion concentration versus the neutral reactant concentration is essentially linear, in agreement with previous solutions of the equation. However, when the free diffusion coefficient of the product ion is less than that of the reactant ion, significantly greater curvature is observed.

These results have been applied to our experimental study of charge transfer from the negative ions F^-, Cl^-, Br^-, I^-, and SF_6^- to UF_6 (Ref. 179). In all cases, plots of the logarithm of the reactant ion signal versus the UF_6 flow were curved, like the calculated plot mentioned above. This is consistent with the fact that our best

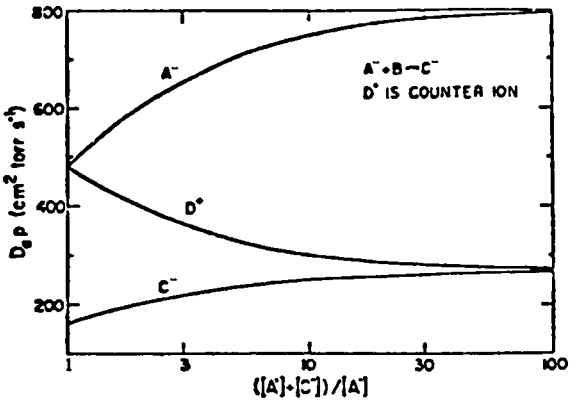

Fig. 35.
Ambipolar diffusion coefficients for a three-ion system as a function of counter-ion-to-reactant-ion ratio or $1 + (C^-)/(A^-)$.

estimate for the free diffusion coefficient for UF_6 is considerably smaller than for the reactant ions. For all the reactions, however, the experimental curvature was greater than the curvature calculated with the diffusion coefficient of the reactant ion as a function of extent of reaction. This is illustrated in Fig. 36 for the $Cl^- + UF_6$ reaction. The best calculated lines through the first and

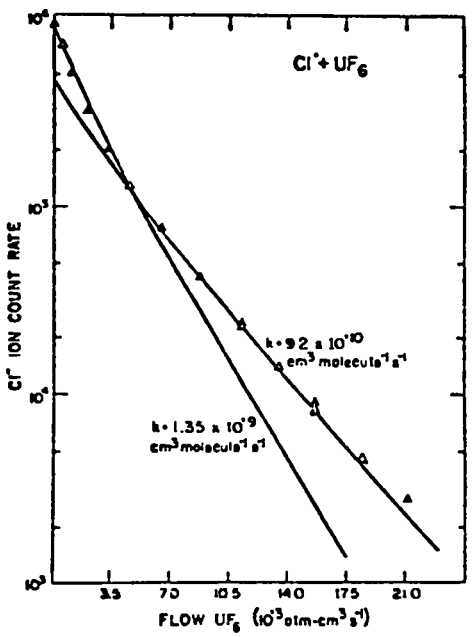

Fig. 36.
Data for the reaction $Cl^- + UF_6 = Cl + UF_6^-$ plotted as log ion signal vs UF_6 flow. Δ indicates experimental data. Solid lines indicate computed fits with the indicated rate coefficients in cm^3 molecules^{-1} s^{-1}.

last portions of the data give rate constants that differ from the mean by about 25%.

Our results for charge transfer reactions to UF_6 are summarized in Table XXI and show that all the rate constants are slightly lower than for ion-induced dipole orbiting collisions, the Langevin limit; the rate constants depend on the square root of the reduced masses of the reactants; and the rates appear to be independent of the energy of reaction. Our value of SF_6^- lies between the previous two values.

D. Ion-Molecule Reactions by the Flowing Afterglow Technique: A New Technique: A New Determination of $D°_{298}(F_5S\text{-}F)$ and of the Ionization Potential of SF_5 (L. M. Babcock and G. E. Streit)

In addition to using the flowing afterglow technique in determining rate constants of ion-molecule reactions, it may be used to obtain thermodynamic information, such as ionization potentials (IP) and heats of reaction.

Thermochemical information can be obtained from the two types of flowing afterglow measurement. The first is a "yes/no" method by which limits for the ionization potential of A may be set based on whether it undergoes a charge exchange reaction with B, for which the ionization potential is known. That is, if the reaction $A^+ + B \rightarrow A + B^+$ occurs, then IP(A) $\geq$ IP(B). Conversely, if the reaction does not occur, then IP(A) < IP(B). The second method is measuring the equilibrium constant for a reaction, thus yielding the free energy of reaction. This may be accomplished only if the reaction is thermoneutral within a few tenths of an electron volt and if the neutral product is not a labile species.

We have investigated some ion-molecule chemistry of SF_6 and SF_5 and, in addition to several rate constant measurements (Table XXII), have determined values for $IP(SF_5)$, $AP(SF_5^+/SF_6)$, the appearance potential of SF_5^+ from SF_6, and $D°_{298}(F_5S\text{-}F)$.[182] An examination of charge exchange reactions of SF_5^+ with the neutral molecules NO_2 (IP = 9.75 eV), NH_3(10.17 eV), H_2S(10.43 eV), Br_2(10.51 eV), and Cl_2(11.48 eV) leads to the establishment of the ionization potential of SF_5 at 10.5 ± 0.1 eV. We have also determined an equilibrium constant for the reaction system $CF_3^+ + SF_6 \leftrightarrows CF_4 + SF_5^+$. The equilibrium constant, $K = (5.9 \times 10^3) \pm 50\%$, yields a $\Delta G°_{298} = -0.22 \pm 0.01$ eV, and by using standard entropies we obtain $\Delta H°_{298} = -0.17 \pm 0.02$ eV.

The appearance potential $AP(SF_5^+/SF_6)$ is obtained from the following thermochemical cycle.

$SF_6 \rightarrow SF_5^+ + F + e$	$AP(SF_5^+/SF_6)$
$CF_3^+ + e \rightarrow CF_3$	-9.17 ± 0.08 eV
$CF_3^+ + F \rightarrow CF_4$	-5.42 ± 0.17 eV
$CF_3^+ + SF_6 \rightarrow CF_4 + SF_5^+$	$\Delta H_{298} = -0.17 \pm 0.02$ eV

TABLE XXI

NEGATIVE ION-UF_6 ELECTRON TRANSFER REACTIONS

Reaction	[E.A. (UF_6) - E.A. (X)][a] eV	Rate Constant (cm^3 molecule^{-1} s^{-1}) This Work[b]	Langevin	Prior Work
$F^- + UF_6 \rightarrow F + UF_6^-$	1.7	1.3×10^{-9}	1.9×10^{-9}	
$Cl^- + UF_6 \rightarrow Cl + UF_6^-$	1.5	1.1×10^{-9}	1.5×10^{-9}	6.5×10^{-10} +100% −50%[c]
$Br^- + UF_6 \rightarrow Br + UF_6^-$	1.7	9.3×10^{-10}	1.0×10^{-9}	
$I^- + UF_6 \rightarrow I + UF_6^-$	2.0	7.7×10^{-10}	8.5×10^{-10}	
$SF_6^- + UF_6 \rightarrow SF_6 + UF_6^-$	4.6	6.9×10^{-10}	8.1×10^{-10}	2.4×10^{-10} +100% −50%[c]; 1.5×10^{-9} ±20%[d]

[a]Based on E.A. (UF_6) = 5.1 eV.

[b]± 50%.

[c]Ref. 180.

[d]Ref. 181.

TABLE XXII

ION-MOLECULE REACTIONS INVOLVING SF_6 OR SF_5

Reaction		k ($cm^3 molecule^{-1} s^{-1}$)
$SF_6 + He^+ \rightarrow$	$SF_5^+ + F + He$ $SF_4^+ + 2F + He$ $SF_3^+ + 3F + He$	2.0×10^{-9}
$SF_6 + N_2^+ \rightarrow$	$SF_5^+ + F + N_2$	1.3×10^{-9}
$SF_6 + N^+ \rightarrow$	$SF_5^+ + NF$	1.4×10^{-9}
$SF_6 + CO_2^+ \rightarrow$	$SF_5^+ + CO_2F$	1.4×10^{-11}
$SF_6 + SO_2^+ \rightarrow$	$SF_5^+ + SO_2F$	2.8×10^{-10}
$SF_6 + SO^+ \rightarrow$	$SF_5^+ + SOF$	4.5×10^{-10}
$SF_6 + H_3O^+ \not\rightarrow$		$<5 \times 10^{-12}$
$SF_6 + NO_2^+ \not\rightarrow$		$<5 \times 10^{-12}$
$SF_6 + NO^+ \not\rightarrow$		$<5 \times 10^{-12}$
$SF_5^+ + NO_2 \rightarrow$	$NO_2^+ + SF_5$	2.3×10^{-11}
$SF_5^+ + NH_3 \rightarrow$	$NH_3^+ + SF_5$	1.2×10^{-9}
$SF_5^+ + H_2S \rightarrow$	$H_2S^+ + SF_5$	5.6×10^{-11}
$SF_5^+ + Br_2 \rightarrow$	$Br_2^+ + SF_5$	$<4 \times 10^{-12}$
$SF_5^+ + Cl_2 \rightarrow$	$Cl_2^+ + SF_5$	$<4 \times 10^{-12}$

Thus the appearance potential of SF_5^+ from SF_6 is 14.42 ± 0.27 eV. Combining this with the ionization potential of SF_5 yields $D°_{298}(F_5S\text{-}F) = 3.9$ eV.

Early work on the energy of the SF_5-F bond placed it at 3.29 ± 0.17 eV based on shock tube studies[183] and at 3.38 eV based on thermodynamic studies.[184] More recently, chemiluminescence experiments done by Kiang et al.[185] yield a somewhat higher value: 3.87 ± at 0.15 eV. Our work is in excellent agreement with this and represents the only other experimental determination of $D°_{-298}(F_5S\text{-}F)$ that corroborates the theoretical value of 3.99 eV calculated by Lyman[186] using Rice-Ramsperger-Kassel-Marcus unimolecular rate theory. Because SF_6 has been used as a model compound for the study of laser induced chemistry and also because the ir multiphoton dissociation of SF_6 has received much attention, an accurate knowledge of its thermodynamic parameters is of importance.

IX. MOLECULAR SPECTROSCOPY

A. Ultrahigh-Resolution Coherent Raman Spectroscopy in Molecular Beams (J. J. Valentini, P. Esherick,* and A. Owyoung*)

Supersonic molecular beams provide a unique environment for molecular spectroscopic studies. By variation of the beam operating conditions, specifically the nozzle orifice size, the pressure behind the nozzle, and the distance downstream of the nozzle where the spectra are recorded, it is possible to select the temperature (300 to <10 K) of the molecules in the beam. This selectivity allows the spectroscopist to control the distribution of the molecules over rotational and vibrational states and hence simplifies the analysis of complex molecular spectra. Significantly, this temperature control can be effected while maintaining pressures in the beam that are

*Sandia National Laboratories, Albuquerque.

orders of magnitude greater than equilibrium vapor pressures, allowing otherwise unresolvable or uninterpretable Raman spectra to be simplified and analyzed, even for relatively involatile compounds.

We have recently completed the first experiments to use coherent Raman techniques, specifically quasi-cw inverse Raman spectroscopy, in obtaining ultrahigh resolution (0.002 cm^{-1}) Raman spectra in pulsed as well as cw molecular beams.[187] Figure 37 shows typical spectra obtained for the ν_1 vibration of methane in both static gas and cw molecular beam. The substantial Doppler width reduction and controlled cooling possible in the beam are evident here.

We are presently applying this technique to the study of the high-resolution spectra of moderately large polyatomic molecules, such as sulfur hexafluoride and ethane, as well as to the study of weakly bound molecules, such as the argon dimer, which can be studied only in molecular beams.

B. Remote Detection of Ionizing Radiation by Raman Scattering from N_2^+ (A. H. Zeltmann)

We have investigated the feasibility of remotely detecting covert radiation sources by Raman scattering from

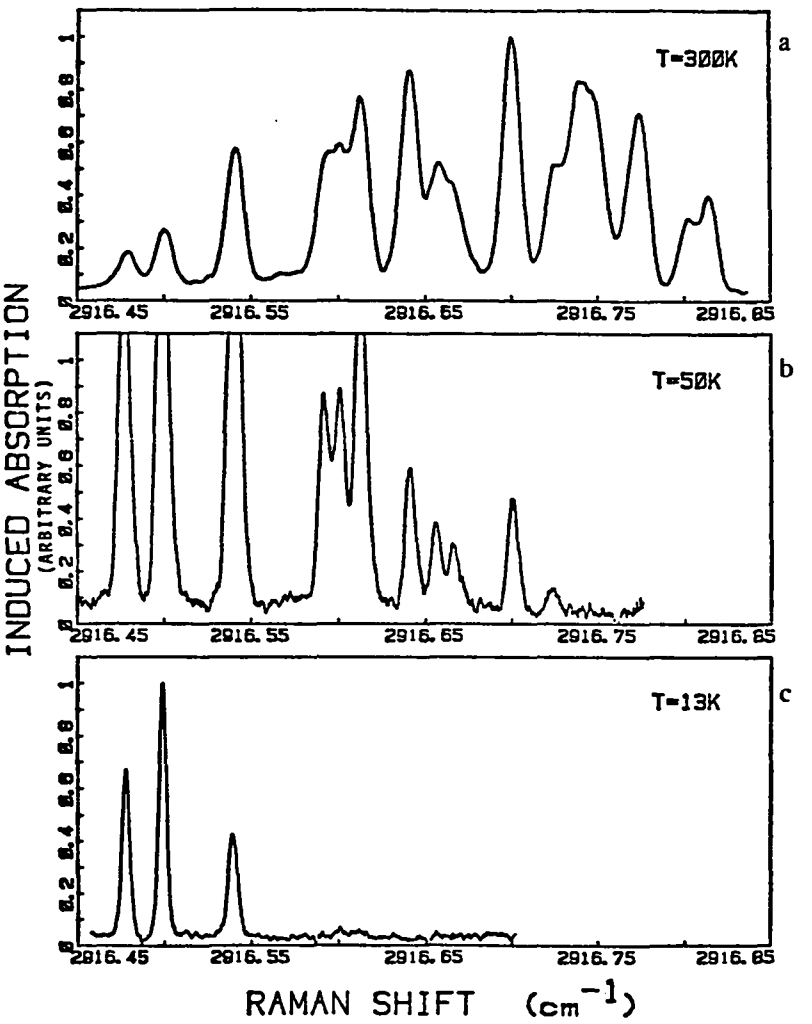

Fig. 37.
Inverse Raman spectra of ν_1 Q-branch of $^{12}CH_4$. Bandhead at 2916.472 cm^{-1}, with higher J transitions extending to higher frequency. (a) Static gas, 1 torr, 300 K, ≈1-deg optical crossing angle; (b) molecular jet, 350-μm nozzle, 4.8 psi backing pressure, 1.8 mm downstream, estimated density (cf. Ref. 188) 1.5×10^{16} cm^{-3}, ≈5-deg optical crossing angle; (c) molecular jet, 100-μm nozzle, 55 psi backing pressure, 4.5 mm downstream, estimated density (cf. Ref. 188) 2.2×10^{15} cm^{-3}, ≈5-deg optical crossing angle.

ions (specifically N_2^+) that are produced in air by the radiation. The air above the source is probed by a laser and the Raman scattered light then collected by a large telescope and focused through a narrow-band light filter onto a photomultiplier detector. N_2^+ ions are the chosen indicator ions because of the predominance of N_2 in the atmosphere.

We have conducted laboratory experiments in which N_2^+ ions in air and in pure N_2 were produced by x radiation at levels of 4×10^5 R/h. To detect these ions we used resonant Raman scattering from the most abundant rovibrational states of N_2^+ in the P-branch near K = 8, with the exciting wavelength at 3914 Å.[189] The Raman scattered light was observed at 4278 Å with a photomultiplier detector. Because the width of the dye laser line is ~0.13 Å and the absorbing line width at 3914 Å is estimated to be ~0.02 Å, much of the dye laser power is off resonance under the best conditions. The dye laser wavelength cannot be controlled more closely than 0.05 Å over a 1-h period, and the drift over the long periods necessary for measurement increases the experimental uncertainty.

Calculations indicated that the rapid charge exchange process

$$N_2^+ + O_2 \rightarrow N_2 + O_2^+$$

would reduce greatly the steady-state concentration of N_2^+. However, the N_2^+ first negative band fluorescence efficiency in air and in pure N_2 is roughly the same.[190] Nitrogen bands involving neutral species have their fluorescence reduced by a factor of 20 in air. Thus, it appears possible to make measurements equally well in air as in pure nitrogen.

Solomon and Silva[191] have made a preliminary study of N_2^+ produced by x rays. Much of our effort was concerned with duplicating their Raman cross-section measurements. We have observed the x-ray fluorescence spectrum reported in the literature[190] and have detected Raman scattering from N_2^+ at 4278 Å. The cross-section estimate from our measurements agrees with those reported by Solomon and Silva.

Calculations based on this cross-section for Raman scattering indicate that this method for detection of covert radiation sources is not feasible. Our most optimistic estimate of the signal at 250 m is 0.05 photons detected per second. This signal cannot be reliably detected unless the observation time is intolerably long in a system whose time stability is measured in fractions of an hour in the laboratory. We have not assumed any background noise, which must be considered for a real system. Even with optimistic parameters our calculations indicate that the signal strength would be too low for reliable detection by at least two orders of magnitude. The basic limitations of the method are threefold:

- Laser power and stability; 1 j/pulse; drift, 0.05 Å^1/h.
- The time that can be devoted to scanning a portion of an area, ~1/min.
- The level of radiation, 1 R/h.

It is a fair generalization that increasing laser power tends to decrease stability and increases bandwidth. Both are detrimental. Without a major breakthrough, no improvements can be expected.

The laboratory ion-producing and Raman detection system we have constructed can, however, be profitably employed to study ionic processes in gases by laser spectroscopy.

C. Optogalvanic Double-Resonance Spectroscopy: Experimental Observations[192] (R. Engleman, Jr., and R. A. Keller)

The optogalvanic effect (laser-induced impedance changes in gaseous discharges) has become an important spectroscopic tool. When two lasers with wavelengths corresponding to different optical transitions are used to induce impedance changes in a discharge, a conjunctive signal is present when there is a common intermediate energy level involved in the two transitions.

The elements studied were neon, uranium, and sodium. The energy levels irradiated in uranium and sodium are shown in Fig. 38 and the data are summarized in Table XXIII. It is apparent that large effects are observed: optogalvanic signals associated with laser B can be tripled when laser A irradiates a transition terminating in a common intermediate level.

Inspection of Fig. 38 and the data in Table XXIII shows that, in sodium, energy transfer can occur to a nearby level, which is not common to both laser irradiations, and can result in a conjunctive signal. Similar effects occur in uranium. Energy transfer will always be a problem when this technique is used to determine a common intermediate energy level involving these two transitions. On the other hand, this effect can lead to interesting information concerning energy-transfer processes in atoms and molecules.

Finally, it should be noted that, although this method can be used to discern connecting energy levels and help

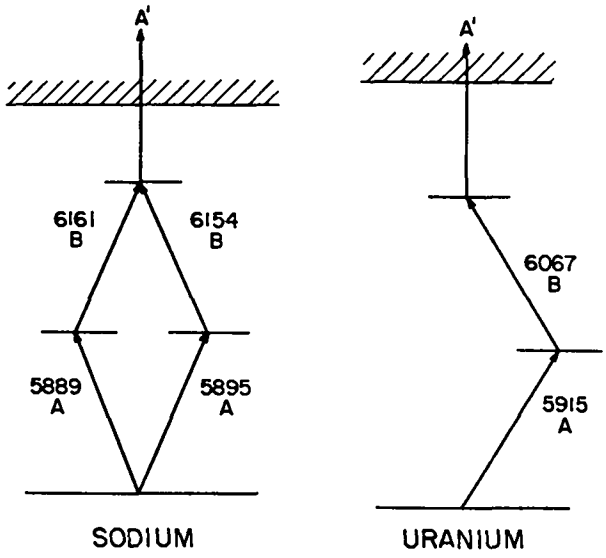

Fig. 38.
Energy levels and irradiated transitions in sodium and uranium for optogalvanic double-resonance spectroscopy. Laser A tuned off resonance (A') had no effect on OGE(B).

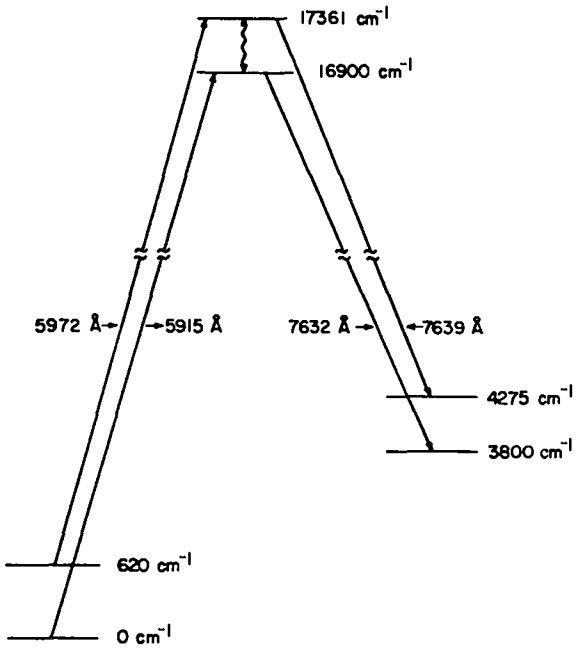

Fig. 39.
Energy levels and irradiated transitions in uranium for laser-enhanced emission studies. The wavy line denotes the occurrence of energy transfer but does not imply a specific mechanism for this transfer.

in spectral assignments, it is no more sensitive than measuring changes in emission intensity, and it is significantly more complicated. An example of finding connecting levels in uranium by inducing changes in emission intensities is shown in Figs. 39 and 40. The spectral assignments shown in Fig. 40 were obtained from the data in the Los Alamos National Laboratory's uranium atlas. Note that the 7639-Å emission is from the energy level at 17 361 cm^{-1}. The intensity of this emission is doubled (Fig. 40a and c) when the laser is tuned to irradiate the 5972-Å transition that terminates

TABLE XXIII

CONJUNCTIVE EFFECTS FOR DUAL-LASER IRRADIATION OF A HOLLOW-CATHODE DISCHARGE

λ_A (Å)	λ_B (Å)	Power A (mW)	Power B (mW)	OGE (B) (mV)	OGE (B + A) (mV)[c]
Sodium					
5895	6154	120	140	5	10
5889	6154	140	140	5	6[b]
5889	6161	140	130	7	10
5895	6161	140	150	10	11[b]
Uranium					
5915	6067	120	50	25	70

[a]Laser A, dc. Signal is B ac signal enhanced by A.

[b]No common energy levels. (See Fig. 38.)

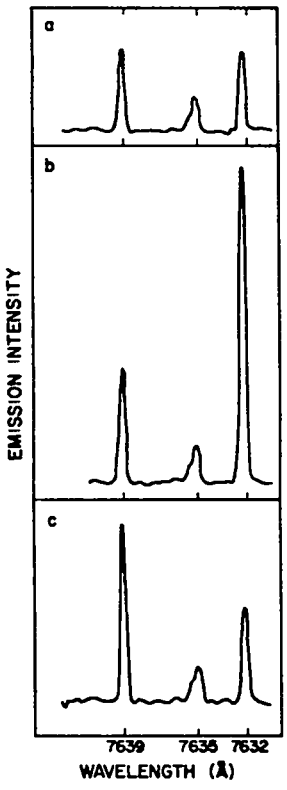

Fig. 40.
Uranium-emission spectra from a hollow-cathode discharge. The vertical axis is the same for all spectra. a. No laser irradiation; b. 240 mW of laser irradiation at 5915 Å; c. 270 mW of laser irradiation at 5972 Å.

in the 17 361-cm^{-1} level. Similar results were obtained with emission at 7632 Å when the laser was tuned to 5915 Å. Energy transfer is also apparent in Fig. 40 by the increase in the 7632-Å emission when the laser is tuned to 5972 Å, or by the increase in 7939-Å emission when the laser is tuned to 5915 Å. The emission line at 7635 Å is from an energy level at 20 420 cm^{-1}, which is too far removed from 17 361 cm^{-1} for appreciable energy transfer to occur.

Optogalvanic double-resonance spectroscopy would be useful for laser-wavelength control in experiments requiring sequential photoexcitation involving a common intermediate level. There may also be some cases in which emission cannot be readily observed because of small quantum yields or highly luminous backgrounds; in those cases, the double-resonance technique would present distinct advantages for discerning common intermediate-energy levels.

D. Locking of cw Dye Laser Emission onto the Wavelength of Molecular Fluorescence by Intracavity Gain: Example I_2[193] (K. A. Truesdell, R. A. Keller, and E. F. Zalewski*)

Locking of laser emission to wavelengths of molecular fluorescence is potentially useful for wavelength standards, molecular excitation for photochemical reactions or fluorescence analysis, gain measurements, and state selection by stimulation emission. In a few cases, that is, I_2, Na_2, Li_2, Bi_2, and Te_2, cw dimer lasers have been developed for these purposes, but we believe that the technique using the gain present in the dye medium will be more generally applicable.

For state selection by stimulated emission there is considerable advantage to placing the sample inside the cavity of the dye laser. State selection by stimulated emission involves the use of a pump laser to excite a molecule to a specific v′, J′ level of an excited electronic state and then stimulation of emission from this state to a specific v″,J″ level of the ground electronic state. It is difficult to use two independent lasers for this purpose because the wavelengths of each laser must be controlled to within a few MHz so that the same portion of the Doppler distribution is addressed by each laser. Placing the sample inside the dye laser cavity automatically pulls the dye laser emission onto the desired fluorescence wavelength. An additional advantage of this technique for some applications is the high circulating power available inside the dye cavity.

The introduction of small optical losses inside the cavity of a broadband dye laser decreases the laser power at wavelengths corresponding to the absorption losses. The laser output is extremely sensitive to these losses, and this phenomenon forms the basis for intracavity absorption spectroscopy. In a similar fashion it has been demonstrated that introduction of small optical gains into the laser cavity results in the laser locking onto wavelengths corresponding to these gains. For example, gains as small as 0.0003 were sufficient to lock a dye laser to emission wavelengths from a helium-selenium discharge placed within the laser cavity. The small optical gain required for laser locking means that this technique should be applicable for many molecular systems in addition to those that exhibit sufficient gain to act as lasers by themselves.

---

*National Bureau of Standards, Washington, D. C.

In the present work a single mode Ar^+ laser is tuned to excite the P(13) and/or R(15), 43′ ← 0″, $B^3\Pi_{o_u^+}$ ← $X^1\Sigma_{o_g^+}$ transition in molecular iodine. The Ar^+ laser radiation is then passed through the dichroic end mirror of the dye laser cavity and into a sample cell of iodine. Iodine flurescence has been detected on transitions v′ = 43, J′ = 12 and/or 16 to J″ = 11, 13 and/or 15, 17, v″ = 0 to 86. This fluorescence introduces gain into the optical cavity at the corresponding wavelengths; when the dye laser is tuned near to one of the fluorescence wavelengths, locking occurs, with the result that a substantial amount of the dye laser output is at a wavelength corresponding to a particular iodine fluorescence (Fig. 41).

The major conclusions from this work are:

(1) An organic dye laser is sensitive to small optical gains as low as 0.0001 are sufficient to lock a portion of used effectively to lock a large portion of the laser output onto wavelengths corresponding to molecular fluorescence. We have demonstrated that single-pass gains as low as 0.001 are sufficient to lock a portion of the dye laser output onto I_2 fluorescence frequencies.

(2) The intracavity gain-probing technique requires wavelength control of the pump-down laser of only ±6 Å. In contrast, if a single-frequency extracavity method were used for gain detection, the pump-down frequency would have to be controlled to within a few MHz.

(3) The dye-laser-assisted I_2 laser should be useful for state selection and photochemical applications. These experiments could be performed either extracavity or intracavity, and the efficiency of the system can be maximized by judicious choice of the transmission characteristics of the output coupler.

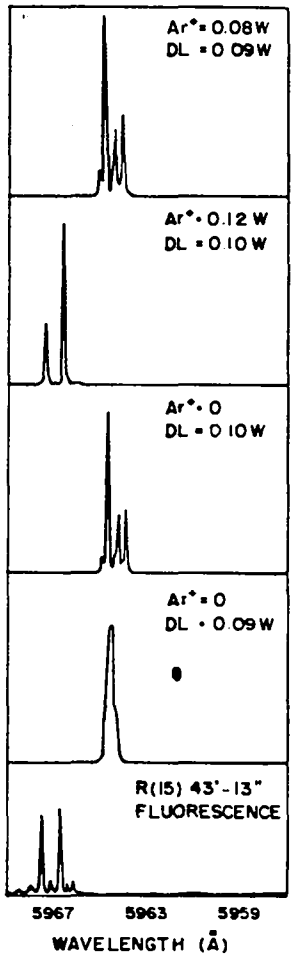

Fig. 41.
Dye laser assisted I_2 laser spectra for 43′ − 13″ transitions. $Ar^+ = Ar^+ - I_2$ pump laser power, DL = dye laser circulating power, 19 cm I_2 cell. (a) Dye laser with I_2 inside the cavity and the $Ar^+ - I_2$ pump laser tuned off the 43′ − 0″ absorption, P_{I_2} = 0.3 torr. (b) Dye laser with I_2 inside the cavity, $P_{I_2} = 0.3$ torr. $Ar^+ - I_2$ laser is tuned to $R(15)43' - 0''$ absorption. (c) Dye laser with I_2 inside the cavity (no Ar^+ laser), $P_{I_2} = 0.3$ torr. (d) Dye laser without I_2 inside the cavity (no Ar^+ laser), $P_{I_2} = 0$. (e) I_2 fluorescence, $P_{I_2} = 0.3$ torr, $Ar^+ = 0.11$ W⊙, $Ar^+ - I_2$ laser tuned as indicated in (b). The intensity scale is the same for a—d.

E. Photoionization of Polymers of Hydrogen Sulfide and of Carbonyl Sulfide (N. C. Blais and E. Walters*)

The photoionization work currently being conducted in Group CNC-2 is directed at obtaining properties of ions of van der Waals molecules and, where possible, the properties of the neutral molecules.[194,195] By comparing the variation of some of the measured properties, such as the ionization potential, with the size of the molecular cluster, we can begin to obtain values for bulk properties from those of the individual molecules. We report here on the photoionization yields of carbonyl sulfide and its dimer and of hydrogen sulfide and several of its polymers.

The apparatus consists of a monochromatic photon source, a free jet expansion molecular beam source, and a moderate resolution mass spectrometer.[194] Besides cooling the beam molecules sufficiently to produce measurable concentrations of molecular clusters, the free jet expansion also collapses the distribution of initial rotational states of the molecules to that characteristic of a temperature of less than 100 K. As a result, the resolution of the photoion yield curves approaches the optical resolution of the monochromator. For the

*University of New Mexico.

monomeric species the optical resolution is about 12 meV (1.5 Å), whereas for the polymers the optical resolution is 32 meV (3.7 Å) because wider slits are used.

Figures 42 and 43 show the photoion yield per photon for the carbonyl sulfide (OCS) system. Figure 42 is for the monomer OCS^+ and Fig. 43 is for the dimer $(OCS)_2^+$. The energy threshold is clearly lower for the dimer than for the monomer. The autoionization peak at about 1010 Å is sharp and narrow for the monomer and centered at 1017 Å. For the dimer it is broadened considerably and shifted slightly upward in energy. Both changes are the result of the presence of the other moiety, the neutral OCS partner. Application of the Born-Haber cycle gives a value of 0.45 ± 0.01 eV for the van der Waals bond energy of $(OCS)_2^+$. Table XXIV summarizes some of the transitions of the OCS molecule that we have identified in the photoion spectrum of the monomer.

Figures 44 and 45 show the photoion yields of the H_2S molecule and its dimer, respectively. Autoionization makes the monomer spectrum of H_2S more complicated

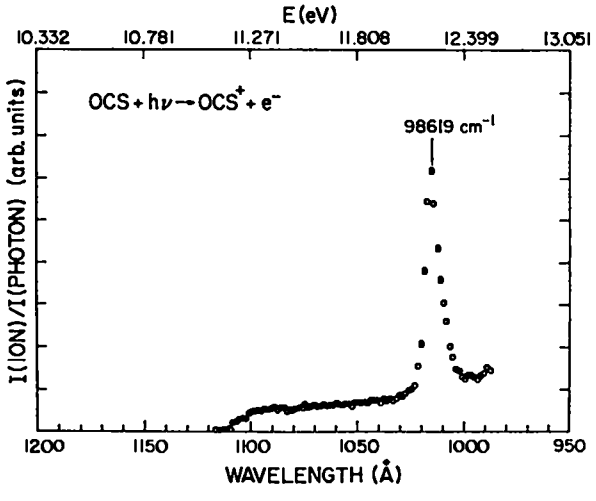

Fig. 42.
The photoion yield per photon for OCS^+. Error bars are less than the size of the circled points.

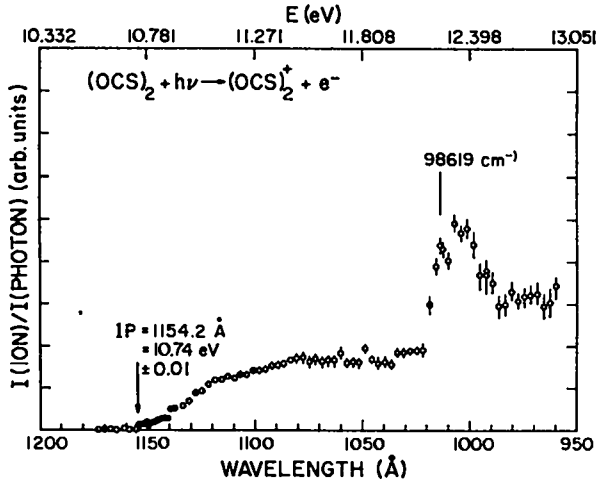

Fig. 43.
The photoion yield per photon for the dimer, $(OCS)_2^+$.

TABLE XXIV

IONIZATION THRESHOLDS AND SPECTRAL ASSIGNMENTS FOR OCS^+ AND $(OCS)_2^+$

Ion	Ionization Threshold	Wavelength
$OCS^+(^2\Pi_{3/2})$	11.179	1109.1
$OCS^+(^2\Pi_{1/2})$	11.213	1105.7
$(OCS)_2^+$	10.74	1154.2

Wavelength	ΔE (cm^{-1}, ±50)	Spectral Assignment
1100.7	688	$^2\Pi_{3/2} + \nu_1$
1097.4	684	$^2\Pi_{1/2} + \nu_1$
1093.5	1286	$^2\Pi_{3/2} + 2\nu_1$
1090.1	1294	$^2\Pi_{1/2} + 2\nu_1$
1085.2	1986	$^2\Pi_{3/2} + \nu_3$ or $3\nu_1$
1081.7	2007	$^2\Pi_{1/2} + \nu_3$ or $3\nu_1$

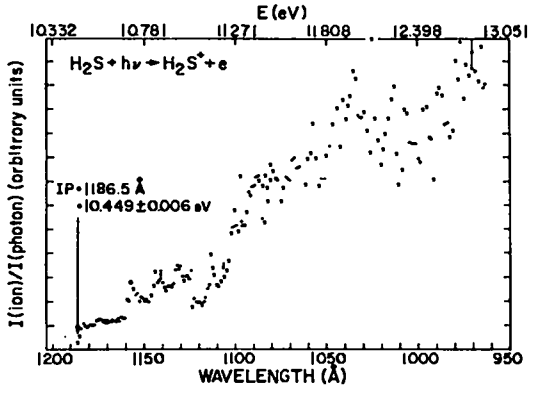

Fig. 44.
The photoion yield per photon for H_2S^+. Typical error bars are shown. Near threshold, the statistical errors are less than the circled points.

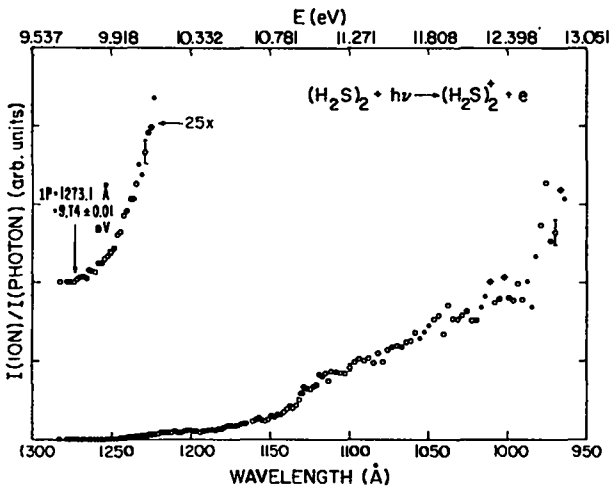

Fig. 45.
The photoion yield per photon for $(H_2S)_2^+$. The insert is the region near threshold and has the same wavelength scale.

than the spectra of CS_2 or OCS within the same energy range. As was the case with OCS, considerable broadening of the autoionization peaks occurs in the $(H_2S)_2^+$ spectrum. Much of the analysis of the H_2S^+ spectrum remains to be done, but several very interesting properties of the polymers are quickly obtained. Figure 46 shows the variation of the ionization threshold energy with the number of H_2S units comprising the van der Waals molecule. In contrast to results for other polymers,[194,196,197] a straight line does not fit these data because the relative strengths of the bonds as monomeric units are added to the polymer. One can conjecture that

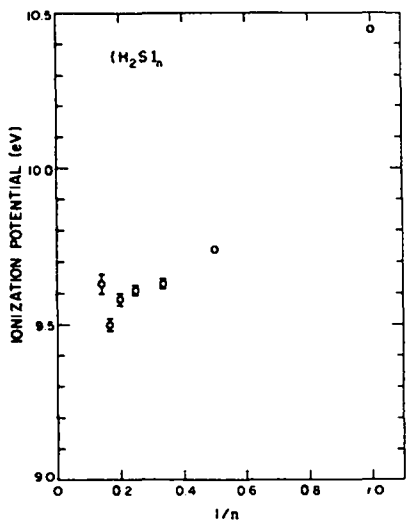

Fig. 46.
The ionization potential in electron volts of H_2S polymers, $(H_2S)_n$, where n is the number of H_2S units in the polymer, plotted as a function of 1/n.

hydrogen bonding, which should occur as with H_2O, is responsible for the departure from a straight line, but virial coefficient data indicate an unexceptional bond strength for the neutral dimer, 0.028 eV.[198,199] The dimer ion is bound by 0.74 ± 0.01 eV. Bonding of each additional H_2S unit in the ion can be obtained from Fig. 46 with additional assumptions about the small nuetral bond strengths.

F. Evaluation of the Vibrational Transition Moment for the υ_2 Bands of $^{14}ND_3$ and $^{15}ND_3$ (L. H. Jones and B. J. Krohn)

In connection with the development of lasers for irradiation in certain regions of the infrared, we desired to know the vibrational transition moment for the υ_2 bands of $^{14}ND_3$ and $^{15}ND_3$. These vibration-rotation bands had been previously observed and analyzed by one of us[200] at relatively high resolution (0.04 cm^{-1}, full width half maximum). The best approach is to measure the true integrated intensities of a number of individual lines of known vibration-rotation transition. To resolve individual lines this requires a pressure of 10 torr or less. The true line widths are then narrower than our resolution. This required development of a computer program for deconvolution of the true line intensity from the observed width and peak absorbance. The line shape assumed was a Voigt function, which combines Gaussian character because of Doppler broadening and Lorenzian character because of pressure broadening. Applying this treatment led to a transition moment of 0.179 ± 0.010 Debye for both $^{14}ND_4$ and $^{15}ND_3$. These lead to a derivative of the dipole moment, $|\partial\mu/\partial Q_2| = 93$ $cm^{3/2}$ $s.^{-1}$ A manuscript describing these studies is now in press.[201]

G. Low-Temperature Impurity-Doped Solids

1. High-Resolution Infrared Absorption Studies of SF_6 and SeF_6 Trapped in Noble Gas Solids (L. H. Jones, B. I. Swanson, and S. A. Ekberg). Matrix isolation spectroscopy has become widely used to study molecular structure, isotope shifts, free radicals, V-V energy transfer and other effects for which lack of rotational and collisional complications is desirable. A premixed gas is deposited onto a sample plate at cryogenic temperature. The guest, or impurity, is generally quite dilute (mole fraction 10^{-3} or less) in the host matrix to minimize

aggregation and resonance interactions. The host is commonly a noble gas (neon, argon, krypton, xenon) or nitrogen because these are relatively inert species and will not affect significantly the structure or vibrational energy levels of the guest molecules. Although it is generally recognized that there is always some host-guest interaction, the nature of such matrix effects is not well understood, and they are generally ignored. However, for such little understood phenomena as energy transfer and molecular dynamics in matrices, it is important to understand the matrix-molecule interactions. For example, it has been reported that CH_3F does not rotate in a low-temperature argon matrix;[202] yet recent V-V energy transfer studies of CH_3F in argon matrices[203] indicate that relaxation occurs by transfer of a quantum of the C-F stretching vibration to a rotational level of high quantum number (14-18). We hope to resolve such contradictory results by detailed studies of matrix-molecule interactions using high resolution.

In the past, and even today, most infrared matrix studies are carried out at fairly low resolution ($\sim$1 cm^{-1}), leading to concealment of many of the enlightening details of the absorption spectra. With the use of high-resolution infrared studies (0.035 cm^{-1}), we have resolved structure revealing new and important matrix effects. Much of this work has been carried out with SF_6 in noble gas matrices. As an example of the value of high resolution, we present Fig. 47, which shows the ν_3 absorption band of SF_6 in argon at both 0.5- and 0.035-cm^{-1} resolution. SF_6 is an octahedral molecule for which ν_3, the antisymmetric S-F stretching mode, is triply degenerate for the truly unperturbed molecule. The 0.5-cm^{-1} spectrum shows little detail; however, the high-resolution spectrum, as reported earlier,[204] shows much sharp, fine structure, which indicates multiple trapping sites and site symmetry splittings.

In Fig. 48 we show the effect of temperature variation on the observed vibrational spectrum. Note that in heating from 10-16 K, peak H disappears (actually it merges with I). This temperature effect is *completely reversible*, although in some cases spectral changes with temperature indicate irreversible phenomena, such as aggregation, change in site structure, or change in crystallite size. We attribute this temperature reversible coalescence to dynamic site exchange induced by vibrational dephasing[205] and will discuss it further in Sec. IX.G.2. We believe that peaks H and I are site symmetry split components from one site and that E and F are from another site. Including the other peaks observed, we conclude that there are at least six different trapping sites

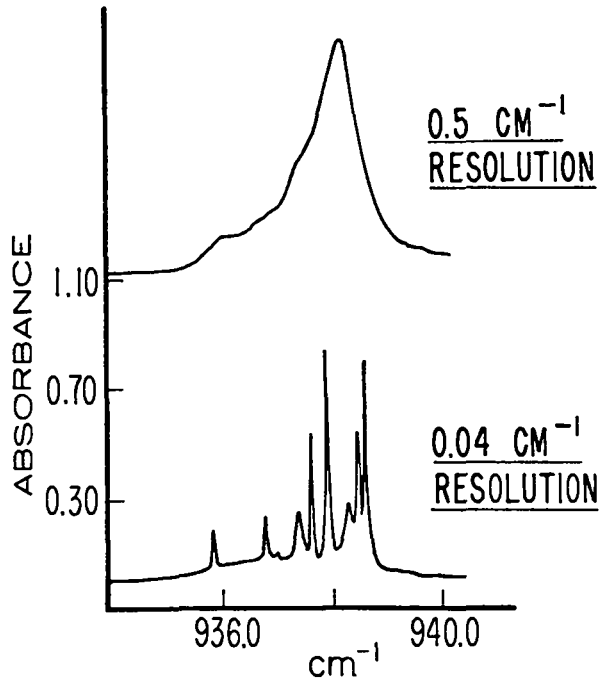

Fig. 47.
Spectrum of SF_6 in argon at 10 K at a ratio of 1/10 000. Resolution is as indicated.

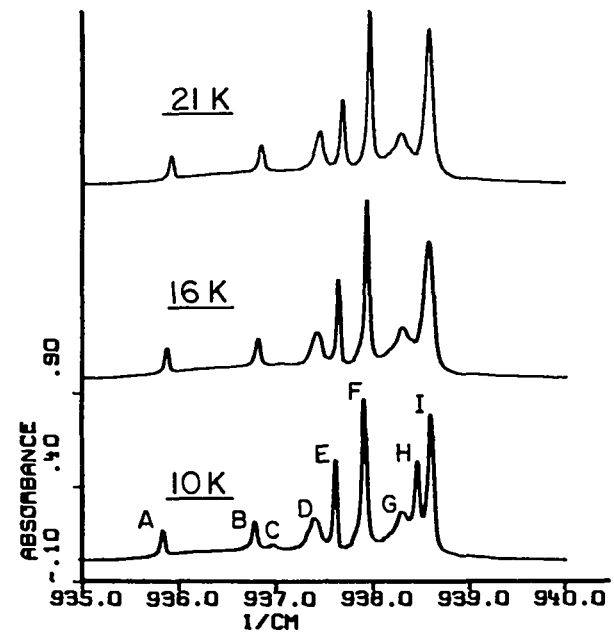

Fig. 48.
ν_3 absorption, Ar/SF_6 = 10 000 annealed at 30 K. Temperatures as indicated.

for SF_6 in an argon matrix under the conditions of Fig. 48.

SF_6 in a krypton matrix shows rather different structure. Of particular interest is a striking difference for

$^{34}SF_6$ and $^{32}SF_6$ as shown in Fig. 49. This compares the spectrum of the two isotopic species in a matrix containing equal amounts of $^{32}SF_6$ and $^{34}SF_6$. In particular, note that the strong $^{34}SF_6$ peak is sharper and more symmetrical than the analogous peak for $^{32}SF_6$, which has a side-band structure. The only explanation that occurs at present is that the vibrational amplitudes differ, particularly in the excited state. The greater amplitude for ν_3 of $^{32}SF_6$ may lead to greater interaction with the phonons, leading to phonon side bands. This requires further investigation. One other point to notice is that the two high-frequency doublets coalesce with increase in temperature, another example of dynamic site exchange.[206]

Temperature dependent studies of SF_6 in a xenon matrix show that a high-frequency doublet of ν_3 exhibits dynamic site exchange and amazingly shows a kinetic isotope effect (see Sec. IX.G.2)[207]. Other groups are studying V-V energy transfer of SF_6 in noble gas matrices by pumping the ν_3 mode with a CO_2 laser and studying the relaxation from excited vibrational states.* To interpret such results satisfactorily, it is important to understand what transitions are being pumped. For example, for SF_6 in argon at 10 K there are only two near coincidences of CO_2 laser lines with SF_6 absorption lines—10P26 (936.83) is slightly below peak B. (Fig. 48). We note that the absorption lines shift slightly, in an unpredictable fashion, as temperature is changed. Thus, with a knowledge of the high-resolution spectrum and the frequency shifts with temperature, one can hope to optimize the pumping efficiency. For a krypton matrix at 10 K, the only near coincidence is from 10P30 (934.92 cm^{-1}), which hits on the low-frequency side of the strong peak. For SF_6 in xenon at 10K, 20P34 (931.05 cm^{-1}) of a CO_2 laser falls on the low-frequency wing of the strong peak whereas 10P32 (933.00 cm^{-1}) lies in the middle of the high-frequency coalescing doublet.

We have also studied the spectra of SeF_6 isolated in noble gas matrices. It is somewhat larger than SF_6 and thus gives us a probe into the effect of change in size of the guest within a given matrix host. In Fig. 50 we see a rich display of absorption peaks because five isotope species contribute significantly, each one giving rise to seven peaks. Fortunately, the isotope shift for a mass change of two is greater than the spread of peaks for one isotope. Thus it is not difficult to assign peaks to a given isotope. The fine structure is duplicated for each isotope with the appropriate intensity. By comparison of lattice constants of the matrix and molecular sizes, we might expect SeF_6 in krypton to have a spectrum similar in structure to SF_6 in argon. Although the spectra are not duplicates, there is some correspondence. In particular we note that the doublet slightly above 772.0 cm^{-1} shows dynamic site exchange and coalescence in the same temperature range as does SF_6 in argon.[208] This is discussed further in Sec. IX.G.2.

SeF_6 in xenon shows structure and dynamics similar to SF_6 in xenon. In an argon matrix, however, SeF_6 does not resemble any of the SF_6 matrices and does not show evidence of dynamic site exchange.[209]

*This information was provided by L. Abouaf-Marguin, Université de Paris-Sud.

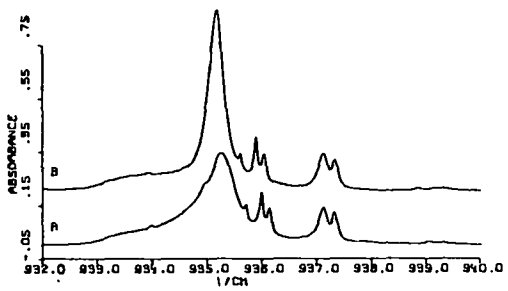

Fig. 49.
ν_3 absorption for $^{32}SF_6$ and $^{34}SF_6$ at 10 K. Kr/$^{32}SF_6$/$^{34}SF_6$ = 10 000/0.5/0.5, A = $^{32}SF_6$; B = $^{34}SF_6$. Frequency scale is shifted by ~17 cm^{-1} for $^{34}SF_6$.

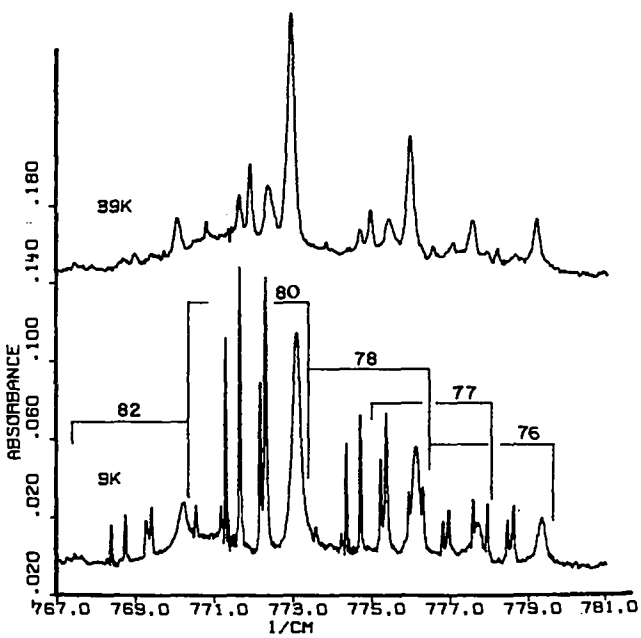

Fig. 50.
ν absorption for SeF_6, natural abundance Kr/SeF_6 = 10 000; annealed at 39 K. Numbers over bracketed regions indicate selenium isotopic mass.

We have not yet discussed the trapping cages we expect for these octahedral molecules in noble gas matrices, which have a face-centered cubic structure. In Ref. 206, we conclude that in argon, krypton, and xenon, SF_6 and SeF_6 are too small to fit satisfactorily in place of six host atoms. However, they will fit rather snugly in a four-atom substitutional site in Td (tetrahedral) symmetry. Therefore, the relevant spectroscopic point groups for these molecules are Td (a subgroup of O_h) and the subgroups of Td. This tells us, for example, that SF_6 could reside on a site of symmetry C_{3v} or C_s or any of the other subgroups of Td within a Td trapping cage resulting in splitting of the ν_3 mode. We have not yet been able to sort out the symmetries of the various observed sites.

Finally we would like to discuss results for both SF_6 and SeF_6 in a neon matrix. From the size we conclude that these molecules must replace six neon atoms and may thus maintain octahedral symmetry.[206] Because of distortions, however, the ν_3 mode could be split into two or three absorption peaks. We note that the major absorption in each case consists of three peaks, suggesting low symmetry because of distortion from O_h symmetry. If it were possible to follow these absorptions to high enough temperature, we might observe coalescence from dynamic averaging. The absorptions in neon are fairly close to the gas phase values for ν_3 [~947.7 for SF_6 (Ref. 210) and 778.5 for SeF_6 (Ref. 211)]. Also the isotope shifts can be measured quite accurately. These facts indicate that an accurate potential function can be calculated from the spectra. The ν_3 frequencies for $^{80}SeF_6$ and the various isotope shifts are given in Table XXV. Using the gas phase frequencies[211] for ν_3 and ν_4 (778.5 ± 2 cm^{-1} and 436.0 ± 5 cm^{-1}), we have calculated the potential constants for SeF_6. The computer program was altered to refine on the isotope shifts as well as on the frequencies of the main isotope, using weights in accord with the above estimated error limits. The results are listed in Table XXVI along with earlier values of Abramowitz and Levin[211] estimated with the aid of the Coriolis constant ζ_4 calculated from band contour analysis of $\bar{\nu}_4$. Within experimental error our results are in agreement with those of Ref. 211; however, ours are determined with greater precision. This is another demonstration that accurate isotope shifts measured in a neon matrix are quite useful for estimation of potential constants.

2. Dynamic Site Exchange and Vibrational Dephasing on a Picosecond Time Scale (B. I. Swanson and L. H. Jones). Matrix isolated molecules are expected to exhibit rich dynamics ranging from rigid structural arrangements at low temperature (T <10 K) to diffusion at temperatures well below the melting point of the host matrix. Surprisingly, the only dynamic process that has been studied in any detail for low-temperature matrices is hindered molecular rotation of diatomics and other small molecules.[212] These earlier studies were carried out at relatively low resolution (~0.5 cm^{-1}). In an effort to further clarify dynamics in low-temperature matrices, we have studied the high-resolution (0.035 cm^{-1}) ir spectra of trapped species as a function of temperature, where irreversible spectral

TABLE XXV

FREQUENCIES FOR ν_3 OF $^{80}SeF_6$ AND ISOTOPE SHIFTS FOR $^{1}SeF_6$ IN A NEON MATRIX[a]

	ν	Δν(cm^{-1})				
Peak	$^{80}SeF_6$	80-82	80-78	80-77	80-76	80-74
A	775.986	2.955	−3.105	−4.720	−6.382	−9.840
B	776.069	2.951	−3.108	−4.723	−6.385	−9.843
C	776.186	2.947	−3.108	−4.720	−6.384	---
D	776.543	2.955	−3.108	---	---	---
E	776.751	2.951	−3.112	---	---	---
Ave Δν		2.952	−3.108	−4.721	−6.384	−9.841

[a]Neon/SeF_6 = 10 000/1; T = 4.2 K.

TABLE XXVI

POTENTIAL CONSTANTS FOR F_{1u} MODES OF SeF_6

	A[a,b]	B
C_{33}	0.2176(3)	---
C_{44}	0.584 (3)	---
C_{34}	−0.0907(5)	---
F_{33}[c]	4.916 (6)	4.88 ± 0.10
F_{44}	1.823 (13)	1.817 ± 0.03
F_{34}	0.765 (6)	0.74 ± 0.04

[a]A (gas phase, uncorrected for anharmonicity); B (calculated by Abramowitz and Levin, Ref. 207).

[b]Numbers in parentheses are least squares standard deviations in units of last decimal place.

[c]Symmetry force constants are as defined in Ref. 211. Units are millidynes A^{-1} for F_{33}, millidyne · rad^{-1} for F_{34}, and millidynes · $A \cdot rad^{-2}$ for F_{44}. Units for compliance constants, C_{ij}, are inverse of those for F_{ij}.

changes have been eliminated by prior annealing of the matrix (see Sec. IX.G.1).

Noble gas (neon, argon, krypton, and xenon) matrices of SF_6 and SeF_6 exhibit substantial spectral changes with temperature that are completely reversible. The most striking result is the broadening and coalescence of site symmetry split components of degenerate modes to give single peaks as temperature is raised; the results obtained for ν_3 of SF_6 in an argon matrix, which are typical, are shown in Fig. 51. Similar studies for $^{80}SeF_6$ are shown in Fig. 52. We have been able to show that the motional collapse of site symmetry split components results from rapid exchange among equivalent low symmetry trapping sites on the ir time scale, much like motional averaging of NMR, which is often observed for nonrigid molecules.[213] Our results represent the first observation of motional averaging on the vibrational time scale and can be treated using modern theories of vibrational dephasing.[214-216] Essentially, the two high-frequency fundamentals of the trapped species undergo phase relaxation through anharmonic coupling of both modes to a low-frequency site local phonon mode. Excitation and de-excitation of the site phonon mode through coupling to the phonon bath modulates phase exchange between the two fundamentals. As temperature is raised, the rate of excitation and de-excitation of the low-energy dephasing mode increases, resulting in exchange averaging of

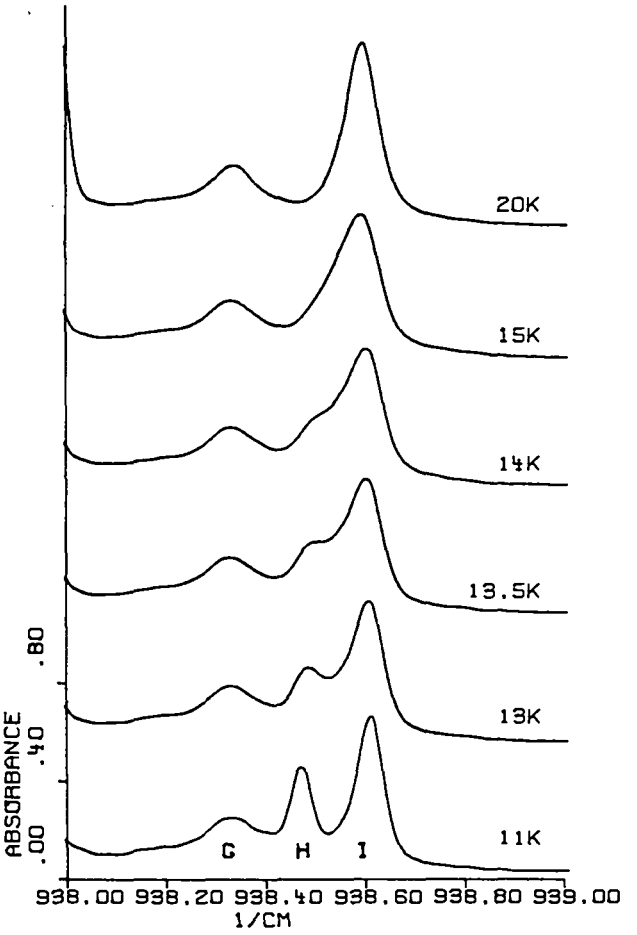

Fig. 51.
Temperature dependence of portion of ν_3 region of SF_6 in argon matrix. Argon/SF_6 = 10 000; deposited at 9 K and annealed at 30 K.

the two fundamentals. It is stressed that several systems studied to date exhibit motional collapse of vibrational bands, indicating that dynamic site exchange is a general phenomenon for matrix isolated species and, no doubt, is important for other impurity doped solids.

We have used a modifed Bloch equation to estimate the activation energies for site exchange where the frequency spectrum is given by

$$I(\nu) = \mathrm{Im}\,\frac{i\tau[I_+(\alpha_-\tau + 1) + I_-(\alpha_+\tau + 1) + 2(I_+I_-)^{1/2}]}{(\alpha_+\tau + 1)(\alpha_-\tau + 1) - 1}$$

and $\alpha_\pm = 1/T_\pm + 2\pi i(\nu - \nu_0 \pm \delta\nu/2)$. Here $T_\pm$, $I_\pm$, and $\delta\nu$ are the pure dephasing times, the intensities, and the peak separations in the low-temperature zero exchange limit. The spectral changes as a function of temperature have been used with the above equation to evaluate the activation energies for exchange, E_a, and the

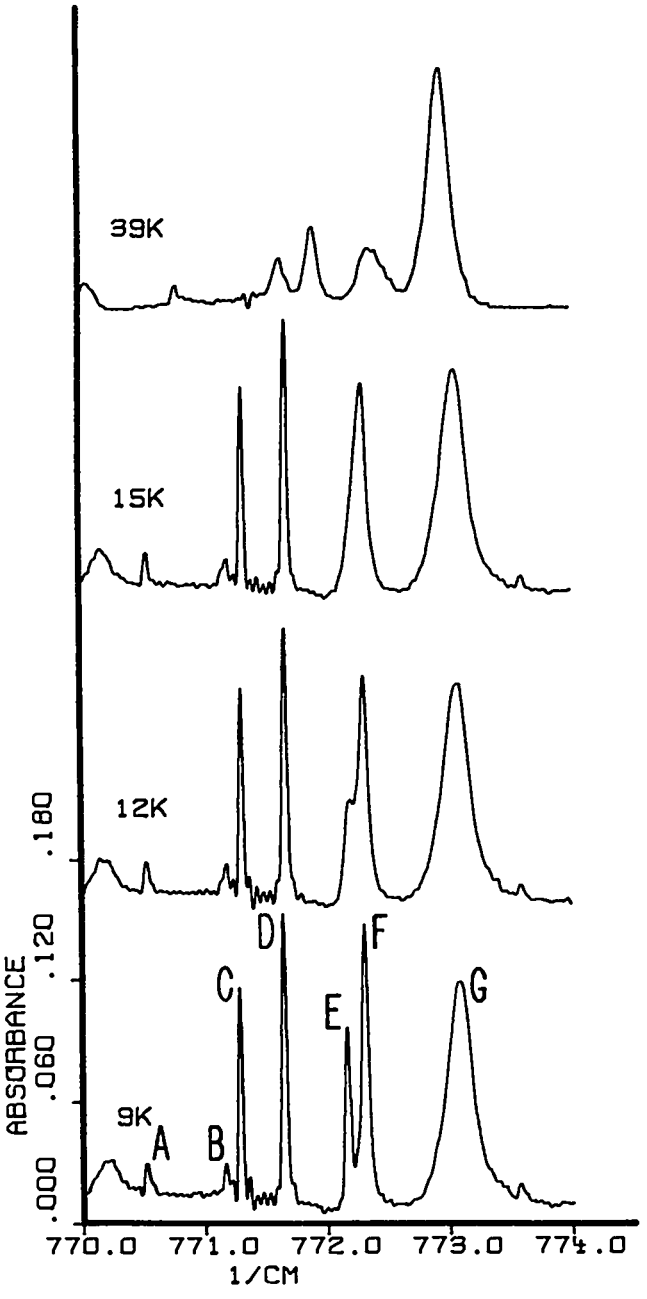

Fig. 52.
ν_3 region for $^{80}SeF_6$ in a krypton matrix deposited at 20 K and annealed at 39 K; 1:10 000.

high-temperature exchange rates; these are presented in Table XXVII for several systems. This is essentially an Orbach type activation process, where E_a gives the energy of the dephasing mode.[214,215] The frequencies of the dephasing modes calculated using the above procedure all fall within the broad phonon bands[217] of the host matrix materials. Thus, it is reasonable that the dephasing modes correspond to resonances in the phonon structure induced by the impurity molecules.

TABLE XXVII

BARRIERS AND HIGH-TEMPERATURE EXCHANGE TIMES FOR DYNAMIC SITE EXCHANGE FOR SF_6 AND SeF_6 IN NOBLE GAS MATRICES

	E_a (cm^{-1})	τ_o ps
SF_6/Ar	21	11
SF_6/Kr	9	65
$^{32}SF_6$/Xe	17	54
$^{34}SF_6$/Xe	17	45
SeF_6/Kr	31	4
SeF_6/Xe	23	65

Although theories of vibrational dephasing provide a model for interpretation of the matrix results, current observations point to the need for further development of current theories. First, we observe asymmetric line shapes for the fundamentals undergoing phase exchange, whereas current theories predict Lorentzian lines. Surprisingly, we observe an inverse kinetic isotope effect for the site exchange process in the case of SF_6 in xenon. Essentially, the $^{34}SF_6$ species shows motional collapse at a significantly lower temperature than $^{32}SF_6$. It is difficult at present to rationalize a kinetic isotope effect for such a subtle mass change. The theory for vibrational dephasing must be modified to explain adequately the matrix results.

In addition to vibrational dephasing, the temperature dependence studies show unusual relative intensity and line-width changes for monomer trapping sites. Results obtained for SeF_6/Kr are presented in Fig. 52, where the ν_3 peaks for several sites are shown to lose intensity and broaden as temperature is raised. The relative intensity changes do not result from changes in equilibrium among the various monomer sites because none of these grow in intensity. Rather, the intensity appears to go reversibly to a broad absorption underlying the sharp monomer peaks. This broad band is consistent with that expected for a trapped molecule that is undergoing rapid (on the vibrational time scale) pseudo-rotation to give an averaged external environment for the molecule. The fact that the relative intensity changes are accompanied by a

concommitant line broadening points to dynamics as the source of the spectral changes. Note, however, that current theories for dynamics perturbations to vibrational structure do not allow for intensity changes. Additional experimental and theoretical work is needed to understand fully the rich and unusual dynamics exhibited by matrix isolation species.

Dynamics of molecules trapped in low-temperature matrices plays an important role in both V-V energy transfer processes and energy relaxation. It has been shown[218,219] that the efficiency of V-V energy transfer is strongly dependent on the mismatch in energies of the vibrational states involved and is, therefore, assisted by low-energy modes, which provide and receive excess energy. In energy relaxation, a quantum of vibrational energy is transferred directly to several quanta of rotational, resonance phonon, or bulk phonon modes.[219] Much of the early work with V-V energy transfer and energy relaxation phenomena focused on diatomic molecules trapped in inert gas matrices where rotation of the diatomic was known to play a dominant role.[219] Spectroscopic studies of the fundamental stretch of several diatomics clearly exhibited rovibrational structure consistent with the diatomics acting as free or hindered rotors in the matrices.[212]

More recently, interest in V-V energy transfer and relaxation in condensed phase materials has shifted to larger molecules such as CH_3F and SF_6. The tendency has been to attribute the dominant low-energy mode in energy transfer processes to free or hindered rotational motion by analogy to the earlier work on diatomics. It is quite clear from our work on SF_6 in a variety of matrices and CH_3F in argon that these molecules do *not* undergo rotation. Accordingly, we believe that for these systems the dominant receiver modes for energy relaxation and phonon assisted V-V energy transfer must involve local site phonon modes and not rotational modes. The fact that we observe vibrational dephasing for site symmetry split components of degenerate vibrations of trapped molecules is prima facie evidence for substantial anharmonic coupling between these modes and a low-energy dephasing mode. Thus, the mechanism for energy relaxation to such dephasing modes is present in these systems and, no doubt, provides the dominant pathway for energy transfer and relaxation. It is our contention that local site phonon modes will dominate V-V energy transfer and relaxation for most large molecules trapped in a host crystal.

3. Estimation of True Line Shapes, Widths, and Intensities for Sharp Absorption Peaks in Low-Temperature Matrices (L. H. Jones). In our low-temperature matrix experiments, we have observed a number of sharp absorption lines using our high-resolution ir Fourier transform spectrometer. To understand the matrix-molecule interactions and dynamics, it is important to be able to estimate the integrated intensities, widths, and shapes of these lines. Our spectrometer can resolve lines having a full width at half maximum (FWHM) of ~ 0.035 cm^{-1}. Even so, we find some lines in low-temperature matrices that are considerably narrower than the available resolution. To estimate the true intensity and width of such lines, one must deconvolute this information from the observed spectrum and the known instrumental line shape (ILS). This has been carried out satisfactorily for lines that are only slightly narrower than the ILS; however, for lines that are considerably narrower (by a factor of 1/4 or less) significant discrepancies appear, as evidenced in studies of N_2O and CO vapor, for which transition moments are known.

We record our highest resolution spectra without apodization. This results in a sin x/x function for the ILS. For the narrower lines this leads to undulations on either side of the peak. One can remove these undulations by applying an apodization function to the interferogram before transforming it; however, it degrades the resolution, which is undesirable for our purposes. Figure 53 presents calculated spectra for Lorentzian lines of different true widths but the same integrated intensity convoluted with our instrumental line shape. We see that if the true line width is equal to or larger than the instrumental line width, the undulations disappear. However, as we go to narrower lines, the undulations become more pronounced. It appears that the amplitude of these undulations will be a useful measure of the true line width—more so than the observed width. The instrumental line shape is primarily determined from the mirror travel and the aperture of the source. It appears that another experimental factor may be affecting our results to some extent, and we are trying to pin this down for better accuracy.

Note, in Fig. 53, how the observed peak area decreases dramatically as the true line width becomes much smaller than the instrumental line width (resolution). Thus, the apparent intensities of narrow lines can be quite deceiving without thorough analysis.

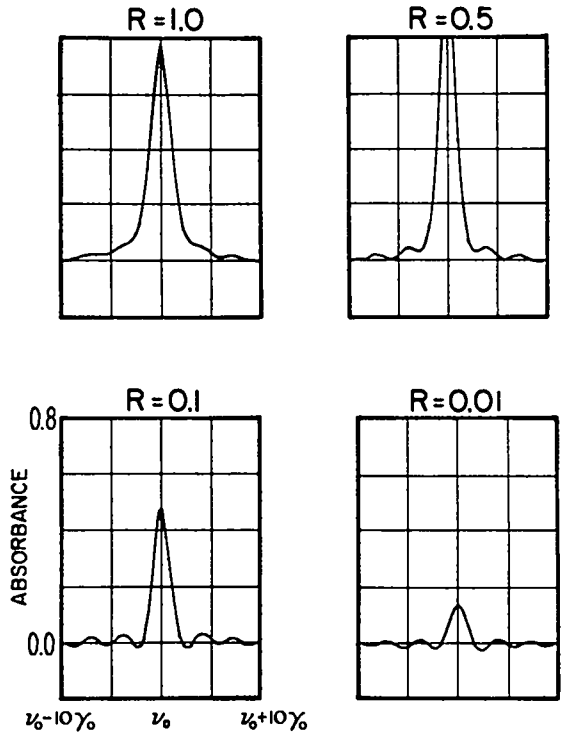

Fig. 53.
Convolution of Lorentzian lines of fixed integrated absorbance (0.037 π) but varying width, γ, with instrumental line shape of width γ_0. $R = \gamma/\gamma_0$. Scale is the same for all four curves. γ and γ_0 are half widths at half maximum.

H. Laser and Photo-Chemistry

1. Isotopically Selective Dissociation of SPF_3 Using a High-Energy Pulsed CO_2 Laser (L. B. Asprey, L. H. Jones, and S. A. Ekberg). This experiment was designed to investigate the dissociation, and accompanying isotopic selectivity induced in SPF_3 by irradiation with a high-energy pulsed CO_2 laser. The analyses were carried out with infrared absorption spectroscopy for extent of reaction and mass spectroscopy for $^{32}S/^{34}S$ isotopic ratio. For greater sensitivity we required SPF_3 enriched to about 50% in ^{34}S. Both $^{32}SPF_3$ and $^{34}SPF_3$ were prepared by the reactions

$$S + PCl_3 \xrightarrow[100°]{AlCl_3} SPCl_3;$$

$$SPCL_3 + 3\ KF \rightarrow SPF_3 + 3\ KCl\,.$$

We have irradiated a 0.1-torr sample of SPF_3 (about 50% ^{34}S) with 28 000 shots of a sharply focused CO_2 laser beam of R_{34} (001-100) at 984.4 cm^{-1}, ~1 J/pulse. The Q branch maximum of the symmetric PF stretch lies at 984.8 cm^{-1} for $^{32}SPF_3$ and at 982.8 cm^{-1} for $^{34}SPF_3$. The SPF_3 molecule is remarkably stable in that so many pulses are required to decompose it to S and PF_3. The fraction of $^{32}SPF_3$ decomposed was about 0.36 as estimated from the ir spectrum. Mass spectra of the gas before and after irradiation gave for the 34/32 ratio 0.920 ± 0.005 and 0.998 ± 0.021, respectively. Using these numbers with the fraction decomposed yields an α_{34} of 0.84, which represents the ratio of the probabilty of decomposing $^{34}SPF_3$ to that of decomposing $^{32}SPF_3$.

A similar experiment with R_{20} (975.9 cm^{-1}) showed very little isotopic separation, if any, which is as expected because it falls in the P branch of both isotopes. Using 30 000 shots of R_{38}, which is to the blue of the Q branch of $^{32}SPF_3$, gave an even better selectivity than R_{34}, namely, $\alpha_{34} \approx 0.68$. The results are tabulated in Table XXVIII.

Though the values of α_{34} for SPF_3 do not appear to be competitive with those for SF_6 (0.1 to 0.2),[220] the separation of products should be simple as the reaction yields solid sulfur.

$$SPF_3\ (gas) \xrightarrow{h\nu} S\ (solid) + PF_3\ (gas).$$

The vibrational mode being pumped with the CO_2 laser is the symmetric PF stretch. This leads to fracture of the weakest bond (PS). Though the selectivity is not great, it is remarkable that it is as significant as observed, inasmuch as the isotope shift is only 2 cm^{-1} and the two isotopic vibration-rotation bands badly overlap.

TABLE XXVIII

ISOTOPIC SELECTIVITY FOR DISSOCIATION OF SPF_3 USING A CO_2 LASER

Line	$\alpha 34$[a]
10 R_{38} (986.64 cm^{-1})	0.68 ± 0.04
10 R_{34} (984.43 cm^{-1})[b]	0.84 ± 0.04
10 R_{20} (975.94 cm^{-1})	~1.0

[a] α_{34} is the ratio of the probability of decomposing $^{34}SPF_3$ to that of decomposing $^{32}SPF_3$.

[b] The Q branch for $^{32}SPF_3$ peaks at 984.8 cm^{-1}; that for $^{34}SPF_3$ peaks at 982.8 cm^{-1}.

2. Photoreduction of UF_6 at 10 K (L. H. Jones and S. A. Ekberg). As part of our continuing effort to understand photolytic reactions of UF_6 in the condensed phase, we have studied the photoreduction of UF_6 dimers, trimers, etc., in argon matrices at 10 K. The idea was to investigate the possibility that UF_5 combines with UF_6 to form U_2F_{11}. Although we do not find evidence for formation of U_2F_{11}, we do find, as described below, that aggregates of UF_6 are more readily reduced to UF_5 than are UF_6 monomers in low-temperature argon matrices. This result is of importance to separation of uranium isotopes using laser excitation of UF_6.

In a typical experiment we deposited a matrix at 10 K with the ratio argon/UF_6 = 60/1. Before irradiation, we see the usual UF_6 monomer ν_3 absorption at 619 cm^{-1} with considerable absorption because of dimer and higher aggregates on either side of the monomer peak. Upon irradiation with an unfocused mercury arc, the aggregation UF_6 peaks diminish much more readily than the monomer peak; broad peaks attributable to UF_5 aggregates are seen to grow in at a much faster rate than UF_5 monomer peaks appear. Though U_2F_{11} cannot be ruled out, the resulting spectra can be explained without invoking its existence. The conclusion is that aggregated UF_6 is more readily photolyzed than UF_6 monomer in an argon matrix, perhaps because when a UF bond is excited, the fluorine can readily attach itself to another nearby fluorine, forming an F_2 molecule and leaving behind $(UF_5)_2$, thus inhibiting the recombination $UF_5 + F \rightarrow UF_6$.

X. MUONIC X RAYS

A. Muonic X-Ray Evidence for the Molecular Dipole Orientation $^-NO^+$ (J. D. Knight, C. J. Orth, M. E. Schillaci, R. A. Naumann,* F. J. Hartmann,** J. J. Reidy†, and H. Schneuwly††)

The Coulomb capture of stopped negative mesons or muons and the subsequent de-excitation of the resulting mesonic or muonic atoms are known to be significantly affected by the chemical structure of the stopping material. The effect is usually observed as a variation in the mesonic x-ray intensities with structure: variation in relative intensities of the individual members of a series and variation in total series intensities that serve as measures of atomic capture probabilities. Modern experimental programs are involved in eliciting the correlations between these variations and known structural features. An important goal is a theory of meson capture and cascade that adequately explains these effects and that might then be employed, in conjunction with experimental measurements, to provide chemical structure information not easily available by other means.

As part of our study of muonic x-ray spectra of gaseous target systems, we have obtained experimental data on NO that provide evidence for the dipole orientation of this molecule. Our experiment involved measurement of Coulomb capture ratios for negative muons stopped in three targets: 5 atm N_2 + 5 atm O_2, 10 atm NO, and 10 atm CO. The target gases were contained in an aluminum pressure vessel exposed to a beam of negative muons (p_μ = 82 MeV/c) from the Los Alamos Meson Physics Facility Stopped Muon Channel, and the muonic x rays were detected with an intrinsic germanium detector suitably shielded to minimize muonic x rays originating from stops in the container. Areas of the peaks of interest in the muonic x-ray spectrum were determined with the peak-fitting program SAMPO; analysis of the data took into account absorption and distributed source effects, backgrounds, and in the case of the $N_2 + O_2$ target, the uncertainty in the composition of the mixture.

The results are shown in Table XXIX where the uncertainties indicated are ± 1σ. The column "Z Law" refers to the original treatment of Fermi and Teller,[221] in which they predicted that for low-gap materials like metal solid solutions the relative captures of mesons in the individual elements of a compound should be propor-

TABLE XXIX

MUON CAPTURE RATIOS

Target	Ratio	Experiment	Z Law (Ref. 221)
5 atm N_2 + 5 atm O_2	N/O	0.834 ± 0.031	0.875
10 atm NO	N/O	0.959 ± 0.030	0.875
10 atm CO	C/O	0.766 ± 0.030	0.750
$\frac{(N/O)_{mixture}}{(N/O)_{NO}}$		0.870 ± 0.032	1.000

*Princeton University, Princeton, New Jersey.
**Technical University of Munich, D-8046 Garching, Germany.
†University of Mississippi, University, Mississippi.
††University of Fribourg, CH-1700 Fribourg, Switzerland.

tional to Z; the law is commonly cited as a reference mark for all substances.

The most striking feature of these data is that the fraction of muons captured by the nitrogen in the NO target is clearly greater than that for the $N_2 + O_2$ mixture of the same atomic composition. There is at present no realistic theoretical model by which this result can be interpreted in terms of the electronic structure of the molecules involved. It is commonly accepted, however, that meson capture should be related to electron density, and there has recently appeared a semi-empirical formulation[222] that takes into account the ionicity of the N-O bond in computing the N/O capture ratio. In this formulation, muon capture occurs through Auger ejection of loosely bound electrons, and the probability of capture by an atom is related to the number of such electrons near it. Applying the computation to the NO with the valence structure :N≡O: , we find that the experimental capture ratio can be reproduced only if the bond ionicity is such as to give the polarity $^-NO^+$. Similarly, for the valence form :C≡O: , the experimental data can be fitted only by assigning the polarity $^-CO^+$; this dipole orientation for the CO molecule is in accord with the one inferred from microwave spectroscopy.[223] We are not aware of a corresponding assignment for NO, but an *ab initio* generalized valence bond calculation of the electronic structure[224] has led to the theoretical assignment $^-NO^+$ for the molecular ground state. Thus, although the muon capture data cannot yet be interpreted as firm proof for the NO polarity, in conjunction with the correct prediction for CO they can be considered as experimental support.

B. Target Density Effects in Muonic Atom Cascades (J. D. Knight, C. J. Orth, M. E. Schillaci, R. A. Naumann, F. J. Hartmann, J. J. Reidy, and H. Schneuwly)

Our principal source of experimental information on the processes involved in Coulomb capture of stopped negative mesons or muons is the mesonic or muonic x-ray spectrum generated as the captured particle cascades from its initial capture state down to its atomic ground state. Because only the last few steps of the cascade produce x rays at detectable levels (the preceding steps are dominated by Auger election transitions, which practically we cannot measure), we need a model to help us bridge the gap between observation and phenomenon. In employing current muonic atom cascade models, we usually start with the assumption that the muons are captured into some arbitrary distribution of the ℓ substates of one n level, say $n_\mu = 14$. The subsequent de-excitation cascade is computed with the model code, finally yielding predicted intensity patterns for the members of the muonic Lyman, Balmer, etc., x-ray series. Fitting of theoretical to experimental patterns is attempted by adjustment of the original ℓ distribution. Apart from experiments done with hydrogen gas, almost all measurements done so far have been carried out on condensed materials, where Auger electrons lost from muonic atoms are believed to be replaced so rapidly that electron depletion has no significant effect on the Auger widths in the cascade.

We have been examining the electron depletion effect by measuring muonic x-ray spectra in a series of gas targets at various pressures. Our main sequence of targets consisted of N_2, argon, and SF_6, measured in the condensed phase (liquid or solid) and in the gas phase at pressures up to 20 atm. Muonic x-ray intensity patterns for argon in liquid and gas states are shown in Figs. 54 and 55, where the experimental data are represented by the points and the predicted values are represented by the junctions of the straight line segments. We used the cascade of Akylas and Vogel,[225] with the initial ℓ distribution given by the function $P(\ell) = e^{\alpha\ell}(2\ell+1)$, where α is an adjustable constant. Taking initial $n_\mu = 14$, setting the K electron refilling width at 0.1 eV, and adjusting α for best fit to the observed Lyman intensities for the liquid argon, we obtained the results shown in Fig. 54. Using the same n and α, but adjusting the code parameters to give *zero* refilling rate for all electrons, we obtained the muonic K and L intensity patterns shown in Fig. 55. The fits for both the liquid and gaseous argon data are reasonably good, although it is evident that theory overestimates the higher muonic Balmer members for liquid argon. The fit

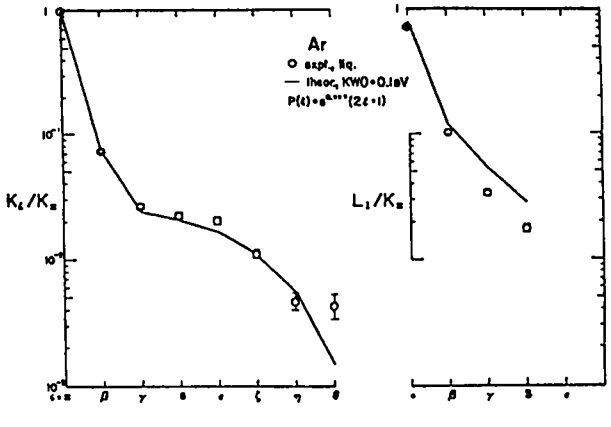

Fig. 54.
Muonic Lyman and Balmer intensity patterns, liquid argon.

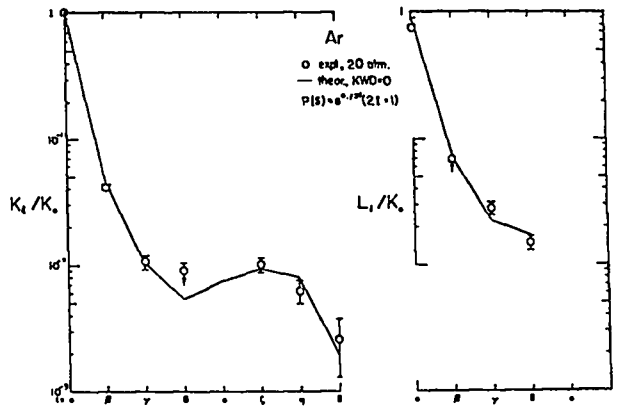

Fig. 55.
Muonic Lyman and Balmer intensity patterns, gaseous argon.

of the zero-refill calculation to the data for argon at 20 atm is not as strange as it may appear. For monatomic gases such as argon, whose muonic atoms start out and travel at near thermal energies, the time to first collision at 20 atm is of the order of 10^{-11} s, whereas the de-excitation cascade should have run its course, on the average, in $<10^{-12}$ s; the average cascade proceeds under approximately zero-refill conditions. For molecules such as N_2 and SF_6, on the other hand, the muonic atom should be starting out with a kinetic energy of the order of several eV and thus should have a high probability of colliding with a potential electron donor in time to influence the course of the de-excitation cascade.

Our data on N_2 and SF_6 show a prominent pressure effect, as expected, but thus far we have not succeeded in finding a simple set of initial model parameters that yield a fit to the experimental data.

In studies of the relative muon capture probabilities of the individual elements in a compound, the so-called "muon capture ratio," the question arises: "Does the capture ratio depend on the pressure (of a gas) or on the state of aggregation?" For relatively covalent molecules the effect is expected to be small, because the slowing down and capture of the muon are determined by the electronic structure, and the electronic structure should not be significantly affected by the presence of neighboring molecules. We have had an opportunity to test this conclusion in our studies with SF_6. Results are shown in Table XXX, where the indicated uncertainties are $\pm 1\sigma$. We note that the F/S capture ratios are constant within experimental error.

TABLE XXX

MUON CAPTURE RATIOS IN SF_6 TARGETS

Target	F captures/S captures
SF_6 solid	6.37 ± 0.30
SF_6 gas 5 atm	5.96 ± 0.50
SF_6 gas 20 atm	6.54 ± 0.45
Z Law	3.38

XI. NUCLEAR COSMOCHEMISTRY

A. Variations of Average Solar-Proton Fluxes During the Last 10 Million Years (R. C. Reedy)

The sun once was believed to be perfect. The invention of the telescope led to the discovery that dark spots often appear on the sun's surface. Over a century ago, the numbers of these sunspots were found to vary regularly with an 11-yr cycle. Each sunspot cycle starts at the time of fewest sunspots, called solar minimum, and the number of sunspots then increases roughly sinusoidally until the peak in sunspot number, solar maximum. Although the total radiative output of the sun does not appear to change during a sunspot cycle, many other outputs of the sun, especially particles and magnetic fields, are known to vary over these 11-yr solar-activity cycles.[226]

Until recently, these many forms of solar activity were believed to have always varied regularly with 11-yr cycles. However, in 1976, Eddy[227] showed that there was a prolonged period of very few sunspots from 1645 to 1715, the "Maunder Minimum." Data for aurorae, solar corona during eclipses, and activities of cosmic-ray-produced ^{14}C in dated tree rings showed the same trend of greatly reduced solar activity throughout this period. The 7000-yr record of ^{14}C in dated tree rings showed that other long periods of either very low or very high solar activity have occurred. For longer time spans, the only data for studying solar variations are the record of the exposure of solar-system matter to cosmic-ray particles or the paleoclimate of the Earth. However, terrestrial climatic changes could have may causes.

Variations in solar activity change the fluxes of cosmic-ray particles,[226] with decreased solar activity increasing the intensities of the galactic cosmic rays

(GCR) and decreasing the numbers of solar-cosmic-ray (SCR) particles. These cosmic-ray flux variations are recorded by the radioactive and stable nuclides that these particles produce in solar-system matter.[228] Almost all of the cosmic-ray-produced nuclides in the Earth or meteorites are made by GCR particles. The flux variations of GCR particles also can be caused by changes in their sources or in their transport to the solar system. Cosmogenic nuclides in lunar samples have recorded the past variations of SCR particles. Although this lunar data set is not very complete, it does extend back millions of years and is the best record of solar activity over such an extended period.

In the moon, the depth-activity profiles of nuclides made by GCR and SCR particles are very different,[228] slowly varying to depths of meters for GCR reactions and steep profiles in the top few centimeters for SCR reactions. Thus, the experimental depth-activity profiles can be readily divided into the parts made by each type of cosmic rays. Fluxes of SCR particles can be determined from cosmogenic nuclide data if the sample's chemical composition and the cross sections for the nuclear reactions making the nuclide are known.[229]

Lunar radioactivity data for fairly short-lived nuclides, like 78-day ^{56}Co, were in good agreement with the profiles expected for the solar-proton fluxes measured by detectors on satellites.[230,231] The low-energy-proton reactions that produce 2.6-yr ^{22}Na and 7.3 x 10^5-yr ^{26}Al in lunar rocks are similar.[228] Because similar depth-activity profiles were measured for these radionuclides in Apollo 11 and 12 samples, Finkel et al.[230] and others concluded that the intensity and spectral shape of solar protons averaged over the last million years were similar to those observed recently. However, the great similarity of the ^{22}Na and ^{26}Al SCR-produced activities was largely accidental, as about 80% of the SCR-produced ^{22}Na activities in Apollo 11, 12, and 14 samples were made by solar protons emitted during a number of intense flares about a decade (four half-lives) before the Apollo missions.[231] Adopting satellite-measured solar-proton fluxes for 1965-1972 (sunspot cycle 20), lunar depth-activity profiles for ^{22}Na and 2.7-yr ^{55}Fe were used to determine the fluxes for solar protons during 1954-1965 (sunspot cycle 19).[231] The fluxes adopted for solar cycle 20 and determined for solar cycle 19 are included in Table XXXI.

The radioactivity data for ^{26}Al and 3.7 x 10^6-yr ^{53}Mn in a number of lunar samples have shown that the solar-proton fluxes over the last 0.5-10 million yr have varied little[230,232] and are similar to the average fluxes for sunspot cycle 20 (see Table XXXI). This sunspot cycle had sunspot numbers that were like the average of those observed during the last two centuries, whereas sunspot cycle 19 had about twice this number of sunspots,[231] the most ever seen over a sunspot cycle. Thus, sunspot cycle 20 seems typical of long-term averages in both solar-proton fluxes and sunspot numbers. However, as noted in Table XXXI, most of the solar protons during this period were from two very large solar-flare events in August 1972.

TABLE XXXI

AVERAGE SOLAR-PROTON FLUXES OVER VARIOUS PERIODS AS DETERMINED FROM LUNAR RADIOACTIVITY MEASUREMENTS

Period (Data)	Fluxes (protons/cm^2 s) E > 10 MeV	E > 30 MeV	E > 60 MeV	E > 100 MeV
1965-1975 (SPME[a]) (Ref. 231)	89	28	8.0	--
1965-7/72[b] (SPME[a]) (Ref. 231)	25	4.2	0.9	--
1954-1964 (^{22}Na, ^{55}Fe) (Ref. 231)	378	136	59	26
~5 × 10^3 y (TL) (Ref. 235)	~60	~14	~6	~3
10^4 y (^{14}C) (Ref. 233)	≅200	72	26	9
3 × 10^5 y (^{81}Kr) (Ref. 229)	--	--	≅18	≅9
10^6 y (^{26}Al) (Ref. 232)	70	25	9	3
5 × 10^6 y (^{53}Mn) (Ref. 232)	70	25	9	3

[a]SPME is the Solar Proton Monitor Experiment (Ref. 231).

[b]Averaged over 11 yr.

The only other lunar radionuclide that had been used to study ancient solar-proton fluxes is 5730-yr ^{14}C, made mainly by the $^{16}O(p,3p)^{14}C$ reaction. The solar-proton fluxes determined from its depth-activity profiles (Table XXXI) are much higher than those for the last million years.[233] These ^{14}C-deduced solar-proton fluxes have been questioned because of three reasons: (1) the possibility of solar-wind-implanted ^{14}C in lunar samples;[234] (2) considerable uncertainties in the cross sections for the $^{16}O(p,3p)^{14}C$ reaction;[229] and (3) the much lower solar-proton fluxes determined for a similar period using thermoluminescence (TL) data for a lunar rock[235] (see Table XXXI). However, the presence of solar-wind-implanted ^{14}C does not affect the solar-proton fluxes, because the same flux is obtained when one excludes the data for the surface layer (where all the solar-wind ^{14}C is implanted). The mean-life for radiation-damage-produced trapped electrons (the source of TL) is not well determined, and the solar-proton production rate of such radiation damage is not well known. Mainly because of these reasons and uncertainties, the large differences between the solar-proton fluxes determined from data for ^{14}C and the other radionuclides often have been ignored. An independent determination of ancient variations in solar-photon fluxes would help to confirm the ^{14}C-deduced results.

Concentrations of 2.1 x 10^5-yr ^{81}Kr have been measured in lunar rocks, but, until recently, the data have never been analyzed for solar-proton fluxes. Using the unpublished data for ^{81}Kr in lunar rock 12002* shown in Fig. 56 and the krypton-production cross sections of Regnier et al.[236] the solar-proton fluxes given in Table XXXI were obtained. The total-less-GCR component of Fig. 56 gives a good SCR depth-activity profile that is considerably higher than that calculated using the solar-proton fluxes for the last 10^6 yr. No fluxes are given in Table XXXI for energies below 60 MeV because the main reactions producing ^{81}Kr in lunar samples have threshold energies about 60 MeV.[236]

There are several factors contributing to the uncertainties of the solar-proton fluxes determined from this ^{81}Kr data. Chemical abundances of the target elements (rubidium, strontium, yttrium, and zirconium) were not measured in the samples used for krypton measurements. Measurements made with other samples of rock 12002 and similar rocks show that these elements are fairly homogeneous, and the uncertainties of the elemental abundances used here are about ±10%. Only a few cross sections have been measured for ^{81}Kr production from

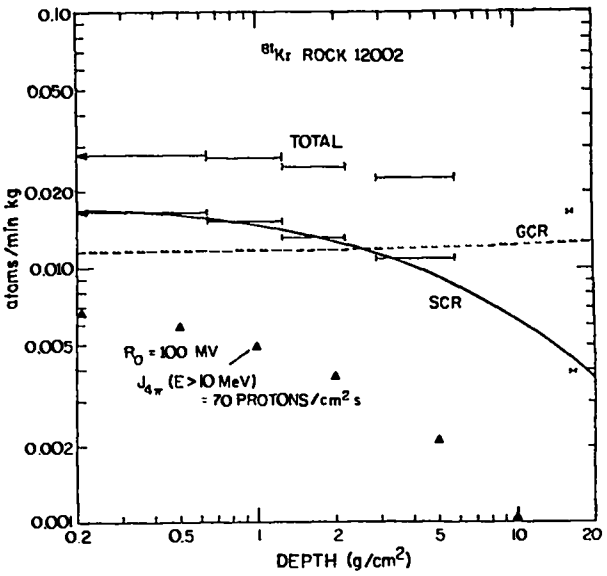

Fig. 56.
The measured and calculated activity of 2.1 × 10^5-y ^{81}Kr is shown as a function of depth in lunar rock 12002. "TOTAL" is the observed data, "GCR" is the estimated contribution of galactic-cosmic-ray reactions, and "SCR" is the solar-proton-produced part [both inferred and (solid line) calculated]. The solid triangles are the calculated production rates of ^{81}Kr using the average solar-proton fluxes over a million years as determined from ^{26}Al and ^{53}Mn radioactivities.

these target elements; most of the cross sections are estimated on the basis of nuclear systematics.[236] If earlier, estimated ^{81}Kr-production cross sections[237] are used, the solar-proton fluxes obtained are about 0.75 of those given here. Another large source of uncertainty in these solar-proton fluxes is the GCR-production normalization factor used to correct for GCR production of ^{81}Kr (Ref. 229). The deepest sample in which ^{81}Kr was measured in rock 12002 (2-6 cm) appears to have considerable SCR-produced activity of ^{81}Kr. Regnier et al.[236] compared the observed and calculated krypton isotopic abundances in 10 samples (none of which was deeper than 6 cm), and the average value of observed-to-calculated ^{81}Kr activities in the deeper samples was 0.97, the value adapted here, but with a 25% standard deviation. The ^{81}Kr activity in the 0- to 1-mm layer of rock is 1.7 times that in the 2- to 6-cm layer, so variations in the GCR normalization factor should not greatly change the solar-proton fluxes. An uncertainty of ±25% in this normalization factor affects the solar-proton flux by about ±20%. New cross-section data and additional lunar-rock analyses for ^{81}Kr are being made to reduce the uncertainty (~±40%) for the solar-proton fluxes given here.

*This information was furnished by K. Marti.

Yaniv and Marti recently measured noble-gas concentrations in samples of lunar rock 68815, which was shielded from cosmic rays until only 2 million yr ago when it was placed in the position it was found by the Apollo 16 astronauts. Comparisons of ^{81}Kr, made mainly over the last 3 x 10^5 yr, and stable krypton isotopes, made over the last 2 x 10^6 yr, allow the ratio of solar-proton fluxes over these two periods to be fairly well determined almost independently of the uncertainty sources listed above (because these nuclides are made from the same target elements and because only relative production ratios need to be known). Preliminary evaluation of the krypton data for rock 68815[238] is consistent with the solar-proton flux variations previously determined from lunar radionuclide activities (Table XXXI).

Although the similarity of solar-proton fluxes averaged over the last few million years and observed recently is noteworthy, the evidence for considerably larger fluxes over the last 10^4 and 10^5 yr is intriguing. Although I believe the results given in Table XXXI are generally correct, much work could be done to improve the accuracies of the fluxes given there and to add results for additional radionuclides or periods. Additional cross sections for protons producing certain radionuclides, especially ^{14}C and ^{81}Kr, need to be measured. Concentrations of ^{81}Kr and other noble-gas isotopes should be measured in more lunar samples and at depths where SCR production is negligible, in addition to the surface layers where SCR effects prevail. Measurements of SCR-produced nuclides in rocks with known exposure ages would provide fluxes for periods other than mean-lives of radionuclides and help to convert average integral fluxes into fluxes for "differential" periods in the past.

Cosmogenic nuclides provide good evidence that the ancient sun was not constant but had variations in its activity. It is to be hoped that the fluctuations observed in cosmic-ray fluxes can be combined with other fossil records in the moon, meteorites, and the Earth to improve our knowledge of the ancient sun.

B. Silver Isotopic Anomalies in Iron Meteorites: Cosmic-Ray Production and Other Possible Sources (R. C. Reedy)

When different solid samples of the Earth, moon, or meteorites are analyzed, the relative abundances of the isotopes for each element usually are identical to within very small experimental uncertainties. The few exceptions generally are produced by isotopic fractionation while changing chemical or physical states or, as in meteorites, by cosmic-ray-induced reactions. Recently, some unusual isotopic anomalies have been measured in some inclusions found in meteorites. For example, excesses of ^{26}Mg in several meteoritic inclusions with high aluminum/magnesium ratios have been ascribed to the decay of 7.3 x 10^5-yr ^{26}Al after the inclusion solidified.

The presence of excess ^{107}Ag in samples of iron meteorites with large ($\sim 10^4$) palladium/silver ratios, initially reported by Kelly and Wasserburg,[239] has been confirmed by Kaiser et al.[240] The new work showed that most of the silver previously measured in meteorites was surface contamination. Kaiser et al. found that the central pieces of two different iron meteorites (Piñon and Santa Clara) has $^{107}Ag/^{109}Ag$ ratios of up to 2.8, whereas normal silver has a $^{107}Ag/^{109}Ag$ ratio of 1.08. Ratios of the two silver isotopes and of the excess ^{107}Ag (denoted $^{107}Ag^*$) to palladium isotopes are given in Table XXXII. The source of the $^{107}Ag^*$ was ascribed by Kelly and Wasserburg to the decay of ^{107}Pd (half-life of 6.5 x 10^6 yr) in the meteorite shortly after it formed. However, Kaiser et al. felt that other factors, such as irradiation by energetic particles or *in situ* fission, could be possible sources of the small amounts of silver found in these meteorites.

The isotope ^{107}Ag can be produced by nuclear reactions with ^{108}Pd (atom abundance of 26.7%) and ^{110}Pd (11.8% abundance), but ^{109}Ag can be made only from ^{110}Pd. Thus, a high fluence of energetic cosmic-ray particles would produce an excess of ^{107}Ag relative to ^{109}Ag by nuclear reactions with palladium isotopes. Cross sections for the production of ^{107}Ag and ^{109}Ag from ^{108}Pd and ^{110}Pd were evaluated or estimated and used to determine the production rates of these silver isotopes to see if the observed excesses could be of cosmogenic origin.

There are several measured and theoretical cross sections for the $^{110}Pd(n,2n)^{109}Pd$ reactions[241,242] that were evaluated to provide an excitation function for the production of ^{109}Ag (produced by the decay of ^{109}Pd) by GCR-produced neutrons. Cross sections for the reactions $^{110}Pd(p,pn)^{109}Pd$ and $^{110}Pd(p,2n)^{109}Ag$ by high-energy protons were estimated from cross sections for similar reactions with other nuclei. Because of the long half-life for ^{107}Pd, no $^{108}Pd(n,2n)^{107}Pd$ or $^{108}Pd(p,pn)^{107}Pd$ cross sections have been measured. Cross sections for (n,p), (n,α), (n,np), and other reactions of 14-MeV neutrons with ^{108}Pd are very low and similar

TABLE XXXII

COMPARISONS OF THE RATIOS OF SILVER ISOTOPES AND EXCESS ^{107}Ag (DENOTED $^{107}Ag^*$) TO PALLADIUM ISOTOPES AS MEASURED IN CENTRAL PIECES FROM TWO IRON METEORITES (REF. 240) WITH THOSE CALCULATED FOR COSMIC-RAY-INDUCED SPALLATION AND NEUTRON-CAPTURE REACTIONS WITH PALLADIUM OVER THE LAST 10^9 YEARS

Sample or Source	$^{107}Ag/^{108}Pd$	$^{107}Ag^*/^{108}Pd$	$^{109}Ag/^{110}Pd$
Piñon #D	3.3×10^{-5}	1.3×10^{-5}	4.3×10^{-5}
Piñon #2B	2.6×10^{-5}	1.5×10^{-5}	2.4×10^{-5}
Santa Clara #106.1	2.3×10^{-5}	0.9×10^{-5}	2.9×10^{-5}
Santa Clara #9	2.7×10^{-5}	1.0×10^{-5}	3.5×10^{-5}
Spallation[a]	2.4×10^{-7}	1.4×10^{-7}	2.1×10^{-7}
Neutron capture[b]	$\sim 4 \times 10^{-9}$	--	$\sim 4 \times 10^{-7}$

[a]Upper limits. (Typical values are expected to be $\cong 0.35$ of these values.)

[b]Order of magnitude estimates. (Such rates are highly variable in meteorites.)

to the cross sections for the same reactions with ^{110}Pd, so it seemed safe to assume that the cross sections for the $^{108}Pd(n,2n)^{107}Pd$ reaction are essentially the same as those for the $^{110}Pd(n,2n)^{109}Pd$ reaction. Measured and theoretical cross sections[243] for (n,xn) reactions with ^{107}Ag were used to help construct the excitation function for the $^{110}Pd(n,4n)^{107}Pd$ reaction.

The radionuclide ^{53}Mn is made by low-energy reactions with iron similar to the reactions that make ^{107}Ag and ^{109}Ag from palladium, so using calculated production ratios for these silver isotopes from palladium and for ^{53}Mn from iron and using measured ^{53}Mn activities seemed the best way to estimate the production rates of silver isotopes. The cross sections used for the production of ^{53}Mn from iron were estimated ones[244] for energies below 35 MeV and experimental proton-induced cross sections[245] above 45 MeV. The measured ^{53}Mn activities in lunar samples are about 1.4 times those calculated using these ^{53}Mn production cross sections.[244] This ^{53}Mn normalization factor of 1.4 will be ignored below because the production ratios $^{107}Ag/^{53}Mn$ and $^{109}Ag/^{53}Mn$ are calculated and we want upper limits for production of silver isotopes.

Various extremes in flux shapes for GCR particles in meteorites and lunar samples were used with the above cross sections to get the following average production ratios: ^{107}Ag (atoms/min/kg-Pd)/^{53}Mn (atoms/min/kg-Fe) = 1.15 (±27%), ^{109}Ag(atoms/min/kg-Pd)/^{53}Mn(atoms/min/kg-Fe)= 0.45 (±29%), and $^{107}Ag/^{109}Ag = 2.60$ (±3%). The calculated ratios of the production rates for the silver isotopes from palladium to those of ^{36}Cl from iron (made only by high-energy particles) had standard deviations of over 100%, showing the need to compare silver production with a low-energy product from iron, like ^{53}Mn.

In iron meteorites, ^{53}Mn activities up to 600 dis/min/kg have been measured, with typical values ~200-300 dis/min/kg. Assuming 600 atoms/min/kg as the upper limit for ^{53}Mn production rates, upper limits for ^{107}Ag and ^{109}Ag production rates are 690 and 270 atoms/min/kg-Pd, respectively. The production rate of excess ^{107}Ag would be 690 − 270 x (0.5183/0.4817) = 400 (atoms/min/kg-Pd) (where 0.5183 and 0.4817 are atom abundances of natural ^{107}Ag and ^{109}Ag, respectively). Assuming 10^9 years as an upper limit for the time iron meteorites were exposed to cosmic rays,[246] the ratio of excess ^{107}Ag to ^{108}Pd is 1.4×10^{-7} (see Table XXXII). This is only ~1% of the excess observed in the iron meteorites. Thus, cosmic-ray-induced spallation reactions during the last several billion years could not produce the observed excess ^{107}Ag.

Neutron-capture reactions with mass 106 and 108 isotopes also could produce silver isotopes. The neutron-capture cross sections for ^{106}Cd and ^{108}Cd are ~1 b, and the abundance of cadmium in iron meteorites is very low, so reactions with cadmium could not produce much

silver. Palladium is fairly abundant (~10 ppm) in iron meteorites. However, the neutron-capture cross sections for ^{108}Pd are much larger than those for ^{106}Pd, so neutron-capture reactions with palladium would produce silver with a ^{109}Ag/^{107}Ag ratio of about 40. Rates for neutron-capture reactions in iron meteorites are highly variable and not well known. I used ^{60}Co activities measured in iron meteorites to estimate the orders of magnitude of the rates for neutron-capture reactions with palladium isotopes. The estimated rate for the ^{108}Pd(n,γ)^{109}Pd reactions is ~500 (atoms/min/kg-Pd). Because the rate for producing excess ^{107}Ag by spallation reactions is ≅400 (atoms/min/kg-Pd), neutron-capture reactions with palladium in iron meteorites would lower or cancel entirely the production of cosmogenic ^{107}Ag*. The production of silver isotopes by neutron-capture reactions could not account for the silver seen in these meteorites (see Table XXXII).

Libby, Libby, and Runcorn[247] have proposed that many elements in iron meteorites, like silver, are produced *in situ* by the spontaneous fission of a siderophilic super heavy element (SHE). The normal palladium isotopic composition in Santa Clara[239] showed that such a fission source is not likely. The mode by which an SHE would fission is not known. If an SHE undergoes binary fission, trends for product yields from the fission of transuranic elements[248] indicate that more ^{109}Ag than ^{107}Ag would be produced because, for elements heavier than fermium, the lowest yield peak would have A ≧ 110.

Lee[249] has proposed that an early intense proton irradiation of a small part of the solar system produced the isotopic anomalies observed in some meteoritic samples. The protons had an energy spectrum of the shape $E^{-4.5}$. Lee proposed that the excess ^{26}Mg that is found in such samples, believed to be made by the *in situ* decay of 7 x 10^5-yr ^{26}Al, is made by these protons by way of the ^{26}Mg(p,n)^{26}Al reaction. The ^{26}Al/^{26}Mg ratios in meteorites, inferred from ^{26}Mg anomalies and cosmic abundances, were ≅ 4 × 10^{-5}, about three times the ^{107}Pd/^{108}Pd ratios inferred from ^{107}Ag* in iron meteorites. The major reaction for making ^{107}Pd by protons is ^{108}Pd(p,pn)^{107}Pd. Cross sections for this reaction were estimated and used with measured ^{26}Mg(p,n)^{26}Al cross sections[244] and an $E^{-4.5}$ proton spectrum to calculate a (^{26}Al/^{26}Mg)/(^{107}Pd/^{108}Pd) production ratio of 9, which is much bigger than the observed ratio. This production ratio would be lower if small grains (r ~ 0.1 g/cm^2) were irradiated. Radioactive decay after the irradiation terminated would lower this ratio. Alpha-particle-induced reactions [for example, ^{23}Na(α,n)^{26}Al and ^{104}Ru(α,n)^{107}Pd] or a harder proton spectrum (for example, $E^{-3.5}$) would change the production ratios but would produce isotopic anomalies in other elements, which have not been found. Variable proton fluxes in different parts of the irradiated region would yield different production rates. Other tests, such as those proposed by Lee,[249] would be needed to check his hypothesis for an early proton irradiation, as the excess ^{107}Ag observed in iron meteorites is compatible with such a model.

The excess ^{107}Ag observed in iron meteorites cannot be produced by a long exposure to cosmic-ray particles, and its production by *in situ* fission seems very unlikely. Thus, there is good evidence for the existence of ^{107}Pd in the early solar system. It is hard to make the amount of ^{107}Pd observed in these iron meteorites by an early intense proton irradiation, so the excess ^{107}Ag is probably due to the decay of nucleosynthetic ^{107}Pd in these iron meteorites.

C. Gamma-Ray Spectroscopy of Comets (R. C. Reedy)

Comets can be spectacular objects in the night sky, but very little is known about them. Scientifically, they are among the most interesting objects in the solar system, probably being the most primitive and pristine bodies accessible to direct study. Their chemical compositions are more like that of the sun than most other objects in the inner solar system,[250] having considerably more volatile elements (hydrogen, carbon, and nitrogen) than even the most primitive meteorites, the CI chondrites. Comets that pass near the sun are believed to originate from the Oort cloud, a large reservoir of comets at the outer edges of the solar system.[251] The giant, outer planets like Jupiter possibly accumulated from many comet-like planetesimals. A comet probably is a dirty snowball, the nucleus, a few kilometers in diameter which, when heated by the sun, produces a coma, a spherical cloud of dimension ~10^4-10^5 km, and both ion and dust tails up to ~10^8 km long.[251] Various groups that advise the National Aeronautics and Space Administration (NASA) have urged detailed studies, especially with spacecraft, of comets. The Comet Working Group concluded that the most important objective of a comet mission is the characterization of the chemical and physical nature of the nucleus.

Gamma-ray spectroscopy is an excellent method to determine the chemical composition of a comet's nucleus. Atomic nuclei that are excited by radioactive decay

or cosmic-ray-induced reactions emit γ-rays that usually have unique energies characteristic of that nucleus. Among the strongest γ-ray lines emitted from a planetary body with their sources,[252] are those at 2.614 MeV, ^{208}Tl daughter of ^{232}Th; 6.129 MeV, ^{16}O(n,nγ); a doublet at 7.64 MeV, ^{56}Fe(n,γ); and 0.847 MeV, ^{56}Fe(n,nγ). The Apollo 15 and 16 spacecraft carried NaI(Tl) detectors, which measured these and other γ rays and which allowed about 20% of the moon's surface to be geochemically mapped.[253] To help plan for future missions to the moon with high-resolution germanium spectrometers, a large catalogue of expected fluxes of γ-ray lines was compiled.[254] These γ-ray fluxes can be used for other planetary bodies that do not contain much hydrogen. However, because hydrogen can greatly modify the energy spectrum of γ-ray-producing cosmic-ray particles,[255] new calculations were done to predict the fluxes of γ rays emitted from a comet.

A chemical model for a comet's nucleus was adopted that consisted of 47% CI chondrite, 42% water, 8% CO_2, 2% hydrocarbons, and 1% sulfur.* Many years ago, neutron-transport calculations had been made for a chondritic composition with 6% water,[255] and the energy spectrum and the depth-flux profile of neutrons were considerably different from those for the same medium without water. These calculations showed that new neutron transport calculations were needed for the model-comet composition. Neutron fluxes in a comet were calculated independently by groups at NASA's Goddard Space Flight Center** and at the Brookhaven National Laboratory.† I used these neutron fluxes to calculate the fluxes of γ-ray lines escaping from the comet.

The fluxes for neutron-capture γ-ray lines are about three times those of an average lunar composition.[254] Because the CI-plus-H_2O chemical composition has a high macroscopic thermal-neutron cross section, which would have depressed lunar neutron-capture γ-ray fluxes by a factor of 2 (Ref. 254), the effect of such a large concentration of water was to make the flux of neutron-capture γ-ray lines about six times that of a similar medium with no water. The cause of this enhancement is the much higher flux of low-energy neutrons near the surface when water is present (peak thermal-neutron flux being at depth of ~30 g/cm^2) compared to when water is absent (peak at ~150 g/cm^2).

The fluxes of the energetic neutrons ($1 \leqq E \leqq 15$ MeV) were calculated by the neutron-transport codes to be lower than those for the case of no water by about a factor of 3, a trend consistent with that previously calculated.[255] These lower fluxes for energetic neutrons mean that the fluxes of the inelastic-scattering (n,nγ) γ rays in a medium with 42% water are about 1/3 of those for a similar composition with no water. The net effect of the presence of 42% water compared to a medium with no water is to increase the ratio of neuton-capture γ rays to inelastic-scattering γ rays by a factor of ~9. The great change in this ratio for neutron-capture to inelastic-scattering reactions means that hydrogen can be detected both by its 2.22-MeV γ ray and by changes in the flux ratio.

The greater fluxes of neutron-capture γ rays compared to those for nonelastic-scattering γ rays make the calculation of γ-ray line fluxes, especially relative values, much easier for a comet than for a lunar-like composition. Nonelastic-scattering (n,xγ) reactions occur over a wide range of energies, so both particle fluxes for several depths and cross sections are needed for many energies. Both these particle fluxes and cross sections can have appreciable uncertainties. Neutron-capture (n,γ) reactions are induced mainly by thermal neutrons, and (n,γ) cross sections and γ-ray yields usually are known quite well.

An important advantage of (n,γ) reactions compared to (n,nγ) reactions is that the former usually produce γ-ray lines unique to that element, whereas the excited levels made by (n,nγ) reactions also can be made by (n,xγ) or (p,xγ) reactions with heavier nuclei. These multiple sources for certain γ rays are a serious problem for low-abundance elements just before elements in the periodic table that are present in high abundances. For example, the 1.434-MeV γ-ray line from excited ^{52}Cr can be made both by ^{52}Cr(n,nγ)^{52}Cr and ^{56}Fe(n,nαγ)^{52}Cr reactions, with the latter reaction producing a larger flux of this γ ray than the former one.[254] However, the ^{53}Cr(n,γ) reaction produces γ rays, such as one of 8.884 MeV, that essentially are not made by any other reactions.

Because the flux of a γ-ray line escaping from an object depends on the absorber half-thickness for that γ ray, the absorber half-thicknesses for silicate media like that of the moon (which has no water or carbon) were compared with those for water and carbon. For most energies, carbon and water have slightly larger and smaller, respectively, half-thicknesses than do silicates. The net effects of carbon and water on half-thicknesses,

*This information was provided by A. Delsemme.
**This information was provided by J. Lapides.
†This information was provided by M. Spergel.

and hence on γ-ray-line fluxes, were usually less than 5% and never more than about 10% when compared to a pure lunar medium. For the calculation of γ-ray fluxes from a comet, these small changes in absorber half-thicknesses can be ignored, because the presence of water greatly changes the source strengths for neutron-capture and nonelastic-scattering γ rays.

The γ-ray spectrometers that have been proposed for future missions would use high-purity germanium crystals and have resolutions for γ rays of a few keV. However, some γ-ray lines have large energy spreads because of Doppler broadening.[256] This broadening of line energy is worst for light nuclei (which get larger recoil velocities immediately following the nuclear reaction producing the γ ray) and for excited levels with very short mean-lives (where the γ ray is emitted while the excited nucleus is still recoiling). Most excited levels that produce major γ-ray lines have mean-lives of $\sim 10^{-11}$ s or longer,[256] which is long enough that the recoiling excited nucleus has stopped moving in a solid before it emits its γ ray; therefore, there is no line broadening. However, the first excited level of ^{12}C, which emits the 4.438-MeV γ ray, has a mean-life of 5×10^{-14} s. The recoil velocity of a ^{12}C nucleus excited by a $^{12}C(n,n')^{12}C^*$ reaction is relatively large and produces a full-width at half maximum (FWHM) of >60 keV for the 4.438-MeV γ-ray line.[257] For the spectrum of neutrons producing the 4.438-MeV γ ray in a planetary body, the FWHM of this line would be ≅100 keV. This line broadening makes the detection of the 4.438-MeV γ ray from ^{12}C much harder than if the line was not Doppler broadened.

The Doppler broadening of the 4.438-MeV γ of ^{12}C makes detection of carbon difficult because there are no other good γ rays from carbon for use in planetary γ-ray spectroscopy. Most excited levels of ^{12}C decay by alpha-particle emission. The only other ^{12}C level (besides the 4.438-MeV one) that emits a high yield of γ rays is the one at 15.11 MeV. This level has an exceedingly short mean-life of 1×10^{-17} s, so its γ-ray line will be Doppler broadened with a FWHM of ≅300 keV (because of its higher recoil velocity). In a γ-ray spectrometer the background around 15 MeV would be much lower than that at 4.4 MeV, but the cross section for exciting this 15-MeV level is much lower.[258] The flux of the 15.11-MeV γ-ray line probably would be ≅1% of that for the 4.438-MeV line. Spallation reactions with carbon produce other radioactive or excited nuclei, but these nuclei emit no (for example, ^{11}C) or few (for example, ^{12}B) γ rays, and these same nuclei would be made in large yields by cosmic-ray reactions with oxygen.

The $^{12}C(n,\gamma)^{13}C$ reaction produces several γ rays that are not produced by any reactions with other nuclei, but the cross section for this reaction with thermal neutrons is small (only 3.4 mb), so the fluxes of these neutron-capture γ rays are low. The most intense line produced by the $^{12}C(n,\gamma)$ reaction has an energy of 4.9455 MeV. The only possible interference with this line in a planetary γ-ray spectrum is a weak $^{16}O(n,n\gamma)$ line at 4.95 ± 0.03 MeV. The energy of this 4.95-MeV line from ^{16}O needs to be determined better. If the energy of this line from ^{16}O is within a few keV of 4.9455 MeV, its intensity in a planetary spectrum can be determined because the excited level in ^{16}O (11.08 MeV) that produces the 4.95-MeV line also produces a similar number of 4.16-MeV γ rays. However, the calculated flux of the 4.9455-MeV neutron-capture γ-ray line is so low that the best line for detecting carbon is the Doppler-broadened γ ray at 4.438 MeV. The 4.9455-MeV γ ray would only be observed for long counting times and would be detected best from an object with large quantities of hydrogen to moderate the neutrons to thermal energies.

Except for carbon, the other elements that should be present in cometary nuclei in appreciable quantities emit relatively strong fluxes of narrow γ-ray lines. Most elements emit fairly intense fluxes of (n,γ) lines. A few elements (for example, magnesium and oxygen) have low or very weak fluxes of (n,γ) lines but have strong (n,xγ) lines. Several elements, especially iron and silicon, have fairly intense γ-ray lines made by both types of reactions, so relative elemental abundances determined by either (n,γ) or (n,xγ) γ-ray lines can be normalized. So, although absolute fluxes of emitted γ rays cannot be calculated very well, almost all of the most abundant elements can be measured, and the relative concentrations can be normalized to sum to 100%. Besides determining almost all of the major elements, including volatile hydrogen and nonvolatile elements like iron and silicon, γ-ray spectroscopy also can determine the abundances of certain key minor elements, such as potassium, titanium, and nickel. Thus, a γ-ray spectrometer near a comet's nucleus would provide valuable chemical abundances that would help in understanding the nature of these interesting objects.

D. Boron Abundances in the Early Solar System (D. B. Curtis)

1. Introduction. Meteorites are extraterrestrial objects that have fallen to the Earth's surface. Since this was recognized, they have been objects of considerable scientific research. Perhaps the most profound reason for the study of meteorites is their antiquity. With very few exceptions, the chronometers provided by the decay of radioactive nuclides show that these objects were formed as solid bodies 4.5 billion yr ago and have remained largely unaltered since that time. Meteorites represent 0.5 x 10^9 to 1.0 x 10^9 yr of solar system history that has been largely obliterated on the Earth and the Earth's moon, the only other objects available for direct laboratory study. In addition, recent measurements have shown that some of the meteoritic material solidified almost instantaneously (within a few million years) after the end of stellar nucleosynthesis. The study of meteorites bears directly on physical and chemical processes before, during, and shortly after the formation of this solar system.

Meteorites represent a broad spectrum of material types. Many of them are highly differentiated chemically relative to what is believed to be the average composition of the solar system. Others have compositions that are, in most aspects, similar to the composition of the sun (99% of the mass in the solar system) and thus are thought to be relatively undifferentiated. Meteorites of the latter type are called chondrites. Within the broad chondrite classification there are subtle chemical, mineralogical, and petrological differences that have resulted in many subclassifications. For our purposes only two broad subgroups will be identified, ordinary chondrites and carbonaceous chondrites. The latter are thought to be the least differentiated of all meteorites and as such their composition has been used to define the average abundance of many elements in the solar system (the "cosmic abundance"). In this sense, these meteorites represent a kind of compositional benchmark in the history of the solar system. Chemical differences between carbonaceous chondrites and other objects are used to infer the nature of processes of differentation in the solar system. Because carbonaceous chondrites are considered to be a relatively unfractionated sampling of the processes of nucleosynthesis, their composition represents an important constraint on theories of the formation of the elements.

Before the work of Curtis et al.[259] boron was thought to be one of the few elements that is significantly overabundant in meteorites relative to estimates of its cosmic abundance. There are many similarly underabundant elements in chondritic meteorites and many hypothetical processes in the early solar system that might produce such deficiencies.[260-263] However, boron was one of the few elements that appeared to manifest processes of chemical enrichment in chondrites. As such, it could provide a unique clue to one aspect of the physical and chemical history of the early solar system.

The elements lithium, beryllium, and boron cannot be formed in stellar interiors because of the instability of their isotopes at stellar temperatures. Fowler et al.[264] suggested that these elements could be formed at stellar surfaces. However, Ryter et al.[265] demonstrated that the energetics required for production at stellar surfaces were unrealistic. Reeves et al.[266] proposed a plausible method of producing ^{6}Li, ^{9}Be, ^{10}B, and ^{11}B in intergalactic space by spallation of carbon, nitrogen, and oxygen isotopes with high-energy galactic cosmic rays (GCR). Because these theories of nucleosynthesis attempt to explain the formation of only four nuclides, two of which are isotopes of boron, an accurate measure of the unfractionated abundance of boron relative to lithium and beryllium is one of the few tests of such hypotheses.

Because boron abundances in meteorites may manifest unusual physical and chemical processes in the early and presolar system, an experiment was initiated to measure boron abundances in a large number of meteorites and meteoritic material.

2. Experiments. Boron abundances were determined using a neutron activation analysis technique in which γ rays emitted "instantaneously" after neutron capture are measured.[267] The isotope ^{10}B has an exceptionally large thermal neutron capture cross section of 3838 b.[268] Neutron capture produces the nuclear reaction $^{10}B(n,\alpha)^7Li^*$. The excited state ^{7}Li* de-excites with a half-life of $\sim 10^{-13}$ s by the emission of a 478-keV γ ray.[268] Because the γ ray is emitted from a recoiling ^{7}Li nucleus, it is Doppler broadened and produces a unique rectangular peak in the prompt γ-ray energy spectrum.

Samples are encapsulated in polyethylene containers and irradiated in a fixed position in the thermal column of the Los Alamos National Laboratory Omega West Reactor. During the irradiation a collimated beam of γ rays from the sample is analyzed by a Ge(Li) detector coupled in anticoincidence with a NaI annulus to a 4096 channel pulse height analyzer. The neutron fluence in the thermal column is monitored by a gas flow fission

counter during data accumulation. All data are normalized to this fluence. Boron abundances are calculated by direct comparison with the National Bureau of Standards certified standard orchard leaves (NBS-SRM-1571) and with various quantities of gravimetrically prepared boric acid solution that were dried in standard counting vials at room temperature.

3. Discussion of Results. A blank is a measured quantity of boron that is not indigenous to the sample. We have identified three general sources of blank in our procedure and have tried to evaluate the effect of each on the results of the experiment.

The most direct source of blank is the components of the irradiation facility. Because the measurements were made "on line," boron-containing components that reside in the neutron flux and emit γ rays that encounter the Ge(Li) detector are indistinguishable from boron in the sample. The magnitude of such a source was evaluated by regularly analyzing empty polyethylene containers (the system blank). All results have had the appropriate system blank subtracted. Uncertainties for the results reflect the uncertainty in this blank correction.

Another potential source of blank is boron introduced into the sample during sample preparation *at this laboratory*. To monitor boron introduced into the samples, a piece of reactor-grade graphite was routinely prepared and analyzed. The results showed that boron that may have been introduced to the sample during preparation was indistinguishable from the system blank.

The final consideration of blanks addresses the problem of boron introduced into samples before arrival at our laboratory. Initial measurements were made on 70 meteorites of all varieties obtained from 6 institutions in Europe and the United States. Most of these samples were encapsulated at the curatorial facility, shipped, and analayzed directly with no further processing. It was required that samples be from material that was observed to fall, but otherwise the terrestrial histories of the rocks were not known. For convenience these 70 will be referred to as "unknown" samples. Highly variable boron concentrations were obtained from different unknown pieces of the same meteorite and from different unknown chondrites from the same subgroup. To attempt to determine whether these variable results reflect boron contamination or truly represent heterogeneity of indigenous boron, samples were taken specifically for this work from the interiors of meteorites.

Surprisingly, boron abundances in unknown samples of meteorites are systematically higher than in interior samples. The median boron abundance in unknown carbonaceous chondrites is four times greater than it is in interior pieces of the same type of meteorite. Even more dramatically, 80% of the results on unknown pieces (53 analyses) are greater than the maximum abundance measured in an interior piece.

The median abundance in unknown samples of ordinary chondrites is 40% greater than it is in interior pieces of the same type of meteorite. Twenty-five percent of the reported abundances in unknown samples (12 analyses) are greater than the maximum abundance measured in an interior sample.

We conclude that there is a significant probability that measured boron abundances in chondritic meteorites are adversely influenced by terrestrial contamination. Consequently, only a few tenths of a gram of recently prepared interior pieces are considered to be representative of uncontaminated chondritic material. Results from samples of this type will be considered in the conclusions.

4. Conclusions.

a. *The Cosmic Abundance of Boron.* When there are significant compositional differences between ordinary and carbonaceous chondrites, the carbonaceous chondrites are used to evaluate the cosmic abundance of the differentiated elements. Because the data show no basis for identifying a generalized fractionation pattern between chondritic subgroups, the results from analyses of all 10 meteorites of different chondritic types have been used to evaluate the cosmic abundance of boron. The logrithmic average is $6.6^{+6.5}_{-3.3}$ B/10^6Si; uncertainties represent 1 standard deviation of the 10 results. The result is a factor of 6.7 less than the previous low estimate based upon measured meteoritic abundances.

Assuming $(Si/H)_{meteorites} = (Si/H)_{solar} = 4.5 \times 10^{-5}$ (Ref. 269), the newly evaluated atomic ratio in meteorites is $3.0^{+3.0}_{-1.5}$ B/10^{10}H. The comparisons in Table XXXIII show that this new meteoritic value is in excellent agreement with the solar limit established by Engvöld[270] and with the $(B/H)_{solar}$ based upon the only positive spectroscopic observation of a boron species in the sun.[271] The meteoritic value is higher than the limit established by Hall and Engvöld.[272] It is likely that the previous discrepancy between meteoritic and solar boron abundances was an artifact of terrestrial boron contamination in carbonaceous chondrites. It is no longer necessary to consider processes that enrich boron in carbonaceous chondrites[273] or deplete boron in the solar

TABLE XXXIII

ESTIMATES OF THE COSMIC ABUNDANCE OF BORON

	$B/10^{10}H$
Meteoritic	160 (Ref. 283)
Meteoritic	65 (Ref. 273)
Meteoritic	20 (Ref. 274)
Meteoritic	$3.0^{+3.0}_{-1.5}$
Solar	$\leq$1.2 (Ref. 272)
Solar	<3.2 (Ref. 270)
Solar	4 (Ref. 271)

photosphere[274] to account for differences between the two.

b. Constraints on the Nucleosynthesis of Light Elements. The isotopes ^{7}Li, ^{9}Be, ^{10}B, and ^{11}B cannot be made by thermonuclear reactions in stars. Reeves et al.[275] suggested that the light isotopes were produced in intergalactic space by spallation reactions of nuclei of carbon, nitrogen, and oxygen induced by high-energy galactic cosmic rays (GCR). Meneguzzi et al.[276] used this theory to predict the relative production rates of the light isotopes. They assumed an energy spectrum for the GCR that was proportional to $(E_o + E)^{-2.6}$, where E_o = 0.931 GeV and E is the kinetic energy of the particle. This energy spectrum predicted a $^{10}B/^{11}B$ ratio that was significantly outside the uncertainty of measured values. To compensate for this failure, several authors have introduced a contribution of low-energy particles. This additional component to the GCR energy spectrum is added to the standard energy spectrum by an exponential term of the form $E^{-\gamma}$ where γ typically falls between 1.5 and 5 (Refs. 266, 277). Moyle et al.[277] suggest that this low-energy contribution to the GCR spectrum is attributable to stellar flares.

Table XXXIV[278-282] contains element and isotope ratios of the light elements using our newly calculated value for the cosmic abundance of boron. When the data were available, element ratios have been calculated for individual meteorites. The ratios in individual rocks fall within reasonable limits of the average values. Also included in Table XXXIV are relative element and isotope production model-predicted rates of light elements production by spallation reactions induced by

TABLE XXXIV

COMPARISON BETWEEN THEORETICAL LIGHT ISOTOPE PRODUCTION AND RELATIVE METEORITIC ABUNDANCES

Source	B/Be	$B/^6Li$[a]	$^{11}B/^{10}B$
Measured			
Chondritic Average	9.3 (Ref. 278)	2.1 (Ref. 279)	4.03 $\pm$ 0.01 (Ref. 280)
Murchison	11.4 (Ref. 281)	—	—
	15.1 (Ref. 282)		
Allende	4.5 (Ref. 282)	1.1 (Ref. 279)	—
	3.4 (Ref. 282)		
Richardton		1.2 (Ref. 279)	—
Saratov	—	2.0 (Ref. 279)	—
Bruderheim	16.8 (Ref. 278)	2.3 (Ref. 279)	4.05
Leedey	—	0.62 (Ref. 279)	—
Calculated			
(Ref. 276) $\phi(E)\ \alpha\ (E_o + E)^{-2.6}$	15	3.75	2.4
(Ref. 277) $\phi(E)\ \alpha\ (E_o + E)^{-2.6} + E^{-3}$	30	2.5	4.1
(Ref. 266) $\phi(E)\ \alpha\ (E_o + E)^{-2.6} + E^{-5}$	21	2.3	$\equiv$4.05
(Ref. 266) $\phi(E)\ \alpha\ (E_o + E)^{-2.6} + E^{-7}$	24	4.8	$\equiv$4.05

[a]Assumes $^7Li/^6Li$ = 12.5.

GCR with different particle energy spectra. The model that enhances the low-energy portion of the GCR spectrum with the form E^{-5} most closely matches the elemental and isotopic abudances in meteorites. Given the spread in the data, the model predictions are in reasonable agreement with the meteoritic composition.

XII. NUCLEAR STRUCTURE AND REACTIONS

A. Measurement of 14-MeV Neutron Cross Sections on Radioactive Nuclides (R. J. Prestwood and K. W. Thomas)

The measurement of fast neuton (~14 MeV) cross sections on radionuclides that have been produced at the Los Alamos Meson Physics Facility (LAMPF) is an ongoing program in CNC-11. These experiments, conducted in collaboration with members of the Lawrence Livermore National Laboratory (LLNL) radiochemistry group, are unique as they are the only published work of this kind. They have had significant impact on the nuclear model calculations upon which we partially depend for our radiochemical test diagnostics.

In this program, we make sophisticated measurements of the interaction processes of fast neutrons with radioactive isotopes on the neutron deficient side of nuclear stability. The results provide a rigorous test of complex nuclear model calculations of these reaction probabilities. In the broadest sense, the program contributes significantly to our basic knowledge of atomic nuclei, and in addition, the specific elements we choose for these studies have direct application to our current weapons test diagnostics. Thus, two important aspects of the Los Alamos National Laboratory mission are served.

The first measurement in this program was the 14.8-MeV cross section for the reaction 106d $^{88}Y(n,2n)^{87m,g}Y$ conducted in September 1975. The measurement of $^{87,88}Y$ isotopes produced in nuclear explosions provides the keystone of the Laboratory's determination of thermonuclear yields.

Since that time a number of additional mesurements using 14.8-MeV neutrons available at the LLNL ICT facility have been made:

533-day $^{173}Lu(n,2n)^{172}Lu$
74.6-yr $^{148}Gd(n,2n + n,np)^{147}Eu$
74.6-yr $^{148}Gd(n,p)^{148}Eu$
1.8×10^6-yr $^{150}Gd(n,2n + n,np)^{149}Eu$
3.3-day $^{89}Zr(n,2n)^{88}Zr$
82.6-day $^{88}Zr(n,2n)^{87}Zr$
82.6-day $^{88}Zr(n,np)^{87m,g}Y$.

The lutetium and zirconium measurements are directly applicable to weapons test results, whereas the gadolinium numbers are a test of nuclear model calculations for neutron deficient isotopes in the rare-earth region. Mass spectroscopy on the gadolinium target material enabled us to determine the correct half-life given above for the ^{148}Gd target isotope, and this supporting work was crucial to the accurate determination of the above cross sections.

We are presently evaluating the possibility for (n,2n) cross section measurements on $^{148,149}Eu$ and/or $^{167,168}Tm$ isotopes. The feasibility of these measurements will depend upon a complex evaluation of the schedule and facilities requisite to the experiments.

- Irradiation of a tantalum target at the LAMPF beam stop.
- Hot cell separations at CNC-3 and 11.
- Target purification and preparation possibly requiring isotope enrichment on the Los Alamos or LLNL radiochemistry machines.
- Mass spectroscopy measurement of isotopic constituency of the final target material.
- Irradiation with 14.8-MeV neutrons at the LLNL ICT facility.
- Measurement of the reaction products by counting techniques; this may require an additional post-irradiation isotope enrichment to enhance the signal/noise ratio, which is a severe restriction in these experiments utilizing such highly radioactive targets.

Because the half-lives of the proposed target isotopes range from 9 days to 93 days, timing and coordination of the various steps described above is clearly crucial to a successful experiment.

All these vanguard experiments have had significant impact on the nuclear model calculations upon which we partially depend for radiochemical test diagnostics. Hence an important adjunct to this work is the continuing comparison of our experimental cross sections with those calculated by Los Alamos Group T-2.

In summary, this continuing program in CNC-11 combines the unique facilities for radionuclide production at LAMPF and 14-MeV neutron production at the LLNL ICT facility in concert with our joint radiochemical expertise to measure hitherto unknown neutron cross sections relevant to our test diagnostic program.

B. Determination of the Half-Lives of ^{87}Zr, ^{87m}Y, and ^{87g}Y (R. J. Prestwood)

As part of a continuing program for the measurement of the 14-MeV-neutron cross sections of radioactive isotopes, it was necessary to have accurate values for the half-lives of ^{87}Zr, ^{87m}Y, and ^{87g}Y. Although half-lives for these species have been reported in the literature,[284-287] recent improvements in counting techniques and computer analyses warranted the redetermination of these values.

1. The Determination of the Half-Life of ^{87}Zr and the Branching to ^{87m}Y and ^{87g}Y. The target for the $^{86}Sr(^3He,2n)^{87}Zr$ reaction was strontium oxide enriched in ^{86}Sr (analysis: ^{86}Sr, 95.72%; ^{84}Sr, 0.02%; ^{87}Sr, 1.24%; ^{88}Sr, 3.01%). The oxide was vacuum-evaporated to a thickness of ~300 μg/cm² on a 1-mil beryllium foil. The target foil was bombarded with 16-MeV $^3He^{2+}$ ions on the Los Alamos Tandem Van de Graaff accelerator for ~100 min at 350 nA.

Following bombardment, the target was dissolved in 6 *M* HCl, about 20 mg of zirconium carrier was added, and the solution was saturated with HCl gas. The solution was then placed on a Bio-Rad AG1-X8 anion exchange resin column (50-100 mesh; 0.8 x 10 cm). The zirconium was adsorbed on the column, and beryllium, yttrium, and strontium passed through quantitatively. The column was washed two or three times with concentrated HCl and the time of the last wash was recorded. The zirconium was eluted with 3 *M* HCl and the column was then washed with 0.2 *M* HCl. The eluates containing the zirconium were combined. The combined eluate was divided into two parts and a zirconium mandelate was precipitated from each by the addition of 15% aqueous mandelic acid.

One sample of zirconium mandelate was mounted for counting in the Trochoidal analyzer (positron counter), and positron decay was followed over a 3-day period. A small number of positrons from ^{89}Zr arising from the $^{88}Sr(^3He,2n)^{89}Zr$ reaction gave a small tail that was removed by means of a least squares analysis of the counting data. For the second zirconium mandelate sample, the 381.3- and 484.4-keV gamma rays from the decay of ^{87}Zr were carefully counted at early times in a Ge(Li) counter. The ratio of the disintegration rate for the 381.3-keV gamma process to that for the 484.4-keV gamma process at early times is a very sensitive measure of the branching to the ^{87m}Y and ^{87g}Y states from the decay of ^{87}Zr.

The counting data from the Trochoidal analyzer, when treated with a least squares program, gave a half-life of 1.684 ± 0.001 h for ^{87}Zr. An independent determination of the half-life from the GAMANAL analysis of the following gamma rays—511.0, 793.8, 1023.9, and 1209.8 keV—gave a value of 1.667 ± 0.006 h. From these results, a final value of 1.68 ± 0.01 h was chosen. Among previously reported values for the half-life are 1.57 h[284] and 1.6 ± 0.1 h.[285]

A computer program was developed for the calculation of the disintegrations of the 391.3- and 484-keV gamma rays as a function of the branching. The observed counting data and the best fit corresponded to a branching of 0.98 ± 0.006 to ^{87m}Y.

2. The Determination of the Half-Lives of ^{87m}Y and ^{87g}Y. The target for the $^{88}Sr(p,2n)^{87m}Y$-^{87g}Y reaction was strontium oxide enriched in strontium-88 (analysis: ^{88}Sr, 99.84%; ^{87}Sr, 0.11%; ^{86}Sr, 0.05%; ^{84}Sr, <0.1%). Target preparation and dimensions were identical to those for the ^{86}Sr target. Two target foils were bombarded, one for about 5 min and the other for 1 h and 20 min, at ~7 μA with 17.0-MeV protons on the Van de Graaff accelerator noted above.

The latter sample was counted immediately in a LEPS Ge(Li) counter, 16 x 4.75 mm, with a resolution of 800 ev at 380 keV. The sample that had been irradiated for 5 min was counted on another Ge(Li) counter, 52 by 47 mm (~95 cm³), with an efficiency of 18.5%.

The decay of the 380.82-keV gamma ray from ^{87m}Y was followed on both counters for many days. The data were processed with the GAMANAL computer program, and a least squares analysis of the information gave a half-life of 13.38 ± 0.01 h from the large Ge(Li) counter and 13.36 ± 0.01 h from the LEPS counter. The value of 13.37 ± 0.03 h was taken as the half-life of the isotope. Other values in the literature are 13.2 ± 0.2 h[286] and 12.5 ± 0.2 h.[287]

The decay of the 484.4-keV gamma ray from ^{87g}Y plus that of the 388.4-keV gamma from ^{87m}Sr, in equilibrium with the 484.4-keV gamma, was followed for about 70 days on a 3- by 3-in. NaI crystal and a least squares program was run on the data to remove the small background of ^{88}Y present. A detailed analysis of the data gave a half-life of 79.6 ± 0.2 h for ^{87g}Y in close agreement with the previously reported value of 80.3 ± 0.3 h.[286]

C. Determination of the Half-Life of ^{148}Gd (R. J. Prestwood, D. B. Curtis, and J. H. Cappis)

In experiments designed to obtain the (n,2n) cross section of ^{148}Gd,[288] a measurement of considerable interest because of the neutron-deficiency of that alpha emitter, an accurate value of the half-life was needed.

A tantalum target was irradiated with 800-MeV protons for 56.3 milliamphours at the Los Alamos Meson Physics Facility (LAMPF). The target was dissolved in a mixture of concentrated nitric and hydrofluoric acids, and lanthanum carrier was added to precipitate lanthanide fluorides. Gadolinium was separated from the other lanthanides by selective elution with α-hydroxyisobutyric through a cation exchange column.[289] Before preparation of the final solution, ^{151}Eu and ^{153}Eu, formed by the decay of gadolinium isotopes, were removed by an additional cation exchange column. The eluate was fumed in concentrated $HClO_4$ to destroy the α-hydroxyisobutyric acid. A final gadolinium-containing sample was prepared by dissolving the residue in 0.2 *M* HCl and carefully weighing the resultant solution.

The concentration of each gadolinium isotope in the sample solution was determined by isotope dilution mass spectrometry. Isotopic ratios were measured on weighed aliquots of spiked and unspiked sample solutions with the Los Alamos National Laboratory Radiochemistry Group's 6-in. solid source mass spectrometer. All mass spectrometric measurements were normalized to the $^{158}Gd/^{160}Gd$ ratio defined by Russ[290] ($^{158}Gd/^{160}Gd$ = 1.13583) to correct for mass fractionation in the instrument. The overall accuracy of the measurements is limited by the accuracy of the assumed value of the ratio.

Two standard solutions of the spike were prepared from 99.999% pure, isotopically normal Gd_2O_3 (source: United Mineral and Chemical Corporation, batch #R1469). The oxide was heated to constant mass in a platinum crucible, a weighed sample dissolved in about 50 mℓ of high-purity hydrochloric acid (source: NBS, batch #4028), and the solution made up to a weighed mass of ~1 kg with water from the Millipore Milli-Q water purification system. Each standard solution was cross calibrated by titration with standard EDTA solution. The results obtained by titration were biased by -0.4 and -0.2% relative to the gravimetrically determined values. Standard results obtained by titration were used for the final determination of isotopic concentrations.

The relative gadolinium isotopic abundances in the standard and the sample solution are shown in Table XXXV. The isotopic composition of the standard solution was assumed to be that measured by Russ.[290] The isotopes of primary interest, the alpha-emitters ^{148}Gd and ^{150}Gd, are absent from normal gadolinium. In addition to the isotopes shown in the table, ^{151}Gd and ^{153}Gd are also present in the sample but are in concentrations too small to be determined by mass spectrometry.

Concentrations of ^{148}Gd were calculated using each of the major isotopes of normal gadolinium. The isotope dilution equation is given below.

$$[^{148}Gd] = \frac{^{1xx}Gd_{std}}{[(^{1xx}Gd/^{148}Gd)_M - (^{1xx}Gd/^{148}Gd)_s]} \times \frac{1}{\text{grams of sample aliquot.}}$$

where $^{1xx}Gd_{std}$ is the number of moles of isotope 1xx added as the standard; $(^{1xx}Gd/^{148}Gd)_M$ and $(^{1xx}Gd/^{148}Gd)_s$ are the appropriate ratios measured in the spiked and unspiked sample, respectively. The equation assumes that $(^{1xx}Gd/^{148}Gd)_{std} = 0$, an assumption that was verified by measurements on the standard. The result is the molar abundance of ^{148}Gd/gram of solution.

The concentrations of ^{148}Gd calculated using ^{155}Gd, ^{156}Gd, and ^{157}Gd systematically differed from those obtained using ^{158}Gd and ^{160}Gd. With two exceptions these differences were less than 1%, The differences can

TABLE XXXV

ISOTOPIC COMPOSITION OF GADOLINIUM

	At.%								
	148	150	152	154	155	156	157	158	160
Sample	19.59	17.45	22.44	1.65	37.29	0.64	0.50	0.24	0.20
Standard			0.20	2.18	14.80	20.47	15.65	24.83	21.86

be ascribed to interferences by other species with mass numbers 155, 156, and 157. Only the results calculated from masses 158 and 160 were used. The concentrations of ^{148}Gd and ^{150}Gd (calculated from the ^{148}Gd/^{150}Gd atomic ratio) are presented in Table XXXVI. Each value shown is the average of seven mass spectrometric measurements on five different spiked solutions using each of the two calibrated standards. The uncertainties are 1 std dev of the seven results.

Several aliquots of the original sample solution were carefully weighed and transferred to platinum alpha-counting plates. The plates were dried, ignited over an open flame to give a virtually weightless sample, and alpha-counted. The result was $2.806 \pm 0.005 \times 10^6$ counts/min/g of original sample solution. Gadolinium-150 has a half-life so long, 1.78×10^6 yr, that it offers no interference in the counting of ^{148}Gd.

The alpha energy of ^{148}Gd is low (3.18 MeV). Because the back-scattering of an alpha particle of low energy is less than that of one of higher energy, it was necessary to determine the counting efficiency for the ^{148}Gd alpha. Using the Low Geometry Alpha Counter, J. Balagna determined the efficiency to be 0.5023 ± 0.0025. Therefore, the number of alpha counts per minute per gram of original sample solution corresponds to 5.587×10^6 disintegrations/min/g of sample solution. From the disintegration rate and the isotopic abundance in nanomoles per gram of sample solution, the half-life of ^{148}Gd was found to be 74.6 ± 3.0 yr. Work reported by previous investigators gave a value of 97.5 ± 6.5 yr.[291]

TABLE XXXVI

CONCENTRATIONS OF ^{148}Gd AND ^{150}Gd IN DILUTION OF GADOLINIUM FROM LAMPF-IRRADIATED TANTALUM

Isotope	Isotopic Abundance (nmole/g of sample solution)
^{148}Gd	0.5254 ± 0.0018
^{150}Gd	0.4680 ± 0.0019

D. The (p,t) Reaction on the Exotic Target ^{148}Gd (R. E. Brown, E. R. Flynn, J. Van der Plicht, G. E. Bentley, J. B. Wilhelmy, L. G. Mann,* and G. L. Struble*)

The nucleus ^{146}Gd has received considerable attention recently because of its supposed "doubly closed" shell character. Its first excited state is thought to be a 3^- and lies relatively high in excitation energy and, therefore, apparently resembles ^{208}Pb. Because ^{146}Gd lies too far from the line of stability to be examined by normal light-ion particle transfer, it has been studied only through xn reactions and heavy-ion two-proton transfer reactions. The nuclear structure of the levels is difficult to extract with the xn measurements, and the heavy-ion reactions are subject intrinsically to poor resolution. To overcome these difficulties we have obtained the radioactive target ^{148}Gd ($t_{1/2}$ = 75 yr) and performed the ^{148}Gd(p,t)^{146}Gd reaction.

The target material was produced by spallation reactions on tantalum with high-intensity protons from the 800-MeV beam at the Los Alamos Meson Physics Facility (LAMPF). The target was 22 g/cm^2 and exposed to $\sim 5.6 \times 10^4$ μA/h primary proton beam. The tantalum was dissolved with an HF/HNO^3 mixture, and the rare earth group was isolated from the bulk solution by adding a lanthanum carrier and precipitating the rare earth fluorides. The rare earths were separated from each other by using standard cation exchange chromatography with α-hydroxyisobutyric acid as the column eluant. These procedures have been adapted to remote operation in the CNC hot cells. The chemically extracted gadolinium fraction was assayed to contain 9.8 μg of ^{148}Gd. A 1-mg carrier of natural gadolinium was added to the solution and then precipitated as a wet hydroxide. The precipitate was shipped to Lawrence Livermore National Laboratory where it was converted to an oxide and isotopically separated. The ^{148}Gd was collected on a 40 μg/cm^2 carbon foil onto a nominal spot size of 2 by 2 mm^2. The target was returned to Los Alamos where a thickness determination was performed using ^{14}C elastic scattering which gave a limit of <16 μg/cm^2.

The (p,t) experiment was performed using the three-stage capability of the Los Alamos Van de Graaff facility and the Q3D spectrometer. Assuming the ground state cross section of the (p,t) reaction to be similar to previously measured ^{142}Ce(p,t), a thickness of 6 μg/cm^2 was obtained. Even with this very thin target an angular distribution on all states below 2.5 MeV was obtained, consisting of nine angles with adequate statistics to identify most final spin values. Initial results are shown in

*Lawrence Livermore National Laboratory.

Fig. 57. These will be complemented in a future experiment involving a study of higher excitation energy in the ^{146}Gd nucleus.

The results presented in Fig. 57 establish that no excited states lie below the 1.575-MeV state given in the literature. The results indicate a 2^+ spin to the 1.980-MeV state and a 0^+ spin to the 2.173-MeV state. This latter state is not the 0^+ pairing vibration, however, as it contains less than 10% of the ground state strength. The 3^- spin of the 1.575-MeV state is not confirmed by the present data.

The results of the present experiment establish that useful nuclear reaction results may be obtained on targets as thin as ~10 μg/cm^2 using the Q3D spectrometer system. This gives rise to a large variety of possible targets from the LAMPF beam stop with a significant number of experiments possible of high physics interest.

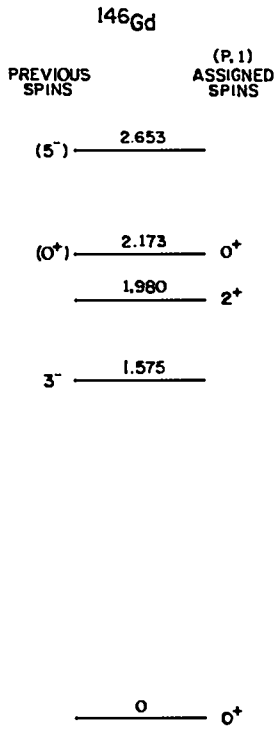

Fig. 57.
Low-lying levels in ^{146}Gd.

E. Search for Neutron-Deficient Light Nuclei near the Proton Drip Line (G. W. Butler, D. J. Vieira, D. G. Perry, A. M. Poskanzer,* L. P. Remsberg,** and J. L. Clark)

Defining the limits of particle stability in the light mass region provides a challenge to both the experimentalist and the theorist. The surprising discoveries of the particle stability of the neutron-rich nuclei ^{11}Li, ^{14}Be, ^{19}C, and ^{32,34}Na, which were predicted to be unstable with respect to one or two neutron emission, pointed out significant deficiencies in the understanding of the nuclear mass surface for light nuclei far from the valley of β-stability. Today such measurements of very neutron rich or very neutron deficient nuclei remain one of the most critical tests of current nuclear mass theories.

Time-of-flight (TOF) techniques have been employed in ongoing experiments at the Clinton P. Anderson Meson Physics Facility (LAMPF) in search of neutron rich[292] or very neutron deficient nuclei near the limits of particle stability. In the present experiment, spallation residues produced by the intense (500-μA average current) 800-MeV proton beam with targets of $^{nat}CaF_2$, ^{nat}Ni, and ^{92}Mo (thickness ~0.5 mg/cm^2) were detected at an angle of 45° in an attempt to establish the proton drip line for the elements magnesium through argon. These measurements were done in the thin target area, which consists of a scattering chamber with several 5-m-long flight tubes. This facility fully utilizes the unique high instantaneous beam intensity and excellent time structure of the main proton beam, allowing TOF experiments such as these to be undertaken.

The observed energy distributions of the spallation residues from such light and medium mass targets were found to decrease rapidly with increasing kinetic energy, with very low yields for nuclei with energies greater than 2 MeV/amu. Therefore a detection system capable of characterizing reaction products to as low an energy as possible was necessary. This system consisted of two fast-timing, secondary-emission channel plate detectors[293] and a standard ΔE-E, gas-Si telescope.[294] A schematic layout of the experimental arrangement is shown in Fig. 58. For each event, nine parameters were recorded, from which the following quantities were determined: (1) the long flight path TOF between the target and CP1 (T_{long}), (2) the total kinetic energy E_{total}, (3) the mass A, and (4) the atomic number Z of the spallation residue. In this experiment the long flight path

*Nuclear Science Division, Lawrence Berkeley Laboratory, Berkeley, California.
**Chemistry Department, Brookhaven National Laboratory, Upton, New York.

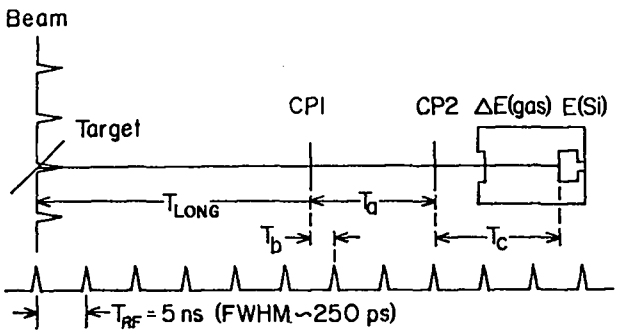

$$E_{TOTAL} = \Delta E + E + \Sigma D.L.'s + PHD$$

$$Mass = 2 E_{TOTAL} (T_{LONG}/D_{LONG})^2$$

Fig. 58.
Schematic layout of the experimental arrangement, the LAMPF beam microstructure, and the important experimental parameters.

TOF was determined to high precision by combining a coarse time measurement, T_a, which was used to determine the long flight time to the nearest rf period, and a fine time measurement, T_b, which measured the time of the event to a fraction of an rf period. After correcting T_a and T_b for time walk with respect to CP1 and CP2 amplitudes, a time resolution of 0.25 ns (FWHM) was obtained over a short flight path (CP1-CP2) of 50 cm, whereas the long flight path (target – CP1 = 4.3 m) time resolution was found to be 1.2 ns.

The total kinetic energy of the reaction product was obtained by adding the pressure and temperature-normalized ΔE-E detector telescope energies. Dead layer corrections for energy losses in the thin carbon foil (20 μg/cm^2) of the channel plate detectors and the polypropylene gas isolation window (60 μg/cm^2) on the detector telescope were made using the dE/dx table lookup method. Owing to the lack of an existing dE/dx table of sufficient accuracy in this energy region, we generated our own table from the data. Finally, an estimate of the pulse height defect (PHD) using the method of Kaufman et al.[295] was added to give the total kinetic energy, E_{total}. The Z of each spallation residue was determined by using the ΔE-E table lookup approach, which was then followed by a mass correction to remove the mass dependence of the Z determinations.

Stringent requirements were used to avoid any ambiguity in the final mass determination and to reduce background events due to random coincidences and other spurious effects. In this analysis a total kinetic energy threshold of 26 MeV was used, resulting in a mass and charge resolution (FWHM) of 0.4 amu and 0.4 charge units, respectively, for a typical spallation product like ^{26}Al.

About 10 million events of the elements nitrogen through calcium were collected from a nickel target in 1 month. The data were analyzed in the fashion previously described, and Fig. 59 shows two of the observed mass spectra. All of the known neutron-deficient isotopes of aluminum and phosphorus are seen out to the currently known limits of particle stability, ^{23}Al and ^{27}P. Beyond these points we find some evidence that ^{22}Al and ^{26}P may be stable; however, the statistics are not sufficient to be convincing. Furthermore, the aluminum spectrum is confused by five potentially spurious events observed below mass 22. Current predictions using Kelson-Garvey mass relationships predict ^{22}Al to be marginally bound by 250 keV, whereas ^{26}P is predicted to be proton unbound by 90 keV.[296] Further experiments to define the neutron-deficient limits of particle stability and, in particular, the possible stability of ^{22}Al and ^{26}P have been performed, and the data analysis is currently in progress.

F. Production of Nuclides Far From Stability (R. Brandt,* W. Faubel, D. C. Hoffman, J. Van der Plicht, and J. B. Wilhelmy)

We are initiating a long-range program with the goal of production and identification of the fission decay properties of heavy actinide nuclei. Recent experiments on difficult to produce fermium and mendelevium isotopes have resulted in the first dramatic deviations from the well-established fission systematics observed in lighter actinide fission. We wish to explore this area more extensively, but efforts to reach the region are hampered by the difficulty of access with conventional techniques and production of many short-lived spontaneous fission activities without adequate methods for specific isotopic assignment. To cope with these problems we are studying the possibility of using neutron rich transfer reactions to produce the isotopes and the development of modern gas counter techniques to enable assignment of the observed fission decay to specific isotopes.

Our initial efforts in studying transfer reactions have been to produce xenon isotopes using ^{14}C and ^{18}O beams

*Los Alamos National Laboratory Visiting Staff Member.

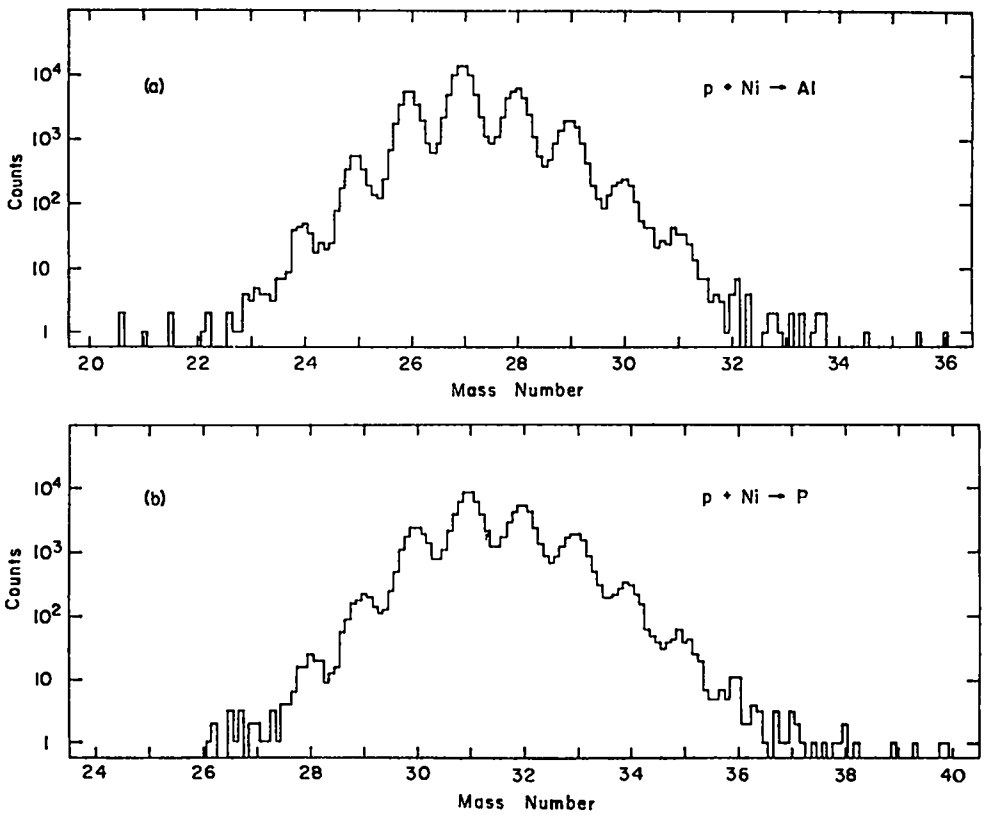

Fig. 59.
Mass spectra observed in 800-MeV proton bombardment of ^{nat}Ni for the elements (a) aluminum and (b) phosphorus.

on targets of tin, antimony, tellurium, and iodine. We have chosen these specific reactions for the following reasons:

- Use of neutron excess projectiles (including ^{14}C, which is uniquely available in the US at Los Alamos).
- Ease of radiochemical isolation of the xenon product from the bulk of the elements produced in the reaction.
- Use of the Los Alamos Van de Graaff facility since the Coulomb barriers are sufficiently low to enable on-site reaction mechanism studies.
- High sensitivity for detection of γ-ray decays from the xenon isotopes.
- Production of a variety of detectable radioactive xenon isotopes from ^{122}Xe-^{135}Xe to permit study of transfer trends.

The first bombardments were with ^{18}O on KI targets. The targets were prepared by evaporating 3-5 mg/cm^2 KI onto a 1.5 mg/cm^2 aluminum foil and then encapsulating the target by evaporation of an ~0.5 mg/cm^2 aluminum layer on top of the KI. The available beam currents of high-energy ^{18}O were limited because of the requirement of stripping the ion to the 7^+ or 8^+ charge state. For the 8^+ ^{18}O, a beam of 83.0 MeV was used at an average current of ~2 pnA. For the 7^+ ^{18}O the energy was 74.5 MeV with an intensity of ~40 pnA. The irradiated targets were dissolved in HCl and the xenon isotopes were cryogenically trapped onto charcoal beads in liquid nitrogen. The beads were γ-ray counted using a high-efficiency well detector. The chemical yield of the xenon trapping was not established in this experiment, and the only detected xenon isotopes were ^{127}Xe and ^{129}Xe. With an assumption of a 10% chemical yield, the ^{129}Xe production was 1 mb for the 7^+ irradiation and 3 mb for the 8^+ irradiation. In the 8^+ irradiation, ^{127}Xe was produced with a cross section of ~100 μb. whereas ^{133}Xe was not observed within the detection sensitivity of ~10 μb.

The second Los Alamos experiment used a ^{14}C beam on targets between tin and iodine and is summarized in Table XXXVII. The xenon fractions were extracted by

TABLE XXXVII

^{14}C BOMBARDMENTS

Run	Target	E (MeV)	Fluence	Chemistry	Chemical Yield
1	KI	66.	9.08×10^{15}	HCl	5.5%
2	KI	57.5	10.04×10^{15}	HCl	>3.8%
3	Te	66.	7.71×10^{15}	$HCl + H_2O_2$	~60%
4	^{130}Te	66.	8.36×10^{15}	$HCl + H_2O_2$	29.3%
5	Te	57.4	7.92×10^{15}	$HCl + H_2O_2$	21.6%
6	Sb	66.	8.44×10^{15}	H_2SO_4	8.6%
7	Sb	57.4	6.54×10^{15}	H_2SO_4	15.7%
8	Sn	66.	6.82×10^{15}	HCl	11.3%

chemically dissolving the target material in the indicated acids and then cryogenically trapping the xenon through a gas vacuum system onto an activated charcoal bead submerged in liquid nitrogen. The beads were counted in a Ge(Li) well counter and the spectra analyzed to extract the yields of the xenon isotopes. Results of the analysis are presented in Table XXXVIII. With a general sensitivity on the order of 1 μb, the neutron excess transfer products seen include "^4H" transfer to make ^{131m}Xe from ^{127}I; "^5He" transfer to produce ^{135}Xe from ^{130}Te; and "^{10}Li" transfer to produce ^{133}Xe from ^{123}Sb. With improved beam intensities and target irradition development, sensitivities on the order of nanobarns are potentially possible. Even at our current sensitivity, we are able to detect a "^{10}Li" transfer which would yield the very exotic isotope ^{264}No with an irradiation of an ^{254}Es target. We plan to continue these studies and extend them to production of neutron rich bismuth isotopes using reactions

$$(^{204}Hg, ^{205}Tl, ^{208}Pb) + ^{18}O \rightarrow ^{212\text{-}214}Bi + \text{residuals}$$

The ^{18}O reactions on these heavier Z targets will require higher beam energies than can be obtained at the Los Alamos Van de Graaff and will be performed at an outside facility. Detection methods of high sensitivity

TABLE XXXVIII

PRODUCTION CROSS SECTIONS (IN μb) FOR XENON ISOTOPES WITH ^{14}C BEAMS

		Xe Isotope							
Run	Target	122	125	127	129m	131m	133m	133	135
1	KI			9.2	940.	40.5		<0.75	
2	KI			<5.	<150.	<23.		<1.2	
3	Te		3.8	46.5	112.	215.	973.	694.	147.
4	^{130}Te					19.7	4700.	2790.	693.
5	Te		3.4	58.0	129.	298.	1390.	1120.	459.
6	Sb		210.	1970.	1000.	230.	<4.1	2.2	
7	Sb			112.	1140.	313.		<2.0	
8	Sn	1880.	13800.	94300.	985.	9120.	<230.	<44.	<30.

should also be available for these neutron rich bismuth isotopes. The half-lives for $^{212-214}$Bi are in the 20 min-1 h range and can be radiochemically isolated from the bulk reaction products. These isotopes β^- decay to very short lived polonium isotopes, which in turn decay by emission of uinique, easily identified high-energy alphas. The majority of the reaction cross section goes into prompt fission decay and the surviving part of the compound cross section results in short-lived α activities that decay to long-lived α emitters that have substantially lower energy emissions than the desired bismuth daughters to be measured.

In pursuit of the ultimate goal of producing and detecting exotic heavy fissioning isotopes, we have begun development work on detection techniques. We envision a system that consists of a recoil-collecting foil for reaction products, a very thin ($\sim$60 μg/cm^2) avalanche counter for a start signal, a position-sensitive parallel plate avalanche counter some 20 cm away to provide fragment velocity information, and finally an ionization counter for residual fragment energy measurement. Prototypes of the position-sensitive avalanche counter are being currently constructed. Realistic detector responses have been simulated, using a Monte Carlo method to select fission distributions. The detector responses were then unfolded, using calculated range-energy relationships to establish fission fragment charge and mass assignments. With as few as 10 fission events, the standard deviation of the charge distribution of the composite fission system was $\sim$1 Z unit, and the mass distribution was $\sim$2 A units. The standard deviation will become narrower as the square root of the number of observations. The final resolution will undoubtedly be limited by systematic errors, but the simulation is encouraging for the possibility of using such detector arrays for assignment of fission events to specific isotopes.

G. Pion-Nucleus Reactions

1. Pion Single-Charge-Exchange in Complex Nuclei

(R. S. Rundberg, G. W. Butler, B. J. Dropesky, G. C. Giesler, S. B. Kaufman,* and E. P. Steinberg*). In their interactions with nuclei, pions of both positive and negative charge may undergo charge exchange. Both single-charge exchange, that is, $A^z(\pi^+,\pi^0)A^{z+1}$ and $A^z(\pi^-,\pi^0)A^{z-1}$ and double-charge exchange, that is, $A^z(\pi^+,\pi^-)A^{z+2}$ and $A^z(\pi^-,\pi^+)A^{z-2}$ can occur. However, the mechanism by which these processes take place is not well understood, in that theoretical calculations cannot explain the observed excitation functions. (Most theoretical models predict a minimum at the (3,3) pion-nucleon resonance.)

Pion single-charge-exchange reactions, which can be studied by radiochemical methods, populate many final states in the product nuclei. Within the limit of many final states, the nuclear structure effects may average out, leaving only the gross features involved in the charge exchange process. In this case, we wish to show how the absolute cross sections and excitation function shapes change as a function of A and/or number of bound levels available for population.

The excitation functions for the pion single-charge-exchange reactions ^{27}Al$(\pi^-,\pi^0)^{27}$Mg (9.4 min), ^{45}Sc$(\pi^+,\pi^0)^{45}$Ti (3.1 h), and ^{65}Cu$(\pi^-,\pi^0)^{65}$Ni (2.5 h) were determined for incident pion energies ranging from 80 to 400 MeV. The results of these experiments will be compared with the Fermi gas model calculations of Kaufman and Hower,[297] and we hope they will stimulate further theoretical work on single-charge-exchange reactions leading to many final states.

Targets were irradiated in the LEP and P^3 pion channels of Los Alamos Meson Physics Facility (LAMPF), and the resulting activities were determined radiochemically. Exposures ranged in duration from one to two half-lives of the reaction products, and the beam intensity was monitored using aluminum monitor foils attached to the target (the aluminum target did not require an additional monitor foil). The pion intensity was determined by measuring the ^{18}F (110-min) or ^{24}Na (15-h) activity in the monitor foil and using the known cross sections for the spallation reactions ^{27}Al$(\pi^\pm$, Spall$)^{18}$F and ^{27}Al$(\pi^\pm$, Spall$)^{24}$Na.[298] The aluminum charge exchange experiment required no chemical separation, and the ^{27}Mg (9.45-min) activity was simply determined by counting the 843.8-keV γ ray using a Ge(Li) spectrometer. The ^{45}Ti was chemically separated from the scandium target, and the 3.078-h β^+ activity was determined using γ-γ annihilation counters. The ^{65}Ni was also chemically separated from the copper target, and the 2.52-h β^- activity was measured in low-background β counters.

Because nucleon-charge-exchange reactions, that is, (n,p) or (p,n) reactions, yield the same products as pion charge exchange, it was necessary to determine the effect of secondary nucleons resulting from primary pion reactions. The secondary effect was determined by measuring the cross section as a function of target

*Argonne National Laboratory Chemistry Department.

thickness. (In the limit of very thin targets, the apparent cross section owing to secondary reactions should scale with the target thickness.) The measured aluminum reaction cross sections, which showed significant contributions from secondary effects, were extrapolated to zero target thickness. The secondary effect was larger in the aluminum cross section for two reasons: (1) the targets used were thicker because the counting efficiency was low; (2) the (n,p) cross section is larger in aluminum because the Coulomb barrier is smaller than, for example, in copper. The secondary effect for scandium and copper targets was shown to be small relative to the experimental uncertainty in the measurements. The resulting excitation functions are shown in Fig. 60.

The Fermi gas model calculations[297] show a strong influence of the (3,3) pion-nucleus resonance. The calculated excitation function has a deep minimum near the (3,3) resonance. These calculations involve the use of

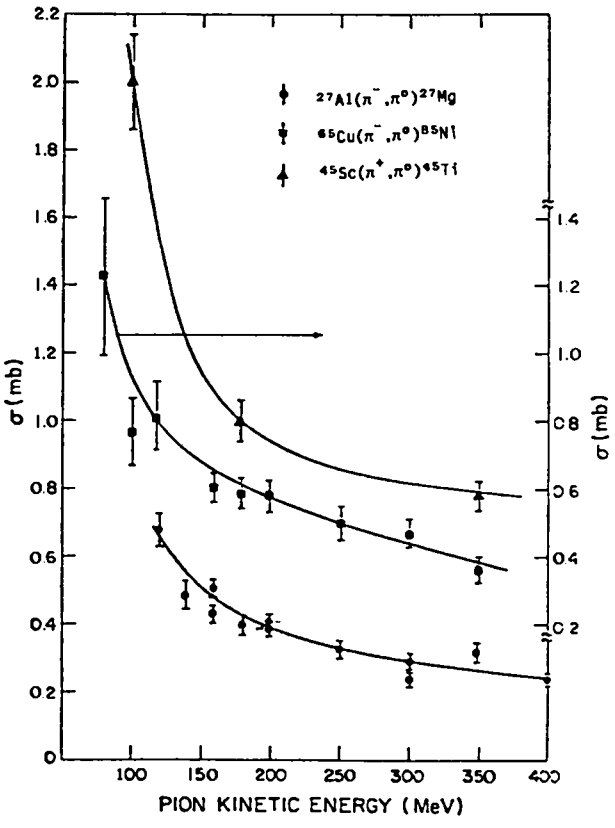

Fig. 60.
Measured excitation functions for the reactions $^{27}Al(\pi^-,\pi^0)^{27}Mg$, $^{45}Sc(\pi^+,\pi^0)^{45}Ti$, and $^{65}Cu(\pi^-,\pi^0)^{65}Ni$.

reduction factors, as defined by T. Ericson et al.[299] and are similar to the distorted wave impulse approximation. The reduction factor is the probability of an incident pion traveling through the nucleus without interacting to a given position in the nucleus, where single-charge exchange takes place, times the probability of the exciting pion traveling out of the nucleus without interracting. The reduction factor becomes smaller near the (3,3) resonance because the mean free path of the pion becomes shorter. When this energy dependence of the reduction factor is removed, the excitation function has a maximum near the (3,3) resonance. The shape of the excitation function was shown not to depend on the Fermi momentum used in the calculation. The magnitude of the cross section, however, was shown to be strongly dependent on the Fermi momentum.

The results of our measurements show no significant structure at all in the excitation function (that is, there is no minimum or maximum near 150 MeV). The lack of structure was common to all the target nuclei used. This lack of structure may be due to broadening of the resonance in the total cross section, resulting in a washout of the minimum in the reduction factor. Although the Fermi gas model failed to predict the correct shape for the excitation function, the relative magnitudes of the cross sections of the various nuclei seem to fit reasonably well with this model (Fig. 61). The single-charge-exchange cross section is predicted to have a $Z/A(E°)^2$ dependence for incident π^-, or $N/A(E°)^2$ for π^+, where $E°$ is the energy required to evaporate a nucleon and Z, N, and A are the proton, neutron, and mass numbers, respectively.

In summary, the excitation function for single-charge exchange in complex nuclei does not have a minimum, in contrast to the prediction of the Fermi gas model. The excitation functions are smooth functions decreasing with increasing pion kinetic energy and suggest a $1/k^2$ function (k is the momentum of the incident pion). The dependence of the magnitude of the single-charge-exchange cross section on target nucleus, however, can be explained using the simple relation predicted by the Fermi gas model. We are continuing this study with measurements of the $^{139}La(\pi^+, \pi^0)^{139}Ce$ reaction cross section as a function of pion kinetic energy. We hope these studies will stimulate more theoretical efforts to understand single-charge exchange in complex nuclei and to calculate new excitation functions for this process.

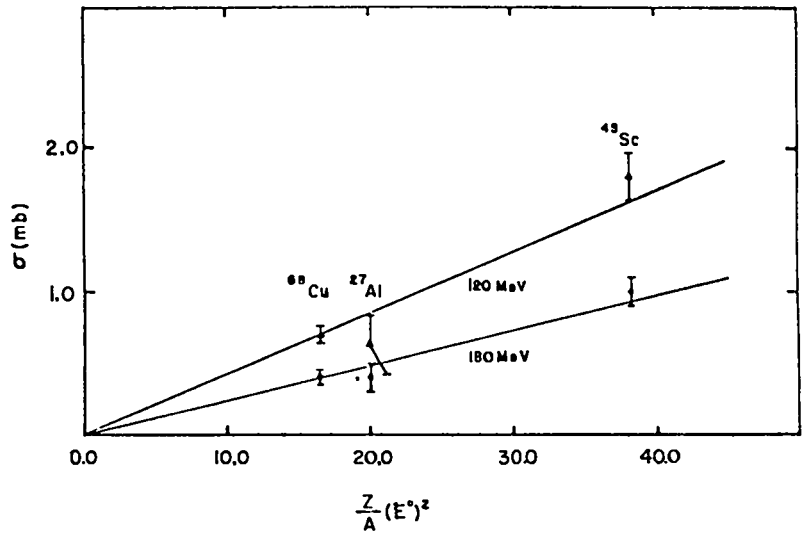

Fig. 61.
The dependence of the single-charge exchange cross section at selected energies on Z(N)/A $(E^*)^2$ as predicted by the Fermi gas model.

2. A Covariant Coupled-Channel Theory for Pion-Nucleus Single-Charge-Exchange Reactions. (L. C. Liu) It has long been known that single-charge exchange scattering of hadrons from nuclei with a neutron excess can shed light on the main features of the isovector component of the nuclear force. Because the basic pion-nucleon scattering amplitude is much better determined than the nucleon-nucleon scattering amplitude, pion-nucleus single-charge-exchange (SCE) reactions have received considerable attention in recent years.[300] Most of the published theoretical work[300,301] made use of the distorted-wave impulse approximation (DWIA) and assumed a one-step reaction mechanism, where the charge exchange takes place between the projectile pion and a single target nucleon. Some researchers also calculated the contribution to SCE arising from two-step processes. However, only the conventional two-step processes related to the scattering of projectiles by correlated nucleon pairs were considered.[302] The question of contributions to SCE due to true pion absorption by two nucleons has not been addressed. Finally, almost all calculations reported in the literature were based on fixed-scatterer approximation (FSA), a calculational scheme that contains many theoretical uncertainties and introduces serious numerical errors into the study of the pion-nucleus interaction at pion energies near and below the (3,3) resonance.

We have developed a covariant coupled-channel theory suitable for the study of pion-nucleus single-charge exchange reactions leading to isobaric analog states (IAS).[303] [The theory is currently being expanded to include the study of pion-nucleus double-charge exchange (DCE) reactions.] The novel features of our approach can be summarized as follows:

(1) The underlying dynamical equations of the theory are fully relativistic.

(2) The pion-nucleus effective interaction used in the theory is covariant and is not based on FSA. At each order, the effective interaction can be evaluated from corresponding reaction diagrams with unambiguous relativistic kinematics, as well as well-defined nuclear dynamics. Fermi motion and the binding effect of the target nucleons are treated from first principles.

(3) Making use of a new *non*perturbative expansion of effective interactions for strongly interacting particles,[304] we construct the second-order effective interaction, which can be related to observable reaction processes through unitarity considerations.

(4) We propose a new two-nucleon reaction mechanism for SCE, which involves the true pion absorption by a pair of target nucleons and the subsequent creation of a pion by the same pair. The foundations of our proposition are the concept of reactive contents of an effective interaction outlined in (3) and the experimental fact that true pion absorption by a

nucleus exhausts more than one-third of the total pion-nucleus reaction cross section in the (3,3) resonance region. Both true pion absorption by two nucleons and pion scattering from correlated nucleon pairs are included in our theory.

(5) We develop an isospin scaling model, which allows the calculation of the second-order SCE interaction from the second-order optical potentials determined in the analysis of the elastic scattering of pions from *neighboring* nuclei.

(6) Finally, we introduce a *momentum-space, coupled-channel,* Coulomb-nuclear matching method to take fully into account macroscopic isospin symmetry-breaking that is due to the pion-nucleous Coulomb interaction, as well as the mass difference between analog nuclei caused by the Coulomb force between the constituent nucleons.

As an application of our theory, we studied the excitation function of the $^{13}C(\pi^+,\pi^0)^{13}N$ (g.s.) reaction and elastic scattering of charged pions from ^{13}C, making use of our knowledge of the pion-^{12}C optical potential. In Fig. 62, we show theoretical and experimental differential cross sections for $\pi^{\pm}$-^{13}C elastic scattering at 180 MeV. The good agreement between the theoretical results and the data[305] is encouraging, in that no adjustable parameters have been used in the present calculation.

On the other hand, calculated excitation functions of the SCE reaction exhibit a strong dependence on the type of the two-nucleon processes being considered (see Fig. 63). Our study indicates therefore that SCE reactions leading to IAS may offer a useful tool for probing pion-nucleus dynamics.[303] In this respect, comparison of our calculated excitation functions with the forthcoming nuclear chemistry measurements of this SCE reaction at Los Alamos Meson Physics Facility will provide useful information as to the composition of the second-order processes.[303]

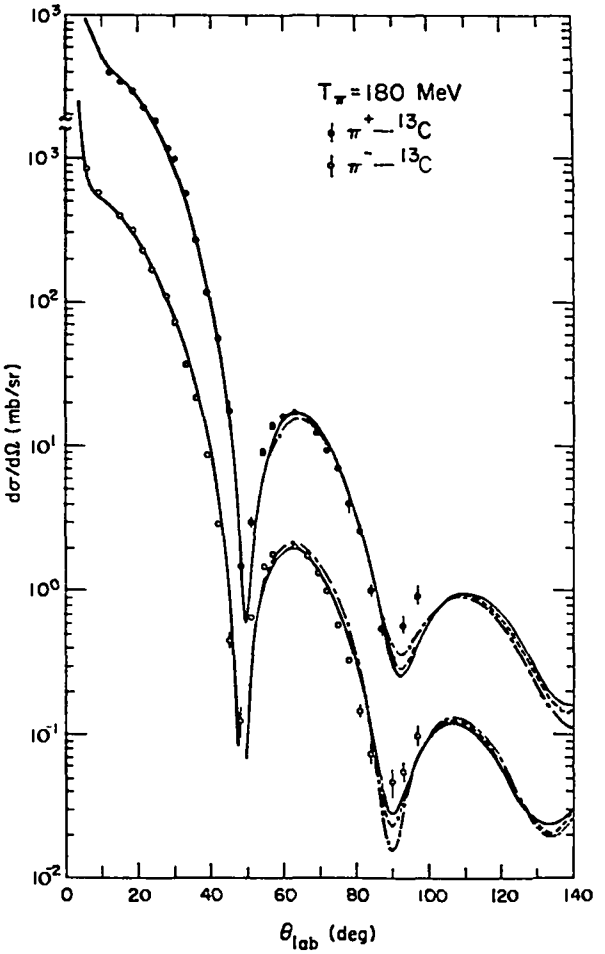

Fig. 62.
Calculated differential cross sections for π^+ ^{13}C and π^- ^{13}C elastic scattering at 180 MeV. Data are taken from Ref. 6. The solid curves correspond to the situation in which only the true pion absorption processes contribute to the second-order SCE potential $V^{(2)}$. Results calculated with the assumption that $V^{(2)}$ is due to pion scattering from correlated pairs are represented by the dot-dash curves. The dashed curves represent theoretical results calculated in the limit that the contributions from these two two-nucleon processes to $V^{(2)}$ cancel each other.

3. Yields of Two-Nucleon-Out Products from Stopped Negative Pion Reactions (C. J. Orth, B. J. Dropesky, G. C. Giesler, L. C. Liu, and R. S. Rundberg). The absorption of a negative pion by the nucleus of an atom into which it has been Coulomb captured is a poorly understood process. To conserve momentum the absorption cannot take place on a single proton, but rather occurs, most likely, on a proton-neutron (pn) or proton-proton (pp) pair. In the process of absorption of a pion on a nucleon pair, a proton is converted to a neutron and the rest mass of the pion (140 MeV) is converted to kinetic energy of the nucleons so that they recoil from each other at 180° in the center of mass system with about 70 MeV each. The counter telescope experiment of Nordberg, Kinsey, and Burman[306] in which coincident nn and np pairs were observed at 180° confirmed this absorption mechanism.

An interesting and important question concerning pion absorption is the relative probability of absorption on a pn pair versus a pp pair. In the Nordberg et al. experiment the ratio R(nn/np) was determined for a series of N = Z nuclei to be 3 ± 1 and for ^{208}Pb to be 4.7

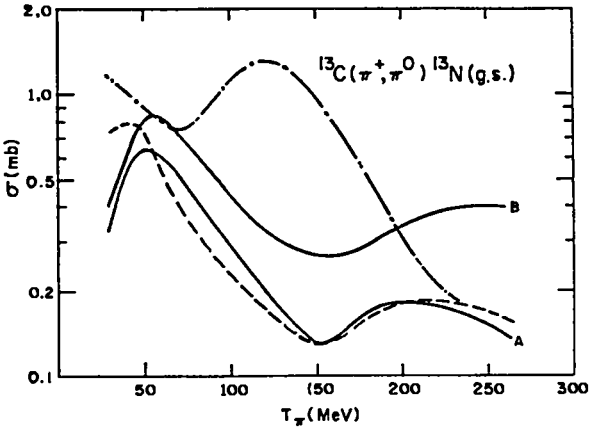

Fig. 63.
Theoretical excitation functions for the SCE reaction $^{13}C(\pi^+,\pi^0)^{13}N(g.s.)$. Curve A corresponds to the situation in which only the true absorption processes contribute to $V^{(2)}$. Results calculated with the assumption that $V^{(2)}$ is due solely to pion scattering from correlated pairs are represented by Curve B. The dashed curve represents the excitation function calculated in the limit that the contributions of these two two-nucleon processes to $V^{(2)}$ cancel each other. The dot-dash curve indicates theoretical results when only the first-order interaction is used.

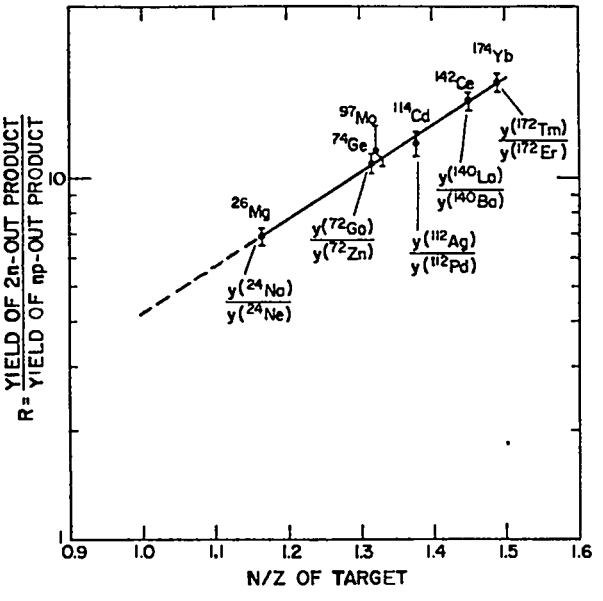

Fig. 64.
Ratios of nn-out to np-out residual product yields versus N/Z of the target nucleus for stopped π^- reactions. The results for ^{97}Mo are preliminary.

± 4.7. These ratios may well differ from the primary ratios because of charge exchange scattering of the outgoing nucleons.

To provide further information about this process, we have measured yields of residual two-nucleon-out products from stopped π^- reactions in ^{26}Mg, ^{74}Ge, ^{97}Mo, ^{114}Cd, ^{142}Ce, and ^{174}Yb using activation techniques. After irradiation the targets were counted with a high-resolution Ge(Li) detector system to determine γ-ray intensities of the radioactive products. With ^{114}Cd it was necessary to do radiochemical separations for silver and palladium products. Although the $\Delta A = 2$ products were our primary interest, we also measured the yields of the other radioactive products to establish the shapes of the yield distributions of the (π^-,xn) and (π^-,pxn) products. The existence of $\Delta A = 2$ residual products requires that the recoiling nucleons escape the nucleus without depositing more than about 6 MeV of excitation energy, otherwise nucleon evaporation would occur, resulting in residual products with $\Delta A \gtrsim 3$. Therefore, these measured yield ratios should correlate closely with the original ratios of absorption on np and pp pairs.

In Fig. 64 we show a semilogarithmic plot of the ratio of the yields of the nn-out and np-out products versus N/Z of the target. Extrapolation of the straight line to N/Z = 1 gives a value of 4.2, and for ^{208}Pb we would predict a ratio of 20, compared with R(nn/np) = 3 ± 1 and 4.7 ± 4.7, respectively, from Nordberg et al.[306]

Whether or not our data correspond directly to the initial ratios of absorption on np and pp pairs is not now known. The large ratios that we have observed may be due to selective sampling of those absorptions that occur on the surface of the nucleus where the ratio of neutrons to protons may be greater than the average for the nucleus. This possibility suggests that these measurements may be a sensitive method for studying the existence of a "neutron skin" in nuclei.

We are attempting to gain further understanding of our measured ratios by comparing them with yields calculated from a model that includes a pionic atom cascade routine followed by intranuclear cascade/evaporation codes (ISOBAR/DFF). The latter codes are being modified to include different nuclear density distributions for the neutrons and the protons.

XIII. RADIOCHEMICAL SEPARATIONS

A. The Chemical Isolation of Spallogenic ^{68}Ge From RbBr. (D. A. Miller,† P. M. Grant, J. W. Barnes, G. E. Bentley, and H. A. O'Brien, Jr.)

Radiogallium, particularly ^{67}Ga, is useful in nuclear medicine for tumor localization and for the detection of inflammatory disease.[307] Because of the increasing interest in positron emission tomography and the existence of its long-lived ^{68}Ge parent, ^{68}Ga from a biomedical generator is predicted to have numerous important applications in positron scintigraphy.[308] The present high cost of ^{68}Ge is a deterrent to extensive research in ^{68}Ga labelling chemistry, however, and the exploration of the production capabilities of Los Alamos Meson Physics Facility (LAMPF) for this system has been initiated.

Experiments have been conducted at the laboratory scale on the synthesis of ^{68}Ge from the spallation of RbBr pressed-salt targets by 800-MeV protons. The activities induced in the target by such an irradiation are given in Table XXXIX. The irradiated pellet is dissolved in 6 *M* HCl, and distillation into a cooled receiver containing a few mℓ of H_2O_2 is effected. The distillate is then adjusted to 8.4 *M* HCl and extracted with CCl_4. A final back-extraction with distilled water completes the separation procedure as it has been developed thus far.

As expected from a previous study of the distillation of NCA[309] radiogermanium from 6 *M* HCl,[310] *Ge quantitatively volatilized and was trapped in the receiver. Moreover, under these conditions, only isotopes of arsenic and selenium codistill with the germanium. The overall chemical yields of these three elements in the separation procedure, from eight independent experiments, are given in Table XL. Following the distillation, the CCl_4 solvent extraction effectively separated germanium from arsenic and selenium, and the back-extraction with distilled water returned *Ge to an aqueous environment. Although this final solution often contained a small fraction of *Se impurity, the *Ge may be suitable for medical use in this medium because it will be used in a ^{68}Ge-^{68}Ga generator system.

A reasonably quantitative recovery of *Ge from irradiated RbBr targets has been demonstrated at the research level, and excellent decontamination from at least 17 neighboring radioelements has been accomplished. The cross section for ^{68}Ge production in RbBr by 800-MeV protons has been measured to be 19 mb (Ref. 311). When this datum is factored with LAMPF target thicknesses and proton intensities, it translates to Ci-level capabilities for ^{68}Ge synthesis in the Isotope Production Facility. The utilization of LAMPF for the supply of ^{68}Ge to the research and medical communities should provide abundant quantities of this material more reliably and economically than was previously possible.

†Department of Chemistry, California State University, Northridge.

TABLE XXXIX

ACTIVITIES IDENTIFIED IN RbBr TARGETS AFTER IRRADIATION WITH 800-MeV PROTONS

Element	Nuclide
Y	88
Sr	82, 83, 85
Rb	81, 82m, 83, 84, 86
Br	75, 76, 77, 80m, 82, 83
Se	72, 73, 75
As	71, 72, 73, 74, 76, 77, 78
Ge	68, 69
Ga	66, 67, 72
Zn	62, 65, 69m
Cu	61, 64, 67
Ni	57
Co	56, 57, 58, 60
Fe	59
Mn	52, 54, 56
Cr	51
V	48
Sc	44, 44m, 46, 47
Be	7

B. A ^{172}Hf-^{172}Lu Isotope Generator for Preclinical Nuclear Medicine (P. M. Grant, R. J. Daniels,* W. J. Daniels,** G. E. Bentley, and H. A. O'Brien, Jr.)

Recent work at Los Alamos has resulted in a practical method for the synthesis, quantitative recovery, and purification of Ci quantities of NCA[312] ^{172}Hf. This long-lived (1.87-yr half-life) nuclide decays to 6.70-d

*Indian Medical Center, Phoenix, Arizona.
**Shell Oil Company, Houston, Texas.

TABLE XL

RADIOCHEMICAL SEPARATION OF ^{68}Ge
FROM PROTON-IRRADIATED RbBr TARGETS

Analytical Step	Chemical Fraction	Overall Chemical Yield (%)		
		Ge	As	Se
Original Solution	—	100	100	100
Distillation	Residue	0	4 ± 2	14 ± 4
	Distillate	98 ± 2	91 ± 2	59 ± 7
CCl_4 Extraction	Aqueous	0.5 ± 0.2	90 ± 3	51 ± 20
	Organic	87 ± 3	0	7 ± 3
H_2O Back-Extraction	Organic	2 ± 1	0	9 ± 4
	Aqueous	87 ± 2	0	1.3 ± 0.3

^{172}Lu, a neutron-deficient isotope of the heaviest rare-earth element. Heavy lanthandies, particularly ^{169}Yb, have found increasing use in nuclear medicine for cisternography, tumor localization, and other diagnostic procedures. Although ^{172}Lu decays to stable ^{172}Yb by electron capture, it produces a number of abundant, high-energy gamma rays that would prohibit its use in patient imaging with present instrumentation. It has been proposed,[313] however, that ^{172}Lu would be useful for compound-labelling investigations and animal biodistribution studies, and its availability would spur increased preclinical research with rare-earth compounds. Following successful preclinical studies, another radiolanthanide with better nuclear properties for diagnostic imaging could be interchanged for ^{172}Lu. The convenience of generator availability and the very long shelf-life of the ^{172}Hf-^{172}Lu system could make it an attractive research tool for medical investigators.

The production of ^{172}Hf is accomplished by irradiating metallic tantalum targets with medium-energy protons at the Los Alamos Meson Physics Facility (LAMPF). The targets are then remotely processed in a hot cell to radiochemically isolate a pure radiohafnium fraction, and significant quantities of ^{172}Hf are thus made available for use in isotopic generators.

A preliminary literature search uncovered a number of potentially useful analytical procedures for the chemical separation of lutetium from hafnium, of which three were selected for evaluation as ^{172}Hf-^{172}Lu generators. These were an anion exchange column eluted with 12 *M* HCl (Ref. 314), solvent extraction utilizing TTA/2 *M* HCl (Refs. 315, 316), and solvent extraction with HDEHP/9 *M* HCl (Ref. 317). Initial experiments employed 10-50 μCi of ^{172}Hf per run, and each separation system was studied in duplicate. Experimental solutions were analyzed for ^{172}Lu yield and (after the reattainment of equilibrium) ^{172}Hf breakthrough by Ge(Li) gamma-ray spectrometry. Comparisons with a primary external standard were made for activity-balance determinations, and agreements to within ±5-10% were obtained.

The anion columns loaded with ^{172}Hf were milked with conc HCl, and average ^{172}Lu yields of 0.92 and ^{172}Hf breakthroughs of 9.6×10^{-5} were measured. The average separation factor for this system was therefore (0.92/9.6 E-5) = 9600. The TTA extraction systems proved to be decidely inferior and resulted in an average separation factor of 39, primarily due to increased ^{172}Hf breakthroughs. Moreover, appreciable radiation damage to the TTA with but μCi quantities of ^{172}Hf was observed over the 3-month duration of this study. Results with the HDEHP generators were 0.95 ^{172}Lu yield and a separation factor of 8300. The HDEHP/9 *M* HCl extraction system and the anion exchange column were therefore comparable in generator performance at μCi activity levels.

For reasons of convenience and resistance to radiolysis effects, it was decided to implement the HDEHP generator in the Laboratory's radiochemistry hot cells

for the processing of LAMPF-irradiated targets. A test of this system under actual hot cell conditions was then performed. A total of 430 mCi of ^{172}Hf was extracted into a 50% HDEHP (by volume) in toluene solution, and ^{172}Lu was then back-extracted from the organic phase with four sequential washings of 9 *M* HCl [multiple extractions are required for quantitative lutetium recovery because the yield from a single step is only ~0.5] (Ref. 317). The HCl fractions were combined, and aliquots of the organic and inorganic phases were assayed for ^{172}Lu and ^{172}Hf. The separation factor obtained in this experiment was 1.7 x 10^4, in reasonable agreement with the results of the laboratory-scale work.

A generator for the separation of ^{172}Lu from ^{172}Hf has thus been developed. Quantitative ^{172}Lu yields are obtainable with a separation factor of 10^4, and the generator has been found to be effective at loadings up to about 0.5 Ci. The HDEHP medium in the hot cell has been very resistant to radiolytic perturbations for nearly 2 yr, with no novel chemical phenomena observed over that period.

The performance parameters of the HDEHP generator should be satisfactory for the proposed preclinical uses of ^{172}Lu. Investigators that are interested in obtaining research quantities of ^{172}Hf-^{172}Lu (or the separated daughter alone) should contact this laboratory.

C. Chemical Recovery of ^{52}Fe From Nickel (H. A. O'Brien, P. M. Grant, G. E. Bentley, J. W. Barnes, and H. M. Zacharis)

In cancer therapy there is a need for an agent to measure radiation effects on bone marrow and to determine the rate of recovery of the red-blood-cell-forming segment of the marrow, that is, the erythropoietic marrow, following radiation therapy. If insufficient active marrow remains, initiation of chemotherapy must be delayed for a period sufficient to allow the marrow to recover.

Indium-III labeled transferrin, as used today, localizes in the reticuloendothelial (RE) system of the marrow and cannot accurately measure erythropoietic marrow activity as can ^{52}Fe. Previous work indicates that at low doses of radiation the erythropoietic marrow is severely affected, whereas the RE portion shows little, if any, effect. At higher doses of radiation and/or drugs, both portions appear to be similarly affected. Thus, ^{52}Fe should prove useful in following the course of radiation/chemotherapy involving the skeletal system.

In 1977, Chauncey et al.[318] reported that ^{54}Mn uptake in canine myocardium was nearly twice that of ^{201}Tl, the most widely used radioactive agent in cardiovascular nuclear medicine today. They also noted that the quantity of ^{54}Mn in the area of myocardial infarction was markedly decreased. Both Chauncey et al. and Atcher et al.[319] have observed very rapid blood clearances of Mn(II) and large heart-to-blood ratios, as shown in Table XLI. These rapid blood clearances, increased myocardial uptake over ^{201}Tl, and large heart-to-blood ratios at short times all point to the potential usefulness of ^{52m}Mn in the diagnosis and study of cardiac diseases.

Sodd, Scholz, and Blue[320] reported in 1974 a cross section of 1.35 ± 0.30 mb for the formation of ^{52}Fe from 588-MeV proton spallation of nickel, whereas corresponding cross sections for targets of cobalt, copper, and manganese were shown to be ~10 times smaller. Our group reported a cross section of 1.54 ± 0.13 mb for ^{52}Fe from nickel bombarded with 800-MeV protons.[321] More recently, Ku et al. reported that the yield from the ^{55}Mn(p,4n)^{52}Fe reaction is somewhat greater than that from 200-MeV proton spallation of nickel.[322] However, it should be noted that their reported overall ^{52}Fe yield of 120 mCi at the end of bombardment (15-h irradiation) is not sufficient for widespread distribution.

Dissolution of the nickel metal is accomplished with 10 *M* HNO_3 and gentle heat. The solution is then made 6 *M* in HCl by the addition of 12 *M* HCl. The extraction procedure is based on the work of Pinajian,[323] in which he demonstrated a K_D of greater than 10^3 for Fe^{+3} using pre-equilibrated MIBK (methylisobutylketone) from 6 *M* HCl. We observed a significant increase in the organic volume (about 30%) at the conclusion of this step.

After phase separation, the organic is washed twice with equal volumes of 6 *M* HCl plus 3% H_2O_2. The remaining contaminants are thus removed, and the iron is stripped from the organic with distilled water.

The chemical yields measured for this radiochemical procedure are shown in Table XLII. Note that chromium, manganese, and nickel are completely eliminated after the first extraction, and that sodium, scandium, vanadium, and cobalt are removed during the acid-peroxide washes. In three separate experiments, long counts were performed on the final product solutions to look for radio-nuclidic contaminants. The results are shown in Table XLIII. The ^{48}V seen in targets 1 and 2 is absent from target 3. This arises from a slight modification in the procedure. For the first two targets, the original solution, containing 10 *M* HNO_3 and 6 *M* HCl, was made 3% in H_2O_2 before the MIBK extraction.

TABLE XLI

TISSUE CONCENTRATION OF ^{54}Mn IN MICE
(Percent of Total Dose/Gram of Tissue[a])

	Time Post Injection			
	5 Min	10 Min	20 Min	2 H
Organ				
Blood	0.18	0.13	0.06	000.04
Myocardium	17.34	16.53	13.00	12.85
Liver	14.82	11.38	11.60	13.18
Kidney	40.57	37.89	34.90	33.57
Lung	8.25	7.03	4.67	6.07
Myocardium/Blood	97.5	123.5	236.	328.9
Myocardium/Liver	1.17	1.47	1.12	0.97
Myocardium/Lung	2.12	2.36	2.78	2.12
Myocardium/Kidney	0.43	0.44	0.37	0.38

[a]R. W. Atcher, et al., J. Nucl. Med. 19(6), 689 (1978).

TABLE XLII

CHEMICAL YIELDS MEASURED
FOR SPALLOGENIC IRON RADIOCHEMICAL PROCEDURE
(RESULTS AVERAGE OF 4 EXPERIMENTS)

	Overall Chemical Yield (%)							
	Na[a]	Sc	V	Cr	Mn	Fe	Co	Ni
Original solution	100	100	100	100	100	100	100	100
Aqueous after MIBK	93	98 ± 1	96 ± 4	100	100	0.30 ± 0.5	99 ± 0.2	100
MIBK 1	6.6	2.0 ± 0.8	4.0 ± 4	0	0	100 ± 0.6	1.1 ± 0.2	0
6 M HCl wash	6.6	2.0 ± 0.8	4.0 ± 4	0	0	0.66 ± 0.5	1.1 ± 0.2	0
MIBK 2	0	0	0	0	0	99 ± 1	0	0
MIBK 3	0	0	0	0	0	0	0	0
H_2O strip (Final solution)	0	0	0	0	0	99 ± 1	0	0

[a]Results of one experiment only.

TABLE XLIII

RADIOCONTAMINANTS IN ^{52}Fe PRODUCTS
(Proton irradiation conditions: 800 MeV, ~1 μA, 20 min)

Target 1	[$T_c = t_0 + 6.5676$ D]	
	^{48}V $A_0 = 2.0987$ E4 DPM	(0.049% of V activity in original solution)
	^{52}Mn $A_0 = 1.1950$ E5 DPM	(^{52}Fe daughter)
	^{59}Fe $A_0 = 2.2579$ E5 DPM	($^{59}Fe/^{52}Fe$ at $t_0 = 0.0018$)
Target 2	[$t_c = t_0 + \sim 10.56$ D]	
	^{48}V $A_0 = 2.566$ E4 DPM	(0.056% of V activity in original solution)
	^{52}Mn $A_0 = 1.4082$ E5 DPM	(^{52}Fe daughter)
	^{59}Fe $A_0 = 1.9412$ E5 DPM	($^{59}Fe/^{52}Fe$ at $t_0 = 0.0016$)
Target 3	[$t_c = t_0 + 6.0504$ D]	
	^{44m}Sc $A_0 = 9.5669$ E3 DPM	(0.0060% of Sc activity in original solution)
	^{52}Mn $A_0 = 2.0969$ E5 DPM	(^{52}Fe daughter)
	^{59}Fe $A_0 = 3.8281$ E5 DPM	($^{59}Fe/^{52}Fe$ at $t_0 = 0.0018$)

For target 3, the peroxide addition was omitted before extraction and a much cleaner product resulted. The overall chemical yield of ^{52}Fe using this procedure is 99 ± 1%.

XIV. THEORETICAL CHEMISTRY

A. Theoretical Chemical Dynamics

1. The Dynamics of Cluster Growth (J. W. Brady, J. D. Doll, and D. L. Thompson). A series of classical trajectory studies has been completed that examines the dynamics of the elementary steps of the early stages of nucleation.[324-327] Specifically, the formation and dissociation of quasi-bound clusters of four, five, and six argon atoms have been investigated and microscopic rate constants computed. This work represents a unique treatment of the nucleation problem, which is usually studied using macroscopic theories or one of two microscopic simulation methods—Monte Carlo simulation or molecular dynamics calculations. Neither of these methods provides information about the individual steps in the mechanism for cluster growth. Our treatment, usually called the chemical dynamics approach, provides fundamental information on the details of the dynamics of cluster growth.

These studies show that the cluster growth process consists of the making and breaking of "bonds" in the same manner as chemical reactions. This suggests that much of the extensive knowledge of chemical reactions can be validly applied to nucleation. For example, our results demonstrate that chemical theories, such as the RRKM unimolecular theory, are directly applicable to dissociation of quasi-bound clusters. The study also shows that cross sections and rate constants are well behaved functions of angular momentum, total energy, and the number of atoms, thus allowing extrapolations to be made and suggesting that with a reasonable number of calculations a complete description of microcluster growth could be obtained. Furthermore, the insight into the fundamental nature of the cluster growth mechanism gained by this study should allow more realistic and accurate macroscopic theories to be formulated. All calculations were performed using CNC-2's Digital Equipment VAX 11/780 minicomputer.

2. Unimolecular Dissociation of Van der Waals Molecules (S. B. Woodruff and D. L. Thompson). Chemical and physical processes involving Van der Waals molecules are related to many traditional areas of research, such as energy transfer, bimolecular and termolecular reactions, unimolecular decay, and spectroscopy. We have made a quasi-classical trajectory study of the dissociation of the Van der Waals molecule $He\cdots I_2$ to $He + I_2$ for collinear geometries as a function of I_2 vibrational state.[328] The agreement between these classical results and those of a quantum mechanical calculation is excellent, showing the validity of trajectory treatments in this important area of chemical dynamics.

This is the first trajectory study of a highly mode-selective molecular decomposition process. The results show that the system undergoes exponential decay, demonstrating that this nonergodic system has random lifetimes. Furthermore, a new method of treating the results was introduced in this work to show that trajectory-computed decay rates can be obtained much more accurately than by previous methods. An important aspect of this research is that the system studied is similar to many models that have been used to study the fundamental behavior of unimolecular dynamics and thus has attracted considerable interest among theoretical chemists.

3. Low-Energy Ion Channeling (J. E. Adams and J. D. Doll). It has been known for a number of years that if an ion beam impinging upon the face of a crystal is oriented so that the ions are incident along one of the major crystallographic axes, then the observed ion penetration depths are much greater than would be expected if the beam were randomly oriented or if the solid were amorphous. Such an effect, known as channeling, is fairly well characterized both experimentally and theoretically in the high-energy (keV-MeV) regime. However, a recent experiment[329] [D^+ on W(110)] performed at ion energies of 80 eV has yielded a penetration depth profile that is qualitatively different from that predicted by an extrapolation of the high-energy results. Because the structure of the depth profile is intimately linked not only to the structure of the solid surface but also to that of any adsorbed overlayers that may block otherwise available channels, ion channeling at low energies would seem to have a great potential as a surface diagnostic tool if a better understanding of the dynamics of the process could be obtained.

Our approach to this problem[330,331] has involved the use of classical trajectory techniques. (Although other workers have employed much the same methods, these earlier studies have assumed that the ion dynamics is influenced exclusively by isolated two-body collisions with the solid atoms, an assumption that seems physically unrealistic. We have, in contrast, explicitly summed all two-body interactions at each step in the trajectory to include the longer range potential effects which our calculations indicate are nonnegligible.) These trajectories are easily generated by direct integration of Hamilton's equations, although the present problem is somewhat more difficult than conventional atom-diatom scattering problems because the interaction of the ion with the electron gas of the metal creates an effective frictional drag on the particle's motion, thereby destroying energy conservation. This velocity-dependent friction is the classical analog (unquantized, of course) of plasmon excitations. Because the energy-loss mechanism causes the ions to come to rest within the crystal, one can generate theoretically a depth profile of ions scattered into the metal and can subsequently compare this prediction with the recent experiments. All calculations were performed using CNC-2's Digital Equipment VAX 11/780 minicomputer.

At present we are able to make the following general comments concerning the channeling simulations. First, one can obtain fair qualitative agreement between theory and experiment even for the case (the only one that we have examined so far) in which the solid atoms are held fixed in their equilibrium positions. Second, ion penetration profiles are quite sensitive to the screening length of the ion-atom elastic potential, whereas the back-scattered ion energy spectra are particularly sensitive to the magnitude of the effective frictional forces. (We have suggested that these two observations might permit experimentalists to obtain more accurate determinations of the interatomic forces involved.) Third, small rotations of the angle of incidence of the ions away from the surface normal do not alter the gross structure of the penetration depth distributions, even though such rotations *can* significantly affect the back-scattered energy spectra. Finally, we can say that one should not ignore the analytic uses of low-energy ion channeling, at least at present; the phenomenon may well provide an independent means for obtaining surface and adsorbate structures.

4. Adsorption/Desorption Kinetics (J. E. Adams and J. D. Doll). Descriptions of adsorption/desorption phenomena represent important components in a general theoretical characterization of heterogeneous catalysis,

but no work has appeared that adequately treats the whole range of kinetic detail that is just now being observed experimentally, We have, however, recently proposed a method for calculating such information that is both uniquely versatile, in that it does indeed permit one to investigate arbitrarily complex real systems, and also quite accurate, with the quality of the calculations being comparable to that obtained in the best of the recent experiments.[332,333] In particular, we are able to evaluate such nonnegligible effects on the rates as adsorbate concentration, system temperature, and concurrent diffusion parallel to the substrate surface. No other work to date has been able to incorporate such a degree of dynamical complexity.

The actual formalism employed in the present study involves a relatively straightforward, two-step procedure. First, a generalization of Slater's theory of unimolecular reaction kinetics[334] is used to generate what is essentially just a transition state theory approximation. (Physically, this is equivalent to calculating the equilibrium vapor pressure of the adsorbed species.) One then applies the dynamical corrections suggested by Chandler[335] to the transition state results, thereby obtaining "exact" rate constants. Nowhere in the development does one need to restrict the dynamical description to only harmonic interactions or to highly idealized surface models.

Initial studies have examined thermal desorption of the ligher rare gases from solid xenon. Below are listed a few of the more important conclusions of this work. All calculations were performed using CNC-2's Digital Equipment VAX 11/780 minicomputer.

- The inclusion of adatom-adatom interactions may increase desorption rates by as much as 100%.
- At sufficiently high temperatures the motion of the surface atoms may be ignored, inasmuch as the desorption depends only upon the average potential interaction of an adatom with a surface unit cell.
- Desorption rates depend on the atomic density of the crystal face and are larger for crystal faces with lower atomic densities.
- For some systems one can see a marked decrease in the rates for finite adsorbate coverages with respect to the analogous infinite dilution results at temperatures just above $\varepsilon\kappa_B^{-1}$, where ε is the adatom-adatom potential well depth. Such an effect should be of particular importance if ε is substantially larger than the adatom-solid atom interaction.

5. Energy Transfer, Reaction, and Dissociation as a Function of Initial State for $H + H_2$ on an Accurate *ab initio* Potential Energy Surface (N. C. Blais and D. G. Truhlar*). We present results of trajectory calculations for the following reactions.

$$H_A + H_BH_C(v, j) \rightarrow H_A + H_BH_C(v', j') \quad \text{(R1)}$$

$$\rightarrow H_AH_B(v', j') + H_C \text{ or } H_AH_C(v', j') + H_B \quad \text{(R2)}$$

$$\rightarrow H_A + H_B + H_C \quad \text{(R3)}$$

We have examined the dependence of these reactions (energy transfer, atom exchange, and dissociation) on the initial internal state of the H_2 molecule, including states at high energy. For the high-energy states the transition probabilities are reasonably high and the concern with zero-point energy is minimized, thereby justifying our use of quasi-classical trajectories for the dynamical calculations.[336,337] We also have used an accurate *ab initio* potential energy surface, the LSTH potential,[338,339] so that the results are the best predictions that can be made presently about the real system.

We were especially interested in how several reaction attributes changed over the manifold of initial bound states. In Fig. 65 we have plotted values of the rate constant for (R2) for each initial state investigated. Both axis scales are linear in energy so that the energy dependence is evident. However, because vibration and rotation energies are not additive, the correspondence between the state and energy is strictly true only on the axes. The dependence of the rate constant on the initial vibrational quantum number and on the initial rotational quantum number is evident. From the change in rate coefficients for the states along the axes it is clear that, with equal amounts of initial internal energy in the molecule, vibration is much more effective than rotation in promoting atom exchange. In fact, vibration is at least 10 times as effective as rotation. However, if vibration and rotation are both present in the molecule in roughly equal amounts (as near the center of the plot), then rotation is almost as effective as vibration in promoting atom exchange.

Figure 66 is a similar plot but with the average final vibrational quantum number indicated at each initial

*University of Minnesota.

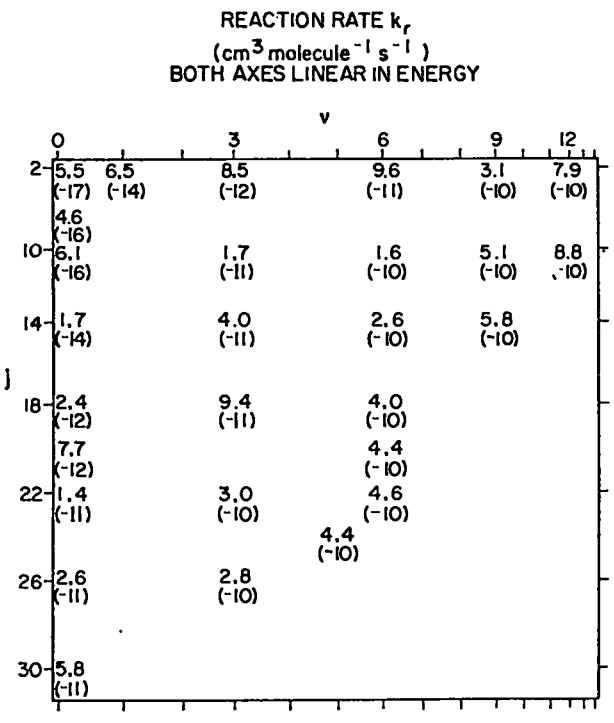

Fig. 65.
The rate constant (in cm^3 $molecule^{-1}$ s^{-1}) for the exchange reaction (R2) for various initial states for a 300 K distribution of relative translational energy. Numbers in parentheses are powers of 10. The initial vibrational and rotational quantum numbers are indicated on the abscissa and ordinate, respectively. The abscissa is chosen to be linear in energy for (v,0) states, and the ordinate scale is chosen to be linear in energy for (0,j) states.

state. There is a clear trend for vibration to be adiabatic during exchange. In fact, along the coordinate $j = 10$, the vibrational quantum number changes very little from reactant to product. But, as might be expected, there is significant transfer of rotational to vibrational energy at high initial j and, conversely, vibrational to rotational energy at low initial j.

In marked contrast to the adiabaticity for vibrational energy, the average final rotational quantum number differs considerably from its initial value, as shown in Fig. 67. Only at very low j is j′ nearly the same as j. For $j \geq 8$ there is a net energy loss from rotation. Because vibration does not change much during exchange, the net energy loss from rotation appears as translation. Therefore exchange when reactants have high internal energies causes the products to be translationally hotter than the reagents.

Energy transfer from the higher energy states of a molecule are of particular importance because, in the

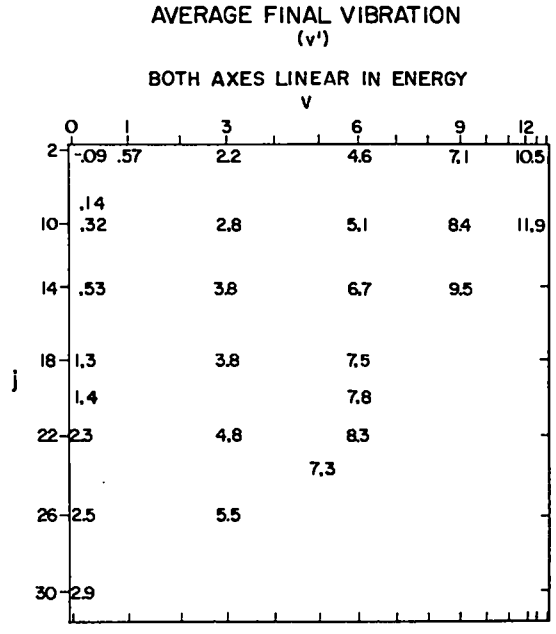

Fig. 66.
The average final vibrational quantum number for the exchange product of reaction (R2) for various initial states for a 300 K distribution of relative translational energy. The quantity given is $\langle v' \rangle$, where $(v' + 1/2)h = J'_r$, where J'_r is the final vibrational radial action variable. The axes are as in Fig. 65.

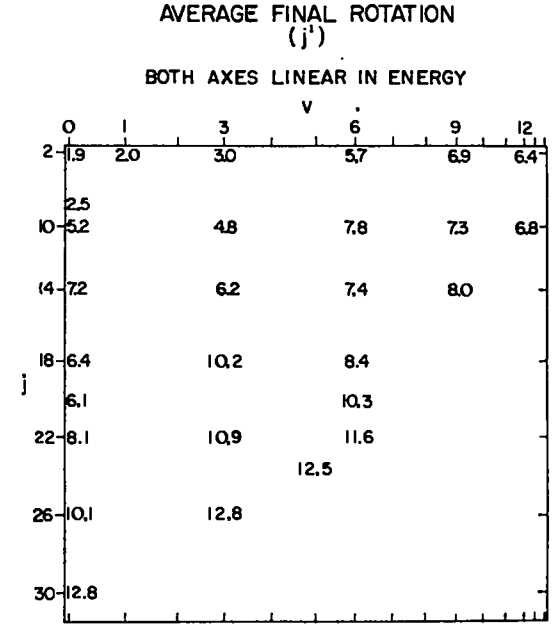

Fig. 67.
The average final rotational quantum number for the exchange product of reaction (R2) for various initial states for a 300 K distribution of relative translational energy. The quantity given is $\langle j' \rangle$, where $(j' + 1/2)h = 2\pi J' = J'_\theta$, where J_θ' is the final rotational action variable and J′ is the final rotational angular momentum. The axes are as in Fig. 65.

laboratory, studies on dissociation and recombination always involve a competition between the dissociation process to higher unbound states and the energy transfer to lower nondissociative states. In Fig. 68 are summarized the results of energy transfer from six initial states at a fixed collision energy of 0.5 eV. The contour lines connect points of equal transition cross section and are spaced at the values 9.0, 3.0, 1.0, 0.36, 0.12, 0.045, 0.015, and 0.005 a_0^2, with the interior contours around the initial state having the highest value. The "flow" of transition probability is a complex function of the initial state. If the initial state has a high j then, for those collisions that change the state, the transition probability is largest for final states of about equal energy. For initial states with low j, transitions to other states are predominantly along constant v', with $v = 0, j = 6$ being an extreme case. Transitions involving large changes in vibration or rotation apparently have no systematic correlation with the initial state. It is also significant that these large multiple quantum transitions are not nearly as unlikely as has been predicted before. (See references in Ref. 340.) The systematics of energy transfer in the H + H_2 system are similar to those in a completely different collision system, Ar + H_2 (Ref. 340).

In Fig. 69 the contour plots are for the transfer of energy with mechanism (R1), nonexchanging collisions, and for (R2), with atom exchange for two of the states presented in Fig. 68. In this figure the contours have the values of 3.75, 1.25, 0.417, 0.139, 0.046, 0.015, and 0.005. The two distributions differ considerably. The distribution for the case of no exchange is generally concave, whereas that for the case with exchange is convex. This implies an even higher probability for large multiple quantum transitions if thermoneutral atom exchange produces the energy transfer.

Figure 70 shows the cross section for dissociation of H_2 molecules on collision with hydrogen atoms and with argon atoms. The results from a calculation using a line of centers (LOC) model, a model often used to describe

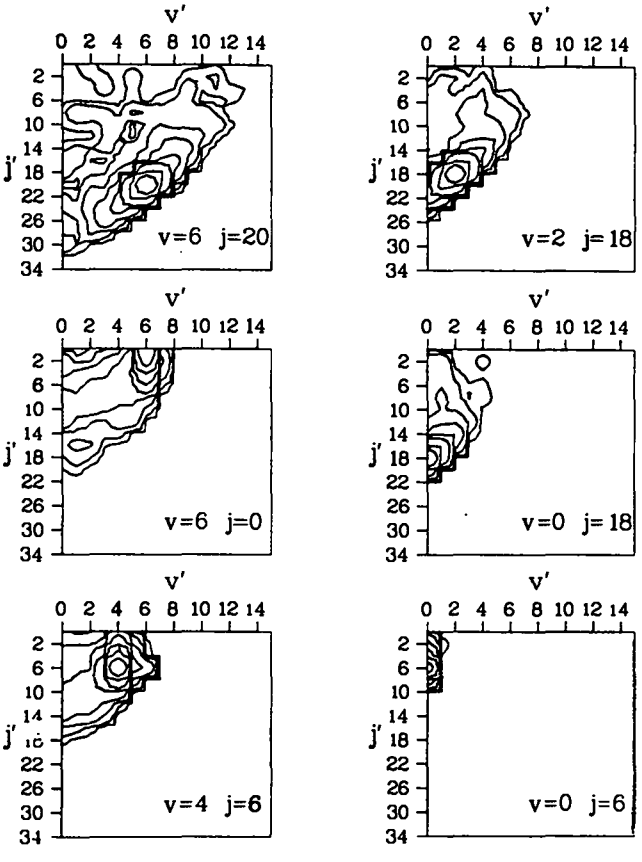

Fig. 68.
Contour plots of equal cross section for molecular energy transfer, process (R1), initial molecular states. Each plot is labeled by the initial state, and the axes indicate the final states. The relative translational energy was 0.5 eV and the contours have the values 9.0, 3.0, 1.0, 0.36, 0.12, 0.045, and 0.015 a_0^2. The contour of 9.0 a_0^2 is the one nearest to the initial molecular state.

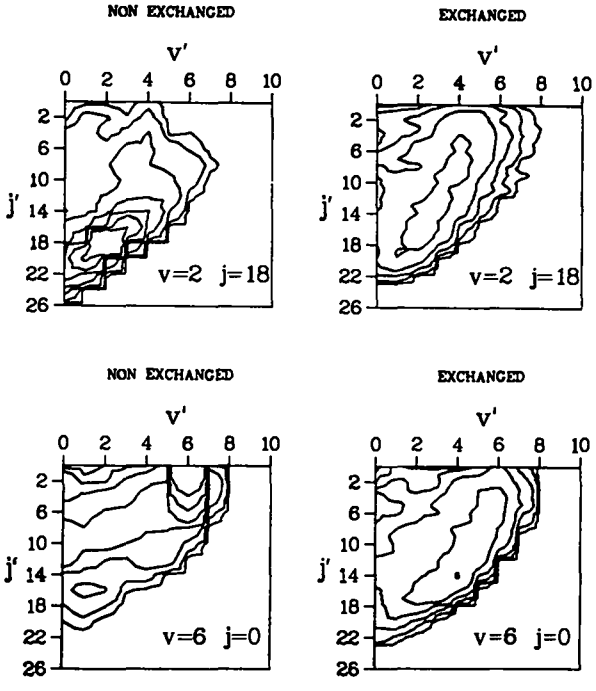

Fig. 69.
Contour plots of equal cross sections for the state-to-state processes (R1) and (R2). The relative translational energy is 0.5 eV and the contours have the values 3.75, 1.25, 0.417, 0.139, 0.046, 0.015, and 0.005 a_0^2. The innermost contours have the largest value and the values diminish monotonically (within statistical error) to the edges.

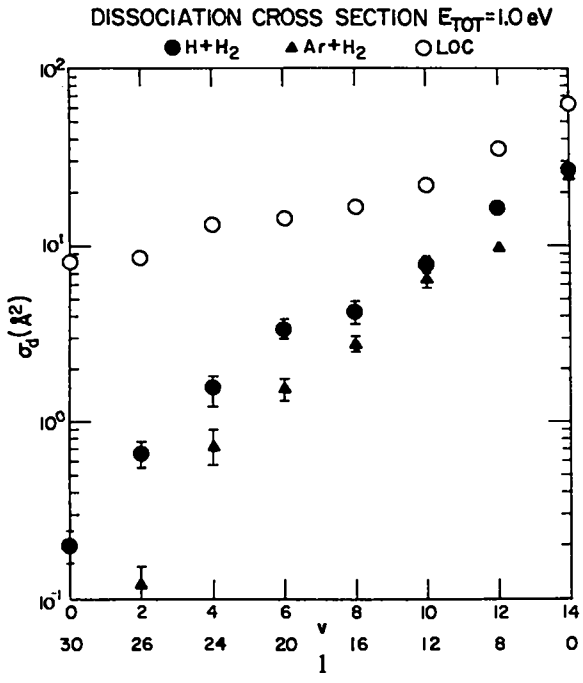

Fig. 70.
The dissociation cross section (in Å²) plotted against the initial molecular state quantum numbers. All the states have approximately the same internal energy. Three sets of points are plotted. Filled circles correspond to H + H_2, filled triangles to Ar + H_2, and open circles are values calculated from a line-of-centers (LOC) model.

dissociation, is also shown for the hydrogen atom collision. The model is clearly inappropriate. The difference in the interatomic forces when a hydrogen atom or an argon atom collides with the H_2 molecule leads to a higher efficiency for dissociation by the hydrogen atom.

We have also calculated the thermal rate constants and activation energies (Table XLIV)[341,342] for (R2) at three different temperatures, 444 K, 875 K, and 2400 K. At the lowest temperatures we compare our results with the most reliable experimental values, and at each temperature we list the best transition state calculation (with tunneling corrections).

Our calculations are among the very few completely *ab initio* calculations of the rate constant and activation energy for any chemical reaction. Of particular interest is the trend for the activation to increase with increasing temperature. An Arrhenius plot of the logarithm of the rate constant versus (1/T) would not be a straight line but would be concave upward.

B. Monte Carlo Based Electronic Structure Techniques (J. D. Doll)

Traditional quantum-chemical approaches to studies of electronic structure are based on the use of the

TABLE XLIV

THE RATE CONSTANT AND THE ACTIVATION ENERGY FOR ATOM EXCHANGE (R2)

	k ($cm^3 molecule^{-1} s^{-1}$)			
T(K)	Trajectories	Ref. 341	Ref. 342	Transition State
444	6.7 ± .8(−15)	7.7(−15)	1.0(−14)	9.49(−15)
875	8.0 ± .7(−13)	[4.4(−13)][a]	[9.9(−13)][a]	8.99(−13)
2400	3.5 ± .3(−11)			4.63(−11)
	Activation energy (eV)			
444	0.34 ± .01	0.350	0.382	0.33
875	0.38 ± .01		[0.414][a]	0.39
2400	0.60 ± .09			0.62

[a]Square brackets indicate extrapolation from a lower temperature range using the Arrhenius constants.

"variational principle." This principle assures that, given proper symmetry constraints, the energy associated with a trail wave function will always exceed that of the true electronic ground state. Trail functions are, thus optimized by varying adjustable parameters to minimize the computed energy. Historically this procedure has evolved in the direction of using trial functions of sufficiently simple functional form that the basic integrals that arise can be calculated essentially analytically. Such simplicity is gained at the expense of using trial functions that are intrinsically inefficient. That is, by virtue of their special functional form (chosen for convenience), these trial functions are often quite unphysical and, as a consequence, must contain many (10^2-10^5) adjustable parameters if chemical accuracy is desired.

From the earliest days of quantum chemistry one has known that compact and extremely accurate wave functions can be developed provided one is willing to build into these functions an explicit dependence on the electron-electron separation distances. Such "correlated" functions were used in the 1930s by James and Coolidge and by Hylleraas to treat simple systems with spectroscopic accuracy. Unfortunately, the functional form of such correlated trial functions makes it very difficult to use them to treat more complex systems within a traditional framework. The basic integrals involved are analytically intractable.

Recently we have examined the use of Monte Carlo (MC) based techniques in conjunction with correlated trial functions.[343] In this approach one foregoes any attempt to perform analytically the basic integrals which arise. Rather all integrations are performed using a modified form of the well-known Metropolis Monte Carlo method, which is especially suited to this application because the method's intrinsic complexity is independent of the dimensionality of the integrations involved. This implies that the method will be applicable to systems with significantly larger numbers of electrons than can be treated conventionally. A second important point is that the present method serves to unify the treatment of finite and extended systems, which will prove especially important for applications such as chemisorption that have both aspects.

Our results thus far involve both formal and computational aspects. On the formal side we have succeeded in establishing a quantitative estimate of the numerical accuracy of the MC method when applied to this problem. The estimate shows that the statistical uncertainty (the standard deviation for the computed energy) behaves as $(|E\Delta E|/N)^{1/2}$, where E is the true electronic energy, ΔE is the difference in the true and approximate energies, and N is the number of MC points used in the calculation.

The result shows that the convergence is more rapid than might have been assumed. One might initially have guessed, for example, that the convergence would be as $|E|/\sqrt{N}$. Such a convergence would have been prohibitively slow because the total energy, E, is often quite large. Because the actual result involves ΔE, which is often quite small, convergence is acceptable. As a related point we note that the MC method becomes *easier* to apply as the quality of the trial function *increases* (ΔE becomes smaller). The known convergence of the method permits one to develop extrapolation estimates of the true energy. The computational feasibility of the method was checked by performing benchmark calculations for a simple (but nontrivial) model system, the H_3^+ molecular ion. Using an extremely simple correlated trial function involving only three adjustable parameters, we reproduced the results obtained by previous investigators[344] using wave functions with over 300 such parameters. This hundredfold decrease in the number of parameters graphically illustrates the potentially increased efficiency of correlated trial functions. All calculations were performed using CNC-2's Digital Equipment VAX 11/780 minicomputer.

XV. UNCLASSIFIED WEAPONS RESEARCH

A. Bismuth: A New Weapons Radiochemical Detector (K. W. Thomas, W. R. Shields, D. J. Rokop, J. S. Gilmore, A. J. Gancarz, G. W. Butler, and D. W. Barr)

One of the primary functions within the Chemistry-Nuclear Chemistry Division is the radiochemical diagnosis of nuclear devices detonated underground at the Nevada Test Site. For the evaluation of the performance of the fission portion of the devices, it is only necessary to measure residual uranium, plutonium, and selected fission products. Assessment of the performance of the fusion parts is less straightforward, and two general approaches are used. One is to measure the amount of ^4He produced in the principal thermonuclear reactions (shown below) and other subsidiary reactions.

A. $^6Li + n \rightarrow \alpha + T + 4.77$ MeV

B. $D + T \rightarrow \alpha + n_{14} + 17.6$ MeV

The alternative approach is to measure the fluence of 14-MeV neutrons produced in reaction B by the use of radiochemical detector elements. These elements, which are ideally monoisotopic, are doped into or placed between different parts or regions of the device. The resultant (n,2n), multiple (n,2n) and (n,γ) products are measured and interpreted for the fluence of neutrons. The reaction products are radioactive and are measured by conventional radiochemical methods. There are 11 of these detector elements now in use at the Los Alamos National Laboratory. This number permits detailed examination of device performance. Such detailed analyses are crucial in understanding the physics of thermonuclear burn and are instrumental in suggesting design modifications and developing new designs. As a result of the interest in detailed diagnoses, we are in the process of trying to develop the class of potential new detectors whose reaction products are too long-lived to be measured by radiochemical techniques, but which, in principle, can be measured mass-spectrometrically.

During this past year we have successfully implemented bismuth as one of these new detectors and here briefly summarize recent results.

The stable bismuth isotope has A = 209. The first- and second-order (n,2n) products, A = 208 and A = 207, are long-lived species that can be detected mass-spectrometrically, although in some cases A = 207 also can be detected radiochemically. In these cases, the values of ^{207}Bi measured by the two techniques are in good agreement, and we have determined a half-life for ^{207}Bi of 32.3 a. The higher order (n,2n) products, A = 206 and A = 205, and the (n,γ) product, A = 210, are relatively short-lived and are measured radiochemically. The ability to detect higher order reaction products is important, because they are sensitive measures of both neutron fluence gradients and/or a mixture of small amounts of the doped portion of the device into high-flux regions. Only two other detectors, lutetium and europium, in addition to the new detector bismuth, can be used to measure fourth-order (n,2n) reaction products.

The implementation of bismuth as a detector has involved development of chemical and radiochemical separation procedures, mass spectrometry procedures for analysis of ^{209}Bi, ^{208}Bi, and ^{207}Bi, and counting procedures for samples with low specific activities.

The chemistry needs (1) to be relatively rapid because of the 6.2-day half-life of ^{206}Bi; (2) to be carrier-free because the addition of bismuth carrier would make the value of ^{209}Bi/^{208}Bi too large for mass spectrometric determination; and (3) to effect a 10^8 separation of bismuth from lead because ^{208}Pb and ^{207}Pb interfere with their respective bismuth isobars in the mass spectrometric analysis. The chemical procedure meeting these requirements as well as the necessity for extreme radiochemical purity is an operation capable of processing 25 g of postshot debris and isolating 1-20 μg of bismuth.

The major steps include (1) extraction of bismuth into tri-*n*-octylamine from a medium 0.1 *M* in each H_2SO_4 and KBr; (2) back-extraction with 0.5 *M* $HClO_4$; (3) adsorption of the element on a cation exchange resin column; (4) elution from the resin by means of 1 *M* HCl; (5) adsorption as a chloro-complex on an anion exchange resin column; and (6) elution with 2 *M* HF. After a portion of the eluate is taken for radiochemical analysis, the remainder is prepared for mass spectrometric analysis by converting the bismuth to the nitrate and electroplating the metal onto a rhenium cathode and the residual lead onto a platinum anode.

The mass spectrometric analysis is done by thermally ionizing bismuth, effecting the mass separation by using two magnet sectors in tandem, and detecting the ions by an electron multiplier operated in the pulse-counting mode. The two main mass spectrometric problems are hydrocarbon interferences and lead isobaric interferences at the mass 207 and 208 positions. These problems, however, can be solved by careful and clean chemical techniques and the use of a tandem-magnet mass spectrometer.

Bismuth has been used as a detector on three recent tests and will be on an upcoming test. On one test it was used with other detectors to provide a cross-calibration at a high specific thermonuclear yield; it will be placed on an upcoming test to provide a cross-calibration at a low specific yield. In another test, it was placed remote from a thermonuclear fuel. Using the previous calibration data, the results from this experiment are in quite reasonable agreement with other detectors and theoretical calculations. This will be confirmed by the additional calibration to be completed shortly.

B. Vibrational Spectra and Normal Coordinates of High Explosives under Ambient Conditions (B. I. Swanson and Scott A. Ekberg)

Very little is known about the behavior for shock initiation of high explosives (HE) at a microscopic level despite the extensive work that has been carried out at Los Alamos National Laboratory and other research

institutions. A shock wave produces a high pressure and temperature front that dominantly perturbs the phonon modes (translational and librational motions of the molecules). A portion of the energy induced in the phonon bath by the shock wave must be transferred to higher energy molecular vibrations before decomposition can take place. One view is that the hydrodynamic heating by shock compression is enough to raise the temperature of a homogeneous explosive to the point where thermal decomposition can take place.[345,346] In nonuniform explosives the argument is modified by postulating that thermal decomposition occurs only in local regions (hot spots) and that these sites then initiate detonation.[347,348] Another view is that the shock forces result in bond breakage by multiphonon energy transfer to selected molecular vibrations.[349,350] The distinction here is whether or not the shock wave results in rapid thermalization of the energy among all the vibrational states as opposed to a nonequilibrium situation in which certain modes are selectively excited. In the event of selective mode excitation, the energy deposited in particular molecular vibrations may undergo vibrational-vibrational (V-V) energy transfer to other molecular modes to build up sufficient energy in the bonds that are initially broken. To understand better the transfer of energy from the phonon bath to molecular vibration and V-V energy transfer, a vibrational spectroscopic study of HEs has been initiated.

The principal goals are to characterize the molecular vibrations in HEs under ambient conditions and to monitor the vibrational spectra under extreme pressure and temperature conditions that simulate the shock wave. We hope to be able to differentiate between equilibrium versus nonequilibrium excitation by determining whether or not particular molecular vibrations are strongly coupled to the phonon bath. If only certain modes are coupled to the phonon bath, it is likely that they can act as receiver modes in a multiphonon energy transfer process. The identity of such receiver modes will then help clarify which bonds are initially broken. Studies of both sensitive and insensitive HEs may also help clarify what makes systems such as triaminotrinitro benzene (TATB) insensitive.

The first step in a vibrational spectroscopic study of HEs is to characterize the molecular vibrations in terms of the internal coordinates (bond stretching and angle deformation). Essentially, the eigenvectors of the fundamental modes of vibration will be evaluated using normal mode analysis where the observed frequencies of vibration and isotopic frequency shifts are used to fit the quadratic potential constants. Accordingly, ir and Raman spectra of normal and isotopically substituted samples of pentaerythritol tetranitrate (PETN) and TATB are being obtained. TATB is well suited for such a detailed vibrational analysis because the molecule is constrained to a high symmetry arrangement (D_{3h}) in the solid state.[351] Raman spectra of TATB labeled with ^{15}N in both the nitro and amino groups, as well as deuterated samples, have been observed. The results show extensive mixing of N-O stretching modes with NH_2 deformations, as well as large spectral changes upon deuteration. Several partially deuterated samples have been studied and their spectra (Fig. 71) give evidence for H-D scrambling in the solid, as no discrete modes involving either hydrogen or deuterium motion are found. Surprisingly, the incorporation of small amounts of deuterium in an otherwise hydrogenated sample, and vice versa, results in completely new modes in the 1000-1600 cm^{-1} region where $-NH_2$ deformation and N-O stretch are expected. These results support the notion that $-HN_2$ and N-O motions are strongly mixed and point to the importance of intermolecular interactions in determining the makeup and energy of molecular modes in the 1000-1600 cm^{-1} region. The implication here is that these same modes are strongly coupled to the phonon modes, which are dependent on intermolecular interactions.

C. Raman Spectra of High Explosives Under Extreme Pressure and Temperature Conditions (B. I. Swanson and D. Schiferl)

The motivation for studying vibrational spectra for high explosives (HEs) under extreme pressure and temperature conditions is to simulate the effect that a shock wave would have on the HEs' vibrational modes. One goal is to follow the dependence of the phonon modes (in both frequency and line shape) on pressure and temperature. Equally important, experiments of this type should help identify those molecular vibrations that are responsive to pressure and temperature and, therefore, are strongly coupled to the lower energy phonon modes. A multiphonon energy transfer process, where several quanta of a low-energy phonon mode are transferred to a high-energy internal vibration, requires strong anharmonic coupling between the phonon modes and the high-energy receiving mode. Finally, spectroscopic studies as a function of pressure may help identify structural phase transformations that occur under the extreme conditions of a shock wave.

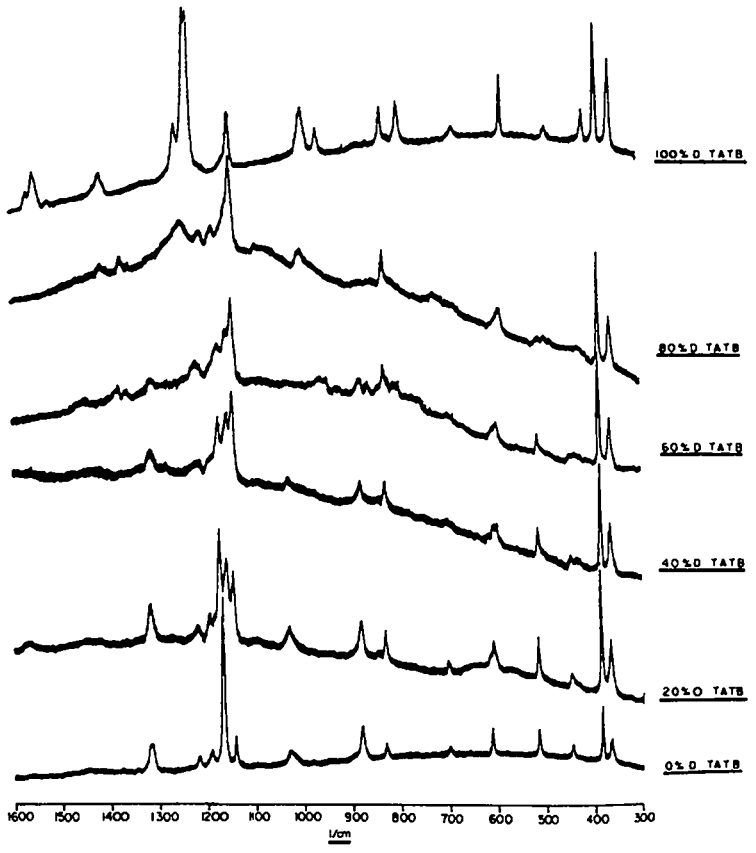

Fig. 71.
Raman spectra of TATB as a function of deuteration.

Typically, the pressures involved in a shock-initiated detonation of HEs are less than 100 kbar. Recent advances in high-pressure technology have made it possible to observe Raman spectra up to 100 kbar.[352,353] The high-pressure diamond anvil cells required for such a study are convenient for laser excitation of the sample and will allow investigation of both the low-energy phonon region and the higher energy molecular modes. Infrared measurements are less useful here because the diamond windows and and the pressurizing mediums are strong ir absorbers, effectively eliminating much of the ir region for study. Nonetheless, it should be possible to carry out ir measurements within the window region of the diamond anvil cells, which include the important N-O stretch region. For the above reasons the work will focus on Raman measurements.

Preliminary Raman measurements of PETN at ~9 kbar have been made. Although the spectral quality was poor by virtue of the low sensitivity of the Cary 82 spectrometer and the absence of signal averaging, we were able to observe several of the lattice and molecular modes. The frequencies of several modes are given in Table XLV. The frequency positions of the phonon modes were all observed to increase substantially with pressure. Surprisingly, several of the higher energy molecular combinations were also observed to shift to higher frequencies with pressure. The results lend support to a multiphonon process involving selected internal modes. The substantial frequency increase observed for the phonon modes is significant in that the efficiency of a multiphonon energy transfer is strongly dependent on the frequency separation of the phonon and receiving modes.

Low-temperature (10 K) Raman spectra have been obtained for several isotopes of TATB and the normal isotopic species of PETN and tetryl. In general, we observe significant sharpening of the modes for all of the samples, resulting in the resolution of a great deal of structure in the phonon region. The frequencies of the phonon modes are observed to increase as temperature is lowered. In the case of TATB, the frequencies of several

TABLE XLV

PRESSURE DEPENDENCE OF SELECTED RAMAN MODES OF PETN

kbar	9 kbar	
41	90	
51	72	
74	92	
96	108	Phonon Modes
	114	
277	290	
871	879	Internal Modes
1291	1297	
2984	2997	
3023	3043	

of the internal modes also exhibit temperature dependence. Surprisingly, the $-^{14}NO_2$, $-^{15}NO_2$ isotopic shifts for three modes known to involve $-NO_2$ motion are observed to change significantly upon cooling, indicating that the mode mixture changing with temperature. These results point to the strong coupling of certain molecular modes to the phonon modes that are most perturbed by temperature.

REFERENCES

1. D. A. Cremers and R. A. Keller, "Thermally Induced Laser Pulsing: A New Technique to Measure Weak Absorptions of Solutions," submitted to Appl. Opt.

2. R. A. Keller and E. F. Zalewski, "Noise Considerations, Signal Magnitudes, and Detection Limits in a Hollow Cathode Discharge by Optogalvanic Spectroscopy," Appl. Opt. 19, 3301 (1980).

3. B. A. Palmer, R. A. Keller, and R. Engleman, Jr., "An Atlas for Uranium Emission Intensities in a Hollow Cathode Discharge," Los Alamos National Laboratory report LA-8251-MS (1980).

4. B. A. Palmer, R. A. Keller, F. V. Kawolski, and J. L. Hall, "Accurate Wave Number Measurements of Uranium Spectral Lines," submitted to J. Opt. Soc.

5. E. F. Zalewski, R. A. Keller, and C. T. Apel, "The Optogalvganic Effect as a Detector for Intracavity Atomic Absorption in a cw Dye Laser," accepted by Appl. Opt. (LA-UR-80-2733).

6. W. W. Berg, P. J. Crutzen, H. E. Grahek, S. N. Gitlin, and W. A. Sedlacek, "First Measurements of Total Chlorine and Bromine in the Lower Stratosphere," Geophys. Res. Lett., in press (1980).

7. A. Mason, G. Hut, and K. Telegadas, "Comparison of Stratospheric Tritium (as HTO) and Zirconium-95 Burdens from the High Yield Chinese Nuclear Tests of June 27, 1973 and November 17, 1976," Environmental Quarterly, USDOE Report EML-371 (April 1980).

8. W. A. Sedlacek, E. J. Mroz, E. S. Gladney, G. H. Heiken, R. Leifer, and R. Chuan, "Physical and Chemical Characteristics of Mt. St. Helens Airborne Debris," Symposium on Mt. St. Helens Eruption: Its Atmospheric Effects and Potential Climatic Impact, Washington, D.C., November 18-19, 1980.

9. *The Microbial Production of Amino Acids*, K. Yamada, S. Kinoshita, T. Isunoda, and K. Aida, Eds. Halsted Press, New York (1972).

10. R. T. Eakin, L. O. Morgan, C. T. Gregg, and N. A. Matwiyoff, FEBS Letters 28, 259 (1972).

11. J. A. Denhollander, T. R. Brown, K. Ugurbil, and R. G. Shulman, Proc. Natl. Acad. Sci., USA 76, 6096 (1979).

12. M. Kainosho, K. Ajisaka, and H. Nakazawa, FEBS Letters 80, 385 (1977).

13. R. Deslauriers, H. C. Jarrell, R. A. Byrd, and I.C.P. Smith, FEBS Letters 118, 185 (1980).

14. A. D. Elbein, Adv. Carbohydr. Chem. Biochem. 30, 227 (1974).

15. R. E. London, J. P. Groff, and R. L. Blakley, Biochem. Biophys. Res. Commun. 86, 779 (1979).

16. R. E. London, V. H. Kollman, and N. A. Matwiyoff, J. Am. Chem. Sec. 97, 3565 (1975).

17. D. Gagnaire, H. Reutenauer, and F. Taravel, Org. Magn. Reson. 12, 679 (1979).

18. E. Bengsch and M. Ptak, in *Stable Isotopes in the Life Sciences*, IAEA Panel Proceedings Series, 1977 (IAEA, Vienna, 1977), pp. 197-206.

19. R. E. London and T. E. Walker, Org. Magn. Reson., in press (1981).

20. J. A. Pople and T. Schaefer, Mol. Phys. 3, 547 (1961).

21. R. E. London, Org. Magn. Reson., in press (1981).

22. R. E. London, J. Magn. Reson. 38, 173 (1980).

23. T. E. Walker, H. P. C. Hogenkamp, T. E. Needham, and N. A. Matwiyoff, J. Chem. Soc., Chem. Commun. 85 (1974).

24. K. A. Krohn, "The Search for a Gamma-Emitting Estrogenic Ligand," J. Nucl. Med. 21, 593-595 (1980).

25. D. S. Wilbur and H. A. O'Brien, Jr., "A-Ring Brominations of Estradiol: An Investigation of the Product Ratios Obtained." Abstract. Third International Symposium on Radiopharmaceutical Chemistry, St. Louis, Missouri, June 1980; J. Labelled Cmpds. Radiopharm., in press (LA-UR-80-652).

26. W. R. Slaunwhite, Jr., and L. Neeley, "Bromination of Phenolic Steroids. I. Substitution of Estrone and 17β-Estradiol in Ring A," J. Org. Chem. 27, 1749-1752 (1962).

27. T. Utne, R. B. Jobson, and F. W. Landgraf, "The Synthesis of 2- and 4-Bromoestradiol," J. Org. Chem. 33, 1654-1656 (1968).

28. R. B. Woodward, "2,4-Dibromo-α-Oestradiol," J. Am. Chem. Soc. 62, 1625-1626 (1940).

29. P. M. Grant, R. E. Whipple, J. W. Barnes, G. E. Bentley, P. M. Wanek, and H. A. O'Brien, Jr., "Radionuclides from Proton Induced Spallation Reactions for Biomedical Applications. III. Bromine-77 Production and Isolation from Molybdenum Targets." Abstract. Joint ACS/CSJ Chemical Congress, April 1979, Honolulu, Hawaii.

30. D. S. Wilbur, G. E. Bentley, and H. A. O'Brien, Jr., "A Rapid Synthesis of A-Ring Bromine-77-Labeled Estrogens with High Specific Activity," J. Labelled Cmpds. Radiopharm., in press (LA-UR-80-3599).

31. F. B. Ballard, W. H. Danforth, S. Naegle, and R. J. Bing, "Myocardial Metabolism of Fatty Acids," J. Clinc. Invest. 39, 717-723 (1960).

32. G. D. Robinson, Jr., "Synthesis of ^{123}I-16-iodo-9-Hexadecenoic Acid and Derivatives for Use as Myocardial Perfusion Imaging Agents," Int. J. Appl. Radiat. Isotopes 28, 149-156 (1977).

33. G. D. Robinson, Jr., and A. W. Lee, "Radioiodinated Fatty Acids for Heart Imaging: Iodine Monochloride Addition Compared with Iodine Replacement Labeling," J. Nucl. Med. 16, 17-21 (1975).

34. H. -J. Machulla, G. Stöcklin, Ch. Kupfernagel, Ch. Freundlieb, A. Höck, K. Vyska, and L. E. Feinendegen, "Comparative Evaluation of Fatty Acids Labeled with C-11, Cl-34m, Br-77, and I-123 for Metabolic Studies of Myocardium," J. Nucl. Med. 19, 298-302 (1978).

35. G. Stöcklin, H. H. Coenen, M. F. Harmand, G. Kloster, R. Weireich, L. E. Feinendegen, K. Vyska, A. Höck, and C. Freundlieb, "15-(p-Bromophenyl-)pentadecanoic Acid: A New Potential Agent for Myocardial Imaging," Abstract. J. Nucl. Med. 21, 58 (1980).

36. D. W. Hart and J. Schwartz, "Hydrozirconation. Organic Synthesis via Organozirconium Intermediates. Synthesis and Rearrangement of Alkylzirconium(IV) Complexes and Their Reaction

with Electrophiles," J. Am. Chem. Soc. 96, 8115-8116 (1974).

37. D. B. Carr and J. Schwartz, "Preparation of Organoaluminum Compounds by Hydrozirconation-Transmetalation," J. Am. Chem. Soc. 101, 3521-3531 (1979).

38. A. I. Meyers and D. L. Temple, Jr., "Synthesis via 2-Oxazolines. II. A Versatile Synthesis of Aliphatic Carboxylic Acids and Esters. Mono- and Dialkylation of Acids Masked by a Simple Protecting Group," J. Am. Chem. Soc. 92, 6644-6646 (1970).

39. W. G. Myers and H. O. Anger, J. Nucl. Med. 3, 183 (1962).

40. B. Christy, G. King, and W. M. Smoak, J. Nucl. Med. 15, 484 (1974).

41. P. Rabin and V. Gregory, Int. J. Appl. Radiat. Isotopes 19, 361-367 (1968).

42. A. A. Sunar and A. E. Mitta, Radiochim. Acta., 12, 119 (1969).

43. U. S. Pharmacopeia XIX (Mack Publishing Co., Easton, Pennsylvania, 1975), p. 467.

44. H. Elias, C. Arnold, and G. Kloss, Int. J. Appl. Radiat. Isotopes 24, 463-469 (1973).

45. M. Tubis, E. Posnick, and R. A. Nordyke, Proc. Soc. Exp. Biol. Med. 103, 497-498 (1960).

46. R. Gillet, M. Gogneau, and G. Mathy, Int. J. Appl. Radiat. Isotopes 27, 61-62 (1976).

47. T. F. Budinger, Y. Yano, and B. Hoop, J. Nucl. Med. 16, 429 (1975).

48. B. Hoop, Jr., R. A. Beh, G. A. Beller, G. L. Brownell, C. A. Burnham, D. J. Hnatowich, et. al., IEEE Trans. Nucl. Sci. NS-23: 584 (1976).

49. H. A. O'Brien, A. E. Ogard, and P. M. Grant, Prog. Nucl. Med. 4, 16 (1978).

50. G. E. Bentley, J. W. Barnes, P. M. Grant, R. E. Whipple, P. M. Wanek, M. A. Ott, T. P. DeBusk, and H. A. O'Brien, Jr., Proc. Joint Amer. Chem. Soc./Chem. Soc. Japan Chem. Cong. (Honolulu, April, 1979), (Abstract).

51. L. Knight, K. A. Krohn, M. J. Welch, B. Spomer, and L. P. Hager, in *Radiopharmaceuticals*, G. Subramanian, B. A. Rhodes, J. F. Cooper and V. J. Sodd, Eds. (Society of Nuclear Medicine, New York, 1975) p. 149.

52. G. Stocklin, Int. J. Appl. Radiat. Isot. 28, 131 (1977).

53. J. A. Spicer, D. F. Preston, R. G. Robinson, D. L. Bradshaw, S. H. Stern, R. D. Dean, N. L. Martin, and B. A. Rhodes, Int. J. Appl. Radiat. Isot. 28, 163 (1977).

54. E. Lebowitz and P. Richards, Semin. Nucl. Med. 4, 257 (1974).

55. R. M. Lambrecht, E. Norton, A. P. Wolf, and S. Treves, J. Labelled Compds. Radiopharm. 13, 245 (1977).

56. H. A. O'Brien, A. E. Ogard, and P. M. Grant, Prog. Nucl. Med 4, 16 (1978).

57. P. M. Grant, R. E. Whipple, J. W. Barnes, G. E. Bentley, P. M. Wanger, and H. A. O'Brien, Abstr. Pap. Am. Chem. Soc. 177, NUCL-31 (1979).

58. G. A. Cowan, E. A. Bryant, W. R. Daniels, and W. J. Maeck, "Some United States Studies of the Oklo Phenomenon," in *The Oklo Phenomenon* (International Atomic Energy Agency, Vienna, 1975), pp. 341-354.

59. W. J. Maeck, F. W. Spraktes, R. L. Tromp, and J. H. Keller, "Analytical Results, Recommended Nuclear Constants, and Suggested Correlations for the Evaluation of Oklo Fission Produced Data," (International Atomic Energy Agency, Vienna, 1975), pp. 319-340.

60. R. P. Walton, Jr., and G. A. Cowan, "Relevance of Nuclide Migration at Oklo to the Problem of Geologic Storage of Radioactive Waste," (International Atomic Energy Agency, Vienna, 1975), pp. 499-506.

61. A. J. Gancarz, "U-Pb Age (2.05×10^9 years) of the Oklo Uranium Deposit," in *Natural Fission Reactors* (International Atomic Energy Agency, Vienna, 1978), pp. 513-519.

62. W. J. Maeck, J. E. Delmore, R. L. Eggleston, and F. W. Spraktes, "The Measurement of Ruthenium in Uranium Ores and ^{238}U Spontaneous Fission Yields," (International Atomic Energy Agency, Vienna, 1978), pp. 535-540.

63. G. A. Cowan, "Migration Paths for Oklo Reactor Products and Applications to the Problem of Geological Storage of Nuclear Wastes," (International Atomic Energy Agency, Vienna, 1978), pp. 693-699.

64. A. J. Gancarz, G. A. Cowan, D. B. Curtis, and W. J. Maeck, "^{99}Tc, Pb, and Ru Migration Around the Oklo Natural Fission Reactors," in *Scientific Basis for Nuclear Waste Management, Vol. 2,* C. J. M. Northrup, Jr., Ed., (Plenum Publishing Corp., New York, 1980), pp. 601-608.

65. D. B. Curtis, and A. J. Gancarz, "An Interim Report on studies of Uranium, Thorium, and Lead Migration of Key Lake, Saskatchewan, Canada," Los Alamos National Laboratory report LA-8440-MS (July 1980).

66. P. P. Raemaekers and C. E. Dunn, "Geology and Geochemistry of the Eastern Margin of the Athabasca Basin," in *Uranium in Saskatchewan,* C. C. Dunn, Ed., Spec. Pub. Sask. Geol. Soc. 3, 297-322 (1977).

67. A. J. Gancarz, "Chronology of the Cluff Lake Uranium Deposit, Saskatchewan, Canada," in *International Uranium Symposium on the Pine Creek Geosyncline.*

68. J. Hoeve and T. I. Sibbald, "On the Genesis of Rabbit Lake and Other Unconformity-Type Uranium Deposits in Northern Saskatchewan, Canada," *Econ. Geol. 73,* 1450-1473 (1978).

69. P. L. Money, "The Wollaston Fold-Belt System, Saskatchewan-Manitoba," Can. J. of Earth Sci. 5, 1489-1504 (1968).

70. G. L. Cummings and B. P. Scott, "Rb/Sr Dating of Rocks from the Wollaston Lake Belt, Saskatchewan," Can. J. Earth Sci. 13, 355-364 (1976).

71. F. J. Dahlkamp, "Geology Appraisal of the Key lake U-Ni Deposits, Northern Saskatchewan," Econ. Geol. 73, 1430-1449 (1978).

72. D. C. Hoffman, R. Stone, and W. W. Dudley, Jr., "Radioactivity in the Underground Environment of the Cambric Nuclear Explosion at the Nevada Test Site," Los Alamos National Laboratory report LA-6877-MS (July 1977).

73. D. C. Hoffman, "A Field Study in Radionuclide Migration," in *Radioactive Waste in Geologic Storage,* S. Fried, Ed., ACS Symposium Series 100 (Am. Chem. Soc., Washington, D.C., 1979), p. 149.

74. J.-P. Sauty, "An Analysis of Hydrodispersive Transfer in Aquifers," Water Resources Research 16, 145 (1980).

75. C. S. Ross and R. L. Smith, "Ash-Flow Tuffs: Their Origin, Geologic Relations, and Identification," U. S. Geol. Soc. Prof. Paper 366 (1961).

76. G. H. Heiken and M. L. Bevier, "Petrology of Tuff Units from the J-13 Drill Site, Jackass Flats, Nevada," Los Alamos National Laboratory report LA-7563-MS (February 1979).

77. M. L. Sykes, G. H. Heiken, and J. R. Smyth, "Mineralogy and Petrology of Tuff Units from the UE25A-1 Drill Site, Yucca Mountain, Nevada," Los Alamos National Laboratory report LA-8139-MS (November 1979).

78. B. R. Erdal, R. D. Aguilar, B. P. Bayhurst, P. Q. Oliver, and K. Wolfsberg, "Sorption-Desorption Studies on Argillite," Los Alamos National Laboratory report LA-7455-MS (March 1979).

79. B. R. Erdal, R. D. Aguilar, B. P. Bayhurst, W. R. Daniels, C. J. Duffy, F. O. Lawrence, S. Maestas, P. Q. Oliver, and K. Wolfsberg, "Sorption-Desorption Studies on Granite," Los Alamos

National Laboratory report LA-7456-MS (February 1979).

80. K. Wolfsberg, B. P. Bayhurst, B. M. Crowe, W. R. Daniels, B. R. Erdal, F. O. Lawrence, A. E. Norris, and J. R. Smyth, "Sorption-Desorption Studies on Tuff. I. Initial Studies with Samples from the J-13 Drill Site, Jackass Flats, Nevada," Los Alamos National Laboratory report LA-7480-MS (April 1979).

81. E. N. Vine, B. P. Bayhurst, W. R. Daniels, S. J. DeVilliers, B. R. Erdal, F. O. Lawrence, S. Maestas, P. Q. Oliver, J. L. Thompson, and K. Wolfsberg, "Sorption-Desorption Studies on Tuff. II. A Continuation of Studies with Samples from Jackass Flats, Nevada and Initial Studies with Samples from Yucca Mountain, Nevada," Los Alamos National Laboratory report LA-8110-MS (January 1980).

82. J. Grisham, "T-2 Calculated Source Term for H. B. Robinson-2 Fuel Element B05-E-14," Los Alamos National Laboratory office memorandum, September 15, 1978.

83. C. F. Baes, Jr., and R. E. Mesmer, *The Hydrolysis of Cations*, (John Wiley & Sons, Inc., New York, 1976).

84. T. W. Newton, R. D. Aguilar, and B. R. Erdal, "Estimation of U, Np, and Pu Solubilities vs Eh and pH," in "Laboratory Studies of Radionuclide Distribution Between Selected Groundwater and Geologic Media," B. R. Erdal, Ed., Los Alamos National Laboratory report LA-8339-PR (May 1980).

85. Y. B. Katayama, D. J. Bradley, and C. O. Harvey, "Status Report on LWR Spent Fuel IAEA Leach Tests," Pacific Northwest Laboratory report PNL-3173 (1980).

86. B. R. Erdal, Ed., "Laboratory Studies of Radionuclide Distributions Between Selected Groundwaters and Geologic Media, October 1—December 31, 1979," Los Alamos National Laboratory report LA-8210-PR (March 1980).

87. B. R. Erdal, Ed., "Laboratory Studies of Radionuclide Distributions Between Selected Groundwaters and Geologic Media, January 1—March 31, 1980," Los Alamos National Laboratory report LA-8339-PR (May 1980).

88. B. R. Erdal, Ed., "Laboratory Studies of Radionuclide Distributions Between Selected Groundwaters and Geologic Media, April 1—June 30, 1980," Los Alamos National Laboratory report LA-8472-PR (September 1980).

89. W. R. Daniels, Ed., "Laboratory Studies of Radionuclide Distributions Between Selected Groundwaters and Geologic Media, Annual Report, October 1, 1979—September 30, 1980," Los Alamos National Laboratory report LA-8586-PR (January 1981).

90. B. Allard, H. Kipatsi, and J. O. Liljenzin, "Expected Species of Uranium, Neptunium, and Plutonium in Neutral Aqueous Solutions," J. Inorg. Nucl. Chem. 42, 1015 (1980).

91. J. Fuger and F. L. Oetting, *The Chemical Thermodynamics of Actinide Elements and Compounds. Part 2. The Actinide Aqueous Ions* (IAEA, Vienna, 1976).

92. T. M. Ottaway, "Oxidation Reduction Indicators of $E_0' < 0.76$ Volt," in *Indicators*, E. Bishop, Ed., (Pergamon Press, Oxford, 1972), p. 469.

93. F. A. H. Schreinemakers, "In-, Mono-, and Divariant Equilibria," Proc. of Koninklijke Akademie van Wetenschappen Te Amsterdam, reprinted by the Pennsylvania State University, University Park, Pennsylvania, p. 325.

94. D. Korzhinskii, *Physiochemical Basis of the Analysis of the Paragenesis of Minerals*, (Consultants Bureau, Inc., New York, 1959), p. 142.

95. E-an Zen, "Construction of Pressure Temperature Diagrams for Multicomponent Systems after the Method of Schreinemakers—A Geometrical Approach," USGS Bull. 1225, (1966), p. 56.

96. E-an Zen, "Prehnite- and Pumpellyite-Bearing Mineral Assemblages, West Side of the Appalachian Metamorphic Belt, Pennsylvania to Newfoundland," J. Pet. 15, 197-242 (1974).

97. R. O. Fournier, "The Solubility of Amorphous Silica at High Temperatures and High Pressures," Proc. Conf. Scale Manage. Geotherm. Energy Dev., (San Diego, California, August 2-4, 1976), p. 20.

98. G. W. Morey, R. O. Fournier, and J. J. Rowe, "The Solubility of Quartz in Water in the Temperature Interval from 25° to 300°C," Geochim. Cosmochim. Acta 26, 1029 (1962).

99. J. A. Van Lier, P. L. de Bruyn, and J. Th. G. Overbeek, "The Solubility of Quartz," J. Phys. Chem. 64, 1675 (1960).

100. R. K. Iler, *The Chemistry of Silica* (John Wiley & Sons, Inc., New York, 1979), p. 30.

101. R. A. Robie, B. S. Hemmingway, and J. R. Fisher, "Thermodynamic Properties of Minerals and Related Substances at 298.15K and 1 Bar (10 Pascals) Pressure and at Higher Temperatures," USGS Bull. 1452, 456 (1979).

102. R. W. Charles, "Amphiboles on the Join Pargasite-Ferropargasite," Am. Mineral. 65, 996-1001 (1980).

103. B. B. McInteer, "Isotope Separation by Distillation: Design of a Carbon-13 Plant," Sep. Sci. Technol. 15, 491 (1980).

104. T. E. Madley, J. T. Yates, and R. C. Stern, J. Chem. Phys. 42, 1372 (1965); R. P. H. Gasser, P. M. Gowan, and D. G. Newman, Surf. Sci., 11, 317 (1968).

105. E. R. S. Winter, J. Chem. Soc., 5781 (1964).

106. Yi-De Hsieh, Ph.D. Thesis, University of Akron (1977) and references therein.

107. D. L. Murdock and G. A. Atwood, Ind. Eng. Chem., Process Des. and Dev. 13, 254 (1974).

108. M. Uchida and A. T. Bell, J. Catal. 60, 204 (1979).

109. D. T. Clay and S. Lynn, AIChE J. 21, 466 (1975); D. B. Hibbert and A. C. C. Tseung, J. Chem. Soc. 1981 (1978); J. Happel, M. A. Hnatow, L. Bajars, and M. Kundrath, Ind. Eng. Chem., Prod. Res. Dev. 14, 264 (1975); J. G. I. Bazes, L. S. Caretto, and K. Nobe, Ind. Eng. Chem., Prod. Res. Dev. 14, 264 (1975).

110. J. J. Helstron and G. A. Atwood, Ind. Eng. Chem., Process des. and Dev. 17, 114 (1978); N. G. Vilesov, A. D. Biba, V. M. Rasputko, V. J. Skripko, and N. N. Ljevchik, Khim. Tekh. 3, 3 (1976).

111. D. C. Moody and R. R. Ryan, J. Chem. Soc., Chem. Commun. 503 (1976); D. C. Moody and R. R. Ryan, Inorg. Chem. 16, 2473 (1977).

112. J. Valentine, D. Valentine, Jr., and J. P. Collman, Inorg. Chem. 10, 219 (1971).

113. R. D. Wilson and J. A. Ibers, Inorg. Chem. 17, 2134 (1978).

114. G. J. Kubas, Inorg. Chem. 18, 182 (1979).

115. P. G. Eller and G. J. Kubas, J. Am. Chem. Soc. 99, 4346 (1977); P. G. Eller, G. J. Kubas, and R. R. Ryan, Inorg. Chem. 16, 2454 (1977).

116. L. Pauling, 3rd Ed. (Cornell University Press, Ithaca, New York, 1960).

117. D. M. P. Mingos, Trans. Met. Chem. 3, 1 (1978).

118. R. R. Ryan, G. J. Kubas, D. C. Moody, and P. G. Eller, "Structure and Bonding," submitted for publication.

119. D. C. Moody and R. R. Ryan, Cryst. Struct. Commun. 5, 145 (1976).

120. G. J. Kubas, J. Chem. Soc., Chem. Commun. 61 (1980).

121. T. Yoshida, T. Matsuda, T. Okano, T. Kitani, and S. Otsuka, J. Am. Chem. Soc. 101, 2027 (1979).

122. D. C. Moody and R. R. Ryan, Inorg. Chem. 16, 2473 (1977).

123. G. J. Kubas, R. R. Ryan, and V. McCarty, Inorg. Chem. 19, 3003 (1980).

124. R. R. Ryan, G. J. Kubas, D. C. Moody, and P. G. Eller, "Structure and Bonding," in press (1981).

125. D. A. Johnson and V. C. Dew, Low-temperature photolysis of a Ru-η^1-SO_2 complex has been observed to produce an η^2-SO_2 form: Inorg. Chem. 18, 3273 (1979).

126. The ^{31}P NMR spectra were obtained from samples sent to the Colorado State University Regional NMR Center, funded by National Science Foundation Grant No. CHE 78-18581. The ^{17}O NMR studies were carried out in collaboration with Dr. Lee J. Todd of Indiana University.

127. P. G. Eller, J. R. Peterson, D. D. Ensor, and A. C. Larson, Inorg. Chim. Acta., 37, 129 (1979).

128. G. W. Halstead, P. G. Eller, L. B. Asprey, and K. V. Salazar, Inorg. Chem. 17, 2967 (1978).

129. G. W. Halstead and P. G. Eller, Inorg. Synth., accepted for publication (1980).

130. G. W. Halstead, P. G. Eller, and M. P. Eastman, Inorg. Chem. 18, 2867 (1979).

131. M. P. Eastman, P. G. Eller, and G. W. Halstead, J. Inorg. Nucl. Chem., submitted.

132. H. Gilman, et al., J. Am. Chem. Soc. 78, 4287, 4289, 6027, 6030 (1956).

133. D. C. Bradley, R. C. Mehratra, and D. P. Gaur, *Metal Alkoxides*, (Academic Press, New York, 1978) and references contained therein.

134. P. G. Eller and P. J. Vergamini, Inorg. Chem., in press (1980), (LA-UR-80-1808).

135. G. W. Halstead, P. G. Eller, L. B. Asprey, and K. V. Salazar, Inorg. Chem. 17, 2967 (1978).

136. G. W. Halstead and P. G. Eller, Inorg. Synth., in press (1980), (LA-UR-80-85).

137. P. G. Eller, to be published.

138. P. C. Wailes, H. Weigold, and A. P. Bell, J. Organomet. Chem. 33, 181 (1971); J. Organomet. Chem. 34, 155 (1972).

139. L. D. McIsaac, J. D. Baker, J. F. Krupa, R. E. LaPointe, D. H. Meikrantz, and N. C. Schroeder, "Study of Bidentate Compounds for Separation of Actinides from Commercial LWR Reprocessing Waste," Idaho Falls National Engineering Laboratory report ICP-1180 (1979).

140. S. M. Bowen, R. T. Paine, C. F. Campana, P. G. Eller, and N. C. Schroeder, Inorg, Chem., submitted. (LA-UR-81-0031).

141. AB Teleplan, "Handling of Spent Nuclear Fuel and Final Storage of Vitrified High Level Reprocessing Waste," Solna, Sweden, 1978/Ultraoffset AB Solna.

142. C. K. Jorgensen and R. A. Penneman, in *Heavy Element Properties, 1975* (North-Holland Publishing Co., Amsterdam, 1976) pp. 117-121.

143. W. H. Zachariasen, "Bond Lengths in Oxygen and Halogen Compounds of the d- and f-Elements," J. Less-Common Met. 62, 1-7 (1978).

144. R. A. Penneman, R. G. Haire, and M. H. Lloyd, "Polymolybdates as Plutonium(IV) Hosts," ACS Symp. Ser. 117, *Actinide Separations*, (American Chemical Society, Washington, D.C., 1980) Chap. 39, pp. 571-581.

145. A. S. Saprykin, V. I. Spitsyn, M. M. Orlova, O. P. Zhuravleva, and N. N. Krot, Radiokhimiya 2, 247-252 (1978).

146. A. S. Saprykin, V. I. Spitsyn, and N. N. Krot, "Determination of the Formal Potentials of Pu(IV)-Pu(III) and Am(IV)-Am(II) Couples in Presence of $P_2W_{17}O_{61}^{10-}$ Ions," Dokl. Akad. Nauk SSSR 228, 649-651 (1976).

147. V. N. Kosyakov, G. A. Timofeev, E. A. Erin, V. I. Andreev, V. V. Kopytov, and G. A. Simakin, "Production and Stability of Americium(IV), Curium(IV), and Californium(IV) in Solutions of Potassium Phosphotungstate," Radiokhimiya 19, 511-517 (1977).

148. M. H. Lloyd, "Solution Instabilities and Solids Formation," LWR Reprocessing Solutions," Trans. Am. Nuclear Soc. 24, (1957).

149. M. H. Lloyd, "Chemical Behavior of Plutonium in LWR Fuel Cycle Reprocessing Solutions," Conference: Plutonium Fuel Cycle Process, ANS National Topical Meeting, Miami, Florida, May 1977.

150. "Polymolybdates as Plutonium(IV) Hosts," R. A. Penneman, R. G. Haire, and M. H. Lloyd, in *Actinide Separations*, ACS Symposium Series 117, J. D. Navratil and W. W. Schultz, Eds. (ACS, Washington, D.C., 1980), Chap. 39, pp. 571-581.

151. P. G. Eller, T. C. Cremers, R. A. Penneman, and C. Herrick, to be published.

152. L. M. Kovba and V. K. Trunor Radiokhim (Engl. Transl.) 7, 314 (1965).

153. K. V. Skrostsova and G. A. Sidorenko, Zop. Uses. Mineralog. Obsh., 94, 548 (1965).

154. V. N. Serezkin, L. M. Kovba, and V. K. Truner, Radiokhim. (Engl. Transl.) 16, 231 (1972).

155. B. O. Loopstra, "Neutron Diffraction Investigation of U_3O_8," Acta Cryst. 17, 651 (1964).

156. B. O. Loopstra, "The Structure of β-U_3O_8," Acta Cryst. B26, 656 (1970).

157. J. C. Levet, M. Patel, J. Y. LeMerouille, "Structure Cristalline de UO_2Br," Acta Cryst. B33, 2542 (1977).

158. R. Chevalier and M. Gasperin, "Structure Cristalline de UVO_5," Bull. Soc. Fr. Minéral. Cristallogr. 93, 18 (1970).

159. W. H. Zachariasen and R. A. Penneman, "Application of Bond Length-Strength Analysis to 5f Element Flourides," J. Less-Common Met. 69, 369-377 (1980).

160. W. H. Zachariasen, "Bond Lengths in Oxygen and Halogen Compounds of the d- and f-Elements," J. Less-Common Met. 62, 1-7 (1978).

161. D. Cohen, "The Preparation and Spectrum of Uranium(V) Ions in Aqueous Solutions," J. Inorg. Nucl. Chem. 32, 3525 (1970).

162. J. C. Levet, "Preparation d'un nouvel oxyhalogenine d'uranium pentavalent UO_2Cl," C. R. Acad. Sci. Paris 268, 703 (1969); J. C. Levet, "Sur un nouvel oxybromine d'uranium pentavalent," C. R. Acad. Sci. Paris 268 4775 (1965).

163. J. C. Levet, M. Potel, and J. V. Merouille, "Structure Cristalline de UO_2Br," Acta Cryst. B33, 2542 (1977).

164. G. W. Halstead, P. G. Eller, and M. P. Eastman, "Nonaqueous Chemistry of Uranium Pentafluoride," Inorg. Chem. 18, 2867 (1979).

165. K. Tatsumi and R. Hoffmann, "Bent Cis d^0 MoO_2^{2+} vs. linear d^0f^0 UO_2^{2+}: A Significant Role for Nonvalence 6p Orbitals in Uranyl," Inorg. Chem. 19, 2656 (1980).

166. D. T. Meshri and W. B. White, Technical Data, Ozark-Mahoning-Pennwalt Co., Tulsa, Oklahoma.

167. W. R. Hasek, W. C. Smith, and V. A. Engelhardt, J. Am. Chem. Soc. 82, 543 (1960).

168. G. A. Olah and J. Welch, J. Am. Chem. Soc. 100, 5396 (1978).

169. B. B. McInteer, Sep. Sci. Technol. 15, 491-508 (1980).

170. D. Rittenburg, A. S. Keston, F. Rosebury, and R. Schoenheimer, J. Biol. Chem. 127, 291 (1939).

171. A. E. Redpath, M. Menzinger, and T. Carrington, "Molecular Beam Chemiluminescence xI: Kinetic and Internal Energy Dependence of the $NO+O_3 \rightarrow NO_{23}^* \rightarrow NO_2$ Reaction," Chem. Phys. 27, 409 (1978); D. Van den Ende and S. Stolte, "Influence

of Translational and Internal Energy upon the Chemiluminescent Part of the Exothermic Reaction $NO+O_3 \rightarrow NO_2^* \rightarrow NO_2 + h\nu + O_2$," Chem. Phys. 45, 55 (1980).

172. F. C. Fehsenfeld, "Diagnostics of the Flowing Afterglow," Int. J. Mass Spectrom. Ion Phys. 16, 151 (1975).

173. E. E. Ferguson, F. C. Fehsenfeld, and A. L. Schmeltekopf, "Flowing Aftergow Measurements of Ion-Neutral Reactions," Adv. At. Mol. Phys. 5, 1 (1969).

174. R. W. Huggins and J. H. Cahn, "Metastable Measurements in Flowing Helium Afterglow," J. Appl. Phys. 38, 180 (1967).

175. R. C. Bolden, R. S. Hemsworth, M. J. Shaw, and N. D. Twiddy, "Measurements of Thermal Energy Ion-Neutral Reaction Rate Coefficients for Rare-Gas Ions," J. Phys. B. 3, 45 (1970).

176. D. K. Bohme, R. S. Hemsworth, H. W. Rundle, and H. I. Schiff, "Determination of Proton Affinity from the Kinetics of Proton Transfer Reactions. II. Kinetic Analysis of the Approach to the Attainment of Equilibrium," J. Chem. Phys. 58, 3504 (1973).

177. G. E. Streit and T. W. Newton, "The Effects of Chemical Reaction on Diffusive Ion Loss Processes in a Flowing Afterglow," Int. J. Mass Spectrom. Ion Phys., in press (LA-UR-80-1809).

178. H. J. Oskam, "Microwave Investigation of Disintegrating Gaseous Discharge Plasmas," Philips Res. Rep. 13, 335 (1958).

179. G. E. Streit and T. W. Newton, "Negative Ion-Uranium Hexafluoride Charge Transfer Reactions," J. Chem. Phys. 73, 3178 (1980).

180. J. L. Beauchamp, "Properties and Reactions of Uranium Hexafluoride by Ion Cyclotron Resonance Spectrosocpy," J. Chem. Phys. 64, 718 (1976).

181. J. A. D. Stockdale, R. N. Compton, and H. C. Schweinler, "Negative Ion Formation in Selected Hexafluoride Molecules," J. Chem. Phys. 53, 1502 (1970).

182. L. M. Babcock and G. E. Streit, "Ion-Molecule Reactions of SF_6: Determination of $IP(SF_5^+)$, $AP(SF_5^+/SF_6)$ and $D(SF_5\text{-}F)$," J. Chem. Phys. (in press) (LA-UR-80-3399).

183. J. F. Bott and T. A. Jacobs, "Shock-Tube Studies of Sulfur Hexafluoride," J. Chem. Phys. 50, 3850 (1969).

184. D. L. Hildenbrand, "Mass Spectrometric Studies of Some Gaseous Sulfur Flourides," J. Phys. Chem. 77, 897 (1973).

185. T. Kiang, R. C. Estler, and R. N. Zare, "Upper and Lower Bounds on the $F_5S\text{-}F$ Bond Energy," J. Chem. Phys. 70, 5925 (1979).

186. J. L. Lyman, "A Model for Unimolecular Reaction of Sulfur Hexafluoride," J. Chem. Phys. 67, 1868 (1977).

187. J. J.Valentini, P. Esherick, and A. Owyoung, "Use of a Free-Expansion Jet in Ultra-High-Resolution Inverse Raman Spectroscopy," Chem. Phys. Lett., 75, 590 (1980).

188. G. M. McClelland, K. L. Saenger, J. J. Valentini, and D. R. Herschbach, "Vibrational and Rotational Relaxation of Iodine in Seeded Supersonic Beams," J. Phys. Chem., 83, 947 (1979).

189. W. H. J. Childs, "Perturbations and Rotation Constants of Some First Negative Nitrogen Bands," Proc. Roy. Soc., A 137, 641 (1932).

190. G. Davidson and R. O'Neil, "Optical Radiation from Nitrogen and Air at High Pressure Excited by Energetic Electrons," J. Chem. Phys. 41, 3946 (1964).

191. J. E. Solomon and D. M. Silva, "Detection of N_2^+ Produced by Ionizing Radiation in the Atmosphere (Preliminary Results)," NUC TN 1497, 1975.

192. R. Engleman, Jr. and R. A. Keller, "Optogalvanic Double-Resonance Spectroscopy: Experimental Observations," Opt. Lett. 5, 465 (1980).

193. K. A. Truesdell, R. A. Keller, and E. F. Zalewski, "Locking of cw Dye Laser Emission onto the Wavelength of Molecular Fluorescence by Intracavity Gain: Example I_2," J. Chem. Phys. 73, 1117 (1980).

194. W. M. Trott, N. C. Blais, and E. A. Walters, "Molecular Beam Photoionization Study of Acetone and Acetone-d_6," J. Chem. Phys. 69, 3150 (1978).

195. W. M. Trott, N. C. Blais, and E. A. Walters, "Photoionization of Carbon Disulfide Monomers and Dimers in a Supersonic Molecular Beam," J. Chem. Phys. 71, 1692 (1979).

196. Y. Ono, S. H. Linn, H. F. Prest, M. E. Gress, and C. Y. Ng, "Molecular Beam Photoionization Study of Carbon Disulfide, Carbon Disulfide Dimer, and Clusters," J. Chem. Phys. 73, 2523 (1980).

197. S. L. Anderson, T. Hiroka, P. W. Tiedeman, B. H. Mahan, and Y. T. Lee, "Photoionization of $(H_2)_2$ and Clusters of O_2 Molecules," J. Chem. Phys. 73, 4779 (1980).

198. F. Khoury and D. B. Robinson, "Second Virial Coefficients and Intermolecular Force Constants of the Ethane-Hydrogen Sulfide System," J. Chem. Phys. 55, 834 (1971).

199. P. Seal and P. K. Bandyopadhyay, "Contributions of Non-Spherical Interactions to the Second Virial Coefficient of Ethane and Hydrogen Sulfide Gases," Indian J. Phys. 48, 684 (1974).

200. L. H. Jones, J. Mol. Spectrosc. 74, 409 (1979).

201. B. J. Krohn and L. H. Jones, J. Mol. Spectrosc., in press.

202. A. J. Barnes, H. E. Hallam, J. D. R. Howells, and G. F. Schrimshaw, J. Chem. Soc., Faraday II, 69, 738 (1973).

203. L. Abouaf-Marguin and B. Gauthier-Roy, Chemical Physics 51, 213 (1980).

204. L. H. Jones, B. I. Swanson, and S. A. Ekberg, Chem. Phys. Lett. 68, 499 (1979).

205. B. I. Swanson and L. H. Jones, J. Chem. Phys. 73, 986 (1980).

206. B. I. Swanson and L. H. Jones, "Matrix-Molecule Interactions, Dynamics, and Exchange Phenomena in Low Temperature Matrices: SF_6 in Argon and Krypton," J. Chem. Phys. in press (1981). (LA-UR80-2511).

207. B. I. Swanson and L. H. Jones, "On the Observation and Origin of Kinetic Isotope Effects in Exchange Dephasing: Motional Collapse of Vibrational Structure for SF_6 Isolated in a Xenon Matrix," Chem. Phys. Lett. in press (1981). (LA-UR80-1627).

208. L. H. Jones, B. I. Swanson, and S. A. Ekberg, Chem. Phys. Lett. 74, 330 (1980).

209. L. H. Jones and B. I. Swanson, "High Resolution Studies of Dynamics in Low Temperature Matrices: Vibrational Dephasing for SeF_6 in Noble Gas Solids," J. Chem. Phys., in press (1981). (LA-UR80-2846).

210. P. S. McDowell, J. P. Aldridge, and R. F. Holland, J. Phys. Chem. 80, 1203 (1976).

211. S. Abramowitz and I. W. Levin, Inorg. Chem. 6, 538 (1967).

212. H. E. Hallam, *Vibrational Spectroscopy of Trapped Species* (John Wiley and Sons, Inc., New York, 1973).

213. R. M. Golding in *Physical Chemistry, an Advanced Treatise*, Vol. IV, D. Henderson, Ed. (Academic Press Inc., New York, 1970), Chap., 9. p. 440.

214. R. M. Shelby, C. B. Harris, and P. A. Cornelius, J. Chem. Phys. 70, 34 (1979); C. B. Harris, R. M. Shelby, and P. A. Cornelius, Chem. Phys. Lett. 57, 8 (1978); Phys. Rev. Lett. 38, 1415 (1977).

215. R. J. Abott and D. W. Oxtoby, J. Chem. Phys. 70, 4203 (1979).

216. R. Kosloff and S. A. Rice, J. Chem. Phys. 72, 4591 (1980).

217. B. M. Powell and G. Dolling in *Rare Gas Solids*, Vol. 2, M. L. Klein and J. A. Venables, Eds. (Academic Press Inc., New York, 1977), p. 969.

218. R. Orbach in *Optical Properties of Ions in Crystals*, H. M. Crosswhite and H. W. Moos, Eds. (John Wiley and Sons, Inc., New York, 1967), p. 445.

219. F. Legay in *Chemical and Biochemical Applications of Lasers*, Vol. 2, C. B. Moore, Ed. (Academic Press Inc., New York, 1977), p. 43.

220. J. L. Lyman, S. D. Rockwood, and S. M. Freund, J. Chem. Phys. 67, 4545 (1977).

221. E. Fermi and E. Teller, Phys. Rev. 72, 399 (1947).

222. H. Schneuwly, V. I. Pokrovsky, and L. I. Ponomarev, Nucl. Phys. A312, 419 (1978).

223. B. Rosenblum, A. H. Nethercot, Jr., and C. H. Townes, Phys. Rev. 109, 400 (1958).

224. S. P. Walch and W. A. Goddard III, Chem. Phys. Lett. 33, 18 (1975).

225. V. R. Akylas and P. Vogel, Computer Phys. Commun. 15, 291 (1978).

226. M. A. Pomerantz and S. P. Duggal, Rev. Geophys. Space Phys. 12, 343 (1974).

227. J. A. Eddy, Science 192, 1189 (1976).

228. R. C. Reedy and J. R. Arnold, J. Geophys. Res. 77, 537 (1972).

229. R. C. Reedy, *Proc. Conf. on the Ancient Sun*, Boulder, Colorado, October 16-19, 1979 (Pergamon Press, Inc., Elmsford, New York, 1980), p. 365.

230. R. C. Finkel, J. R. Arnold, M. Imamura, R. C. Reedy, J. S. Fruchter, H. H. Loosli, J. C. Evans, A. C. Delany, and J. P. Shedlovsky, *Proc. Lunar Sci. Conf. 2nd*, Houston, Texas, January 11-14, 1971 (M.I.T. Press, Cambridge, Massachusetts, 1971), p. 1773.

231. R. C. Reedy, *Proc. Lunar Sci. Conf. 8th*, Houston, Texas, March 14-18, 1977 (Pergamon Press, Inc., Elmsford, New York, 1977), p. 825.

232. C. P. Kohl, M. T. Murrell, G. P. Russ, and J. R. Arnold, *Proc. Lunar Planet. Sci. Conf. 9th*, Houston, Texas, March 13-17, 1978 (Pergamon Press, Inc., Elmsford, New York, 1978), p. 2299.

233. R. S. Boeckl, Earth Planet. Sci. Lett. 16, 269 (1972).

234. E. L. Fireman, *Proc. Lunar Planet. Sci. Conf. 9th*, Houston, Texas, March 13-17, 1978 (Pergamon Press, Inc., Elmsford, New York, 1978), p. 1647.

235. H. P. Hoyt, R. M. Walker, and D. W. Zimmerman, *Proc. Lunar Sci. Conf. 4th*, Houston, Texas, March 5-8, 1973 (Pergamon Press, Inc., Elmsford, 1973), p. 2489.

236. S. Regnier, C. M. Hohenberg, K. Marti, and R. C. Reedy, *Proc. Lunar Planet. Sci. Conf. 10th*, Houston, Texas, March 19-23, 1979 (Pergamon Press, Inc., Elmsford, New York, 1979), p. 1565.

237. C. M. Hohenberg, K. Marti, F. A. Podosek, R. C. Reedy, and J. R. Shirck, *Proc. Lunar Planet. Sci. Conf. 9th*, Houston, Texas, March 13-17, 1978 (Pergamon Press, Inc., Elmsford, New York, 1978), p. 2311.

238. A. Yaniv, K. Marti, and R. C. Reedy, *Lunar Planet Sci. XI*, (Lunar and Planetary Institute, 1980), p. 1291.

239. W. R. Kelly and G. J. Wasserburg, Geophys. Res. Lett. 5, 1079 (1978).

240. T. Kaiser, W. R. Kelly, and G. J. Wasserburg, Geophys. Res. Lett. 7, 271 (1980).

241. W. Augustyniak, M. Herman, A. Marcinkowski, and B. Zwieglinski, Nucl. Phys. A285, 145 (1977).

242. M. Bormann, H. H. Bissem, E. Magiera, and R. Warnemünde, Nucl. Phys. A157, 481 (1970).

243. B. P. Bayhurst, J. S. Gilmore, R. J. Prestwood, J. B. Wilhelmy, N. Jarmie, B. H. Erkkila, and R. A. Hardekopf, Phys. Rev. C. 12, 451 (1975).

244. R. C. Reedy and J. R. Arnold, J. Geophys. Res. 77, 537 (1972).

245. R. Gensho, O. Nitoh, T. Makino, and M. Honda, Phys. Chem. Earth 11, 11 (1979).

246. H. Voshage and H. Feldmann, Earth Planet. Sci. Lett. 45, 293 (1979).

247. L. M. Libby, W. F. Libby, and S. K. Runcorn, Nature 278, 613 (1979).

248. D. C. Hoffman and M. M. Hoffman, Ann. Rev. Nucl. Sci. 24, 151 (1974).

249. T. Lee, Astrophys. J. 224, 217 (1978).

250. *Comets, Asteroids, Meteorites*, A. E. Delsemme, Ed. (Univ. of Toledo Press, Toledo, Ohio, 1977).

251. F. Whipple, in *Cosmic Dust*, J. A. M. McDonnell, Ed. (John Wiley and Sons, Inc., New York, 1978).

252. R. C. Reedy, J. R. Arnold, and J. I. Trombka, J. Geophys. Res. 78, 5847 (1973).

253. I. Adler, J. I. Trombka, P. Lowman, R. Schmadebeck, H. Blodget, E. Eller, et al., The Moon 7, 487 (1973).

254. R. C. Reedy, *Proc. Lunar and Planet. Sci. Conf. 9th*, Houston, Texas, March 13-17, 1978. (Pergamon Press, Inc., Elmsford, New York, 1978), p. 2961.

255. R. E. Lingenfelter, E. H. Canfield, and W. N. Hess, J. Geophys. Res. 66, 2665 (1961).

256. R. Ramaty, B. Kozlovsky, and R. E. Lingenfelter, Astrophys. J. Suppl. 40, 487 (1979).

257. Z. Janout, S. Pospisil, and M. Vobecky, J. Radioanal. Chem. 56, 71 (1980).

258. C. J. Crannell, H. Crannell, and R. Ramaty, Astrophys. J. 229, 762 (1979).

259. D. B. Curtis, E. S. Gladney, and E. T. Jurney, "A Revision of the Meteorite Based Cosmic Abundance of Boron," Geochim. Cosmochim Acta. (1980).

260. H. C. Lord III "Molecular Equilibria and Condensation in a Solar Nebula and Cool Stellar Atmospheres," Icarus 4, 279-288 (1965).

261. J. W. Larimer and E. Anders, "Chemical Fractionation in Meteorites -II. Abundance Patterns and Their Interpretation," Geochim. Cosmochim. Acta 31, 1239-1279 (1967).

262. M. Blander and J. L. Katz, "Condensation of Primordial Dust," Geochim Cosmochim. Acta 31, 1025-1034 (1967).

263. A. Arrhenius and H. Alven, "Fractionation and Condensation in Space," Earth and Planet Sci. Lett. 10, 253-267 (1971).

264. W. A. Fowler, G. R. Burbidge, and E. M. Burbidge, "Nuclear Reactions and Element Synthesis in the Surfaces of Stars," Ast. J. Supp. 17, 11, 167-194 (1955).

265. C. Ryter, H. Reeves, E. Gradsztajn, and J. Audouze, "The Energetics of L-Nuclei Formation in Stellar Atmospheres and its Relevance to X-Ray Astronomy," Astr. Astrophys. 8, 389-397 (1970).

266. H. Reeves and J. P. Meyer, "Cosmic-Ray Nucleosynthesis and the Infall Rate of Extragalactic Matter in the Solar Neighborhood," Astophys. J. 226, 613-631 (1978).

267. E. S. Gladney, E. T. Jurney, and D. B. Curtis "Nondestructive Determination of Boron and Cadmium by Thermal Neutron-Prompt γ-Ray Spectrometry," Anal. Chem. 48, 2139-2142 (1976).

268. C. M. Lederer, V. S. Shirley, E. Browne, J. M. Dairiki, R. E. Doebler, A. A. Shihab-Elden, L. J. Jardine, J. K. Truli, and A. B. Buyrne, *Table of Isotopes*, Seventh Edition (John Wiley and Sons, Inc., New York, 1978).

269. J. E. Ross and L. H. Aller, "The Chemical Composition of the Sun," Science 191, 1223-1220 (1976).

270. O. Engvöld "The Diatomic Molecules BH, BN, and BO in Sunspots on the Solar Abundance of Boron," Solar Physics 11, 183-197 (1970).

271. J. L. Kohl, W. H. Parkinson, and G. L. Withbroe, "The Solar Boron Abundance," Astrophys. J. (Letters) 212, L101-L104 (1977).

272. D. N. B. Hall and O. Engvöld "A Reduced Upper Limit to the Solar Boron Abundance," Astrophys. J. 197, 513-515 (1975)

273. A. A. Mills, "Boron in Carbonaceous Chondrites," Nature 220, 1113-1114 (1968).

274. M. R. Weller, M. Furst, T. A. Tombrello, and D. S. Burnett, "Boron Concentrations in Carbonaceous Chondrites," Geochim. Cosmochim. Acta 42, 999-1010 (1978).

275. H. Reeves, W. A. Fowler, and F. Hoyle, "Galactic Cosmic Ray Origin of Li, Be, and B in Stars," Nature 226, 727-729 (1970).

276. M. Meneguzzi, J. Andouze, and H. Reeves, "The Production of the Elements Li, Be, and B by Galactic Cosmic Rays in Space and its Relation with Stellar Observations," Astron. Atrophys. 15, 337-356 (1971).

277. R. A. Moyle, B. G. Glagola, G. J. Mathews, and V. E. Viola, Jr., "Nucleosynthesis of Li, Be, and B: Contributions from the p + ^{16}O Reaction at 50-90 MeV" Phys. Rev. C 19, 631-640 (1979).

278. C. W. Sill and C. P. Willis, "The Beryllium Content of Some Meteorites," Geochim. Cosmochim. Acta 26, 1209-1214 (1962).

279. W. Nichiporuk and C. B. Moore, "Lithium in Chondritic Meteorites," Earth Plant. Sci. Lett. 9, 280-286 (1970).

280. E. K. Agyei and C. C. McMullen, "Determination of the Isotopic Abundance of Boron in Meteorites and Tektites," *Short Papers of the Fourth International Conference, Geochronology, Cosmochronology, Isotope Geology*, R. Zartman, Ed., Geol. Surv. Open-File Report 78-701 (1978), pp. 3-6.

281. K. J. Eisentraut, D. J. Griest, and R. E. Sievers, "Ultratrace Analysis for Beryllium in Terrestrial, Meteoritic, and Apollo 11 and 12 Lunar Samples Using Electron Capture Gas Chromatography," Anal. Chem.. 43, 2003-2007 (1971).

282. U. Quant and W. Herr, "Beryllium Abundance in Meteorites Determined by Non-Destructive Photon Activation," Earth Plant. Sci. Lett. 24, 53-58 (1974).

283. A. G. W. Cameron, S. A. Colgate, and L. Grossman, "Cosmic Abundance of Boron," Nature 243, 204-207 (1973).

284. F. D. S. Butement and G. B. Briscoe, J. Inorg. Nucl. Chem., 25, 151 (1963).

285. E. K. Hyde and G. D. O'Kelley, Phys. Rev., 82, 944 (1944).

286. W. H. Zoller, W. B. Walters, and C. D. Coryell, Phys. Rev., 185, 1537 (1969).

287. M. Kazumasha, J. Phys. Soc. Japan, 23, 1191 (1967).

288. R. J. Prestwood, D. R. Nethaway, and N. L. Smith, to be published.

289. K. Wolfsberg, "Collected Radiochemical Procedures," Los Alamos National Laboratory report LA-1721, 4th Ed. (1976), p. 73.

290. G. P. Russ III, Earth Planet. Sci. Lett. 19, 275 (1973).

291. A. M. Freeman, J. Milsted, D. Metta, D. Henderson, J. Lerner, A. L. Harkness, and D. J. Rokop, Radiochim. Acta. 5, 192 (1966).

292. G. W. Butler, D. G. Perry, L. P. Remsberg, A. M. Poskanzer, J. B. Natowitz, and F. Plasil, Phys. Rev. Lett. 38, 1380 (1977).

293. A. M. Zebelman, W. G. Meyer, K. Halbach, A. M. Poskanzer, R. G. Sextro, G. Gabor, and D. A. Landis, Nucl. Instrum. Methods 141, 439 (1977).

294. M. M. Fowler and R. C. Jared, Nucl. Instrum. Methods 124, 341 (1975).

295. S. B. Kaufman, E. P. Steinberg, B. D. Wilkins, J. Unik, A. J. Gorski, and M. J. Fluss, Nucl. Instrum. Methods 115, 47 (1974).

296. I. Kelson and G. T. Garvey, Phys. Lett. 23, 689 (1966); J. Jänecke, At. Data Nucl. Data Table 17, 455 (1976); A. H. Wapstra and K. Bos, At. Data Nucl. Data Table 19, 177 (1977).

297. S. B. Kaufman and C. O. Hower, Phys. Rev. 140, B1272 (1965).

298. B. J. Dropesky, G. W. Butler, G. C. Giesler, C. J. Orth, and R. A. Williams, Los Alamos National Laboratory, unpublished data, 1980.

299. T. Ericson, F. Selleri, and R. T. Van de Walle, Nucl. Phys. 36, 353 (1962).

300. J. E. Spencer, in *Proc. Int. Conf. High-Energy Phys. Nucl. Struct, 7th*, Zurich, Switzerland, 29 August-2 September, 1977, M. P. Locher, Ed., (Birkauser Verlag, Basel and Stuttgart, 1977), pp. 153-172.

301. M. Johnson, D. Bowman, and H. Baer, "Workshop on Pion Single Charge Exchange," January 22-24, 1979, Los Alamos National Laboratory report LA-7892-C (July 1979).

302. J. Warzawski, A. Gal, and J. M. Eisenberg, Nucl. Phys. A294, 321 (1978).

303. L. C. Liu, Phys. Rev. C 23, 814 (1981).

304. L. C. Liu and C. M. Shakin, Phys. Rev C 20, 2339 (1979).

305. E. Schwarz, J.-P. Egger, F. Goetz, P. Gretillat, and C. Lunke, Phys. Lett. 43B, 1578 (1979).

306. M. E. Nordberg, K. F. Kinsey, and R. L. Burman, Phys. Rev. 165, 1096 (1968).

307. P. Hoffer, J. Nucl. Med. 21, 282, 394, and 484 (1980).

308. D. J. Hnatowich, Int. J. Appl. Radiat. Isotopes 28, 169 (1977).

309. A. P. Wolf and J. S. Fowler, in *Radiopharmaceuticals II* (Society of Nuclear Medicine, New York, 1979), p. 73.

310. S. Mirzadeh, M. Kahn, P. M. Grant, and H. A. O'Brien, Radiochim. Acta, in press.

311. P. Grant and D. Miller, unpublished data.

312. A. P. Wolf and J. S. Fowler, in *"Radiopharmaceuticals II* (Society of Nuclear Medicine, New York, 1979), p.73.

313. R. J. Daniels, P. M. Grant, and H. A. O'Brien, Int. J. Nucl. Med. Biol. 5, 11 and 207 (1978).

314. K. A. Kraus and F. Nelson, Proc. Int. Conf. Peaceful Uses of At. Energy 1st Geneva, Vol. 7, p. 113.

315. G. H. Morrison and H. Freiser, *Solvent Extraction in Analytical Chemistry* (John Wiley and Sons, Inc., New York, 1957), p. 160.

316. J. Hala, J. Inorg. Nucl. Chem. 29, 187 (1967).

317. I. H. Qureshi, L. T. McClendon, and P. D. LaFleur, *Modern Trends in Activation Analysis*, NBS Spec. Publ. 312, Vol. I, 1969, p. 666.

318. D. M. Chauncey, S. E. Halpern, P. M. Hagan, M. L. McKegney, K. E. Berstein, and H. A. O'Brien, Jr., Proc. Soc. Nucl. Med. 2nd Ann. Western Reg. Mtg., Las Vegas, Nevada, October 21-23, 1977.

319. R. W. Atcher, A. M. Friedman, J. R. Huizenga, G. V. S. Rayudu, E. A. Silverstein, and D. A. Turner, J. Nucl. Med. 19(6): 689 (1978).

320. V. J. Sodd, K. L. Scholz, J. W. Blue, Med. Phys. 1(1): 25 (1974).

321. P. M. Grant, H. A. O'Brien, Jr., B. P. Bayhurst, J. S. Gilmore, R. J. Prestwood, R. E. Whipple, and P. M. Wanek, J. Label. Cmpd. Radiopharm. 16, 212 (1979).

322. T. Ku, P. Richards, L. G. Stang, and T. Prach, Proc. 2nd Int. Symp. Radiopharm., Soc. Nucl. Med., p. 745 (1979).

323. J. J. Pinajian, Oak Ridge National Laboratory report ORNL-TM-1481 (April 1966).

324. J. W. Brady, J. D. Doll, and D. L. Thompson, "Cluster Dynamics: A Classical Trajectory Study of $A + A_n \leftrightarrows A^*_{n+1}$," J. Chem. Phys. 71, 2467 (1979).

325. J. W. Brady, J. D. Doll, and D. L. Thompson, "Cluster Dynamics: Further Classical Trajectory Studies of $A + An \rightarrow A^*_{n+1}$," J. Chem. Phys. 73, 2767 (1980).

326. J. W. Brady, J. D. Doll, and D. L. Thompson, "Cluster Dynamics: A Classical Trajectory Study of $A^*_n \rightarrow A_{n-1} + A$," J. Chem. Phys. 74, 1026 (1981).

327. J. W. Brady, J. D. Doll, and D. L. Thompson, "Classical Trajectory Studies of Homogeneous Nucleation of a Rare Gas," to appear in *Potential Energy Surfaces and Dynamics Calculations*, D. G. Truhlar, Ed. (Plenum Press, New York, 1981).

328. S. B. Woodruff and D. L. Thompson, "A Quasi-Classical Trajectory Study of Vibrational Predissocation of Van der Waals Molecules," J. Chem. Phys. 71, 376-380 (1979).

329. J. A. Panitz, "Deuterium Depth Profiles in Metals using Imaging Field Desorption," J. Vac. Sci. Technol. 14, 502 (1977).

330. J. E. Adams and J. D. Doll, "Dynamics of Ion Channeling at Low Energies: Preliminary Trajectory Studies," J. Chem. Phys. 73, 2137 (1980).

331. J. E. Adams and J. D. Doll, "Dynamics of Ion Channeling at Low Energies: Non-Normal Incidence," J. Chem. Phys., accepted for publication. (LA-UR-80-2706).

332. J. E. Adams and J. D. Doll, "Desorption from Solid Surfaces via Generalized Slater Theory," J. Chem. Phys. 74, 1467 (1981).

333. J. E. Adams and J. D. Doll, "Dynamical Corrections to Transition State Theory Adsorption Rates: Effect of a Precursor State," submitted to Surface Science (LA-UR-80-2081).

334. N. B. Slater, *Theory of Unimolecular Reactions* (Cornell University, Ithaca, 1959).

335. David Chandler, J. Chem. Phys. 68, 2959 (1978).

336. D. L. Bunker and N. C. Blais, "Monte Carlo Calculations. V. Three-Dimensional Study of a General Bimolecular Interaction Potential," J. Chem. Phys. 41, 2377 (1964).

337. N. C. Blais and D. G. Truhlar, "Monte Carlo Trajectory Study of $Ar + H_2$ Collisions. I. Potential Energy Surface and Cross Sections for Dissociation, Recombination, and Inelastic Scattering," J. Chem. Phys. 65, 5335 (1976).

338. P. Sieglbahn and B. Liu, "An Accurate Three-Dimensional Potential Energy Surface for H_3," J. Chem. Phys. 68, 2457 (1978).

339. D. G. Truhlar and C. J. Horowitz, "Functional Representation of Liu and Siegbahn's Accurate *ab initio* Potential Energy Calculations for $H + H_2$," J. Chem. Phys. 68, 2466 (1978).

340. J. W. Duff, N. C. Blais and D. G. Truhlar, "Monte Carlo Trajectory Study of $Ar + H_2$ Collisions: Thermally Averaged Vibrational Transition Rates at 4500 K," J. Chem. Phys. 71, 4304 (1979).

341. W. R. Schulz and D. J. LeRoy, "Kinetics of the Reaction $H + p - H_2 \rightarrow 0 - H_2 + H$," Can. J. Chem. 42, 3869 (1965).

342. K. A. Quickert and D. J. LeRoy, "Test of Transition-State Theory using the Experimentally Determined Rate Constant Ratio for the Reactions $H + H_2$ and $H + D_2$," J. Chem. Phys. 53, 1325 (1970) and "Erratum: .," J. Chem. Phys. 54, 5444 (1971), combined with A. A. Westenburg and N. de Haas, "Atom-Molecule Kinetics using ESR Detection. II. Results for $D + H_2 \rightarrow HD + H$ and $H + D_2 \rightarrow HD + D$," J. Chem. Phys. 47, 1393 (1967).

343. J. D. Doll, J. Chem. Phys. submitted.

344. G. D. Carney and R. N. Porter, J. Chem. Phys. 60, 4251 (1974).

345. A. W. Campbell, W. C. Davis, and J. R. Travis, Phys. Fluids 4, 498, (1961).

346. C. L. Mader, Phys. Fluids 6, 375 (1963).

347. A. W. Campbell, W. C. Davis, J. B. Ramsey, and J. R. Travis, Phys, Fluids 4, 511 (1961).

348. C. L. Mader, Phys. Fluids 8, 1811 (1965).

349. F. Owens, Army Armament Research and Development Command Large Caliber Weapons Systems Laboratory, Technical Report ARLCD-TR-79037 (1979).

350. A. M. Karo, J. R. Hardy, and F. E. Walker, Acta Astronaut. 5, 1041 (1970).

351. H. C. Cady and A. C. Larson, Acta Cryst. 18, 485 (1965).

352. L. Merrill and W. A. Bassett, Rev. Sci, Instrum. 45, 290 (1974).

353. R. LeSar, S. A. Ekberg, L. H. Jones, R. L. Mills, L. A. Schwalbe, and D. Schiferl, Solid State Commun. 32, 131 (1979).

APPENDIX A

PUBLICATIONS

CNC-2
PUBLICATIONS 1978-80

J. E. Adams and J. D. Doll, "Dynamics of Ion Channeling at Low Energies: Preliminary Trajectory Studies," J. Chem. Phys. 73, 2137 (1980).

N. C. Blais and D. G. Truhlar, "Monte Carlo Trajectory Study of Ar+H_2: Vibrational Selectivity of Dissociative Collisions at 4500 K and the Characteristics of Dissociation under Equilibrium Conditions," J. Chem. Phys. 70, 2962 (1979).

N. C. Blais and D. G. Truhlar, "*Ab initio* Calculation of the Vibrational Energy Transfer Rate of H_2 in Ar using Monte Carlo Classical Trajectories and the Forced Quantum Oscillator Model," J. Chem. Phys. 69, 846 (1978).

J. W. Brady, J. D. Doll, and D. L. Thompson, "Cluster Dynamics: Further Classicial Trajectories Studies of $A+A_n \leftrightarrows A^*_{n+1}$," J. Chem. Phys. 73, 2767 (1980).

J. W. Brady, J. D. Doll, and D. L. Thompson, "A Classical Trajectory Study of Xenon Atom-Chlorine Dimer Collisions," J. Chem. Phys. 73, 292 (1980).

J. W. Brady, J. D. Doll, and D. L. Thompson, "Cluster Dynamics: A Classical Trajectory Study of $A+A_n \leftrightarrows A^*_{n+1}$," J. Chem. Phys. 71, 2467 (1979).

J. W. Brady, J. D. Doll, and D. L. Thompson, "Angular Dependence of Velocity Distributions in Gas/Solid-Surface Collisions: Relationship to the Interaction Potential," J. Chem. Phys. 69, 3458 (1978).

I. J. Brink and C. E. Holley, "The Enthalpy of Formation of Strontium Monoxide," J. Chem. Thermodyn. 1978, 10, 259-266.

J. C. Brown, H. E. Bass, and D. L. Thompson, "A Quasi-Classical Trajectory Study of the Four-Center Reactions: HBr+ClI_2 and HBr+BrCl," J. Chem. Phys. 70, 2326 (1979).

J. M. Bunch, J. G. Hoffman, and A. H. Zeltmann, "On the Nature of Features Seen by TEM in Fast Neutron Irradiated Al_2O_3," J. Nuclear Mater. 73, (1978) 65-69.

R. W. Charles, C. E. Holley, Jr., J. W. Tester, L. A. Blatz, and C. O. Grigsby, "Experimentally Determined Rock-Fluid Interactions Applicable to a Natural Hot Dry Rock Geothermal System," The Metallurgical Society of AIME, TMS Paper Selection A80-8 (1980).

J. D. Doll, "A Unified Theory of Dissociation," J. Chem. Phys. 73, 2760 (1980).

J. D. Doll, "Anharmonic Corrections in Unimolecular Theory: A Monte Carlo Approach," Chem. Phys. Lett. 72, 139 (1980).

J. D. Doll, "Generalized Langevin Theory of Gas/Solid-Surface Dynamics: A Formulation for Thermal Desorption," J. Chem. Phys. 68, 3158 (1978).

J. W. Duff, N. C. Blais, and D. G. Truhlar, "Monte Carlo Trajectory Study of Ar+H_2 Collisions: Thermally Averaged Vibrational Transition Rates at 4500 K," J. Chem. Phys. 71, 4304 (1979).

J. W. Duff and P. Brumer, "Statistical Behavior and the Detailed Dynamics of Collinear F+H_2 Trajectories," J. Chem. Phys. 71, 3895 (1979).

T. H. Dunning, Jr., and P. J. Hay, "The Covalent and Ionic States of the Rare Gas Monofluorides," J. Chem. Phys. 69, 134 (1978).

T. H. Dunning, Jr., M. Valley, and H. S. Taylor, "Theoretical Studies of the Low-Lying Electronic States of GaKr, Including Extrapolation to InKr and TlKr," J. Chem. Phys. 69, 2672 (1978).

R. Engleman, Jr., R. A. Keller, and B. A. Palmer, "Hyperfine Structure and Isotope Shift of the 1.3 μm Transition of ^{129}I," Appl. Opt. 19, 2767 (1980).

C. E. Holley, Jr., and E. J. Huber, Jr., *Combustion Calorimetry, V.1. Experimental Chemical Thermo-*

dynamics, S. Sunner and M. Mansson, Eds., "Combustion Calorimetry of Metals and Simple Metallic Compounds," (Pergamon Press, Inc., 1979), Chap. 10, pp. 211-237.

C. E. Holley, Jr., "Funding of Research in Thermodynamics," TRC Current Data News 7, No. 2 (1979).

C. E. Holley, Jr., "Funding of Research in Thermodynamics," Editorial J. Chem. Engr. Data 23, No. 4, 4A (1978).

R. A. Keller, R. Engleman, Jr., and B. A. Palmer, "Atlas for Optogalvanic Wavelength Calibration," Appl. Opt. 19, 836 (1980).

R. A. Keller and E. F. Zalewski, "Noise Considerations, Signal Magnitudes and Detection Limits in a Hollow Cathode Discharge by Optogalvanic Spectroscopy," Appl. Opt. 19, 3301 (1980).

R. A. Keller, R. Engleman, Jr., and E. F. Zalewski, "Optogalvanic Spectroscopy in a Uranium Hollow Cathode Discharge," J. Opt. Soc. Am. 69, 738 (1979).

P. M. Kroger, S. J. Riley, and G. H. Kwei, "Polyhalide Photofragment Spectra. II. Ultraviolet Photodissociation Dynamics of UF_6," J. Chem. Phys. 68, 4195 (1978).

G. H. Kwei and V. W. S. Lo, "Crossed Beam Studies of the Hydrogen Exchange Reaction: The Reaction of H and D Atoms with T_2 Molecules," J. Chem. Phys. 72, 6265 (1980).

G. H. Kwei and D. R. Herschbach, "Optical Model Analysis of $H+H_2$ Reactive Scattering," J. Phys. Chem. 83, 1550 (1979).

G. H. Kwei, "Classical Trajectory Studies of Alkali Halide Collision Dynamics," Chap. 14 in *Alkali Halide Vapors: Structure, Spectra, and Reaction Dynamics*, P. Davidovits and D. L. McFadden, Eds. (Academic Press, New York, 1979), pp. 441-477.

G. H. Kwei, Book review of *Molecular Scattering: Physical and Chemical Applications*, K. P. Lawley, Ed., J. Am. Chem. Soc. 100, 3268 (1978).

W. B. Lewis and A. H. Zeltmann, "Opto-Acoustic Spectroscopy and the Energy of Photodissociation of Uranium Hexafluoride," J. Photochem. 12, 51 (1980).

D. R. McLaughlin and D. L. Thompson, "Ground- and Lower Excited-State Discrete *ab initio* Electronic Potential-Energy Surfaces for Doublet HeH_2," J. Chem. Phys. 70, 2748 (1979).

R. K. Preston, D. L. Thompson, and D. R. McLaughlin, "A Theoretical Prediction of Vibrational Enhancement for Dissociative Charge Transfer in the HeH_2^+ System," J. Chem. Phys. 68, 13 (1978).

J. A. Silver, N. C. Blais, and G. H. Kwei, "Crossed Beam Studies of the $Na(3p^2P_{3/2})$ Atoms by N_2, O_2, CO, and NO Molecules," J. Chem. Phys. 71 3412 (1979).

K. C. Smyth, R. A. Keller, and F. F. Crim, "Photon-Induced Ionization Changes in a Neon Discharge," Chem. Phys. Lett. 55, 473 (1978).

G. E. Streit and T. W. Newton, "Negative Ion-Uranium Hexafluoride Charge Transfer Reactions," J. Chem. Phys. 73, 3178 (1980).

H. H. Suzukawa, M. Wolfsberg, and D. L. Thompson, "A Quasi-Classical Trajectory Study of the Energy Transfer in CO_2-Rare Gas Systems," J. Chem. Phys. 68, 455 (1978).

D. L. Thompson, "On the Rate and Activation Energy of the $Br+Br_2$ Atom-Exchange Reaction," Chem. Phys. Lett. 55, 424 (1978).

W. M. Trott, N. C. Blais, and E. A. Walters, "Photoionization of Carbon Disulfide Monomers and Dimers in a Supersonic Molecular Beam," J. Chem. Phys. 71, 1692 (1979).

W. M. Trott, "Photoionization Mass Spectrometric Studies of Selected Compounds in a Molecular Beam," Los Alamos National Laboratory report LA-7727-T (March 1979).

W. M. Trott, N. C. Blais, and E. A. Walters, "Molecular Beam Photoionization Study of Acetone and Acetone-d_6," J. Chem. Phys. 69, 3150 (1978).

K. A. Truesdell, R. A. Keller, and E. F. Zalewski, "Locking of cw Dye Laser Emission onto the Wavelength of Molecular Fluorescence by Intracavity Gain: Example I_2," J. Chem. Phys. 73, 1117 (1980).

D. G. Truhlar, N. C. Blais, J.-C. J. Hajduk, and J. H. Kiefer, "Monte Carlo Trajectory Study of Ar+H_2 Collisions: Master-Equation Simulation of a 4500 K Shock Wave Experiment with Thermal Rotation," Chem. Phys. Lett. 63, 337 (1979).

S. P. Walch and T. H. Dunning, Jr., "Calculated Barrier to Hydrogen Atom Abstraction from Methane by Triplet P Oxygen Atoms," J. Chem. Phys. 72, 3221 (1980).

S. B. Woodruff and D. L. Thompson, "A Quasi-Classical Trajectory Study of Vibrational Predissociation of Van der Waals Molecules: Collinear He$\cdots I_2(B^3\Pi)$," J. Chem. Phys. 71, 376 (1979).

E. F. Zalewski, R. A. Keller, and R. Engleman, Jr., "Laser Induced Impedance Changes in a Neon Hollow Cathode Discharge. A Mechanistic Study," J. Chem. Phys. 70, 1015 (1979).

PAPERS ACCEPTED FOR PUBLICATION IN FY 1980

J. E. Adams and J. D. Doll, "Dynamics of Ion Channeling at Low Energies: Non-Normal Incidence," J. Chem. Phys.

J. E. Adams and J. D. Doll, "Desorption from Solid Surfaces via Generalized Slater Theory," J. Chem. Phys.

J. E. Adams and J. D. Doll, "Dynamical Corrections to Transition State Theory Adsorption Rates: Effect of a Precursor State," Surf. Sci.

N. C. Blais and D. G. Truhlar, "Reaction, Dissociation, and Energy Transfer as a Function of Initial State for H+H_2 on an Accurate *Ab Initio* Potential Energy Surface," to appear in *Potential Energy Surfaces and Dynamics Calculations*, D. G. Truhlar, Ed. (Plenum Press, New York, 1981).

J. W. Brady, J. D. Doll, and D. L. Thompson, "Cluster Dynamics: A Classical Trajectory Study of $A^*_n \rightarrow 1A_{n+11}+A$," J. Chem. Phys.

J. W. Brady, J. D. Doll, and D. L. Thompson, "Classical Trajectory Studies of Homogeneous Nucleation of a Rare Gas," to appear in *Potential Energy Surfaces and Dynamics Calculations*, D. G. Truhlar, Ed. (Plenum Press, New York, 1981).

J. D. Doll, "Monte Carlo Sampling Techniques and the Evaluation of Unimolecular Rate Constants," J. Chem. Phys.

R. Engleman, Jr., and R. A. Keller, "Optogalvanic Double Resonance Spectroscopy: Experimental Observations," Opt. Lett.

C. E. Holley, Jr., M. H. Rand, and E. K. Storms, "The Actinide Carbides," book chapter in *The Chemical Thermodynamics of Actinide Elements and Compounds* (IAEA).

G. H. Kwei, "Crossed Beam Studies of Chemical Kinetics Using Radiotracer Techniques," to be published in book form in the American Chemical Society's ADVANCES IN CHEMISTRY series.

G. E. Streit and T. W. Newton, "The Effect of Chemical Reaction on Diffusive Ion Loss Processes in a Flowing Afterglow," Int. J. Mass Spectrom. Ion Phys.

J. J. Valentini, P. Esherick, and A. Owyoung, "Use of a Free-Expansion Jet in Ultra-High Resolution Inverse Raman Spectroscopy," Chem. Phys. Lett.

LA REPORT

B. A. Palmer, R. Engleman, and R. Keller, "An Atlas of Uranium Emission Intensities in a Hollow Cathode Discharge," LA-8251-MS (July 1980).

PAPERS AND TALKS PRESENTED AT SCIENTIFIC MEETINGS IN FY 1980

G. E. Streit, "Flowing Afterglow Studies of Negative Ion-UF_6 Electron Transfer Reactions," 32nd Annual Gaseous Electronics Conference, Pittsburgh, Pennsylvania, October 9-12, 1979.

G. E. Streit, "Negative Ion-UF_6 Electron Transfer Reactions: Detailed Modelling of Rate and Diffusion Coefficients in the Flowing Afterglow," 32nd Annual Gaseous Electronics Conference, Pittsburgh, Pennsylvania, October 9-12, 1979.

D. L. Thompson, "Effects of Vibrational Energy on Rotational Relaxation: He + H_2," Southwest Regional ACS Meeting, Austin, Texas, December 6-7, 1979.

*J. J. Valentini, "Crossed Molecular Beam Study of the $NO+O_3 \rightarrow NO_2+O_2$," University of California, Berkeley.

*J. D. Doll, "Review of Long Range Force Problems in Gas/Solid Surface Scattering," National Resource in Computational Chemistry workshop on Long Range Forces, Menlo Park, California, January 8-11, 1980.

*N. C. Blais, "Energy Transfer, Reaction and Dissociation as a Function of Initial State for $H+H_2$ on an Accurate *ab initio* Potential Energy Surface," ACS Meeting, Las Vegas, Nevada, August 25-29, 1980.

J. E. Adams, "Dynamics of Ion Channeling at Low Energies: Preliminary Trajectory Studies," 2nd West Coast Theoretical Chemistry Conference, California Institute of Technology, Pasadena, California, April 9-11, 1980.

J. D. Doll, "Unified Theory of Dissociation," 2nd West Coast Theoretical Chemistry Conference, California Institute of Technology, Pasadena, California, April 9-11, 1980.

C. E. Holley, "Geothermal Energy from Hot Dry Rock," Southwestern and Rocky Mountain Division, AAAS, 56th Annual Meeting, Las Vegas, Nevada, April 9-12, 1980.

J. D. Doll, "Nucleation Dynamics," Theoretical Chemistry Conference, Banff, Canada, June 15-20, 1980.

J. D. Valentini, "Ultra-High Resolution Inverse Raman Spectroscopy of Methane in a cw Free-Expansion Jet," 11th International Quantum Electronics Conference, Boston, Massachusetts, June 23-27, 1980.

*Invited talk.

R. A. Keller, "Tunable Lasers in Analytical Chemistry," ACS Meeting, Kansas City, Missouri, April 17-18, 1980.

*R. A. Keller, "Analytical and Spectroscopic Applications of Optogalvanic Spectroscopy," the University of Nebraska, April 15-16, 1980; the University of Missouri, April 17-18, 1980; and the University of Arkansas, April 19, 1980.

J. E. Adams, "Desorption from Solid Surfaces via Generalized Slater Theory," poster session, National ACS Meeting, Las Vegas, Nevada, August 25-29, 1980.

L. Babcock, "Study of Reactions of Small Positive Ions with Selected Metal Hexalfluorides," poster session, National ACS Meeting, Las Vegas, Nevada, August 25-29, 1980.

L. A. Blatz, "The Interaction of Water and Biotite-Granodiorite Rock at 198°C, 235°C and 275°C," 3rd International Symp. Water-Rock Interactions, Edmonton, Alberta, Canada, July 14-24, 1980.

*D. L. Thompson, "Classical Trajectory Studies of Homogeneous Nucleation of a Rare Gas," Potential Energy Surfaces and Dynamics Calculations at the National ACS Meeting, Las Vegas, Nevada, August 25-29, 1980.

C. E. Holley, "Interaction of Water with Crystalline Basement Rock in Fractured Hot Dry Rock Geothermal Reservoirs," 3rd International Symp. Water-Rock Interactions, Edmonton, Alberta, Canada, July 14-24, 1980.

CNC-3
PUBLICATIONS 1978-80

R. J. Daniels, P. M. Grant, and H. A. O'Brien, Jr., "The Production, Recovery, and Purification of Hf-172 for Utilization in Nuclear Medicine as the Generator of Lu-172," Int. J. Nucl. Med. Biol. 5, 11-17 (1978).

*Invited talk.

P. M. Grant, B. R. Erdal, R. E. Whipple, R. J. Daniels, and H. A. O'Brien, Jr., "The Half-Lives of Sr-82 and Rb-82," Phys. Rev. C 18(6), 2799-2800 (1978).

P. M. Grant, H. A. O'Brien, Jr., S. Mirzadeh, and R. E. Whipple, (Letter to Editor) "Premature Evaluation of a $^{68}Ge/^{68}Ga$ Distillation Generator," J. Nucl. Med. 21, 702-703 (1980).

P. M. Grant, R. E. Whipple, H. A. O'Brien, Jr., and S. Kulprathipanja, "The Influence of Carrier Strontium Level and Eluant Volume on the Performance of Sr-82/Rb-82 Biomedical Generators," J. Nucl. Med. 19 1250-1255 (1978).

H. B. Hupf, P. M. Wanek, and H. A. O'Brien, Jr., "Rapid Radioiodination of Rose Bengal at Room Temperature," J. Nucl. Med. 19, 525-529 (1978).

S. Mirzadeh, M. Kahn, P. M. Grant, and H. A. O'Brien, Jr., "A Procedure for the Preparation of Chloride-Free Solutions of Carrier-Free Germanium-68," Radiochem. Radioanal. Letters 42(6), 361-364 (1980).

H. A. O'Brien, Jr., "Accelerator Preparation of Radioistopes for Medical Applications," Trans. Amer. Nucl. Soc. 33, 222-224 (1979).

H. A. O'Brien, Jr., A. E. Ogard, and P. M. Grant, "The LASL Medical Radioisotope Research Program: An Overview of LAMPF and the Isotope Production Facility," Prog. Nucl. Med. 4, 16-22 (1978).

H. A. O'Brien, Jr., P. M. Grant, and A. E. Ogard, "The LASL Medical Radioisotope Research Program: Radiochemistry Problems and New Developments," Prog. Nucl. Med. 4, 93-99 (1978).

Y. Yano, T. F. Budinger, H. A. O'Brien, Jr., and P. M. Grant, "Evaluation and Application of Alumina Column Rb-82 Generators," J. Nucl. Med. 20, 961-966 (1979).

PAPERS ACCEPTED FOR PUBLICATION IN FY 1980

P. M. Grant, R. J. Daniels, W. J. Daniels, G. E. Bentley, and H. A. O'Brien, "A Heavy Rare Earth Nuclide Generator," J. Label. Cmpds. Radiopharm.

D. A. Miller, P. M. Grant, J. W. Barnes, G. E. Bentley, and H. A. O'Brien, "Research Scale Experimentation on the Production and Purification of Spallogenic ^{68}Ge at Los Alamos for Nuclear Medicine Applications," Pergamon Press.

H. A. O'Brien, Jr., and P. M. Grant, "Biomedical Positron Generators," Pergamon Press.

D. S. Wilbur and H. A. O'Brien, Jr., "A-Ring Brominations of Estradiol. An Investigation of the Product Ratios," J. Label. Cmpds. Radiopharm.

PAPERS AND TALKS PRESENTED AT SCIENTIFIC MEETINGS IN FY 1980

R. E. Gibson, A. Mazaitis, B. Francis, R. Patt, W. C. Eckelman, R. C. Reba, and H. A. O'Brien, "In Vivo Receptor Binding of Radiolabeled Estrogens," J. Nucl. Med. 21, 36 (1980).

P. M. Grant, P. M. Wanek, R. E. Whipple, G. E. Bentley, J. W. Barnes, and H. A. O'Brien, "Novel Research Radioisotopes from the Los Alamos Meson Physics Facility," Abstracts of Papers, 146th Nat. Mtg., AAAS, A. Herschman, Ed. 126 (1980).

C. Haydock, K. S. Sastry, H. A. O'Brien, P. Grant, J. W. Barnes, and G. E. Bentley, "Bromine-77: A Promising New Probe for Biomolecular Research Through PAC," Proc. Int. Conf. Nucl. Phys. (1980).

D. A. Miller, P. M. Grant, J. W. Barnes, G. E. Bentley, and H. A. O'Brien, "Radionuclides from Proton-Induced Spallation Reactions for Biomedical Applications. V. Ge-68 Recovery from RbBr Targets," Abstracts of Papers, 2nd Chem. Cong. No. Amer. Cont. Amer. Chem. Soc., Part 1, NUCL No. 45, (August 1980).

H. A. O'Brien, Jr., "A Review of Biomedical Generators Yielding Positron Emitters of Interest in Medicine," Abstracts of Papers, 2nd Chem. Cong. No. Amer. Cont. Amer. Chem. Soc., Part 1, NUCL No. 42, (August 1980).

L. Rosen, D. C. Hoffman, B. J. Dropesky, and H. A. O'Brien, Jr., "Nuclear and Radiochemistry Facilities at LAMPF," Abstracts of Papers, 2nd Chem. Cong. No. Amer. Cont. Amer. Chem. Soc., Part 1, NUCL No. 62, (August 1980).

CNC-4
PUBLICATIONS 1978-80

M. Alei, Jr., "Rapid Synthesis of Isotopically Labelled Methanes," J. Labelled Compd. & Radiopharm. XVII(1), 115-19 (1980).

M. Alei, Jr., L. O. Morgan, and W. E. Wageman, "^{15}N Magnetic Resonance of Aqueous Imidazole and Zn(II)-Imidazole Complexes. Evidence for Hexacoordination," Inorg. Chem. 17, 2288-93 (1978).

M. Alei, Jr., L. O. Morgan, W. E. Wageman, and T. W. Whaley, "pH Dependence of ^{15}N NMR Shifts and Coupling Constants in Aqueous Imidazole and 1-Methylimidazole. Comments on Estimation of Tautomeric Equilibrium Constants for Aqueous Histidine," J. Am. Chem. Soc. 102(9), 2881-2887 (1980).

M. Alei, Jr., and William E. Wageman, "^{15}N NMR Shifts for Imidazole and 1-Methyl Imidazole in CH_2Cl_2 Relative to Aqueous Solution," Tetrahedron Let. 8, 667-70 (1979).

M. Alei, Jr., and W. E. Wageman, "Gas Phase ^{13}C Chemical Shifts and Coupling Constants in the Deuteromethanes," J. Chem. Phys. 68, 783-84 (1978).

M. Alei, Jr., W. E. Wageman, and L. O. Morgan, "Nitrogen-15 Chemical Shifts for Imidazole in Aqueous CD^{2+} Solutions," Inorg. Chem. 17, 3314-15 (1978).

M. Alei, Jr., P. J. Vergamini, and William E. Wageman, "^{15}N NMR of *cis*-Diamine-Platinum(II) Complexes in Aqueous Solution," J. Am. Chem. Soc. 101(18), 5415-17 (1979).

D. E. Armstrong, B. B. McInteer, T. R. Mills, and J. G. Montoya, "Isotopic Enrichment of ^{15}N, ^{17}O, and ^{18}O," in *Stable Isotopes*, Proc. 3rd Int. Conf., May 23-26, 1978, Oak Brook, Illinois, E. R. Klein and P. D. Klein, Eds. (Academic Press, New York, 1979) p. 175.

D. E. Armstrong, T. R. Mills, B. B. McInteer, J. G. Montoya, C. A. Lehman, R. C. Vandervoort, and M. Goldblatt, "The COLA Column for ^{13}C Production," in *Stable Isotopes*, Proc. 3rd Int. Conf., May 23-26, 1978, Oak Brook, Illinois, E. Roseland Klein and Peter D. Klein, Eds. (Academic Press, New York, 1979) p. 177.

D. L. Anton, H. P. C. Hogenkamp, T. E. Walker, and N. A. Matwiyoff, "Carbon-13 Nuclear Magnetic Resonance Studies of the Monocarboxylic Acids of Cyanocobalamin. Assignments of the *b*-, *d*-, and *e*-Monocarboxylic Acids," J. Am. Chem. Soc. 102, 2215-19 (1980).

L. B. Asprey and R. T. Paine, "Metal Pentafluorides," in *Inorganic Sythesis XIX*, D. F. Shriver, Ed. (Wiley-Interscience, New York, 1979), pp. 137-40.

J. E. Barefield, L. H. Jones, and R. Liepens, "Vibration-Rotation Analysis of Deuterium Tritide," J. Mol. Spectrosc. 80, 233-236 (1980).

R. Barker and T. E. Walker, "^{13}C NMR Spectroscopy of Isotopically Enriched Carbohydrates," in *Methods in Carbohydrate Chemistry* (Academic Press, 1980), Vol. VIII, Chap. 21, pp. 151-165.

R. L. Blakley, L. Cocco, R. E. London, T. E. Walker, and N. A. Matwiyoff, "Nuclear Magnetic Resonance Studies on Bacterial Dihydrofolate Reductase Containing [*methyl*-^{13}C]-Methionine," Biochemistry 17, 2284-93 (1978).

J. R. Cann, R. E. London, J. M. Stewart, and N. A. Matwiyoff, "Effect of Temperature upon the Circular Dichroism of Bradykinin," Int. J. Pept. Protein Res. 14(5), 388-92 (1979).

L. Cocco, R. L. Blakley, R. E. London, J. P. Groff, T. E. Walker, and N. A. Matwiyoff, "NMR Studies of ^{13}C Labeled Dihydrofolate Reductase," in *Chemistry and Biology of Pteridines*, Proc. Sixth Int. Symposium, La Jolla, California, Sept. 25-28, 1978, R. L. Kisliuk and G. M. Brown, Eds. (Developments in Biochemistry, Vol. 4) (Elsevier/North-Holland, New York, 1979) pp. 383-388.

L. Cocco, R. L. Blakley, T. E. Walker, R. E. London, and N. A. Matwiyoff, "Nuclear Magnetic Resonance Studies on Bacterial Dihydrofolate Reductase Containing [Guanidino-^{13}C]-labeled Arginine," Biochemistry 17, 4285-4290 (1978).

P. G. Eller, book review of *Structure and Bonding, Volume 28, Electrons in Oxygen- and Sulphur-Containing Ligands*, (Springer-Verlag, New York, 1976), in J. Am. Chem. Soc. 100(9), 2938 (1978).

P. G. Eller and G. J. Kubas, "Synthesis, Properties, and Structure of Iodosulfinate Salts," Inorg. Chem. 17, 894-97 (1978).

P. G. Eller, A. C. Larson, J. R. Peterson, D. D. Ensor, and J. P. Young, "Crystal Structures of α-UF_5 and U_2F_9 and Spectral Characterization of U_2F_9," Inorg. Chem. Acta 37, 129-133 (1979).

P. G. Eller and R. R. Ryan, "Crystal and Molecular Structures of Two Square-Pyramidal Rhodium(I)-Sulfur Dioxide Complexes. Bonding Effects in Pyramidal-SO_2 Complexes," Inorg. Chem. 19(1), 142-47 (1980).

H. Flicker and L. H. Jones, "Integration of Absorption Lines Using the Nicolet FT-IR Spectrometer," Nicolet Instr. Corp. Newslet., FT-IR Spectral Lines II No. 1, (March 1980) p. 6.

E. Fukushima, book review of *Magnetic Resonance of Phase Transitions*, F. J. Owens, C. P. Poole, Jr., and H. A. Farach, Eds. (Academic Press, New York, 1979), in J. Magn. Resonan. 40, 409-412 (1980).

E. Fukushima, A. A. V. Gibson, and T. A. Scott, "Carbon-13 NMR of Carbon Monoxide. II. Molecular Diffusion and Spin-rotation Interaction in Liquid CO," J. Chem. Phys. 71(4), 1531-36 (1979).

E. Fukushima, A. A. V. Gibson, and T. A. Scott, "ERRATUM: Carbon-13 NMR of Carbon Monoxide. I. Pressure Dependence of Translational Motion in Beta-CO, [J. Chem. Phys. 66, 4811-17 (1977)]," J. Chem. Phys. 68, 2022 (1978).

E. Fukushima and G. Halstead, "NMR of Polycrystalline $NaUF_6$," in *Magnetic Resonance and Related Phenomena (1978)*, Proc. XX Congress Ampere, Tallinn, USSR, Aug. 21-26, 1978, E. Kundla, E. Lippmaa and T. Saluvere, Eds. (Springer-Verlag, Berlin, 1979) p. 378.

E. Fukushima and S. B. W. Roeder, "Spurious Ringing in Pulse NMR," J. Magn. Reson. 33, 199-203 (1979).

E. Fukushima and K. D. Swenson, "Use of CAMAC for Computer Interface in NMR," J. Magn. Reson. 39, 325-328 (1980).

C. T. Gregg, J. Rudnick, B. B. McInteer, T. W. Whaley, and W. W. Shreeve, "The Effect of Ethanol on Galactose Tolerance in Man," in *Stable Isotopes*, Proc. 3rd Int. Conf. May 23-26, 1978, Oak Brook, Illinois, E. R. Klein and P. D. Klein, Eds. (Academic Press, New York, 1979), pp. 515-25.

G. W. Halstead, P. G. Eller, L. B. Asprey, and K. V. Salazar, "Convenient Multigram Syntheses of Uranium Pentafluoride and Uranium Pentaethoxide," Inorg. Chem. 17, 2967-69 (1978).

G. W. Halstead, P. G. Eller, and M. P. Eastman, "Nonaqueous Chemistry of Uranium Pentafluoride," Inorg. Chem. 18(10), 2867-72 (1979).

H. P. C. Hogenkamp, N. A. Kohlmiller, R. Howsinger, T. E. Walker, and N. A. Matwiyoff, "Interaction of *cis*-Diamminediaquoplatinum(II) with (Adenosyl-) cobalamin and Alkylcobalamins," J. Chem. Soc., Dalton Trans. 9, 1668-1673 (1980).

L. H. Jones, "Measurement and Analysis of the ν_2 Bands of $^{14}ND_3$ and $^{15}ND_3$," J. Mol. Spectrosc. 73(3), 409-22 (1979).

L. H. Jones and S. A. Ekberg, "Vibrational Spectrum and Potential Constants for S_2F_{10}," Spectrochim. Acta 36A, 761-767 (1980).

L. H. Jones and S. A. Ekberg, "Photoinduced Reaction of UF_6 with SiH_4 in a Low Temperature SiH_4 Matrix," J. Chem. Phys. 71(11), 4764-65 (1979).

L. H. Jones, S. Ekberg, and L. B. Asprey, "Laser Excitation of SF_6 in Low Temperature Matrices," J. Chem. Phys. 70, 1566-67 (1979).

L. H. Jones, Craig Kennedy, and S. Ekberg, "Potential Constants of CF_4," J. Chem. Phys. 69, 833-838 (1978).

L. H. Jones, B. J. Krohn, and R. C. Kennedy, "The ν_4 Fundamental of Three Isotopic Species of CF_4," J. Mol. Spectrosc. 70, 288-93 (1978).

L. H. Jones and R. R. Ryan, "Potential Constants and Dissociation Pathways," J. Mol. Struct. 46, 35-42 (1978).

L. H. Jones, B. I. Swanson, and S. A. Ekberg, "Temperature Reversible IR Spectral Changes and Site Structure Dynamics for SeF_6 Isolated in Krypton Matrices," Chem. Phys. Lett. 74, 331 (1980).

L. H. Jones, B. I. Swanson, and S. A. Ekberg, "High Resolution Infrared Matrix Isolation Spectroscopy of SF_6 and BCl_3," Chem. Phys. Lett. 68(2,3), 499-500 (1979).

L. H. Jones, R. C. Taylor, and R. T. Paine, "Potential Constants of Borane Carbonyl," J. Chem. Phys. 70, 749-57 (1979).

V. H. Kollman, J. L. Hanners, R. E. London, E. G. Adame, and T. E. Walker, "Photosynthetic Preparation and Characterization of ^{13}C-Labeled Carbohydrates in *Agmenellum quadruplicatum*," Carbohydr. Res. 73, 193-202 (1979).

V. H. Kollman, R. E. London, J. L. Hanners, C. T. Gregg, and T. W. Whaley, "Photosynthetic Preparation of Galactose-$^{13}C_6$ and Glycerol-$^{13}C_3$ Using a Marine Red Alga," J. Labelled Comp. Radiopharm. XVI(6), 833-42 (1979).

V. H. Kollman, R. E. London, J. L. Hanners, and T. E. Walker, "Photosynthetic Preparation of ^{13}C-Labeled Sugars Using a Blue-Green Alga," in *Stable Isotopes*, Proc. 3rd Int. Conf., May 23-26, 1978, Oak Brook, Illinois, E. R. Klein and P. D. Klein, Eds. (Academic Press, New York, 1979), pp. 19-27.

G. J. Kubas, "Five-co-ordinate Molybdenum and Tungsten Complexes, $[M(CO)_3(PCy_3)_2]$, which Reversibly add Dinitrogen, Dihydrogen, and Other Small Molecules," J. Chem. Soc., Chem. Commun. No. 2, 61-62 (1980).

G. J. Kubas, "Tetrakis(acetonitrile)copper(I) Hexafluorophosphate," Inorg. Synth. XIX, 90-92 (1979).

G. J. Kubas, "Diagnostic Features of Transition-Metal-SO_2 Coordination Geometries," Inorg. Chem. 18, 182-188 (1979).

G. J. Kubas, "A Convenient Method for Deoxygenating Solvents for Benchtop Inert-Atmosphere Reactions," Aldrichimica Acta 11(1), 10 (1978).

G. J. Kubas, A. C. Larson, and R. R. Ryan, "Reactions of Quinuclidine *N*-Oxide and Other Amine Oxides with Sulfur Dioxide. Structure of Quinuclidine Sulfur Trioxide," J. Org. Chem. 44(22), 3867-71 (1979).

G. J. Kubas, R. R. Ryan, and V. McCarty, "Bonding of η^2-Sulfur Dixoide: Structures of Tricarbonyl (1,10-phenanthroline)-(η^2-sulfur dioxide)molybdenum(O) and Dicarbonyl(2,2′-bipyridyl)bis-(η^2sulfur dioxide) molybdenum(O)," Inorg. Chem. 19(10), 3003-3007 (1980).

A. C. Larson, "Restrained Refinement of Disodium Adenosine 5′-Triphosphate Trihydrate," Acta, Cryst. B34, 3601-04 (1978).

K. M. Leary, J. L. Lyman, L. B. Asprey, and S. M. Freund, "CO_2 Laser Induced Reactions of SF_5Cl," J. Chem. Phys. 68, 1671-76 (1978).

R. LeSar, S. A. Ekberg, L. H. Jones, R. L. Mills, L. A. Schwalbe, and D. Schiferl, "Raman Spectroscopy of Solid Nitrogen up to 374 kbar," Solid State Commun. 32, 131-134 (1979).

E. K. S. Liu, "Chemistry of Trifluoromethyl Compounds. 2. Synthesis and Characterization of Bis(pyridine)bis(trifluoromethyl)-zinc," Inorg. Chem. 19(1), 266-68 (1980).

E. K. S. Liu and L. B. Asprey, "Chemistry of Trifluoromethyl Compounds. I. NMR Evidence for Bis(trifluoromethyl)zinc and Methyl(trifluoromethyl) zinc," J. Organometal. Chem. 169, 249-254 (1979).

R. E. London, "Correlation of Carboxyl Carbon Titration Shifts and pK Values," J. Magn. Reson. 38, 173-177 (1980).

R. E. London, "Intramolecular Dynamics of Proteins and Peptides as Monitored by Nuclear Magnetic Relaxation Measurements," in *Magnetic Resonance in Biology, I.*, J. S. Cohen, Ed. (John Wiley & Sons, Inc., New York, 1980) Chap. 1, pp. 1-69. Invited review.

R. E. London, "Quantitative Evaluation of γ-Turn Conformation in Proline-Containing Peptides Using ^{13}C NMR," Int. J. Pept. Protein Res. 14, 377-87 (1979).

R. E. London, "Carbon-Carbon Coupling in [90%-^{13}C-2]Histidine," J. Chem. Soc., Chem. Commun. 1070-71 (1978).

R. E. London, "On the Interpretation of ^{13}C Spin Lattice Relaxation Resulting from Ring Puckering in Proline," J. Am. Chem. Soc. **100**, 2678-85 (1978).

R. E. London and J. Avitabile, Jr., "Internal Diffusion Model. Application to Methionine Relaxation in Dihydrofolate Reductase," J. Am. Chem. Soc. **100**, 7159-7165 (1978).

R. E. London and J. W. Avitabile, Jr., "Carbon-13 Relaxation Times in a Hydrocarbon Chain Undergoing Gauch-Trans Isomerism," Proc. Symp. Biomolecular Structure and Function, University of Missouri, Columbia, Missouri, May 1977, P. F. Agris, Ed. (Academic Press, 1978) pp. 78-85.

R. E. London, J. P. Groff, and R. L. Blakley, "^{13}C NMR Evidence of the Slow Exchange of Tryptophans in Dihydrofolate Reductase Between Stable Conformations," Biochem. Biophys. Res. Commun. 86(3), 779-786 (1979).

R. E. London, N. A. Matwiyoff, J. M. Stewart, and J. R. Cann, "A ^{13}C Nuclear Magnetic Resonance Study of the Cis-Trans Isomerism in X-Pro-Pro Tripeptides," Biochemistry 17, 2277-83 (1978).

R. E. London and A. D. Sherry, "Conformation Examination of Uridine Diphosphoglucose Using Lanthanide-Nitrilotriacetate Chelates as Shift Probes," Biochemistry 17, 3662-3666 (1978).

R. E. London, John M. Stewart, John R. Cann, and N. A. Matwiyoff, "^{13}C and ^{1}H NMR Studies of Bradykinin and Selected Peptide Fragments," Biochemistry 17, 2270-7 (1978).

R. E. London, J. M. Stewart, J. R. Cann, R. Williams, and N. A. Matwiyoff, "Carbon-13 NMR Spectroscopy of [20%-1,2-$^{13}C_2$-Gly^6]-Bradykinin. Role of Serine in Reducing Structural Heterogeneity," J. Am. Chem. Soc. 101(9), 2455-2462 (1979).

R. E. London, T. E. Walker, V. H. Kollman, and N. A. Matwiyoff, "Studies of the pH Dependence of ^{13}C Shifts and Carbon-Carbon Coupling Constants of [U-^{13}C] Aspartic and Glutamic Acids," J. Am. Chem. Soc. **100**, 3723-29 (1978).

R. E. London, T. E. Walker, D. M. Wilson, and N. A. Matwiyoff, "Application of Doubly Decoupled $^{13}C\{^{1}H, ^{14}N\}$NMR Spectroscopy to Studies of the Conformation and Dynamics of the Choline Headgroup of Phospholipids," Chem. Phys. Lipids 25, 7-14 (1979).

N. A. Matwiyoff, "Architecture and Dynamics of Isotopically Labelled Marcomolecules by Nuclear Magnetic Resonance Spectroscopy," in *ESR and NMR of Paramagnetic Species in Biological and Related Systems*, I. Bertini and R. S. Drago, Eds. (D. Reidel Publ. Co., Hingham, Massachusetts, 1979), pp. 28-53.

N. A. Matwiyoff, R. E. London, T. E. Walker, R. Blakley, and L. Cocco, "^{13}C NMR Studies of Bacterial Dihydrofolate Reductase Containing [Methyl-^{13}C] Methionine and [Guanido-^{13}C]Arginine," in *Stable Isotopes*, Proc. 3rd Int. Conf., May 23-26, 1978, Oak Brook, Illinois, E. R. Klein and P. D. Klein, Eds. (Academic Press, New York, 1979) pp. 299-305.

B. B. McInteer, "Isotope Separation by Distillation: Design of a Carbon-13 Plant," Sep. Sci. Technol. 15(3), 491-508 (1980).

T. R. Mills, "Carbon Isotope Separation by Absorptive Distillation," Sep. Sci. Technol. 15(3), 475-490 (1980).

D. C. Moody and J. D. Odom, "The Chemistry of Trivalent Uranium. The Synthesis and Reaction Chemistry of the Tetrahydrofuran Adduct of Uranium Trichloride, $UCl_3(THF)_x$," J. Inorg. Nucl. Chem. 41, 533-35 (1979).

D. C. Moody, R. A. Penneman, and K. V. Salazar, "The Chemistry of Trivalent Uranium. 2. Synthesis of UCl_3(18-crown-6) and $U(BH_4)_3$(18-crown-6)," Inorg. Chem. 18, 208-209 (1979).

D. C. Moody and R. R. Ryan, "Novel Reactivity and Low Temperature (–60°C) Structure of $Ru(CO)_2(\eta^2\text{-}SO_2\cdot SO_2)(PPh_3)_2$," J. Chem. Soc., Chem. Commun. No. 24, 1230-1231 (1980).

D. C. Moody and R. R. Ryan, "Di[(benzo-15-crown-5)sodium]Tetrachloro-dioxouranate, $C_{28}H_{40}Cl_4Na_2O_{12}U$," Cryst. Struct. Comm. 8(4), 933-36 (1979).

D. C. Moody and R. R. Ryan, "Structures of (Sulfur dioxide)tris-(triphenylphosphine)nickel(O), $Ni(SO_2)(PPh_3)_3$, and Bis(sulfur dioxide)bis-(triphenylphosphine)nickel(O), $Ni(SO_2)_2(PPh_3)_2$," Inorg. Chem. 18, 223-227 (1979).

D. C. Moody, R. R. Ryan, and A. C. Larson, "Structure of Nitrosyl(sulfur dioxide)bis(triphenylphosphine) cobalt," Inorg. Chem. 18, 227-229 (1979).

R. T. Paine, R. W. Light, and M. Nelson, "Vibrational Spectra of Uranium(IV) Borohydride and Uranium(IV) Borodeuteride," Spectrochim. Acta 35A(3), 213-16 (1979).

G. Makorovich, Yu. V. Gagarinskii, and S. V. Borisov, "Crystal Chemical Regularities in Uranium and Analogous Fluorides," Moscow, Atomizdat (1975) (in Russian); also, Los Alamos National Laboratory report LA-TR-79-15 (1979) (R. A. Penneman, Ed. and A. D. Cernicek, Trans.).

R. A. Penneman, R. G. Haire, and M. H. Lloyd, "Polymolybdates as Plutonium(IV) Hosts," in *Actinide Separations*, ACS Symposium Series 117, J. D. Navratil and W. W. Schulz, Eds. (American Chemical Society, Washington, D.C., 1980), Chap. 39, pp. 571-581.

M. J. Reisfeld, H. Flicker, and M. Goldblatt, "Analysis of the Fourier Transform Spectra of $^{12}C^{17}O_2$ and $^{12}C^{17}O^{18}O$: The ν_2 (15 μm) Region," J. Mol. Spectrosc. 82, 411-417 (1980).

M. J. Reisfeld, H. Flicker, and M. Goldblatt, "Analysis of the Fourier Transform Spectrum of $^{13}C^{18}O_2$ in the 4.3 μm and 16 μm Regions," J. Mol. Spectrosc. 83(1), 175-184 (1980).

R. R. Ryan and G. J. Kubas, "Lability and Reactivity of SO_2-Transition Metal Complexes: Crystal and Molecular Structure of $OsHCl(CO)[P(C_5H_{11})_3]_2(SO_2)\cdot 2CHCl_3$," Inorg. Chem. 17(3), 637-41 (1978).

R. R. Ryan, J. R. Smyth, and B. I. Swanson, "Structural Phase Transformations in Dicesium Sodium Ferricyanide," Acta Cryst. B35, 264-65 (1979).

R. R. Ryan and B. I. Swanson, "Comment on the Room-Temperature Structure of Dicesium Lithium Chromium Hexacyanate," Acta Crystallogr. B34, 1398-99 (1979).

B. I. Swanson and L. H. Jones, "Temperature Reversible Site Structural Change for SF_6 Isolated in an Argon Matrix," J. Chem. Phys. 73(2), 986-87 (1980).

B. I. Swanson, B. C. Lucas, and R. R. Ryan, "Structural Phase Transformations and Temperature Dependent Raman Spectra of $Cs_2LiFe(CN)_6$," J. Chem. Phys. 69(10), 4328-34 (1978).

P. J. Vergamini, "Reaction of UF_6 with Methanol to Form UF_5OMe," J. Chem. Soc., Chem. Commun. 54-55 (1979).

P. J. Vergamini and P. G. Eller, "The ^{13}C NMR Spectrum of $Pt(PPh_3)_2(\eta^2\text{-}CS_2)$ - a Non-fluxional π-CS_2 Complex," Inorg. Chem. Acta Lett. 6, L291-L292 (1979); Inorg. Chem. Acta 34, L291-L292 (1979).

T. E. Walker, R. E. London, R. Barker, and N. A. Matwiyoff, "Dihedral Angle Dependence of Geminal Scalar Coupling Constants in ^{13}C-1 Amino Sugars," Carbohyd. Res. 60, 9-18 (1978).

W. H. Zachariasen, "Bond Lengths in Oxygen and Halogen Compounds of *d* and *f* Elements," J. Less-Common Metals 62, 1-7 (1978).

W. H. Zachariasen and R. A. Penneman, "Application of Bond Length-Strength Analysis to 5f Element Fluorides," J. Less-Common Metals 69, 369-77 (1980).

LA REPORTS

J. W. Conant, H. H. Cady, R. R. Ryan, J. L. Yarnell, and J. M. Newsam, "The Atom Positions of Pentaerythritol Tetranitrate (PETN, $C_5H_8N_4O_{12}$) Determined by X-Ray and by Neutron Diffraction," Los Alamos National Laboratory report LA-7756-MS (December 1979).

B. B. McInteer, "Fractional Distillation for Carbon Isotope Separation," Los Alamos National Laboratory Mini-Review LASL-78-76 (October 1978).

D. F. Shepard, "Kinetics and Thermodynamics of Nickel(II): Glycine Complexes Using Carbon Magnetic

Resonance," Thesis, University of New Mexico, 1979: Los Alamos National Laboratory report LA-7774-T (April, 1979).

PAPERS ACCEPTED FOR PUBLICATION FY 1980

M. Alei, Jr., L. O. Morgan, and W. E. Wageman, "^{15}N NMR Study of Complexation of 1-Methylimidazole by Zn(II) and Cd(II) in Aqueous Solution," Inorg. Chem.

M. J. O. Anteunis, F. Borremans, J. M. Stewart, and R. E. London, "A 360 MHz ^{1}HNMR Conformational Analysis of Gly-Pro-X Peptides (X = Ala, Cha, Phe)," J. Am. Chem. Soc.

P. G. Eller and R. A. Penneman, "Physicochemical Properties of Curium," in *Chemistry of the Actinides*, Seaborg and Katz, Eds. (Invited chaper).

P. G. Eller and P. J. Vergamini, "Nuclear Magnetic Resonance and Chemical Studies of Uranium(V) Alkoxides," Inorg. Chem.

C. T. Gregg, J. Rudnick, B. B. McInteer, and W. W. Shreeve, "The Effect of Ethanol on Complete Oxidation of C-13 Galactose in Alcoholic Liver Disease," J. Nucl. Med.

G. W. Halstead and P. G. Eller, "Uranium(V) Fluorides and Alkoxides," Inorg. Synth.

G. J. Kubas and R. R. Ryan, "Chlorobis (Tricyclohexylphosphine)-(Sulfur Dioxide)Rhodium(I). A Square Planar SO_2-Transition Metal Complex," Inorg. Chem. Acta.

G. J. Kubas, R. R. Ryan, and V. McCarty, "Bonding of η^2-Sulfur Dioxide: Structures of Tricarbonyl-(1,10-phenanthroline)-(η^2-sulfur dioxide)molybdenum(O) and Dicarbonyl(2,2′-bipyridyl)bis-(η^2-sulfur dioxide) molybdenum(O)," Inorg. Chem. 19(10), 3003-3007 (1980).

G. J. Kubas and P. J. Vergamini, "Synthesis, Characterization and Reactions of Iron-Sulfur Clusters containing the S_2 Ligand. $[Cp_2Fe_2(S_2)(SR)_2]^{0,+1}$, $[Cp_4Fe_4S_5]^{0,+1,+2}$, and $[Cp_4Fe_4S_6]$," Inorg. Chem.

R. E. London, "Carbon-Carbon Coupling in [13-$^{13}C_1$]Tryptophan," Org. Magn. Reson.

R. E. London and T. E. Walker, "Asymmetric NMR Spectra of Weakly Coupled Nuclei: A Common Characteristic in the ^{13}C NMR Spectra of [U-^{13}C] Labeled Molecules and in Natural Abundance Proton-Coupled ^{13}C Spectra," Org. Magn. Reson.

B. B. McInteer and J. G. Montoya, "An Automated Mass Spectrometer for Nitrogen Isotope Analysis," Anal. Biochem.

D. C. Moody, M. Goldblatt, B. B. McInteer, and T. R. Mills, "Alumina Catalyzed Isotope Exchange in CO," J. Catal.

D. C. Moody and R. R. Ryan, "*Trans*-Hydridocarbonyltris-(triphenylphosphine)cobalt(I), $CoP_3OC_{55}H_{46}$," Cryst. Struct. Commun.

D. C. Moody and R. R. Ryan, "Novel Reactivity and Low Temperature (−60°C) Structure of $Ru(CO)_2(\eta^2\text{-}SO_2\cdot SO_2)(PPh_3)_2$," J. Chem. Soc., Chem. Commun.

R. A. Penneman, "Americium,"in *Encyclopedia of Science and Technology*, 5th Ed. (McGraw-Hill Book Co.)

R. A. Penneman, "Neptunium," in *Encyclopedia of Science and Technology*, 5th Ed., (McGraw-Hill Book Co.)

W. W. Schulz and R. A. Penneman, "Physicochemical Properties of Americium," in *Chemistry of the Actinides*, Seaborg and Katz, Eds. (Invited chapter).

B. I. Swanson and L. H. Jones, "Matrix-Molecule Interactions, Dynamics, and Exchange Phenomena in Low Temperature Matrices: SF_6 in Argon and Krypton," J Chem. Phys.

PAPERS AND TALKS PRESENTED AT SCIENTIFIC MEETINGS IN FY 1980

M. Alei, Jr., L. O. Morgan, and W. E. Wageman, "^{15}N NMR Study of Complexation of Histidine by Zn(II) and Cd(II) in Aqueous Solution," 180th ACS National Meeting, Las Vegas, Nevada, August 24-29, 1980.

L. B. Asprey and P. G. Eller, "Fluorination Reactions of UF_6," 7th European Symp. Fluorine Chemistry, Venice, September 15-19, 1980.

L. B. Asprey and L. H. Jones, "Laser-Induced Separation of Sulfur Isotopes in Thiophosphoryl Fluoride," 35th Northwest - 5th Biennial Rocky Mountain ACS Joint Regional Meeting, Salt Lake City, Utah, June 12-14, 1980.

P. G. Eller, "SO_2 Insertion Reactions of d- and f-Element Complexes," Southwest Regional ACS Meeting, Austin, Texas, December 5-7, 1979.

P. G. Eller, "Crystal Structure of Hg(DHDECMP-H)(NO_3)," (Presented by R. T. Paine), Actinide Workshop IV, Los Alamos, New Mexico, May 13-14, 1980.

*P. G. Eller, "SO_2 Interactions with f- and d-Element Organometallics," Ohio State University, Columbus, Ohio, May 30, 1980.

P. G. Eller, "SO_2 Interactions with f- and Early d-Element Organo-metallics," 180th ACS National meeting, Las Vegas, Nevada, August 24-29, 1980.

E. Fukushima and K. D. Swenson, "Use of CAMAC for Computer Interface in NMR," 21st Experimental Nuclear Magnetic Resonance Spectroscopy Conference, Florida State University, Tallahassee, Florida, March 16-20, 1980.

G. D. Jarvinen, G. J. Kubas, and R. R. Ryan, "Sulfur Dioxide Complexes of Mo(O) and W(O): Interconversion of η^1 and η^2 Geometries and a Novel SO_2 Bridging Structure," ACS Combined Regional Meeting Southeast-Southwest, New Orleans, Louisiana, December 10-13, 1980.

G. J. Kubas and R. R. Ryan, "Coordinatively-Unsaturated Mo(O) and W(O) Complexes $M(CO)_3(PCy_3)_2$, which Reversibly Add N_2, H_2, and Other Small Molecules," 179th ACS National Meeting, Houston, Texas, March 24-28, 1980. ACS Abstracts of Papers 179, INOR-28 (1980).

G. J. Kubas, "New Aspects of the Coordination Chemistry and Bonding of SO_2, an Exceptionally Versatile Small Molecule," Gordon Research Conference on Inorganic Chemistry, New Hampton, New Hampshire, August 4-8, 1980.

B. B. McInteer, "Isotope Separation by Distillation: Design of a Carbon-13 Plant," Symposium on Separation Science and Technology for Energy Applications, Gatlinburg, Tennessee, October 30 - November 2, 1979. Sep. Sci. Technol. 15(3), 491-508 (1980).

B. B. McInteer, "Automation of a Mass Spectrometer for Nitrogen Isotope Ratio Analysis," 7th Int. Symp. Mass Spectrometry in Biochemistry Medicine, and Environmental Research, Milan, Italy, June 16-18, 1980.

T. R. Mills, "Carbon Isotope Separation by Absorptive Distillation," Symposium on Separation Science and Technology for Energy Applications, Gatlinburg, Tennessee, October 30 - November 2, 1979. Sep. Sci. Technol. 15(3), 475-490 (1980).

*D. C. Moody, "The Chemistry of Trivalent Uranium," University of South Carolina, Columbia, South Carolina, November 30, 1979.

D. C. Moody, R. R. Ryan, and G. J. Kubas, "Activation of S-O Bonds in Transition Metal-Sulfur Dioxide Complexes," 179th ACS Meeting, Houston, Texas, March 24-28, 1980. ACS Abstracts of Papers 179, INOR-34 (1980).

R. A. Penneman, "A Zirconium Molybdate as a Plutonium Host," IAEA Symposium on the Management of Alpha-Contaminated Wastes, Vienna, Austria, June 2-6, 1980.

H. D. Ramsey, D. G. Clifton, S. W. Hayter, R. A. Penneman, and Eldon L. Christensen, "Status of ^{241}Am Recovery and Purification at Los Alamos Scientific Laboratory," ACS Int. Symp. Industrial-Scale Production-Separation-Recovery of Transplutonium Elements," Las Vegas, Nevada, August 24-29, 1980. [To be published in ACS Symposium Series.]

M. J Reisfeld, H. Flicker, and M. Goldblatt, "Analysis of the Fourier Transform Spectrum of $^{13}C^{18}O_2$ in the 4.3 μm and 16 μm Regions," 35th Annual Symp. Molecular Spectroscopy, Columbus, Ohio, June 16-20, 1980.

M. J. Reisfeld, H. Flicker, and M. Goldblatt, "Analysis of the Spectra of $^{12}C^{17}O_2$, $^{12}C^{17}O^{18}O$, and $^{13}C^{17}O_2$ in the ν_2 (15 μm) Region," 35th Annual Symp. Molecular Spectroscopy, Columbus, Ohio, June 16-20, 1980.

---

*Invited talk.

R. R. Ryan, G. J. Kubas, D. C. Moody, and P. G. Eller, "Activation of Sulfur Dioxide by Transition Metal Complexes," 2nd Int. Symp. Homogeneous Catalysis, Düsseldorf, Germany, September 1-3, 1980.

B. I. Swanson and L. H. Jones, "High Resolution Infrared Studies of Dynamics and Exchange Phenomenon in Low Temperature Matrices," poster session, Gordon Conference, Wolfeboro, New Hampshire, August 18-22, 1980.

B. I. Swanson and L. H. Jones, "Application of High Resolution FTIR to the Study of Dynamics in Low Temperature Matrices," Symp. Fourier Transform Methods, 180th ACS National Meeting, Las Vegas, Nevada, August 24-29, 1980.

P. J. Vergamini and G. J. Kubas, "Synthesis, Structure, and Properties of Complexes Containing Organometallic Cluster Ligands," 179th ACS National Meeting, Houston, Texas, March 24-28, 1980. ACS Abstracts of Papers 179, INOR-94 (1980).

T. E. Walker, D. L. Anton, H. P. C. Hogenkamp, and N. A. Matwiyoff, "Carbon-13 Nuclear Magnetic Resonance Studies of the Structure of Vitamin B-12 Derivatives," American Society of Biological Chemists, Biophysical Society, New Orleans, Louisiana, June 1-5, 1980. Abstract in Federation Proc. 39, No. 6, May 1980.

CNC-7
PUBLICATIONS 1978-80

M. Alei, Jr., "Rapid Synthesis of Isotopically Labelled Methanes," J. Labelled Compd. Radiopharm. 17, 115-19 (1980).

M. Alei, Jr., L. O. Morgan, W. E. Wageman, and T. W. Whaley, "pH Dependence of ^{15}N NMR Shifts and Coupling Constants in Aqueous Imadazole and 1-Methyl Imidazole: Comments on Estimation of Tautomeric Equilibrium Constants for Aqueous Histidine," J. Am. Chem. Soc. 102(9), 2881-2887 (1980).

B. P. Bayhurst, J. S. Gilmore, R. J. Prestwood, R. E. Whipple, and P. M. Wanek, "Spallation Yields of ^{52}Fe, ^{67}Cu, ^{67}Ga, and ^{201}Tl from Reactions of 800-MeV Protons with Ni, As, Pb, and Bi Targets," J. Labelled Cmpds. Radiopharm. 16, 212-213 (1979).

J. E. Bonelli, J. P. Greenberg, A. L. Lazrus, J. E. Spencer, and W. A. Sedlacek, "Laboratory Simulation of Impregnated Filter Collection of Stratospheric Hydrogen Chloride and Chlorine Nitrate," Atmospheric Environment 12, 1591-94 (1978).

R. W. Charles, C. E. Holley, Jr., J. W. Tester, L. A. Blatz, and C. O. Grigsby, "Experimentally Determined Rock-Fluid Interactions Applicable to a Natural Hot Dry Rock Geothermal System," TMS Pap. Sel. A80-8 (1980).

C. C. Cummings, A. E. Ogard, and R. H. Shaw, "Target Insertion and Handling System for the Isotope Production Facility," Proc. 26th Conf. Remote Systems Technology, 1978, pp. 201-206.

D. B. Curtis and A. J. Gancarz, "Lead Isotopes as Indicators of Environmental Contamination from the Uranium Mining and Milling Industry in the Grants Mineral Belt, New Mexico," Proc. NEA Seminar for the Management, Stabilization and Environmental Impact of Uranium Mill Tailings OECD, Paris, France, 143 (1978).

D. B. Curtis, E. S. Gladney, and E. T. Jurney, "Potential Interferences in the Determination of Sulfur by Thermal Neutron Induced Prompt γ-Ray Spectrometry," Anal. Chem. 51, 158 (1979).

D. B. Curtis and R. A. Schmitt, "The Petrogenesis of L-6 Chondrites: Insights from the Chemistry of Minerals," Geochem. Cosmochin. Acta 43, 1091-1103 (1978).

H. O. Denschlag, H. Braun, W. Faubel, G. Fischbach, H. Meixler, G. Paffrath, W. Pörsch, M. Weis, H. Schrader, G. Siegert, J. Blachot, Z. B. Alfassi, H. N. Erten, T. Izak-Biran, T. Tamai, A. C. Wahl, and K. Wolfsberg, "Distribution of Nuclear Charge and Angular Momentum in Chains 132-137, 99, and 102 of ^{235}U (n_{th},f) at Various Kinetic Energies and Charge States of the Fragments," *Physics and Chemistry of Fission*, Vol. II, IAEA, Vienna, 153-177 (1979).

B. R. Erdal, B. P. Bayhurst, W. R. Daniels, S. J. DeVilliers, G. H. Heiken, F. O. Lawrence, M. L. Sykes, J. R. Smyth, J. L. Thompson, E. N. Vine, and K. Wolfsberg, "Parameters Affecting Radionuclide Migration in Geologic Media," *Scientific Basis for Nuclear*

Waste Management, Vol. 2, C. J. M. Northrup, Ed. (Plenum Press, New York) pp. 609-616.

B. R. Erdal, B. P. Bayhurst, W. R. Daniels, S. J. DeVilliers, F. O. Lawrence, J. L. Thompson, and K. Wolfsberg, "Parameters Affecting Radionuclide Migration of Argillaceous Media," Proc. of the Workshop on the Use of Argillaceous Materials for the Isolation of Radioactive Waste, Paris, September 10-12, 1979 (Nuclear Energy Agency, Organization for Economic Co-Operation and Development, Paris, France) pp. 55-66.

B. R. Erdal, W. R. Daniels, D. C. Hoffman, F. O. Lawrence, and K. Wolfsberg, "Sorption and Migration of Radionuclides in Geologic Media," *Scientific Basis for Nuclear Waste Management*, Vol. 1, G. J. McCarthy, Ed., (Plenum Press, New York, 1979) pp. 423-426.

A. J. Gancarz, "Chronology of the Cluff Lake Uranium Deposit, Saskatchewan, Canada," Proc. Int. Uranium Symp. Pine Creek Geosyncline, Northwest Territory, Australia, 91-94, (1979).

A. J. Gancarz, "U-Pb Age (2.05×10^9 years) of the Oklo Uranium Deposit," *Natural Fission Reactors*, 513-520 (IAEA, Vienna, 1978).

E. S. Gladney and D. B. Curtis, "Comment on Determination of Fluoride by Neutron Activation Analysis," Anal. Chem. 50, 376 (1978).

E. S. Gladney, D. B. Curtis, and E. T. Jurney, "Multi-Element Analysis of Major and Minor Elements by Thermal Neutron Induced Capture Gamma-Ray Spectrometry," J. Radio. Chem. 46, 299-308 (1978).

E. S. Gladney, L. F. Wangen, D. B. Curtis, and E. T. Jurney, "Observations on Boron Release from Coal Fired Power Plants," Env. Sci. Tech. 12, 1084 (1978).

P. M. Grant, B. R. Erdal, R. E. Whipple, R. J. Daniels, and H. A. O'Brien, Jr., "Half-lives of ^{82}Sr and ^{82}Rb," Phys. Rev. C18, 2799 (1978).

H. A. O'Brien, Jr., P. M. Grant, and A. E. Ogard, "The LASL Medical Radioisotope Research Program: Radiochemistry Problems and New Developments," Prog. Nucl. Med 4, 93-99 (1978).

H. A. O'Brien, Jr., A. E. Ogard, and P. M. Grant, "The LASL Medical Radioisotope Research Program: An Overview of LAMPF and the Isotope Production Facility," Prog. Nucl. Med. 4, 16-22 (1978).

C. J. Orth, J. D. Knight, K. Wolfsberg, and M. W. Johnson, "Nuclear Disintegration of Some Complex Nuclei by 60-MeV Muons," Phys. Rev. C 21, 1967 (1980).

R. J. Otto, G. T. Seaborg, and M. M. Fowler, "Recoil Range Distributions of Heavy Mass Products in Deep Inelastic Reaction with Gold and Uranium Targets," Phys. Rev. C 17, 1071 (1978).

M. A. Shapiro, E. R. Reiter, R. D. Cadle, and W. A. Sedlacek, "Vertical Mass and Trace Constituent Transports in the Vicinity of Jet Streams," Arch. Met. Geoph. Biokl., Ser. B 28, 193-206 (1980).

J. R. Smyth, J. Thompson, and K. Wolfsberg, "Microautoradiographic Studies of the Sorption of U and Am on Natural Rock Samples," *Radioactive Waste Management*, Vol. 1 (1), 13-24 (Harwood Academic Publishers, New York, 1980).

E. N. Vine, D. Young, W. Vine, and W. Wolf, "An Improved Synthesis of ^{18}F-5-fluorouracil," Int. J. Applied Rad. Isot. 30 401 (1979).

K. Wolfsberg, W. R. Daniels, D. C. Hoffman, and B. R. Erdal, "Migration of Radionuclides in Geologic Media — Laboratory and Field Studies," *Effluent and Environmental Radiation Surveillance, ASTM STP 698*, J. J. Kelly, Ed. (American Society for Testing and Materials, 1980) pp. 252-254.

PAPERS ACCEPTED FOR PUBLICATION IN FY 1980

M. Alei, Jr., P. J. Vergamini, and W. E. Wageman, "^{15}N NMR of cis-Diamine-Platinum(II) Complexes in Aqueous Solution," J. Inorg. Chem.

W. W. Berg, P. J. Crutzen, H. E. Grahek, S. N. Gitlin, and W. A. Sedlacek, "First Measurements of Total Chlorine Bromine in the Lower Stratosphere," Geophys. Res. Lett.

D. B. Curtis, E. S. Gladney, and E. T. Jurney, "The Cosmochemistry of Boron," Geochem. Cosmochim. Acta.

B. R. Erdal, B. P. Bayhurst, B. M. Crowe, W. R. Daniels, D. C. Hoffman, F. O. Lawrence, J. R. Smyth, J. L. Thompson, and K. Wolfsberg, "Laboratory Studies of Radionuclide Transport in Geologic Media," Proc. Int. Symp. Underground Disposal of Radioactive Wastes, Otaniemi, Finland.

A. J. Gancarz, G. A. Cowan, D. B. Curtis, and W. J. Maeck, "^{99}Tc, Pb and Ru Migration Around the Oklo Natural Fission Reactors," Proc. Int. Symp. Scientific Basis for Nuclear Waste Mangement.

M. Megan, A. Shaw, W. A. Sedlacek, P. R. Guthals, M. M. Fowler, and R. Megill, "Measurements of Nitric Oxide After a Nuclear Burst," J. Geophys. Res. (green).

W. A. Sedlacek, "Use of Ozone and Aitken Nuclei as Natural Tracers to Examine the Exchange of Air Between the Troposphere and Stratosphere in the Vicinity of The Tropopause Fold," S. Barr and T. Gedayloo, Eds., Proc. Atmospheric Tracers and Tracer Application Workshop, Los Alamos, New Mexico, May 22-24, 1979, Los Alamos National Laboratory report LA-8144-C (December 1979).

E. N. Vine, B. P. Bayhurst, W. R. Daniels, S. J. DeVilliers, B. R. Erdal, F. O. Lawrence, and K. Wolfsberg, "Radionuclide Transport and Retardation in Tuff," Scientific Basis for Nuclear Waste Management, Vol. 3, J. G. Moore, Ed. (Plenum, New York).

E. Vine, A. C. Wahl, "Fractional Independent Yields of ^{104}Tc and ^{105}Tc from Thermal-Neutron Induced Fission of ^{235}U and of ^{239}Pu," J. Inorg. Nucl. Chem.

LA REPORTS

D. B. Curtis and A. J. Gancarz, "An Interim Report on Studies of Uranium, Thorium and Lead Migration at Key Lake, Saskatchewan, Canada," Los Alamos National Laboratory report LA-8440-MS (July 1980).

W. R. Daniels, compiler, "Laboratory Studies of Radionuclide Distributions Between Selected Groundwaters and Geologic Media, October 1, 1979—September 30, 1980," Los Alamos National Laboratory report LA-8586-PR (January 1981).

B. R. Erdal, compiler, "Laboratory Studies of Radionuclide Distribution Between Selected Groundwaters and Geologic Media, October 1—December 31, 1979," Los Alamos National Laboratory report LA-8210-PR (March 1980).

B. R. Erdal, compiler, "Laboratory Studies of Radionuclide Distributions Between Selected Groundwaters and Geologic Media, January 1—March 31, 1980," Los Alamos National Laboratory report LA-8339-PR (May 1980).

B. R. Erdal, compiler, "Laboratory Studies of Radionuclide Distributions Between Selected Groundwaters and Geologic Media, April 1—June 30, 1980," Los Alamos National Laboratory report LA-8472-PR (September 1980).

E. S. Gladney, D. B. Curtis, D. R. Perrin, J. W. Owens, and W. E. Goode, "Nuclear Techniques for the Chemical Analysis of Environmental Materials," Los Alamos National Laboratory report LA-8192-MS (January 1980).

A. E. Norris, "Fission Product Release, July 1—September 30, 1979," Los Alamos National Laboratory report LA-8149-PR (November 1979).

A. E. Norris, "Oklo - Natural Fission Reactor Program July 1—September 30, 1979," Los Alamos National Laboratory report LA-8189-PR (January 1980).

A. E. Norris, "Fission Product Release, October 1—December 31, 1979," Los Alamos National Laboratory report LA-8272-PR (March 1980).

A. E. Norris, "Oklo - Natural Fission Reactor Program, October 1—December 31, 1979," Los Alamos National Laboratory report LA-8281-PR (March 1980).

A. E. Norris, "Fission Product Release, January 1—March 31, 1980," Los Alamos National Laboratory report LA-8389-PR (June 1980).

A. E. Norris, "Oklo - Natural Fission Reactor Program, January 1—March 31, 1980," Los Alamos National Laboratory report LA-8479-PR (August 1980).

A. E. Norris, "Fission Product Release, April 1—June 30, 1980," Los Alamos National Laboratory report LA-8539-PR (September 1980).

W. A. Sedlacek, "Use of Ozone and Aitken Nuclei as Natural Tracers to Examine the Exchange of Air Between the Troposphere and Stratosphere in the Vicinity of the Tropopause Fold," in "Proceedings of the Atmospheric Tracers and Tracer Application Workshop," Los Alamos National Laboratory report LA-8144-C (December 1980).

E. N. Vine, R. D. Aguilar, B. P. Bayhurst, W. R. Daniels, S. J. Devilliers, B. R. Erdal, F. O. Lawrence, S. Maestas, P. Q. Oliver, J. L. Thompson, and K. Wolfsberg, "Sorption-Desorption Studies on Tuff II. A Continuation of Studies with Samples from Jackass Flats, Nevada and Initial Studies with Samples from Yucca Mountain, Nevada," Los Alamos National Laboratory report LA-8110-MS (January 1980).

K. Wolfsberg, B. R. Erdal, and B. M. Crowe, compilers, "Research and Development Related to the Nevada Nuclear Waste Storage Investigations, April 1—June 30, 1980," Los Alamos National Laboratory report LA-8471-PR (October 1980).

K. Wolfsberg, B. R. Erdal, and B. M. Crowe, compilers, "Research and Development Related to the Nevada Nuclear Waste Storage Investigations, July 1—September 30, 1980," Los Alamos National Laboratory report LA-8612-PR (February 1981).

PAPERS AND TALKS PRESENTED AT SCIENTIFIC MEETINGS IN FY 1980

J. C. Banar, "Advances in Lead Isotopic Analysis," 28th Annual Conference on Mass Spectrometry and Allied Topics, New York, May 25-30, 1980.

R. W. Charles, "Rock Alteration in an Experimentally Imposed Temperature Gradient," Int. Assoc. Geochemistry and Cosmochemistry Meeting, Edmonton, Alberta, July 14-24, 1980.

R. W. Charles, C. E. Holley, J. W. Tester, L. A. Blatz, and C. O. Grigsby, "Experimentally Determined Rock-Fluid Interactions Applicable to a Natural Hot Dry Rock Geothermal System," AIME Annual Meeting, 1980, Las Vegas, Nevada.

W. E. Clements, S. Barr, and M. Fowler, "Effective Transport Velocity and Plume Elongation in Nocturnal Valley Wind Fields," Second Joint Conf. Applications of Air Pollution Meterology, New Orleans, Louisiana, March, 1980.

D. B. Curtis, "Boron Abundances in Meteorities: A New Perspective," 43rd Annual Meteoritical Society Meeting, La Jolla, California, September 2—8, 1980.

S. J. DeVilliers, B. P. Bayhurst, W. R. Daniels, F. O. Lawrence, E. N. Vine, and K. Wolfsberg, "Sorptive Properties of Tuff," ACS Meeting, Las Vegas, Nevada, August 24—29, 1980.

S. J. DeVilliers, B. R. Erdal, and K. Wolfsberg, "Groundwater Composition and Element Concentration as Factors Affecting the Sorption Behavior of Geologic Media," ACS 35th Northwest-5th Biennial Rocky Mountain Joint Regional Meeting, Salt Lake City, Utah, June 12—14, 1980.

D. J. Frank, "The Use of Intermediate Range Mass Spectrometry in the Measurement of Heavy Methanes as Atmospheric Tracers," 28th Annual Conference on Mass Spectrometry and Allied Topics, New York, May 25—30, 1980.

P. R. Guthals, "Project Airstream" presentation to Command Staff, 24th Composite Wing, USAF, Panama, November 1979.

C. Holley, C. Grigsby, J. Tester, L. Blatz, and R. Charles, "Interaction of Water with Crystalline Basement Rock in Fractured Hot Dry Geothermal Reservoirs, Tests, and Laboratory Experiments," Int. Assoc. Geochemistry and Cosmochemistry Meeting, Edmonton, Alberta, 1980.

A. E. Norris, "Fission Product Release," National Nuclear Waste Storage Isolation Information Meeting, Columbus, Ohio, October 30—November 1, 1979.

D. J. Rokop, "The Utilization of Electrodeposition and Pulse Counting for Medium Precision Analyses of

Nanogram Size Samples of Uranium and Plutonium," 28th Annual Conference on Mass Spectrometry and Allied Topics, New York, May 25—30, 1980.

W. A. Sedlacek, "Aerial Sampling of Soufriere of St. Vincent," American Geophysical Union Meeting, San Francisco, California, December 3, 1979.

W. A. Sedlacek, "Aircraft Measurements of Volcanic Debris in the Stratosphere," Tenth International Laser Radar Conference Symposium on Mt. St. Helens, Silver Springs, Maryland, October 6—9, 1980.

J. L. Thompson, W. R. Daniels, B. R. Erdal, S. Maestas, E. N. Vine, and K. Wolfsberg, "Microautoradiographic Studies of Radionuclide Sorption in Geologic Media," ACS 35th Northwest-5th Biennial Rocky Mountain Joint Regional Meeting, Salt Lake City, Utah, June 13—14, 1980.

J. L. Thompson, B. R. Erdal, W. R. Daniels, E. N. Vine, and K. Wolfsberg, "Microautoradiography: A Useful Technique for Investigating Radionuclide Transport in Geologic Media," Fourth International Conference on Nuclear Methods in Environmental and Energy Research, Columbia, Missouri, April 14-17, 1980.

CNC-11
PUBLICATIONS 1978-1980

H. Backe, F. Weik, P. A. Butler, V. Metag, J. B. Wilhelmy, D. Habs, G. Himmele, and H. J. Specht, "Direct Observation of Coulomb Fission of ^{238}U with ^{184}W Projectiles," Phys. Rev. Letters 43, 1077-1080 (1979).

S. J. Balestrini, R. Decker, H. Wollnik, K. D. Wünsch, G. Jung, E. Koglin, and G. Siegert, "Independent Yields of Rb and Cs Isotopes from Thermal-Neutron Induced Fission of ^{235}U," Phys. Rev. C 20, 2244-2248 (1979).

R. S. Bhalerao, L. C. Liu, and C. M. Shakin, "Systematic Features of Pion-Nucleus Interaction," Phys. Rev. C 21, 1903-1912 (1980).

R. S. Bhalerao, L. C. Liu, and C. M. Shakin, "Self-Energy of the Δ Resonance in Finite Nuclei and Fermi Broadening," Phys. Rev. C 21, 2103-2106 (1980).

R. S. Bhalerao, L. C. Liu, and C. M. Shakin, "Theoretical Models for the Calculation of the Reaction π+d $\rightarrow$ p+p in the Resonance Region," Nuovo Cimento 56A, 502-506 (1980).

T. J. Bornhorst and J. P. Balagna, "Instrumental Neutron Activation Analysis of French Geochemical Reference Samples," Geostandards Newsletter 3, 177-180 (1979).

H. C. Britt, E. Cheifetz, D. C. Hoffman, J. B. Wilhelmy, R. J. Dupzyk, and R. W. Lougheed, "Fission Barriers for ^{255}Es, ^{256}Es, and ^{255}Fm," Phys. Rev. C 21, 761-763 (1980).

H. C. Britt, A. Gavron, P. D. Goldstone, R. Schoenmackers, J. Weber, and J. Wilhelmy, "Yet More Complexity in Fission: Barriers for Nuclei with N = 150-154," Phys. Rev. Letters 40, 1010-1013 (1978).

H. C. Britt and J. B. Wilhelmy, "Simulated (n,f) Cross Sections for Exotic Actinide Nuclei," Nucl. Sci. Eng. 72, 222-229 (1979).

E. Cheifetz, H. A. Selic, A. Wolf, R. Chechik, and J. B. Wilhelmy, "Even-Even Neutron-Rich Isotopes," in *Nuclear Spectroscopy of Fission Products*, Till von Egidy, Ed., Conference Series 51 (The Institute of Physics, London, 1980), pp. 193-207.

B. J. Dropesky, G. W. Butler, C. J. Orth, R. A. Williams, M. A. Yates-Williams, G. Friedlander, and S. B. Kaufman, "Absolute Cross Sections for the ^{12}C($\pi^{\pm}$, πN)^{11}C Reactions Between 40 and 600 MeV," Phys. Rev. C 20, 1844-1856 (1979).

G. P. Ford, "Calculation of Nuclear Level Densities of ^{56}Fe, ^{59}Co, ^{60}Ni, ^{61}Cu, ^{62}Ni, ^{63}Cu, and ^{65}Cu," Nucl. Sci. Eng. 66, 334-348 (1978).

P. Glässel, D. V. Harrach, Y. Civelekoglu, R. Männer, H. J. Specht, J. B. Wilhelmy, H. Freiesleben, and K. D. Hildenbrand, "Three Particle Exclusive Measurements of the Reactions ^{238}U + ^{238}U and ^{238}U + ^{248}Cm," Phys. Rev. Letters 43, 1483-1486 (1979).

D. C. Hoffman, "Element 107," in McGraw-Hill Yearbook of Science and Technology—1977 Review/1978 Preview, (McGraw-Hill, Book Company, New York, 1978) pp. 156-158.

D. C. Hoffman, "Neutron Multiplicity Measurements for Spontaneous Fission of Cf and Fm Isotopes and Relevance to Neutron Emission for Superheavy Elements," in *Superheavy Elements*, Int. Symp. Superheavy Elements, Texas Technical University, Lubbock, Texas, March 9-11, 1978, M. A. K. Lodhi, Ed. (Pergamon Press, New York, 1978) pp. 89-102.

D. C. Hoffman, G. P. Ford, J. P. Balagna, and L. R. Veeser, "Neutron Multiplicity Measurements of Cf and Fm Isotopes," Phys. Rev. C 21, 637-646 (1980).

D. C. Hoffman, J. B. Wilhelmy, J. Weber, W. R. Daniels, E. K. Hulet, R. W. Lougheed, J. H. Landrum, J. F. Wild, and R. J. Dupzyk, "12.3-min ^{256}Cf and 43-min ^{258}Md and Systematics of the Spontaneous Fission Properties of Heavy Nuclides," Phys. Rev. C 21, 972-981 (1980).

C. M. Hohenberg, K. Marti, F. A. Podosek, R. C. Reedy, and J. R. Shirck, "Comparisons Between Observed and Predicted Cosmogenic Noble Gases in Lunar Samples," in *Proc. Ninth Lunar and Planetary Science Conf.*, Houston, Texas, March 13—17, 1978 (Pergamon Press, New York, 1978) pp. 2311-2344.

E. K. Hulet, R. W. Lougheed, J. H. Landrum, J. F. Wild, D. C. Hoffman, J. Weber, and J. B. Wilhelmy, "Spontaneous Fission of ^{259}Fm," Phys. Rev. C 21, 966-971 (1980).

R. L. Hutson, J. D. Knight, M. Leon, M. E. Schillaci, H. B. Knowles, and J. J. Reidy, "Negative Muon Capture in Noble Gas Mixtures," Phys. Lett. 76A, 226-228 (1980).

S. V. Jackson, J. W. Starner, W. R. Daniels, M. E. Bunker, and R. A. Meyer, "N = 85 Nuclei, II. Decay of 4.15-h ^{149}Tb^{g} to Levels of ^{149}Gd," Phys. Rev. C 18, 1840-1856 (1978).

S. B. Kaufman, E. P. Steinberg, and G. W. Butler, "Spallation of Gold by 100-300 MeV Pions," Phys. Rev. C 20, 2293-2307 (1979).

S. B. Kaufman, E. P. Steinberg, and G. W. Butler, "(π,πN) Reactions on ^{25}Mg and ^{197}Au," Phys. Rev. C 20, 262-266 (1979).

J. D. Knight, C. J. Orth, M. E. Schillaci, R. A. Nauman, F. J. Hartman, J. J. Reidy, and H. Schneuwly, "Coulomb Capture Ratios of Negative Muons in N_2 + O_2, NO, and CO," Phys. Lett. 79A, 377-379 (1980).

D. Liesen, P. Armbruster, F. Bosch, S. Hagmann, P. H. Mokler, H. J. Wollersheim, H. Schmidt-Böcking, R. Schuch, and J. B. Wilhelmy, "Experimental Confirmation of a Scaling Law for the 1sσ Excitation Probability for $Z_1 + Z_2 > 120$, and Its Breakdown in Pb + Cm Collisions at Very Small Internuclear Distances," Phys. Rev. Letters 44, 983 (1980).

L. C. Liu and C. M. Shakin, "Pion-Nucleus Elastic Scattering: Theory and Applications," in *Progress in Particle and Nuclear Physics*, Sir Denys Wilkinson, Ed. (Pergamon Press Ltd., Oxford, 1980), Vol. 5, Chap. 5, pp. 206-243.

L. F. Mausner, M. A. Moinester, J. D. Knight, S. Cochavi, and S. S. Friedland, "In-vivo Beam Localization by Positron Activation in Pion Therapy," Radia. Res. 80, 10-23, (1979).

R. A. Naumann, G. Schmidt, J. D. Knight, L. F. Mausner, C. J. Orth, and M. E. Schillaci, "Negative-Muon Capture Ratios for Alloys and Alkali Halide Solid Solutions," Phys. Rev. A 21, 639-644 (1980).

C. J. Orth, W. R. Daniels, B. J. Dropesky, R. A. Williams, G. C. Giesler, and J. N. Ginocchio, "Products of Stopped-Pion Interactions with Cu and Ta," Phys. Rev. C 21, 2524-2534 (1980).

C. J. Orth, B. J. Dropesky, R. A. Williams, G. C. Giesler, and J. Hudis, "Pion-Induced Spallation of Copper Across the (3,3) Resonance," Phys. Rev. C 18, 1426-1435 (1978).

C. J. Orth, J. D. Knight, K. Wolfsberg, and M. W. Johnson, "Nuclear Disintegration of Some Complex Nuclei by 60-MeV Muons," Phys. Rev. C 21, 1967-1973 (1980).

D. G. Perry and G. C. Giesler, "Philosophy of a Computer-Automated Counting System," IEEE Trans. Nucl. Sci. NS-26, 4591-4595 (1979).

N. T. Porile, B. J. Dropesky, and R. A. Williams, "Emission of ^{24}Na Fragments in the Interaction of ^{197}Au

with Intermediate-Energy Pions and Protons," Phys. Rev. C 18, 2231-2240 (1978).

R. C. Reedy, "Planetary Gamma-Ray Spectroscopy," in *Proc. Ninth Lunar and Planetary Science Conf.*, Houston, Texas, March 13—17, 1978 (Pergamon Press, New York, 1978) pp. 2961-2984.

R. C. Reedy, "Elemental Analysis of Planetary Surfaces Via Orbital Gamma-Ray Spectroscopy," in *Computers in Activation Analysis and Gamma-Ray Spectroscopy, Proc. Am. Nucl. Soc. Topical Conference at Mayaguez, P. R., 1978*, B. S. Carpenter, M. D. D'Agostino, and H. P. Yule, Eds., (Technical Information Center, U. S. DOE, 1979), pp. 684-697.

R. C. Reedy, G. F. Herzog, and E. K. Jessberger, "The Reaction Mg(n,α)Ne at 14.1 and 14.7 MeV: Cross Sections and Implications for Meteorites," Earth Planet, Sci. Lett. 44, 341-348 (1979).

S. Regnier, C. M. Hohenberg, K. Marti, and R. C. Reedy, "Predicted Versus Observed Cosmic-Ray-Produced Noble Gases in Lunar Samples: Improved Kr Production Ratios," in *Proceedings of the Tenth Lunar and Planetary Science Conference*, R. B. Merrill, Ed. (Pergamon Press, New York, 1979) pp. 1565-1586.

H. A. Selic, E. Chiefetz, A. Wolf, and J. B. Wilhelmy, "Neutron-Rich Fragments from Spontaneous Fission of ^{254}Cf," in *Nuclear Spectroscopy of Fission Products*, Till von Egidy, Ed., Conference Series 51 (The Institute of Physics, London, 1980) pp. 316-320.

J. I. Trombka, R. L. Schmadeback, M. J. Bielefeld, L. G. Evans, A. E. Metzger, E. L. Haines, C. S. Dyer, S. M. Seltzer, R. C. Reedy, and J. R. Arnold, "Analytical Methods in Determining Elemental Composition from Apollo X-Ray and Gamma-Ray Spectrometer Data," in *Computers in Activation Analysis and Gamma-Ray Spectroscopy, Proc. Amer. Nucl. Soc. Topical Conference at Mayaguez, P.R., 1978*, B. S. Carpenter, M. D. D'Agostino, and H. P. Yule, Eds., (Technical Information Center, U. S. DOE, 1979) pp. 26-38.

G. D. Westfall, R. G. Sextro, A. M. Poskanzer, A. M. Zebelman, G. W. Butler, and E. K. Hyde, "Energy Spectra of Nuclear Fragments Produced by High-Energy Protons," Phys. Rev. C 17, 1368-1381, (1978).

J. B. Wilhelmy, H. C. Britt, D. C. Hoffman, W. R. Daniels, E. Cheifetz, A. Gavron, J. Weber, E. K. Hulet, J. H. Landrum, R. W. Lougheed, and J. F. Wild, "Fission Properties of the Heavy Actinides," S-Afr. Tydskr. Fis. 1, 116-117 (1978).

K. E. Williams and G. T. Seaborg, "New Isotope ^{242}Bk," Phys. Rev. C 19, 1794-1800 (1979).

PAPERS ACCEPTED FOR PUBLICATION IN FY 1980

E. Cheifetz, H. C. Britt, and J. B. Wilhelmy, "Determination of Fission Probabilities for Actinide Nuclei Excited by the (^{12}C, ^{8}Be$_{g.s.}$) Reaction," Phys. Rev. C.

D. V. Harrach, P. Glässel, Y. Civelekoglu, R. Männer, H. J. Specht, J. B. Wilhelmy, H. Feiesleben, and K. D. Hildenbrand, "Fission Properties of Very Heavy Nuclei Produced in Deep Inelastic Collisions," *Int. Symp. on Physics and Chemistry of Fission*, Jülich, Federal Republic of Germany, May 1979, Paper IAEA-SM-241/D4.

E. S. Gladney, D. R. Perrin, J. P. Balagna, and C. Warner, "Evaluation of a Boron-Filtered Epithermal Neutron Irradiation Facility," Analyt. Chem.

L. C. Liu, "Two-Nucleon Processes in a Coupled-Channel Approach to Pion-Nucleus Single Charge Exchange Reactions," Phys. Rev. C.

J. M. Nitschke, M. Fowler, A. Ghiorso, R. Leber, D. M. Lee, M. J. Nurmia, L. P. Somerville, K. E. Williams, E. K. Hulet, J. Landrum, R. Lougheed, J. Wild, C. Bemis, R. Silva, P. Eskola, "Search for an 80 ms Spontaneous Fission Activity in Bombardments of ^{249}Bk with ^{15}N," Nucl. Phys. A.

R. C. Reedy, "Lunar Radionuclide Records of Average Solar-Cosmic-Ray Fluxes Over the Last Ten Million Years," *Proc. Conf. Ancient Sun.*

R. C. Reedy, "Silver Isotopic Anomalies in Iron Meteorites - Cosmic-Ray Production and Other Possible

Sources," *Proc. Eleventh Lunar and Planetary Sci. Conf.*

G. J. Russell, J. S. Gilmore, R. E. Prael, H. Robinson, and S. D. Howe, "Spallation Target-Moderator-Reflector Studies at the Weapons Neutron Research Facility," *Proc. Symp. Neutron Cross Sections from 10-50 MeV.*

E. P. Steinberg, S. B. Kaufman, and G. W. Butler, "Pion Interactions with Complex Nuclei in the Resonance Region," *Proc. Second Conf. Nuclear Reaction Mechanisms*, Varenna, Italy, June 18—21, 1979.

D. J. Vieira, G. W. Butler, D. G. Perry, A. M. Poskanzer, L. P. Remsberg and J. B. Natowitz, "Search for Light Neutron-Deficient Nuclei Produced in 800 MeV Proton Spallation Reactions," *Proc. Sixth Int. Conf. Atomic Masses*, East Lansing, Michigan, September 18—21, 1979.

LA REPORTS

J. P. Balagna, "Nuclear Radiation Measurement Facilities at the Radiochemistry Laboratory at the Los Alamos Scientific Laboratory," LA-8337-MS (August 1980).

D. M. Holm and T. J. Bornhorst, "Probes: October 1, 1977—September 30, 1978," LA-7796-PR (May 1979).

G. F. Grisham, E. A. Bryant, and K. E. Williams, "Uraninite Leaching: Literature Survey," LA-7799-MS (April 1979).

PAPERS AND TALKS PRESENTED AT SCIENTIFIC MEETINGS IN FY 1980

P. Armbruster, J. B. Wilhelmy, H. Backe, W. Bonin, F. Bosch, P. A. Butler, et al., "Heavy Ions and Heavy Elements: Experimental Measurements in Germany," Am. Chem. Soc. Meeting, Las Vegas, Nevada, August 25—29, 1980.

I. Binder, "Neutron-Induced Reactions of Tin Isotopes," Am. Chem. Soc. Meeting, Las Vegas, Nevada, August 25—29, 1980.

T. J. Bornhorst, W. E. Elston, R. S. Della Valle, and J. P. Balagna, "Distribution of Uranium in Mid-Tertiary Volcanic Rocks, Mogollan-Datil Volcanic Field," Southwest Section of Am. Assoc. of Petroleum Geologists, El Paso, Texas, Feb. 28—29, 1980.

S. J. DeVilliers, B. P. Bayhurst, W. R. Daniels, F. O. Lawrence, E. N. Vine, and K. Wolfsberg, "Sorptive Properties of Tuff," Am. Chem. Soc. Meeting, Las Vegas, Nevada, August 25—29, 1980.

J. D. Knight, C. J. Orth, M. E. Schillaci, R. A. Naumann, F. J. Hartmann, J. J. Reidy, and H. Schneuwly, "Capture of Negative Muons in Some Simple Covalent Molecules—Can it Provide Chemical Structure Information?" ACS 35th Northwest-5th Biennial Rocky Mountain Joint Regional Meeting Salt Lake City, Utah, June 12—14, 1980.

J. R. Lapides, M. S. Spergel, O. W. Lazareth, P. W. Levy, R. C. Reedy, and J. I. Trombka, "The Effects of Hydrogen on Gamma-Ray Emission from Planetary Surfaces," Eleventh Lunar and Planetary Sci. Conf., Houston, Texas, March 17—21, 1980.

L. C. Liu, "Pion-Nucleus Optical Potential: Theory and Applications," seminar MP Division, April 1980.

L. C. Liu, "Dynamics of Single Charge Exchange Reactions," Am. Phys. Soc. Spring Meeting, Washington, D.C., April 28—May 1, 1980.

L. C. Liu, "Importance of Short Range Correlation in Pion-Nucleus Backward Scattering," Int. Conf. Nuclear Physics, Berkeley, California, August 24—30, 1980.

R. J. Prestwood, "Radioactivity in Perspective," 2nd Annual Blue River Trauma Society, Blue River, British Columbia, Canada, March 8—15, 1980.

*R. C. Reedy, "Lunar Radionuclide Records of Average Solar-Cosmic-Ray Fluxes Over the Last Ten Million Years," Conf. Ancient Sun: Fossil Record in the Earth, Moon, and Meteorites, Boulder, Colorado, October 16—19, 1979.

---

*Invited talk.

R. C. Reedy, "Systematics of Nuclear Reactions in Meteorites," 43rd Annual Meteoritical Society Meeting, La Jolla, California, September 2—6, 1980.

L. Rosen, D. C. Hoffman, B. J. Dropesky, and H. A. O'Brien, "Nuclear and Radiochemistry Facilities at LAMPF," ACS Meeting, Las Vegas, Nevada, August 25—29, 1980.

R. S. Rundberg, B. J. Dropesky, G. C. Giesler, G. W. Butler, S. B. Kaufman, and E. P. Steinberg, "Excitation Functions Across the (3,3) Resonance for the Pion Single Charge Exchange Reactions $^{27}Al(\pi^-,\pi^0)^{27}Mg$, $^{65}Cu(\pi^-,\pi^0)^{65}Ni$, and $^{45}Sc\ (\pi^+,\pi^0)^{45}Ti$," 179th National ACS Meeting, Houston, Texas, March 23—28, 1980.

G. J. Russell, J. S. Gilmore, R. E. Prael, H. Robinson, and S. D. Howe, "Spallation Target-Moderator-Reflector Studies at the Weapons Neutron Research Facility," Symp. Neutron Cross Sections from 10-50 MeV, Brookhaven National Laboratory, May 12—14, 1980.

M. E. Schillaci, J. D. Knight, L. F. Mausner, C. J. Orth, R. A. Naumann, and G. Schmidt, "Muonic Lyman X-Ray Intensities in Pure Elements," ACS 35th Northwest-5th Biennial Rocky Mountain Joint Regional Meeting, Salt Lake City, Utah, June 12—14, 1980.

M. S. Spergel, R. C. Reedy, O. W. Lazareth, and P. W. Levy, "Depth Dependence of Cosmogenic Nuclides in Spherical Meteoroids," 43rd Annual Meteoritical Society Meeting, La Jolla, California, September 2—6, 1980.

A. Yaniv, K. Marti, and R. C. Reedy, "The Solar Cosmic-Ray Flux During the Last Two Million Years," Eleventh Lunar and Planetary Science Conf., Houston, Texas, March 17—21, 1980.

M. A. Yates-Williams, A. H. Williams, J. T. Ganley, and J. P. Balagna, "Development of a Radiochemical Diagnostic for the Helios System," Amer. Phys. Soc. Meeting, Boston, Massachusetts, November 12—16, 1979.

APPENDIX B

DIVISION FACILITIES

CHEMICAL SYNTHESIS EQUIPMENT
- PAR electrochemical equipment
- Three gas chromatographs
- Vacuum lines, hoods, inert atmosphere boxes for handling air-sensitive materials and powerful oxidants (F_2)
- High-pressure autoclaves
- High-pressure liquid chromatograph

SPECTROSCOPIC EQUIPMENT
- Nuclear Magnetic Resonance
  - Varian XL-100-Fourier Transform NMR spectrometer for ^{13}C and other nuclei
  - EM-390 fluorine, proton, phosphorous, NMR; EM-360 proton NMR
  - Spectrometers: superconducting and iron core magnets for NMR studies of solids
  - Bruker WM-300 wide-bore spectrometer for high-resolution, multinuclear NMR of liquids
  - Bruker CXP-200 for solid state high-resolution NMR studies
- Infrared
  - Perkin-Elmer 180, 283, and 683 spectrometers
  - Nicolet FT-ir spectrometer
  - Digilab FT-ir far-ir spectrometer (Cryo-Matrix equipment)
- Laser Raman Spectrometers
  - Cary-81 laser-Raman spectrometer
  - SPEX plus Nicolet data system, Spectra Physics 171 with Ar^+, Kr^+ lasers
- Ultraviolet, Visible, Near-IR Spectrometers
  - Hewlett-Packard 8450A uv/visible spectrometer
  - Two Cary-14 spectrometers
  - Molectron N_2-pump and dye laser

X-RAY DIFFRACTION
- Weissenberg precession and powder diffraction cameras

- Picker FACS-1 single-crystal x-ray diffractometer (replacement being ordered)
- Phillips and Picker x-ray diffractometers
- Mettler hot-stage for optical microscopy

INSTRUMENTS FOR ELEMENTAL ANALYSIS
- Atomic absorption spectrometer (in fume hood)
- Plasma emission spectrometer
- X-ray fluorescence spectrometer (automatic read-out and data analysis)
- Dionex ion chromatograph
- Chemical autoanalyzer

HYDROTHERMAL LABORATORY
- Circulation loops
- Rocking vessels
- Permeability systems

INSTRUMENTS FOR THERMOCHEMISTRY
- High-temperature solution calorimeter
- Combustion calorimeter
- Room-temperature solution calorimeter
- Perkin-Elmer TGS-2 thermogravimetric balance
- Differential thermal analyses equipment

ROCK SAMPLE PREPARATION LABORATORY

FLUID TRANSPORT SYSTEMS

MICROSCOPY
- Scanning electron microscope (with nondispersive x-ray analyzer)
- Optical: microautoradiography equipment

MICROORGANISMS PREPARATION FACILITY

INSTRUMENTS FOR *IN VIVO* ANIMAL IMAGING
- Picker 411 gamma camera

INSTRUMENTS FOR CHEMICAL KINETICS, CHEMICAL DYNAMICS, SPECTROSCOPY AND ULTRASENSITIVE ANALYSIS
- Fast-Flow tube
- Crossed molecular beam machine
- Single beam machines
- Stopped-flow kinetics apparatus for plutonium studies
- Excitation lasers uv to ir, pulsed and cw

INSTRUMENTS FOR THEORY
- VAX-11/780 computer

MASS SPECTROMETERS
- Two surface thermal ionization, pulse-counting instruments
- Four surface thermal ionization spectrometers with ion detection by Faraday cage
- One "precision-ratio" gas source
- One gas-source two-stage spectrometer for "heavy methanes"
- Two magnetic deflection isotope separators
- Two cycloidal spectrometers, masses to 80
- Quadrupole with gas chromatograph, masses to 1000
- Time-of-flight and automated nitrogen isotope ratio spectrometer
- Molecular-beam photoionization spectrometer

MEASUREMENT AND HANDLING OF RADIOACTIVITY
- Automatic beta and gamma counting systems
- Alpha, beta, and gamma-ray spectrometers
- Computer control for data collection and data reduction
- Hot cells for high-level gamma- and beta-active materials
- Facilities for alpha-emitting materials

RADIOISOTOPE PRODUCTION FACILITY AT LAMPF

CRYOGENIC SEPARATION FACILITY FOR STABLE ISOTOPES OF CARBON, OXYGEN, AND NITROGEN

☆U.S. GOVERNMENT PRINTING OFFICE: 1981-0-777-022/71

Printed in the United States of America
Available from
National Technical Information Service
US Department of Commerce
5285 Port Royal Road
Springfield, VA 22161

Microfiche $3.50 (A01)

Page Range	Domestic Price	NTIS Price Code	Page Range	Domestic Price	NTIS Price Code	Page Range	Domestic Price	NTIS Price Code	Page Range	Domestic Price	NTIS Price Code
001-025	$ 5.00	A02	151-175	$11.00	A08	301-325	$17.00	A14	451-475	$23.00	A20
026-050	6.00	A03	176-200	12.00	A09	326-350	18.00	A15	476-500	24.00	A21
051-075	7.00	A04	201-225	13.00	A10	351-375	19.00	A16	501-525	25.00	A22
076-100	8.00	A05	226-250	14.00	A11	376-400	20.00	A17	526-550	26.00	A23
101-125	9.00	A06	251-275	15.00	A12	401-425	21.00	A18	551-575	27.00	A24
126-150	10.00	A07	276-300	16.00	A13	426-450	22.00	A19	576-600	28.00	A25
									601-up	†	A99

†Add $1.00 for each additional 25-page increment or portion thereof from 601 pages up.